Cooperative Dynamics of Didodecyldimethylammonium Bromide / Water / n-Dodecane Microemulsions

A Dielectric Relaxation Study

Dissertation
zur Erlangung des
Doktorgrades der Naturwissenschaften
(Dr. rer. nat.)
der Naturwissenschaftlichen Fakultät IV
– Chemie und Pharmazie –
der Universität Regensburg

vorgelegt von
Wolfgang Wachter
aus Pentling

Regensburg 2007

Promotionsgesuch eingereicht am:	16. November 2007
Tag des Kolloquiums:	19. Dezember 2007
Die Arbeit wurde angeleitet von:	apl. Prof. Dr. R. Buchner
Prüfungsausschuss:	Prof. Dr. H. Krienke (Vorsitzender) apl. Prof. Dr. R. Buchner Prof. Dr. G. Schmeer Prof. Dr. J. Daub

meinen Eltern

O sprich mir nicht von jener Datenmenge,
Bei deren Anblick uns der Geist entflieht.
Verhüll' mir das Relaxationsgedränge,
Das wider Willen uns zum Strudel zieht.
Doch helfen mag's, dass man ans Ziel gelänge,
Wo doch dem Forscher reine Freude blüht:
Die Mikroemulsionen, die wir sehen
Zu kennen nicht nur, sondern zu verstehen.

frei nach Johann Wolfgang von Goethe,
Faust I

Vorwort

Diese Dissertation entstand in der Zeit von Februar 2005 bis November 2007 am Institut für Physikalische und Theoretische Chemie der Naturwissenschaftlichen Fakultät IV – Chemie und Pharmazie – der Universität Regensburg.

An erster Stelle gilt mein herzlicher Dank meinem Doktorvater, Herrn apl. Prof. Dr. Richard Buchner, für die Erteilung des Themas und seine großzügige persönliche und wissenschaftliche Förderung. Bei meiner Arbeit gewährte er mir ein außerordentlich hohes Maß an akademischen Freiräumen. Gleichwohl stand er mir jederzeit in allen Belangen mit Rat und Tat zur Seite; die intensiven Diskussionen mit ihm trugen wesentlich zum Gelingen dieser Dissertation bei.

Dem Leiter des Lehrstuhls, Herrn Prof. Dr. Werner Kunz, danke ich für seine großzügige Unterstützung.

In der Arbeitsgruppe von Herrn Prof. Dr. Glenn Hefter, Murdoch University, Perth (Australien), durfte ich im Rahmen dieser Dissertation mehr als fünf unvergessliche Monate verbringen. Ihm danke ich besonders herzlich für seine Gastfreundschaft, die lehrreiche und persönlich bereichernde Zusammenarbeit, sein reges Interesse am Fortschreiten dieser Arbeit und nicht zuletzt für seine Bereitschaft, mir als *native speaker* beim Korrekturlesen des englischen Textes behilflich zu sein.

Meinen aktuellen und ehemaligen Kollegen in der Mikrowellen-Arbeitsgruppe, Herrn Dipl.-Chem. Johannes Hunger, Herrn Dr. Simon Schrödle und Herrn Dipl.-Chem. Alexander Stoppa, danke ich für ihre stete Hilfsbereitschaft und die angenehme Zusammenarbeit. Mein besonderer Dank gilt Herrn Dr. Schrödle für die Einführung in die Geheimnisse der Mikrowellen-Apparaturen bereits während meiner Diplomarbeit.

Allen Mitarbeitern der Werkstätten sei für die zuverlässige, schnelle und gewissenhafte Erledigung meiner Aufträge gedankt. Allen Mitarbeitern des Lehrstuhls in Regensburg und des Chemistry Departments in Murdoch danke ich für ihre Hilfsbereitschaft und die angenehme Arbeitsatmosphäre.

Der *Studienstiftung des deutschen Volkes*, die dieses Dissertationsprojekt äußerst großzügig förderte, fühle ich mich zu besonderem Dank verpflichtet. Auf ihre finanzielle Unterstützung konnte ich mich stets verlassen. Gleichzeitig erhielt ich bei ihren Doktorandenforen und Sommerakademien viele wertvolle Anregungen; die zahlreichen Gespräche mit meinen Mitstipendiaten empfand ich als große persönliche Bereicherung.

Mein Dank gilt ferner der *Deutschen Bunsen-Gesellschaft für Physikalische Chemie e.V.* für die finanzielle Unterstützung meiner Teilnahme an ihrer 105. Hauptversammlung in Erlangen.

Preface

This thesis has been developed from February 2005 until November 2007 at the Institute for Physical and Theoretical Chemistry of the Faculty of Science IV – Chemistry and Pharmacy – at Regensburg University.

First and foremost, I would like to express my gratitude to my PhD supervisor, apl. Professor Dr. Richard Buchner, for raising the issue of my thesis and for his generous personal and scientific support. While doing my work I enjoyed an extraordinary degree of academic freedom. Nevertheless, he was always prepared to help me with words and deeds; the many discussions we had were essential for the success of this thesis.

I would like to thank the head of the institute, Professor Dr. Werner Kunz, for his generous support.

An unforgettable part of my PhD studies was my stay in the group of Professor Dr. Glenn Hefter, Murdoch University, Perth (Australia), where I could work for almost half a year. I feel very much obliged to him for his warm hospitality, the most instructive and personally enriching collaboration, his active interest in the progress of this thesis and not least for offering me a native speaker's expertise for proofreading the English text.

I would like to express my gratitude to my current and former colleagues in the microwave group, Dipl.-Chem. Johannes Hunger, Dr. Simon Schrödle and Dipl.-Chem. Alexander Stoppa, for their steady support and for the enjoyable collaboration. Special thanks go to Dr. Simon Schrödle for introducing me to the mysteries of the microwave instruments already during my diploma thesis.

Thanks to all members of the workshops for completing my orders reliably, diligently and quickly. I would like to thank all members of the Institute at Regensburg and of the Chemistry Department at Murdoch for their cooperativeness and the enjoyable working atmosphere.

I feel very much obliged to the *Studienstiftung des deutschen Volkes* (German National Academic Foundation) for its most generous support of this thesis. Not only could I always rely on its financial aid, but I also had the opportunity to attend its PhD Fora and Summer Academies, which I will remember as very stimulating experiences; the many discussions I had with my fellow scholarship holders were of great personal value to me.

Furthermore, financial support from the *Deutsche Bunsen-Gesellschaft für Physikalische Chemie e.V.* (German Bunsen Society for Physical Chemistry) for my participation in its 105^{th} General Meeting held at Erlangen is gratefully acknowledged.

Contents

Constants and Symbols

Fundamental Physical Constants

elementary charge	e_0	$= 1.60217733 \cdot 10^{-19}\,\mathrm{C}$
permittivity of vacuum	ε_0	$= 8.854187816 \cdot 10^{-12}\,\mathrm{C^2(Jm)^{-1}}$
permeability of vacuum	μ_0	$= 4\pi \cdot 10^{-7}\,\mathrm{(Js)^2(C^2m)^{-1}}$
speed of light in vacuum	c_0	$= 2.99792458 \cdot 10^{8}\,\mathrm{m\,s^{-1}}$
Avogadro constant	N_A	$= 6.0221367 \cdot 10^{23}\,\mathrm{mol^{-1}}$
Boltzmann constant	k_B	$= 1.380658 \cdot 10^{-23}\,\mathrm{J\,K^{-1}}$
Faraday constant	F	$= 9.6485309 \cdot 10^{4}\,\mathrm{C\,mol^{-1}}$
Planck constant	h	$= 6.6260755 \cdot 10^{-34}\,\mathrm{Js}$

Frequently Used Symbols

$\vec{B}$	magnetic induction ($\mathrm{Vs\,m^{-2}}$)	α	damping coefficient ($\mathrm{m^{-1}}$)
$\vec{D}$	electric displacement ($\mathrm{C\,m^{-2}}$)	β	phase constant ($\mathrm{m^{-1}}$)
$\vec{E}$	electric field strength ($\mathrm{V\,m^{-1}}$)	$\hat{\gamma}$	propagation constant ($\mathrm{m^{-1}}$)
$\vec{H}$	magnetic field strength ($\mathrm{A\,m^{-1}}$)	$\hat{\varepsilon}$	complex dielectric permittivity
$\vec{P}$	dielectric polarisation ($\mathrm{C\,m^{-2}}$)	ε'	real part of $\hat{\varepsilon}$
T	temperature (K)	ε''	imaginary part of $\hat{\varepsilon}$
V	volume ($\mathrm{m^3}$)	ε_∞	$\lim_{\nu\to\infty}(\varepsilon')$
c	molarity ($\mathrm{mol\,dm^{-3}}$)	ε	$\lim_{\nu\to 0}(\varepsilon')$
$\vec{j}$	electric current density ($\mathrm{A\,m^{-2}}$)	$\hat{\eta}$	generalised complex dielectric permittivity
$\hat{k}$	complex wavenumber	κ	conductivity ($\mathrm{S\,m^{-1}}$)
m	mass (kg)	μ	dipole moment ($\mathrm{C\,m}$)
r	radius (m)	ν	frequency (Hz)
t	time (s)	ρ	density ($\mathrm{kg\,m^{-3}}$)
Φ	electric potential (V)	τ	relaxation time (s)
ϕ	volume fraction of internal phase	ω	angular frequency ($\mathrm{s^{-1}}$)

Acronyms

AOT	Sodium Bis(2-ethylhexyl) Sulfosuccinate
ATR	Attenuated Total Reflectance
C	Caesium Bromide (CsBr)
CIP	Contact Ion Pair
D	*n*-Dodecane
DDAB	Didodecyldimethylammonium Bromide
DMA	N,N-Dimethylacetamide
DOC	Disordered Open Connected
DR	Dielectric Relaxation
DRS	Dielectric Relaxation Spectroscopy
ESR	Electron Spin Resonance
FD	Frequency Domain
FFEM	Freeze Fracture Electron Microscopy
FTIR	Fourier-Transformed Infrared
IB	Irrotationally Bound
IFM	Interferometer
L	Lithium Bromide (LiBr)
L_2	Microemulsion Phase in the System DDAB/W/D
MD	Molecular Dynamics
N	Sodium Bromide (NaBr)
NMR	Nuclear Magnetic Resonance
OHP	Outer Helmholtz Plane
SAXS	Small-Angle X-Ray Scattering
SDS	Sodium Dodecylsulfate
SIP	Solvent-Shared Ion Pair
2SIP	Solvent-Separated Ion Pair
T	Tetramethylammonium Bromide ($(CH_3)_4NBr$)
TDR	Time-Domain Reflectometry
VNA	Vector Network Analyzer
W	Water (H_2O)
W/O	Water in Oil
5D	Superposition of 5 Debye Equations
6D	Superposition of 6 Debye Equations

Introduction

Microemulsions are a class of chemical substances which is used in nature for at least 100 million years. Since this time, the Australian sawfly larva, a primitive but highly successful insect, encapsulates poisonous terpenes and other compounds of the eucalyptus leaves on which it feeds in a diverticulum; the latter contains the oils in a microemulsion, which is very effective in repelling the larva's predators.[79]

The first reported human use of microemulsions goes back to the Ancient Mesopotamia of Hammurabi ($\sim$ 1750 B.C.), who is known in history for his Code dealing with the laws of property and of damages.[182] In these times, pouring oil on water or water on oil was used as a form of divination. In his book 'Ancient Mesopotamia', Oppenheim describes this practice as follows: 'When the diviner, who was called *baru*, poured oil into a bowl of water which he held in his lap, it was done to establish the will of the deity with regard to the country or to an individual. The movements of the oil in the water, in relation to the surface or the rim of the cup, could portend for the king peace and prosperity or war and rebellion: for the private citizen it might portend progeny, success in business, the recovery of health and the right girl when he was about to marry – or the opposite.'[151] Our knowledge of this practice comes from some Babylonian cuneiform tablets, which were deciphered and translated during the 19$^{\text{th}}$ and the 20$^{\text{th}}$ centuries;[182] in these texts, also the use of oil-water-surfactant mixtures is described.

However, it was not before 1943 that microemulsions became an object of scientific investigation. In this year, Hoar and Schulman published a letter to the editors of *Nature* where they tried to explain why 'oil – alkali-metal soap (or cationic soap, such as cetyl trimethyl ammonium bromide) – water systems of certain concentrations exist as transparent, electrically non-conducting dispersions, in which the oil is the continuous phase'.[111] As an extrapolation from known (macro-)emulsions to this novel kind of substances which was characterized by a lack of turbidity,[92] these authors concluded that the dispersed phase had to consist of 'sub-microscopic micelles';[111] some years later, Schulman *et al.* coined the term 'microemulsion' to describe this phenomenon.[172] Since these times, the concept 'microemulsion' has been defined and redefined repeatedly.[136] According to the definition proposed by Danielsson and Lindman in 1981, which is widely accepted in recent literature,[73,136] a microemulsion is 'a system of water, oil and amphiphile which is a single optically isotropic and thermodynamically stable liquid solution'.[67]

Accordingly, the main difference between macro- and microemulsions – apart from the particle size – consists in their stability: microemulsions are thermodynamically stable systems, whereas (macro-)emulsions are only kinetically stable. It is self-evident that this property makes microemulsions an exciting class of substances for a wide range of technical applications.[73,127] For example, water-in-oil microemulsions are excellent reaction media, increasing the product yield of chemical reactions in which the products are soluble in the oil phase.[173] They are also very useful for the generation of highly dispersed (and hence highly active) catalysts.[73] A further important application of microemulsions is their use for *in vivo* enzymological studies; as in living cells enzymes are usually active near a water/organic interface, water-in-oil microemulsions are an ideal system to investigate enzymatic effects.[143] Beyond that, as Lawrence and Rees illustrate in their review, microemulsions are of great interest to the pharmaceutical scientist because of their ability to act as drug-delivery vehicles.[136]

However, microemulsions are also very useful model systems for water under geometrical confinement. As Levinger points out, 'water is the most ubiquitous bulk liquid on Earth's surface. Yet in biology as well as in natural and synthetic materials, it often is tucked away in tiny crevices inside proteins or in porous materials. [...] Recent investigations have increased our understanding of confined water, showing that in nanoscopic proportions, many water properties differ drastically from those of bulk water.'[139] According to Rosenfeld and Schmuttenmaer, investigating the behaviour of water under confinement is 'essential due to the importance of water trapped in clays, zeolites, porous glasses, and even within proteins.'[163] Water-in-oil microemulsions are an ideal model to study confinement effects on water, as they are relatively simple systems which nevertheless exhibit an aqueous subphase comparable to the aqueous parts of *e.g.* a protein or a zeolite. But also the counterion behaviour in the water droplets of a microemulsion can provide very valuable information for the elucidation of biological processes. It is well known that essential biological properties, like energy biotransformation and excitability, are determined by the local ion concentration at relevant proteolipid sites; however, experimental studies of local ion concentrations in biological membranes are very complicated to conduct, due to the complexity of those systems.[120]

Despite this great potential of applications, microemulsions are still poorly investigated, and many open questions remain regarding their structure, dynamics and properties. Evans *et al.* compare microemulsions to the British Empire in the Victorian age and characterize them as 'elusive, full of contradictions, and yet with an underlying thread of unity.'[79] The first part of this statement can be readily understood given the multitude of contradictions found in the literature dealing with microemulsions; however, its second part seems to be audacious, and maybe even 'preposterous',[79] as Evans *et al.* admit. Freeze Fracture Electron Microscopy (FFEM) images of different microemulsions[123] (see Figure 4.2 for one example) show apparently completely disordered systems exhibiting a variety of microstructures. How is it possible to postulate 'an underlying thread of unity' in view of this obvious diversity?

This question may be answered by a principle proposed by William of Ockham in the 14th century: '*pluralitas non est ponenda sine necessitate*', which translates as 'entities should not be multiplied unnecessarily' and is commonly known as *Ockham's Razor*. This principle, which has been widely accepted in science since the beginnings of modern times, suggests to start investigating an unknown phenomenon by assuming a model being as simple as possible; only if this simple explanation has proven to fail, a more complicated model should be adopted. However, the aim of Ockham's principle is not to elucidate a phenomenon itself; it is merely meant to be a methodological strategy to establish an *applicable* model. In our case, this means that even if the structures of microemulsions are diverse, there may be one model which allows the prediction of properties for a number of these systems.

But there is some deeper reason to suppose 'an underlying thread of unity' in microemulsions. Simplicity as an ontological principle of nature has already been assumed in the natural philosophy of Ancient Greece. Let us think for example of the atomists Leucippus and Democritus ($\sim$ 460 - 400 B.C.) who posited – without any experimental evidence as a result of mere cogitation – that all sensory perceptions like *e.g.* 'sweet', 'bitter', 'warm', 'cold' or the different colours should originate from the same reason, the movement of atoms in a vacuum. About 2000 years later, at the beginnings of the 17th century, Johannes Kepler postulated in his First Law that planets moved on elliptic instead of epicyclic orbits. This meant the rejection of all astronomical principles valid at that time, which Kepler justified saying '*natura amat simplicitates*' ('nature loves simplicities'). Were these postulations of simplicity in nature not much more radical than the assumption of 'an underlying thread of unity' in microemulsions? In this context, it is certainly not unreasonable to assume a simple structure also behind the apparent disorder and diversity of microemulsion systems.

The challenge is to find appropriate tools for an in-depth investigation of the structure and dynamics of microemulsions, and it is the aim of the present study to contribute to this task. It seems to be a promising attempt, due to both the experimental technique and the microemulsion system chosen in this work.

Thanks to its sensitivity to collective modes of hydrogen bond systems and the reorientation of transient dipolar aggregates dielectric relaxation spectroscopy (DRS) is an excellent complement to classical spectroscopic techniques, like IR, Raman or NMR spectroscopy, which basically are only able to monitor molecular dynamics and short-range interactions. In contrast, DRS sheds some light on the dynamics of cooperative processes and on the structural consequences arising from that. This method appears to be particularly suitable for the investigation of microemulsions as it already revealed some characteristic relaxation processes caused by hydrate water molecules surrounding hydrophobic[43,190] and hydrophilic[185] ions and micelles of various cationic[7,8] and anionic[88] surfactants. Micelle-specific relaxation processes should also be detected.[169] One of the merits of DRS is that it is able to monitor the *dynamics* of a system. This is very valuable for the present study given the scarcity of information available in the literature about dynamic properties of microemulsions. As Warr points out, 'although much is not known about the structure of microemulsions, their dynamics have been less well studied.'[194]

Up to now, only few DRS studies of microemulsion systems have been performed, and most of them were suffering from a limited frequency range.[201] However, thanks to the waveguide interferometers available in the Regensburg laboratories covering a frequency range up to 89 GHz, the present work is one of the very first DRS investigations of microemulsions that extends to the water relaxation area. This is very important as the properties of water under confinement are one of the most exciting features microemulsions exhibit. Thus, DRS can provide a valuable contribution to the characterization of the microemulsion system didodecyldimethylammonium bromide / water / *n*-dodecane (DDAB/W/D) microemulsion, which has previously been investigated by NMR self-diffusion,[26,89,176,177] small-angle X-ray scattering (SAXS),[11] conductivity,[51,137] viscosimetry,[51] interfacial tension,[1] rheological,[194]flow and electric birefringence measurements[137] and FFEM images.[123]

The system chosen for this study, DDAB/W/D, forms a homogeneous water-in-oil microemulsion over wide areas of its phase diagram at room temperature and appears to be particularly suitable for investigation. Unlike most microemulsions which require alcohol or another co-surfactant as an additional constituent, DDAB/W/D is a three-component system and thus much easier to manipulate, from both the experimental and theoretical points of view.[3] Additionally, as the surfactant DDAB is a double-chained tetraalkylammonium halide and hence very sparingly soluble in both water and oil, its position within the microemulsion can be well predicted. DDAB has to reside at the oil-water-interface, whereas other surfactants like *e.g.* AOT (sodium bis(2-ethylhexyl) sulfosuccinate) partition between oil and water in a complex manner.[89] Besides, it should be noted that DDAB/W/D microemulsions are not a mere model system which is only of interest because of its structural simplicity. In contrast, DDAB/W/D is widely used as a medium for electrochemical reactions.[121,126,200,202,203]

Although DDAB/W/D may seem to be a relatively simple microemulsion system, it exhibits a perplexing behaviour upon the addition of electrolytes. Sjöblom *et al.* report that replacing pure water by extremely weakly concentrated aqueous solutions of sodium bromide or sodium sulfate ($1 \lesssim c/\mathrm{mM} \lesssim 27$ for NaBr) leads to a dramatic shrinking of the microemulsion phase.[175] The reason for this *co-ion effect* is still obscure; as the bromide concentration in the solution remains virtually constant at such a tiny electrolyte addition, it is obviously due to a cationic effect. Elucidating this phenomenon would certainly mean a major step towards an understanding of this system, of the co-ion influence on ionic microemulsions and of polyelectrolyte solutions in general.

Accordingly, the present work will be subdivided into two parts. First, the system DDAB/W/D will be thoroughly investigated over the entire microemulsion phase, L_2, putting a special emphasis on the properties of water under confinement. In a next step, the influence of different univalent co-ions, namely lithium, sodium, caesium and tetramethylammonium, on the relaxation behaviour of DDAB/W/D microemulsions will be compared.

Gerhard Ertl, who was awarded the Nobel Prize in chemistry this year, recently said that his field of interest, the chemistry of solid interfaces, had been transformed from 'alchemy to exact science.' For the chemistry of the liquid interfaces observed in microemulsions, this transformation is still to be completed. Maybe the present work could act as a little piece of catalyst in this process.

Chapter 1

Fundamentals

1.1 Principles of Electrodynamics

1.1.1 Maxwell and Constitutive Equations

Interactions between electromagnetic fields and matter are described by the four Maxwell equations:[98,179]

$$\vec{\mathrm{rot}}\,\vec{H} = \vec{j} + \frac{\partial}{\partial t}\vec{D} \tag{1.1}$$

$$\vec{\mathrm{rot}}\,\vec{E} = -\frac{\partial}{\partial t}\vec{B} \tag{1.2}$$

$$\mathrm{div}\,\vec{D} = \rho_{\mathrm{el}} \tag{1.3}$$

$$\mathrm{div}\,\vec{B} = 0 \tag{1.4}$$

These principles, which are based on empirical experience and should be regarded as axioms, point out the interrelations between the magnetic field strength $\vec{H}$, the current density $\vec{j}$, the electric induction $\vec{D}$, the electric field strength $\vec{E}$, the magnetic induction $\vec{B}$ and the electric charge density ρ_{el}. Together with Newton's equation of motion

$$m\frac{\partial^2}{\partial t^2}\vec{r} = q(\vec{E} + \vec{v} \times \vec{B}) \tag{1.5}$$

where q denotes a moving charge and $\vec{v}$ its velocity, the Maxwell equations form a complete set of partial differential equations.

For the static case, eq. (1.1) is identical to Ampère's law of magnetomotive force, saying that magnetic fields are created by an Ohmic current of density $\vec{j} = \kappa\vec{E}$ and a displacement current of density $\frac{\partial\vec{D}}{\partial t}$, with closed electric flux lines orbiting the currents.

The temporal changing of the magnetic induction $\vec{B}$ is linked to the surrounding electric field $\vec{E}$ by eq. (1.2), Faraday's law of induction.

Eq. (1.3), Gauß's law, defines electric charges to be the sources of the electric field, whereas eq. (1.4) establishes the solenoidality of the magnetic field.

The force action of electromagnetic fields can be calculated with the help of eq. (1.5).

For homogeneous, non-dispersive, isotropic materials, this set of equations is supplemented by the three constitutive equations

$$\vec{D} = \varepsilon\varepsilon_0\vec{E} \tag{1.6}$$

$$\vec{j} = \kappa\vec{E} \tag{1.7}$$

$$\vec{B} = \mu\mu_0\vec{H} \tag{1.8}$$

defining the relative electrical permittivity ε, the specific conductivity κ and the relative magnetic permeability μ, where ε_0 and μ_0 are the absolute permittivity and permeability of free space, respectively.

Together with the Maxwell equations these three constitutive equations allow a complete characterization of the interactions between an electromagnetic field and any medium.

1.1.2 The Electric Displacement Field

Let us consider now the dynamic case of an electric field $\vec{E}$ oscillating harmonically with the amplitude $\vec{E}_0$ and the angular frequency $\omega = 2\pi\nu$:

$$\vec{E}(t) = \vec{E}_0\cos(\omega t) \tag{1.9}$$

Due to their inertia, dipoles will only be able to follow the electric field instantaneously if it does not exceed a certain frequency, which is determined by the material and the temperature; typical values for liquids range between 1 MHz and 1 GHz.[14] For higher frequencies, a frequency-dependent phase delay, $\delta(\omega)$, is observed between the electric field and the electric displacement field so that:

$$\vec{D}(t) = \vec{D}_0\cos(\omega t - \delta(\omega)) \tag{1.10}$$

Splitting this equation according to the addition theorem of the cosine function

$$\vec{D}(t) = \vec{D}_0\cos(\delta(\omega))\cos(\omega t) + \vec{D}_0\sin(\delta(\omega))\sin(\omega t) \tag{1.11}$$

and introducing – in the style of the material equation (1.6) – the relations

$$\vec{D}_0\cos(\delta(\omega)) = \varepsilon'(\omega)\varepsilon_0\vec{E}_0 \tag{1.12}$$

$$\vec{D}_0\sin(\delta(\omega)) = \varepsilon''(\omega)\varepsilon_0\vec{E}_0 \tag{1.13}$$

the electric displacement field can be expressed as follows:

$$\vec{D}(t) = \varepsilon'(\omega)\varepsilon_0\vec{E}_0\cos(\omega t) + \varepsilon''(\omega)\varepsilon_0\vec{E}_0\sin(\omega t) \tag{1.14}$$

Unlike in the electrostatic case, the relation between $\vec{D}(t)$ and $\vec{E}(t)$ is no longer described by the amplitude $\vec{D}_0$ and the phase shift $\delta(\omega)$, but by the real part, ε', and the imaginary part, ε'', of the frequency-dependent complex permittivity. Their connection to the phase shift is given by equation (1.15):

$$\tan(\delta(\omega)) = \frac{\varepsilon''(\omega)}{\varepsilon'(\omega)} \tag{1.15}$$

Thus, the dielectric displacement field as given by equation (1.14) is composed of a dispersive part $\varepsilon'(\omega)\varepsilon_0\vec{E}_0\cos(\omega t)$ and a dissipative part $\varepsilon''(\omega)\varepsilon_0\vec{E}_0\sin(\omega t)$, the latter being phase-shifted by $\pi/2$ with respect to the driving electric field.

To describe the frequency-dependent energy absorption per units of time and volume we can state for non-conducting systems:

$$\frac{\partial W}{\partial t} = \frac{\omega}{2}\varepsilon''(\omega)\varepsilon_0 E_0^2 = \frac{\omega}{2}E_0 D_0 \sin(\delta(\omega)) \tag{1.16}$$

Mathematical treatment of this issue can be simplified by expressing the field vectors $\vec{E}(t)$ and $\vec{D}(t)$ as exponential functions using complex numbers:

$$\hat{\vec{E}}(t) = \vec{E}_0\cos(\omega t) + \mathrm{i}\vec{E}_0\sin(\omega t) = \vec{E}_0\exp(\mathrm{i}\omega t) \tag{1.17}$$

$$\hat{\vec{D}}(t) = \vec{D}_0\cos(\omega t - \delta) + \mathrm{i}\vec{D}_0\sin(\omega t - \delta) = \vec{D}_0\exp[\mathrm{i}(\omega t - \delta)] \tag{1.18}$$

The real parts of these complex vectors describe the physically measurable, time-depending instantaneous values of the electric field $\vec{E}(t)$ and the electric displacement field $\vec{D}(t)$.

Now, also the constitutive equations (1.6) to (1.8) have to be expressed using real and imaginary parts:[27]

$$\hat{\vec{D}}(t) = \hat{\varepsilon}(\omega)\varepsilon_0\hat{\vec{E}}(t) \tag{1.19}$$

$$\hat{\vec{j}}(t) = \hat{\kappa}(\omega)\hat{\vec{E}}(t) \tag{1.20}$$

$$\hat{\vec{B}}(t) = \hat{\mu}(\omega)\mu_0\hat{\vec{H}}(t) \tag{1.21}$$

The complex permittivity can be obtained comparing eq. (1.19) to eq. (1.14):

$$\hat{\varepsilon}(\omega) = \varepsilon'(\omega) - \mathrm{i}\varepsilon''(\omega) \tag{1.22}$$

Analogous relations hold for the complex specific conductivity $\hat{\kappa}$ and the complex relative permittivity $\hat{\mu}$.

Thus, the constitutive equations in their complex version according to eq. (1.19) to (1.21) extend the description of interactions between electromagnetic fields of any frequency and homogeneous, isotropic bodies to dissipative systems.[27]

1.1.3 Wave Equations

In the case of harmonically oscillating electromagnetic fields,

$$\hat{\vec{E}}(t) = \vec{E}_0\cos(\mathrm{i}\omega t) \tag{1.23}$$

$$\hat{\vec{H}}(t) = \vec{H}_0\cos(\mathrm{i}\omega t) \tag{1.24}$$

Maxwell equation (1.1) can be transformed using the complex constitutive equations (1.19) to (1.21) into:

$$\vec{\mathrm{rot}}\,\vec{H}_0 = (\hat{\kappa}(\omega) + \mathrm{i}\omega\hat{\varepsilon}(\omega)\varepsilon_0)\vec{E}_0 \tag{1.25}$$

Similarly, eq. (1.2) yields:

$$\vec{\mathrm{rot}}\,\vec{E}_0 = -\mathrm{i}\omega\hat{\mu}(\omega)\mu_0\vec{H}_0 \tag{1.26}$$

Applying the rotation operator to eq. (1.25) and taking into account eq. (1.26) and the Legendre vectorial identity

$$\vec{\mathrm{rot}}\,\vec{\mathrm{rot}}\,\vec{H}_0 = \vec{\mathrm{grad}}\,\mathrm{div}\,\vec{H}_0 - \Delta\vec{H}_0 = \vec{\mathrm{grad}}\,(0) - \Delta\vec{H}_0 = -\Delta\vec{H}_0 \tag{1.27}$$

the reduced wave equation of the magnetic field is obtained

$$\Delta\vec{H}_0 + \hat{k}^2\vec{H}_0 = 0 \tag{1.28}$$

for homogeneous, isotropic media with the complex propagation constant $\hat{k}$; the latter is given by

$$\hat{k}^2 = k_0^2\left(\hat{\mu}(\omega)\hat{\varepsilon}(\omega) + \frac{\hat{\mu}(\omega)\hat{\kappa}(\omega)}{\mathrm{i}\omega\varepsilon_0}\right) \tag{1.29}$$

$$k_0 = \omega\sqrt{\varepsilon_0\mu_0} = \frac{2\pi}{\lambda_0} \tag{1.30}$$

$$c_0 = \frac{1}{\sqrt{\varepsilon_0\mu_0}} \tag{1.31}$$

where c_0 is the vacuum speed of light and λ_0 is the length of a monochromatic wave in vacuum.

In the case of a solenoidal medium ($\mathrm{div}\,\vec{E} = 0$) a reduced wave equation for $\vec{E}$ can be obtained accordingly:

$$\Delta\hat{\vec{E}}_0 + \hat{k}^2\hat{\vec{E}}_0 = 0 \tag{1.32}$$

For non-magnetisable matter ($\hat{\mu} = 1$) the complex propagation constant (1.29) is simplified as follows:

$$\hat{k}^2 = k_0^2\left(\hat{\varepsilon}(\omega) + \frac{\hat{\kappa}(\omega)}{\mathrm{i}\omega\varepsilon_0}\right) \equiv k_0^2\hat{\eta}(\omega) \tag{1.33}$$

Here, the generalised complex permittivity $\hat{\eta} = \eta' - \mathrm{i}\eta''$ is introduced. Its real part is given by

$$\eta'(\omega) = \varepsilon'(\omega) - \frac{\kappa''(\omega)}{\omega\varepsilon_0} \tag{1.34}$$

and its imaginary part by

$$\eta''(\omega) = \varepsilon''(\omega) + \frac{\kappa'(\omega)}{\omega\varepsilon_0} \tag{1.35}$$

Eqs. (1.33) to (1.35) point out that dielectric properties and those effects which are due to the conductivity of a system cannot be determined independently.

According to the classical theory by Debye and Falkenhagen there is some dispersion of the complex specific conductivity $\hat{\kappa}$ of electrolyte solutions, which is thought to be caused by the relaxation of the ion cloud.[82] However, from the experimental point of view, this effect is negligible[93] in the microwave frequency range so that we can assume

$$\kappa'(\omega) = \kappa \tag{1.36}$$

and

$$\kappa''(\omega) = 0 \tag{1.37}$$

Hence, the real and the imaginary parts of the complex permittivity are given by

$$\varepsilon'(\omega) = \eta'(\omega) \tag{1.38}$$

and

$$\varepsilon''(\omega) = \eta''(\omega) - \frac{\kappa}{\omega\varepsilon_0} \tag{1.39}$$

On the basis of these equations ε' and ε'' can be calculated from the experimentally accessible quantities η', η'' and κ. The only approximations implied are the neglect of conductivity dispersion and of magnetic loss.

1.2 Dielectric Relaxation

1.2.1 Polarisation

The dielectric displacement field $\hat{\vec{D}}$ can be split into two contributions

$$\hat{\vec{D}} = \hat{\varepsilon}\varepsilon_0\hat{\vec{E}} = \varepsilon_0\hat{\vec{E}} + \hat{\vec{P}} \tag{1.40}$$

with

$$\hat{\vec{P}} = (\hat{\varepsilon} - 1)\varepsilon_0\hat{\vec{E}} \tag{1.41}$$

The term $\varepsilon_0\hat{\vec{E}}$ is independent of the medium, whereas polarisation $\hat{\vec{P}}$ describes the influence of matter on an electric field. Beside this macroscopic definition polarisation can also be interpreted microscopically[27]

$$\hat{\vec{P}} = \hat{\vec{P}}_\mu + \hat{\vec{P}}_\alpha \tag{1.42}$$

as the sum of orientational polarisation

$$\hat{\vec{P}}_\mu = \sum_k \rho_k \langle\vec{\mu}_k\rangle \tag{1.43}$$

and induced polarisation

$$\hat{\vec{P}}_\alpha = \sum_k \rho_k \alpha_k (\hat{\vec{E}}_i)_k \tag{1.44}$$

Here, ρ_k is the density of particles of species k, $\langle\vec{\mu}_k\rangle$ the average dipole moment as obtained by the Langevin theory taking into account all particle orientations, α_k the polarisability and $(\vec{E}_i)_k$ the internal field that is effective at the position of the particle.

Combining eqs. (1.41) and (1.42) gives us the opportunity to establish a link between the experimentally accessible macroscopic quantity polarisation and molecular processes.

Orientational polarisation arises by partial alignment of the permanent dipoles in the electric field; it is countered by the thermal motion of the molecules. For 'simple' dipolar liquids, dipole reorientation takes place on a pico- to nanosecond timescale, corresponding to frequencies in the microwave range. Due to strong coupling effects to the surroundings of the molecules, which may vary considerably, broad bands are observed for relaxation processes in the condensed phase. For (micro-)heterogeneous systems, additional relaxation processes occur, that will be discussed in section 1.5.

The induced polarisation $\hat{\vec{P}}_\alpha$ is composed of two contributions, namely atomic polarisation and electron polarisation. The atomic polarisation is due to the relative shift of the core positions; absorptions arising from it are situated in the infrared region and investigated by molecular vibration spectroscopy. In contrast, the electron polarisation is caused by a shift of the electron sheath density relative to the core. This corresponds to electronic transitions evoking absorptions in the UV/vis part of the spectrum.

Both vibration and electronic transitions occur between discrete energy levels so that sharp absorption bands should be expected.[15]

The timescales of orientational and induced polarisation being significantly different, these two contributions can be separated on the frequency scale and regarded to be linearly independent of each other:[17]

$$\hat{\vec{P}}_\mu = \varepsilon_0(\hat{\varepsilon} - \varepsilon_\infty)\hat{\vec{E}} \tag{1.45}$$

$$\hat{\vec{P}}_\alpha = \varepsilon_0(\varepsilon_\infty - 1)\hat{\vec{E}} \tag{1.46}$$

Situated in the far-infrared, ε_∞ denotes the permittivity after the decay of orientational polarisation, whereas the contribution arising from induced polarisation still remains unchanged. In practice, the limiting value of the permittivity for infinite frequencies as obtained in the microwave range is taken for ε_∞.[15]

1.2.2 Response Function of the Orientational Polarisation

For sufficiently fast variations of the electric field the polarisation does not attain its maximum value any more, as the molecular dipoles are no longer able to follow the field variation without any delay. In this case the relation between $\hat{\vec{E}}$ and $\hat{\vec{P}}$ is given by the response function.

As a prerequisite, we have to assume the principle of superposition for the medium concerned: when a field $\vec{E}_1$ creates a polarisation $\vec{P}_1$ and a field $\vec{E}_2$ a polarisation $\vec{P}_2$, then a field $\vec{E}_1 + \vec{E}_2$ will create a polarisation $\vec{P}_1 + \vec{P}_2$.

To derive the response function, let us consider the following thought experiment. A field $\vec{E}$, evoking a polarisation $\vec{P}$ in the dielectric, is cut off at the time $t = 0$. As the contribution coming from induced polarisation disappears without any delay, the remaining polarisation is expressed as:

$$\hat{\vec{P}}_\mu(t) = \hat{\vec{P}}_\mu(0) \cdot F_P^{\mathrm{or}}(t) \quad \text{with} \quad F_P^{\mathrm{or}}(0) = 1, \quad F_P^{\mathrm{or}}(\infty) = 0 \tag{1.47}$$

The step response function $F_P^{\mathrm{or}}(t)$ of the orientational polarisation is defined as:

$$F_P^{\mathrm{or}}(t) = \frac{\langle \vec{P}_\mu(0) \cdot \vec{P}_\mu(t) \rangle}{\langle \vec{P}_\mu(0) \cdot \vec{P}_\mu(0) \rangle} \tag{1.48}$$

It is a measure of the fraction of the orientational polarisation effective at the time $t = 0$ that is still remaining at time t after the cut-off of the field. One of the methods used in this work, Time Domain Reflectometry (TDR), is based on this principle, making the step response function directly experimentally accessible.

Any time-dependent electric field can be described by a sequence of an infinite number of differential square pulses.[110] In particular, for harmonically oscillating electromagnetic fields of the type

$$\hat{\vec{E}}(t) = \hat{\vec{E}}_0 \exp(-\mathrm{i}\omega t) \tag{1.49}$$

the polarisation at any time t can be expressed as:

$$\hat{\vec{P}}_\mu(\omega, t) = \varepsilon_0(\varepsilon - \varepsilon_\infty)\hat{\vec{E}}(t) \int_0^\infty \exp(-\mathrm{i}\omega t') f_P^{\mathrm{or}}(t')\mathrm{d}t' \tag{1.50}$$

Here,

$$\int_0^\infty \exp(-\mathrm{i}\omega t') f_P^{\mathrm{or}}(t')\mathrm{d}t' = \mathcal{L}_{\mathrm{i}\omega}[f_P^{\mathrm{or}}(t')] \tag{1.51}$$

is the Laplace-transformed pulse response function of the orientational polarisation, which in turn is the negative derivative of the normalised step response function with time:

$$f_P^{\mathrm{or}}(t') = -\frac{\partial F_P^{\mathrm{or}}(t - t')}{\partial(t - t')} \tag{1.52}$$

The pulse response function is normalised according to:

$$\int_0^\infty f_P^{\mathrm{or}}(t')\mathrm{d}t' = 1 \tag{1.53}$$

Taking into account eq. (1.51) the interrelation between the complex permittivity and the pulse response function becomes evident from the two eqs. (1.45) and (1.50) describing the orientational polarisation:[27]

$$\hat{\varepsilon}(\omega) = \varepsilon'(\omega) - \mathrm{i}\varepsilon''(\omega) = \varepsilon_\infty + (\varepsilon - \varepsilon_\infty) \cdot \mathcal{L}_{\mathrm{i}\omega}[f_P^{\mathrm{or}}(t')] \tag{1.54}$$

Plotting of ε' as a function of $\ln(\omega)$ yields the dispersion curve, whereas a plot of ε'' as a function of $\ln(\omega)$ leads to the absorption curve. The real part $\varepsilon'(\omega)$ is a measure of the distortion of the amplitude compared to the static case; the imaginary part $\varepsilon''(\omega)$ describes the extent of the energy absorption of the electromagnetic field by the dielectric.

1.3 Empirical Relaxation Models

Numerous empirical and semi-empirical equations are proposed in the literature to describe dielectric relaxation. For a system where more than one relaxation process is observed dielectric properties can be described in most cases with the help of a suitable linear combination of single processes.

1.3.1 The Debye Equation

A first approach for the description of relaxation processes was made by Debye. He assumed the decrease of orientational polarisation after the cut-off of an external electric field to be proportional to the orientational polarisation itself.[156] This corresponds to a first-order time law:

$$\frac{\partial}{\partial t}\vec{P}_\mu(t) = -\frac{1}{\tau}\vec{P}_\mu(t) \tag{1.55}$$

τ represents the relaxation time, which describes the dynamics of the process. Comparing the solution of this homogeneous differential equation of first order

$$\vec{P}_\mu(t) = \vec{P}_\mu(0)\exp\left(-\frac{t}{\tau}\right) \tag{1.56}$$

to eq. (1.47) yields the step response function:

$$F_P^{\mathrm{or}}(t) = \exp\left(-\frac{t}{\tau}\right) \tag{1.57}$$

According to eq. (1.52) this leads to the pulse response function:

$$f_P^{\mathrm{or}}(t) = \frac{1}{\tau}\exp\left(-\frac{t}{\tau}\right) \tag{1.58}$$

Eq. (1.54) allows determination of the complex permittivity by Fourier transformation of the pulse response function:

$$\hat{\varepsilon}(\omega) = \varepsilon_\infty + (\varepsilon - \varepsilon_\infty)\cdot\mathcal{L}_{\mathrm{i}\omega}\left[\frac{1}{\tau}\exp\left(-\frac{t}{\tau}\right)\right] \tag{1.59}$$

Following the definition of the Laplace transformation

$$\mathcal{L}_s\left[\exp(ax)\right] = \frac{1}{s-a} \tag{1.60}$$

the Debye equation can be obtained immediately from eq. (1.59):[70]

$$\hat{\varepsilon}(\omega) = \varepsilon_\infty + \frac{\varepsilon - \varepsilon_\infty}{1 + \mathrm{i}\omega\tau} \tag{1.61}$$

Splitting into real and imaginary part yields:

$$\varepsilon'(\omega) = \varepsilon_\infty + \frac{\varepsilon - \varepsilon_\infty}{1 + \omega^2\tau^2} \tag{1.62}$$

$$\varepsilon''(\omega) = \omega\tau\frac{\varepsilon - \varepsilon_\infty}{1 + \omega^2\tau^2} \tag{1.63}$$

When the Debye equation applies the dispersion curve, plotted as $\varepsilon' = \varepsilon'(\ln(\omega))$, yields a monotonically decreasing, point-symmetric function, the inflexion point indicating the relaxation time; the absorption curve $\varepsilon'' = \varepsilon''(\ln(\omega))$ yields an axis-symmetric band reaching its maximum at $\omega = 1/\tau$.

1.3.2 Relaxation Time Distributions

For a large number of condensed systems the Debye equation, based on the assumption of *one* relaxation time, is unable to provide a satisfying description. In these cases, a continuous distribution $g(\tau)$ of relaxation times is used instead; for practical reasons logarithmic distributions $G(\ln\tau)$ are applied. Again, it is assumed that the dispersion step observed is due to only *one* relaxation process. The complex permittivity can be expressed as

$$\hat{\varepsilon}(\omega) = \varepsilon_\infty + (\varepsilon - \varepsilon_\infty)\int_0^\infty \frac{G(\ln\tau')}{(1 + \mathrm{i}\omega\tau')}\mathrm{d}\ln\tau' \tag{1.64}$$

with the normalisation

$$\int_0^\infty G(\ln\tau')\mathrm{d}\ln\tau' = 1 \tag{1.65}$$

The Debye equation only provides one relaxation time, *i.e.* a relaxation time distribution in the form of the Dirac delta function. Some of the common empirical equations yielding relaxation time distributions will be presented in the following section.

The Cole-Cole Equation

Introducing the empirical parameter $\alpha \in [0..1[$ into the Debye equation yields the Cole-Cole equation:[56,57]

$$\hat{\varepsilon}(\omega) = \varepsilon_\infty + \frac{\varepsilon - \varepsilon_\infty}{1 + (\mathrm{i}\omega\tau_0)^{1-\alpha}} \tag{1.66}$$

It is based on a symmetric relaxation time distribution around the centre of gravity τ_0, describing symmetric dispersion and absorption curves. Compared to the Debye equation, the dispersion curves are flattened and the absorption curves are both flattened and broadened. For $\alpha = 0$ the Cole-Cole equation becomes equivalent to the Debye equation.

The Cole-Davidson Equation

The Cole-Davidson equation,[68,69] containing the empirical parameter $\beta \in]0..1]$, is based on an asymmetric distribution of relaxation times around the centre of gravity τ_0

$$\hat{\varepsilon}(\omega) = \varepsilon_\infty + \frac{\varepsilon - \varepsilon_\infty}{(1 + \mathrm{i}\omega\tau_0)^\beta} \tag{1.67}$$

and is appropriate for the description of asymmetric dispersion and absorption curves. For $\beta = 1$ this equation is identical to the Debye equation.

The Havriliak-Negami equation

The Havriliak-Negami equation allows description of broad, asymmetric relaxation time distributions. It is obtained by applying both empirical parameters $\alpha \in [0..1[$ and $\beta \in]0..1]$ simultaneously to correct the Debye equation:[108]

$$\hat{\varepsilon}(\omega) = \varepsilon_\infty + \frac{\varepsilon - \varepsilon_\infty}{(1 + (\mathrm{i}\omega\tau_0)^{1-\alpha})^\beta} \tag{1.68}$$

For $\alpha = 0$ and $\beta = 1$ the Havriliak-Negami equation becomes equivalent to the Debye equation.

1.3.3 Superposition of Several Relaxation Processes

When an overall relaxation process is composed of several single processes it is impossible to explain the relaxation behaviour by *one* of the equations described above. In these cases, complex permittivity is described by a superposition of n single processes

$$\hat{\varepsilon}(\omega) = \varepsilon_\infty + \sum_{k=1}^{n} (\varepsilon_k - \varepsilon_{\infty,k}) \int_0^\infty \frac{G_k(\ln \tau_k')}{1 + \mathrm{i}\omega\tau_k'} \mathrm{d} \ln \tau_k' \tag{1.69}$$

taking into account

$$\varepsilon - \varepsilon_\infty = \sum_{k=1}^{n} (\varepsilon_k - \varepsilon_{\infty,k}) = \sum_{k=1}^{n} S_k \tag{1.70}$$

$$\varepsilon_{\infty,k} = \varepsilon_{k+1} \tag{1.71}$$

The single processes are treated as linearly independent from each other. Each of them possesses its own relaxation time distribution and dispersion amplitude S_k.

1.4 Microscopic Relaxation Models

In the preceding sections, dielectric relaxation has been discussed on the microscopic scale without considering the molecular structure of liquids. Hence, let us continue with a short discussion of some models establishing a link between the microscopic and the macroscopic level.

1.4.1 The Onsager Equation

Early models for the description of dipole orientation are based on a continuum ansatz. Following this approach, a single molecule, which is exposed to an electric field, is embedded in – and interacting with – a continuum characterized by the macroscopic properties of the system. Therefore, specific interactions between single particles are not taken into account.

It was on the basis of this approach that Onsager developed the following relation for the interpretation of dielectric data:[27,150]

$$\varepsilon_0(\varepsilon-1)\vec{E} = \vec{E}_\mathrm{h} \cdot \sum_i \frac{\rho_i}{1-\alpha_i f_i}\left(\alpha_i + \frac{1}{3\mathrm{k_B}\,T}\cdot\frac{\mu_{\mathrm{eff},i}^2}{1-\alpha_i f_i}\right) \tag{1.72}$$

Here ρ_i represents the particle density, α_i the polarisability of the continuum, f_i the reaction field factor and $\mu_{\mathrm{eff},i}$ the effective dipole moment of species i.

For the cavity field $\vec{E}_\mathrm{h}$ assuming a spherical cave the following relation applies in a dielectric of permittivity ε:

$$\vec{E}_\mathrm{h} = \frac{3\varepsilon}{2\varepsilon+1}\vec{E} \tag{1.73}$$

Inserting equation (1.73) into equation (1.72) yields the Onsager equation for a system of i components:

$$\frac{(\varepsilon-1)(2\varepsilon+1)\varepsilon_0}{3\varepsilon} = \sum_i \frac{\rho_i}{1-\alpha_i f_i}\left(\alpha_i + \frac{1}{3\mathrm{k_B}\,T}\cdot\frac{\mu_{\mathrm{eff},i}^2}{1-\alpha_i f_i}\right) \tag{1.74}$$

In the case of a single-component dipolar liquid, exhibiting only one dispersion step in the dielectric spectrum, this relation is simplified to:

$$\frac{(\varepsilon-\varepsilon_\infty)(2\varepsilon+\varepsilon_\infty)}{\varepsilon(\varepsilon_\infty+2)^2} = \frac{\rho\mu_\mathrm{eff}^2}{9\varepsilon_0\mathrm{k_B}\,T} \tag{1.75}$$

1.4.2 The Cavell Equation

The Cavell equation represents an extension of the Onsager equation to systems exhibiting several dispersion steps, k. Thus, the following relation can be obtained from eq. (1.74) for spherical particles:[48]

$$\frac{2\varepsilon+1}{\varepsilon}\cdot(\varepsilon_k-\varepsilon_{\infty,k}) = \frac{\mathrm{N_A}\,c_k}{\mathrm{k_B}\,T\varepsilon_0}\cdot\frac{\mu_{\mathrm{eff},k}^2}{(1-f_k\alpha_k)^2} \tag{1.76}$$

Here, f_k represents the reaction field factor for a spherical cavity of radius a_k:[27]

$$f_k = \frac{1}{4\pi\varepsilon_0 a_k^3}\cdot\frac{2\varepsilon-2}{2\varepsilon+1} \tag{1.77}$$

In the form given below

$$c_{k,i} = \frac{(\varepsilon_k - \varepsilon_{\infty,k})\varepsilon_0(2\varepsilon+1)}{\varepsilon} \cdot \frac{(1-\alpha_k f_k)^2}{\mu_k^2} \cdot \frac{\mathrm{k_B}\,T}{\mathrm{N_A}} \tag{1.78}$$

this equation is used for the evaluation of dispersion amplitudes.

The assumption of spherical particles is often quite a rough estimate. For a large number of molecules, an ellipsoid of semi-axes $a_k > b_k > c_k$ provides a much better description. In this case, the following relation can be deduced from eq. (1.72):[20,27]

$$\frac{\varepsilon + A_k(1-\varepsilon)}{\varepsilon} \cdot S_k = \frac{\mathrm{N_A}\,c_k}{3\mathrm{k_B}\,T\varepsilon_0} \cdot \frac{\mu_{\mathrm{eff},k}^2}{(1-f_k\alpha_k)^2} \tag{1.79}$$

Eq. (1.79) establishes a link between the dispersion amplitude S_k and concentration c_k and the effective dipole moment $\mu_{\mathrm{eff},k}$ of a relaxing particle k. In this context, α_k represents the polarisability, f_k the reaction field factor and A_k a parameter describing deviations from spherical shape. For ellipsoidal particles, the following relations apply:[165]

$$f_k = \frac{3}{4\pi\varepsilon_0 a_k b_k c_k} \cdot \frac{A_k(1-A_k)(\varepsilon-1)}{\varepsilon + (1-\varepsilon)A_k} \tag{1.80}$$

and

$$A_k = \frac{a_k b_k c_k}{2} \int_0^\infty \frac{\mathrm{d}s}{(s+a_k^2)^{3/2}(s+b_k^2)^{1/2}(s+c_k^2)^{1/2}} \tag{1.81}$$

For the special case of a prolate rotational ellipsoid of semi-axes a_i and $b_i = c_i$, which can be used for the description of ion pairs, the following analytical solution is given by Scholte:[165]

$$A_k = -\frac{1}{p_k^2-1} + \frac{p_k}{(p_k^2-1)^{1.5}} \ln\left(p_k + \sqrt{p_k^2-1}\right), \qquad p_k = \frac{a_k}{b_k} \tag{1.82}$$

1.4.3 The Kirkwood-Fröhlich Equation

With the help of statistical mechanics macroscopic quantities can be calculated from molecular properties and intermolecular interactions. Thus, it is possible to extend Onsager's approach to interacting particles. Following this idea Kirkwood[129] and Fröhlich[91] succeeded in deducing an expression for a pure dipolar liquid which is very similar to the Onsager equation (1.72):

$$\frac{(\varepsilon-\varepsilon_\infty)(2\varepsilon+\varepsilon_\infty)}{\varepsilon(\varepsilon_\infty+2)^2} = \frac{\rho\mu_{\mathrm{eff}}^2}{9\varepsilon_0\mathrm{k_B}\,T} \cdot g \tag{1.83}$$

The difference from the Onsager equation consists in the additional factor g, the so-called Kirkwood factor, taking into account intermolecular interactions.

When the dipoles of two neighbouring molecules prefer parallel alignment relative to each other a value of $g > 1$ is observed, antiparallel dipole alignment yields $g < 1$, and statistical alignment $g = 1$.

1.4.4 The Debye Model of Rotational Diffusion

In the Debye model of rotational diffusion, a system is regarded to be an accumulation of rigid, spherical dipoles rotating freely in space. This leads to frequent uncorrelated collisions, changing the orientation of the affected dipoles. Therefore, this mechanism is called diffusion of dipolar orientation.[70]

With this model, Debye succeeded in interpreting Brownian motion in terms of the rotation of molecules. However, by doing this, he made use of a number of non-negligible approximations: dipole-dipole interactions and inertia effects are neglected, and the Lorentz field was used as the inner field. Thus, the dipolar correlation function $\gamma(t)$ is described by a microscopic relaxation time τ_s

$$\gamma(t) = \exp\left(-\frac{t}{\tau_\mathrm{s}}\right) \tag{1.84}$$

which can be expressed as a function of the friction factor ζ:

$$\tau_\mathrm{s} = \frac{\zeta}{2\mathrm{k_B}\,T} \tag{1.85}$$

Assuming the hydrodynamical laws – determining the rotation of a sphere in a viscous medium – are valid the Stokes-Debye-Einstein equation is obtained

$$\tau_\mathrm{s} = \frac{3V\eta'}{\mathrm{k_B}\,T} \tag{1.86}$$

where V represents the volume of the sphere and η' the dynamic viscosity of its environment, *i.e.* the microscopic viscosity. However, in most cases this microscopic viscosity deviates from the macroscopic viscosity, η. For example, the viscosity of water situated in the coordination sphere of solvated particles differs from the bulk-water value. To correct these differences, several additional parameters are introduced into eq. (1.86):[76]

$$\tau_\mathrm{s} = \frac{3V\eta}{\mathrm{k_B}\,T} f_\mathrm{stick} C + \tau_\mathrm{s}^0 \tag{1.87}$$

The shape factor, f_stick, accounts for deviations of the molecules from spherical shape; for a sphere with *stick* boundary conditions of rotational diffusion, $f_\mathrm{stick} = 1$. The macroscopic viscosity is corrected by the friction parameter C, yielding $C = 1$ for *stick* and $C = 1 - f_\mathrm{stick}^{-2/3}$ for *slip* boundary conditions. τ_s^0 is an empirical quantity that can be regarded as the correlation time of a free rotor.

1.4.5 Microscopic and Macroscopic Relaxation Time

The development of linear dissipative systems with time can be described by statistical mechanics if it is possible to transfer the macroscopic step response function to the microscopic level.[27]

The decay of orientational polarisation after the cut-off of an electric field is described by eq. (1.48), the macroscopic step response function. Note that the orientational polarisation $\vec{P}_\mu$ is the sum of all permanent molecular dipoles:

$$\vec{P}_\mu(t) = \frac{1}{V}\sum_{i=1}^{n}\vec{\mu}_i(t) \tag{1.88}$$

Inserting this macroscopic definition into eq. (1.48) yields the following relation for the step response function:

$$F_P^{\mathrm{or}}(t) = \frac{\langle\sum_i \vec{\mu}_i(0)\cdot\sum_i \vec{\mu}_i(t)\rangle}{\langle\sum_i \vec{\mu}_i(0)\cdot\sum_i \vec{\mu}_i(0)\rangle} \equiv \Phi(t) \tag{1.89}$$

This macroscopic function $\Phi(t)$ is called the autocorrelation function of orientational polarisation. It can be interpreted on a molecular level with the help of the dipole correlation function $\gamma(t)$. The latter measures the probability for the orientation of a dipole to be still effective at a time t after the cut-off of the external field at a time $t = 0$. $\Theta(t)$ is the angle covered by the particle until t:

$$\gamma(t) = \frac{\langle\vec{\mu}(0)\cdot\vec{\mu}(t)\rangle}{\langle\vec{\mu}(0)\cdot\vec{\mu}(0)\rangle} = \langle\cos\Theta(t)\rangle \tag{1.90}$$

If macroscopic and microscopic correlation function should merge, this means for the scalar product

$$\Big\langle\sum_i \vec{\mu}_i\cdot\sum_j \vec{\mu}_j\Big\rangle = \sum_i\sum_j \vec{\mu}_i\vec{\mu}_j = \sum_i \vec{\mu}_i^2 + \sum_{i\neq j}\vec{\mu}_i\vec{\mu}_j \tag{1.91}$$

that the sum of the cross terms

$$\sum_{i\neq j}\vec{\mu}_i\vec{\mu}_j = \sum_{i\neq j}|\vec{\mu}_i|\cdot|\vec{\mu}_j|\cdot\cos\Theta_{i,j} \tag{1.92}$$

should be equal to zero, *i.e.* no correlations between the dipoles and hence no intermolecular interactions should occur. This may be assumed, approximately, in the gas phase at low pressure; however, in condensed systems the motions of single particles and their orientations are linked together, so that macroscopic and microscopic correlation function are different from each other as a matter of principle.

Consequently, the experimentally available macroscopic relaxation times τ do not coincide with the microscopic relaxation times τ_s. However, if microwave measurements are to be interpreted on a molecular scale, it is essential to establish a link between these two quantities. Various approaches can be found in the literature that account for this problem.

Debye equates the internal field with the Lorentz field; thus, the following relation is obtained:[70]

$$\tau = \frac{\varepsilon + 2}{\varepsilon_\infty + 2} \cdot \tau_\mathrm{s} \tag{1.93}$$

However, this simplification is too strong for polar dielectrics. Hence, this equation may only be applied to apolar systems.

In the case of mere rotational diffusion the equation proposed by Powles and Glarum is regarded to be a reasonable approximation for the link between macroscopic and microscopic relaxation time:[96,161]

$$\tau = \frac{3\varepsilon}{2\varepsilon + \varepsilon_\infty} \cdot \tau_\mathrm{s} \tag{1.94}$$

A more general relation can be obtained by statistical mechanics in the framework of the *corresponding macro-micro correlation theorem*:[128,130,131]

$$\tau = \frac{3\varepsilon}{2\varepsilon + \varepsilon_\infty} \cdot \frac{g}{\dot{g}} \cdot \tau_\mathrm{s} \tag{1.95}$$

In this expression g represents the Kirkwood correlation factor and $\dot{g}$ the so-called dynamic correlation factor. For the limit $\dot{g} = g = 1$ eq. (1.95) reduces to the Powles-Glarum equation (1.94).

1.5 Heterogeneous Dielectrics

1.5.1 The Dielectric Sphere in a Medium

In the previous sections dielectric properties of homogeneous, molecular solutions have been discussed. However, the microemulsions investigated in this work – although macroscopically one-phase systems – consist of water droplets with a radius of approx. 2 to 15 nm, which are embedded in the medium *n*-dodecane. As these particles are much larger than single molecules and as their dielectric properties are completely different from those of the medium it is essential to interpret the results of this study in the framework of dielectric theory of heterogeneous media.

As the most trivial case of a heterogeneous dielectric, let us consider a spherical particle of permittivity ε_P and radius R that is embedded in an infinitely expanded medium of permittivity $\varepsilon_\mathrm{M} \neq \varepsilon_\mathrm{P}$.[27]

Assuming that no electric charges are present, neither in the sphere nor in the medium, the potential of both components follows the Laplace equation:

$$\Delta\Phi_\mathrm{P} = 0 \quad \text{and} \quad \Delta\Phi_\mathrm{M} = 0 \tag{1.96}$$

However, due to the differences in permittivity between the two components an apparent surface charge may occur at the interface. As a general solution of the Laplace equation

(1.96) the following expression is obtained using spherical coordinates (r, θ, φ) and setting the centre of the sphere as the origin and a z-axis parallel to the external field $\vec{E_0}$:

$$\Phi_{\mathrm{M}} = \sum_{n=0}^{\infty} \left[\left(A_n r^n + \frac{B_n}{r^{n+1}} \right) P_n(\cos(\theta)) \right] \tag{1.97}$$

$$\Phi_{\mathrm{P}} = \sum_{n=0}^{\infty} \left[\left(C_n r^n + \frac{D_n}{r^{n+1}} \right) P_n(\cos(\theta)) \right] \tag{1.98}$$

Note that $P_n(\cos(\theta))$ are Legendre polynomials. The following boundary conditions apply:

1. At a large distance from the sphere, the electric field $\vec{E}$ is equal to the external field $\vec{E_0}$, hence:

$$(\Phi_{\mathrm{M}})_{r \to \infty} = -E_0 z = -E_0 r \cos(\theta) \tag{1.99}$$

2. The potential Φ is continuous at the interface:

$$(\Phi_{\mathrm{M}})_{r=R} = (\Phi_{\mathrm{P}})_{r=R} \tag{1.100}$$

3. As the component of the electric displacement field $\vec{D}$ normal to a dielectric interface has to be continuous, the following relation applies:

$$\varepsilon_{\mathrm{M}} \left(\frac{\partial \Phi_{\mathrm{M}}}{\partial r} \right)_{r=R} = \varepsilon_{\mathrm{P}} \left(\frac{\partial \Phi_{\mathrm{P}}}{\partial r} \right)_{r=R} \tag{1.101}$$

4. In the centre of the sphere Φ_{P} may not become infinity.

Taking into account these boundary conditions the following equations are obtained for the potentials:

$$\Phi_{\mathrm{M}} = \left(\frac{\varepsilon_{\mathrm{P}} - \varepsilon_{\mathrm{M}}}{2\varepsilon_{\mathrm{M}} + \varepsilon_{\mathrm{P}}} \cdot \frac{R^3}{r^3} - 1 \right) \cdot E_0 z \tag{1.102}$$

$$\Phi_{\mathrm{P}} = -\frac{3\varepsilon_{\mathrm{M}}}{2\varepsilon_{\mathrm{M}} + \varepsilon_{\mathrm{P}}} \cdot E_0 z \tag{1.103}$$

These potentials can be split into two contributions: $\Phi = -E_0 z$ is the contribution created by the external field, whereas

$$\Phi'_{\mathrm{M}} = \frac{\varepsilon_{\mathrm{P}} - \varepsilon_{\mathrm{M}}}{2\varepsilon_{\mathrm{M}} + \varepsilon_{\mathrm{P}}} \cdot \frac{R^3}{r^3} \cdot E_0 z \tag{1.104}$$

$$\Phi'_{\mathrm{P}} = \frac{\varepsilon_{\mathrm{P}} - \varepsilon_{\mathrm{M}}}{2\varepsilon_{\mathrm{M}} + \varepsilon_{\mathrm{P}}} \cdot E_0 z \tag{1.105}$$

are caused by apparent surface charges on the dielectric interface. Note that eq. (1.104) is identical to the potential of a point dipole situated in the centre of a sphere embedded in vacuum, whose dipole moment

$$\vec{\mu} = \frac{\varepsilon_\mathrm{P} - \varepsilon_\mathrm{M}}{2\varepsilon_\mathrm{M} + \varepsilon_\mathrm{P}} \cdot R^3 \vec{E}_0 \tag{1.106}$$

is parallel to the z axis.

1.5.2 The Effective Static Permittivity in a Suspension of Spheres

Since we are now able to describe one dielectric sphere in a medium let us consider a system containing N spheres characterized by their radius R and permittivity ε_P embedded in a medium of permittivity ε_M. For convenience, we assume that all N spheres are situated in a spherical volume of radius R^* that again is embedded in a medium of permittivity ε_M.[27] Furthermore, for the sake of simplicity, it is assumed that the electric field is static or that both ε_P and ε_M are constant over the frequency range considered.

The Wiener Equation

Provided the interparticle distances are large enough so that dipolar and multipolar interactions can be neglected eq. (1.106) represents the contribution of an individual particle to the total dipole moment. Thus, the latter can be expressed as follows:

$$\vec{\mu} = N \cdot \frac{\varepsilon_\mathrm{P} - \varepsilon_\mathrm{M}}{2\varepsilon_\mathrm{M} + \varepsilon_\mathrm{P}} \cdot R^3 \vec{E}_0 \tag{1.107}$$

Consequently, the potential outside the considered sphere can be written analogously to eq. (1.102):

$$\Phi_\mathrm{M} = \left(N \cdot \frac{\varepsilon_\mathrm{P} - \varepsilon_\mathrm{M}}{2\varepsilon_\mathrm{M} + \varepsilon_\mathrm{P}} \cdot \frac{R^3}{r^3} - 1 \right) \cdot E_0 z \tag{1.108}$$

Ascribing an effective permittivity ε^* to the heterogeneous sphere of radius R^* the same potential can be expressed – again analogously to eq. (1.102) – by

$$\Phi_\mathrm{M} = \left(\frac{\varepsilon^* - \varepsilon_\mathrm{M}}{2\varepsilon_\mathrm{M} + \varepsilon^*} \cdot \frac{R^{*3}}{r^3} - 1 \right) \cdot E_0 z \tag{1.109}$$

Equating both expressions yields the following equation established by Wiener in 1912:[101]

$$\frac{\varepsilon^* - \varepsilon_\mathrm{M}}{2\varepsilon_\mathrm{M} + \varepsilon^*} = \phi \cdot \frac{\varepsilon_\mathrm{P} - \varepsilon_\mathrm{M}}{2\varepsilon_\mathrm{M} + \varepsilon_\mathrm{P}} \tag{1.110}$$

where $\phi = N(R/R^*)^3$ is the volume fraction of the dispersed spheres. Thus, for the effective permittivity of a heterogeneous system, the following result is obtained:

$$\varepsilon^* = \varepsilon_\mathrm{M} \cdot \left(1 + \frac{3\Phi(\varepsilon_\mathrm{P} - \varepsilon_\mathrm{M})}{2\varepsilon_\mathrm{M} + \varepsilon_\mathrm{P} - \Phi(\varepsilon_\mathrm{P} - \varepsilon_\mathrm{M})} \right) \tag{1.111}$$

As this equation has been derived neglecting interactions between the dispersed spheres, it is only valid for dilute dispersions ($\phi \ll 1$).

The Bruggeman Equation

To extend eq. (1.110) to more concentrated dispersions Bruggeman (1935) proposed the following assumptions:[55,101]

1. Eq. (1.110) can be applied for infinitesimal increases in the concentration of the disperse phase.

2. A concentrated dispersion can be thought to be built up by a series of such infinitesimal increases in concentration.

With the help of assumption (1), eq. (1.110) can be transformed to

$$\frac{2\varepsilon' + \varepsilon_\mathrm{P}}{3\varepsilon'(\varepsilon' - \varepsilon_\mathrm{P})}\Delta\varepsilon = \frac{-\Delta\phi'}{1-\phi'} \tag{1.112}$$

where the overall permittivity ε^* has been replaced by $\varepsilon' + \Delta\varepsilon'$, the permittivity of the medium, ε_M, by ε' and the volume fraction ϕ by $\Delta\phi'/(1-\phi')$. Furthermore, as $\Delta\varepsilon$ is an infinitesimal change, the approximation $3\varepsilon' + \Delta\varepsilon' \approx 3\varepsilon'$ has been used in eq. (1.112).

Following assumption (2) eq. (1.112) can be integrated with the boundary conditions $\varepsilon' = \varepsilon_\mathrm{M}$ at $\phi' = 0$ and $\varepsilon' = \varepsilon$ at $\phi' = \phi$ yielding:

$$\frac{\varepsilon - \varepsilon_\mathrm{P}}{\varepsilon_\mathrm{M} - \varepsilon_\mathrm{P}}\left(\frac{\varepsilon_\mathrm{M}}{\varepsilon}\right)^{1/3} = 1 - \phi \tag{1.113}$$

Numerical calculations by Günther and Heinrich[100] show that their results for ε compare favourably with the results of the Bruggeman equation for $\phi \leq 0.4$ if $\varepsilon_\mathrm{P} \gg \varepsilon_\mathrm{M}$ and for $\phi \leq 0.6$ if $\varepsilon_\mathrm{P} \ll \varepsilon_\mathrm{M}$.

1.5.3 The Effective Complex Permittivity in a Suspension of Spheres

The Wagner Equation

In 1914, Wagner proposed a dielectric theory of interfacial polarisation for a dilute disperse system yielding the relation[101]

$$\frac{\hat{\varepsilon}^* - \hat{\varepsilon}_\mathrm{M}}{2\hat{\varepsilon}_\mathrm{M} + \hat{\varepsilon}^*} = \phi \cdot \frac{\hat{\varepsilon}_\mathrm{P} - \hat{\varepsilon}_\mathrm{M}}{2\hat{\varepsilon}_\mathrm{M} + \hat{\varepsilon}_\mathrm{P}} \tag{1.114}$$

This may be regarded as an extension of the Wiener equation (1.110) to complex permittivities.

The Hanai Equation

Following the assumptions made by Bruggeman for the extension of the Wiener equation Hanai (1960) succeeded in developing a theory for concentrated disperse systems on the basis of the Wagner equation. Thus, he obtained the following result:[101]

$$\frac{\hat{\varepsilon}-\hat{\varepsilon}_\mathrm{P}}{\hat{\varepsilon}_\mathrm{M}-\hat{\varepsilon}_\mathrm{P}}\Big(\frac{\hat{\varepsilon}_\mathrm{M}}{\hat{\varepsilon}}\Big)^{1/3}=1-\phi \tag{1.115}$$

with

$$\hat{\varepsilon}-\hat{\varepsilon}_\mathrm{P}=\big[(\varepsilon'-\varepsilon'_\mathrm{P})^2+(\eta''-\eta''_\mathrm{P})^2\big]^{1/2}\cdot\exp\Big(-\mathrm{i}\tan^{-1}\frac{\eta''-\eta''_\mathrm{P}}{\varepsilon'-\varepsilon'_\mathrm{P}}\Big) \tag{1.116}$$

$$\hat{\varepsilon}_\mathrm{M}-\hat{\varepsilon}_\mathrm{P}=\big[(\varepsilon'_\mathrm{M}-\varepsilon'_\mathrm{P})^2+(\eta''-\eta''_\mathrm{P})^2\big]^{1/2}\cdot\exp\Big(-\mathrm{i}\tan^{-1}\frac{\eta''_\mathrm{M}-\eta''_\mathrm{P}}{\varepsilon'_\mathrm{M}-\varepsilon'_\mathrm{P}}\Big) \tag{1.117}$$

$$\hat{\varepsilon}_\mathrm{M}=(\varepsilon'^2_\mathrm{M}+\eta''^2_\mathrm{M})^{1/2}\cdot\exp\Big(-\mathrm{i}\tan^{-1}\frac{\eta''_\mathrm{M}}{\varepsilon'_\mathrm{M}}\Big) \tag{1.118}$$

$$\hat{\varepsilon}=(\varepsilon'^2+\eta''^2)^{1/2}\cdot\exp\Big(-\mathrm{i}\tan^{-1}\frac{\eta''}{\varepsilon'}\Big) \tag{1.119}$$

Inserting eqs. (1.116) to (1.119) into eq. (1.115) and separating the real and imaginary parts yields

$$\frac{[(\varepsilon'-\varepsilon'_\mathrm{P})^2+(\eta''-\eta''_\mathrm{P})^2](\varepsilon'^2_\mathrm{M}+\eta''^2_\mathrm{M})^{1/3}}{[(\varepsilon'_\mathrm{M}-\varepsilon'_\mathrm{P})^2+(\eta''_\mathrm{M}-\eta''_\mathrm{P})^2](\varepsilon'^2+\eta''^2)^{1/3}}=(1-\phi)^2 \tag{1.120}$$

and

$$\tan^{-1}\frac{\varepsilon'\eta''_\mathrm{M}-\varepsilon'_\mathrm{M}\eta''}{\varepsilon'\varepsilon'_\mathrm{M}+\eta''\eta''_\mathrm{M}}=3\tan^{-1}\frac{(\varepsilon'-\varepsilon'_\mathrm{P})(\eta''_\mathrm{M}-\eta''_\mathrm{P})-(\varepsilon'_\mathrm{M}-\varepsilon'_\mathrm{P})(\eta''-\eta''_\mathrm{P})}{(\varepsilon'-\varepsilon'_\mathrm{P})(\varepsilon'_\mathrm{M}-\varepsilon'_\mathrm{P})+(\eta''_\mathrm{M}-\eta''_\mathrm{P})(\eta''-\eta''_\mathrm{P})} \tag{1.121}$$

Eqs. (1.120) and (1.121) are the general expressions from which ε' and η'' can be derived.

1.5.4 The Effective Complex Permittivity in a Suspension of Ellipsoids

General Remarks

In the previous section the dielectric properties of a suspension of spheres have been presented. However, it should be kept in mind that this is probably a very idealized model and it is not certain that the droplets present in 'real' microemulsions as discussed in this work are indeed spheres. Therefore, it is essential to expand our previous discussion to ellipsoids, representing a more realistic geometrical body.

Let us consider an ellipsoid of permittivity $\hat{\varepsilon}_\mathrm{P}$ and of semi-axes R_x, R_y and R_z along the x-, y- and z-axis, respectively, embedded in a continuous medium of permittivity $\hat{\varepsilon}_\mathrm{M}$. When a homogeneous electric field $\vec{E}$ is applied, the electric potentials Φ_P and Φ_M can

be determined analogously to section 1.5.1 by solving the Laplace equation taking into account the boundary conditions. As a result, the following expressions are obtained:[4]

$$\Phi_{\mathrm{M}} = -\sum_{k=x,y,z} E_k k\Big(1 - \frac{\hat{\varepsilon}_{\mathrm{P}} - \hat{\varepsilon}_{\mathrm{M}}}{\hat{\varepsilon}_{\mathrm{M}} + (\hat{\varepsilon}_{\mathrm{P}} - \hat{\varepsilon}_{\mathrm{M}})L_k} L'_k\Big) \tag{1.122}$$

$$\Phi_{\mathrm{P}} = -\sum_{k=x,y,z} E_k k \frac{\hat{\varepsilon}_{\mathrm{M}}}{\hat{\varepsilon}_{\mathrm{M}} + (\hat{\varepsilon}_{\mathrm{P}} - \hat{\varepsilon}_{\mathrm{M}})L_k} \tag{1.123}$$

where

$$L'_k = \frac{R_x R_y R_z}{2} \int_s^\infty \frac{\mathrm{d}s'}{(R_k^2 + s')R_s} \tag{1.124}$$

$$L_k = \frac{R_x R_y R_z}{2} \int_0^\infty \frac{\mathrm{d}s'}{(R_k^2 + s')R_s} \tag{1.125}$$

$$R_s = \sqrt{(R_x^2 + s)(R_y^2 + s)(R_z^2 + s)} \tag{1.126}$$

$$\sum_{k=x,y,z} L_k = 1 \tag{1.127}$$

For a point far away from the ellipsoid L'_k may be approximated as

$$L'_k \approx \frac{R_x R_y R_z}{3} \frac{1}{r^3} \tag{1.128}$$

This approximation can be used to re-write the electric potential outside the ellipsoid, Φ_{M}, along the x-axis:

$$\Phi_{\mathrm{M}} = -E_x r \cos\theta \Big(1 - \frac{\hat{\varepsilon}_{\mathrm{P}} - \hat{\varepsilon}_{\mathrm{M}}}{\hat{\varepsilon}_{\mathrm{M}} + (\hat{\varepsilon}_{\mathrm{P}} - \hat{\varepsilon}_{\mathrm{M}})L_x} \frac{R_x R_y R_z}{3} \frac{1}{r^3}\Big) \tag{1.129}$$

where θ is the angle between the x-axis and the vector r. It can readily be seen that eq. (1.129) is composed of two contributions: the first term is due to the electric field, whereas the second term reflects the influence of the induced dipole moment of the ellipsoid along the x-axis, μ_x. The latter can also be written as

$$\Phi_{\mathrm{M}}^* = \frac{\mu_x}{4\pi r^2 \hat{\varepsilon}_{\mathrm{M}} \varepsilon_0} \cos\theta \tag{1.130}$$

Thus, the second term of eq. (1.129) and eq. (1.130) can be equated, which yields for μ_x:

$$\mu_x = 4\pi \hat{\varepsilon}_{\mathrm{M}} \varepsilon_0 \frac{\hat{\varepsilon}_{\mathrm{P}} - \hat{\varepsilon}_{\mathrm{M}}}{\hat{\varepsilon}_{\mathrm{M}} + (\hat{\varepsilon}_{\mathrm{P}} - \hat{\varepsilon}_{\mathrm{M}})L_x} \frac{R_x R_y R_z}{3} E_x \tag{1.131}$$

The total dipole moment, $\vec{\mu}$, is given by the sum of μ_x, μ_y and μ_z. Assuming the angle φ_k between the k-axis and the direction of the electric field, the component of the dipole moment in the E-direction, μ_E, is obtained as

$$\mu_E = \mu_x \cos\varphi_x + \mu_y \cos\varphi_y + \mu_z \cos\varphi_z = \frac{4\pi R_x R_y R_z}{3} \hat{\varepsilon}_\mathrm{M} \varepsilon_0 E \sum_{k=x,y,z} \frac{\hat{\varepsilon}_\mathrm{P} - \hat{\varepsilon}_\mathrm{M}}{\hat{\varepsilon}_\mathrm{M} + (\hat{\varepsilon}_\mathrm{P} - \hat{\varepsilon}_\mathrm{M}) L_k} \cos^2\varphi_k \tag{1.132}$$

where

$$\cos^2\varphi_x + \cos^2\varphi_y + \cos^2\varphi_z = 1 \tag{1.133}$$

Dilute Suspensions

For a system containing N particles of dipole moment μ_E in the direction of the electric field, the polarisation P is given by

$$P = N \cdot \mu_E \tag{1.134}$$

provided the interparticle distances are large enough so that dipolar and multipolar interactions can be neglected; the electric flux density D can be expressed as:

$$D = \hat{\varepsilon}_\mathrm{M} \varepsilon_0 E + P = \hat{\varepsilon}_\mathrm{M} \varepsilon_0 E + N \mu_E \tag{1.135}$$

With the help of eq. (1.132) we are now able to calculate the complex permittivity of a dilute suspension:

$$\hat{\varepsilon} = \frac{D}{\varepsilon_0 E} = \hat{\varepsilon}_\mathrm{M} \Big(1 + \phi \sum_{k=x,y,z} \frac{\hat{\varepsilon}_\mathrm{P} - \hat{\varepsilon}_\mathrm{M}}{\hat{\varepsilon}_\mathrm{M} + (\hat{\varepsilon}_\mathrm{P} - \hat{\varepsilon}_\mathrm{M}) L_k} \cos^2\varphi_k \Big) \tag{1.136}$$

where ϕ is the volume fraction of particles in the suspension. For randomly orienting ellipsoids, $\langle \cos^2\varphi_k \rangle = 1/3$ so that eq. (1.136) can be transformed to:[4]

$$\hat{\varepsilon} = \hat{\varepsilon}_\mathrm{M} \Big(1 + \frac{1}{3} \phi \sum_{k=x,y,z} \frac{\hat{\varepsilon}_\mathrm{P} - \hat{\varepsilon}_\mathrm{M}}{\hat{\varepsilon}_\mathrm{M} + (\hat{\varepsilon}_\mathrm{P} - \hat{\varepsilon}_\mathrm{M}) L_k} \Big) \tag{1.137}$$

Note that this equation, predicted by a number of authors,[2,90,146,158] postulates three relaxation processes of the Debye type in the general case. For spheroids of $R_x = R_y \neq R_z$, two semi-axes are equal so that only two relaxation processes will occur.

Concentrated Suspensions

Eq. (1.137) describes the complex permittivity of a dilute suspension of ellipsoids. However, when more concentrated dispersions are considered, interactions between the induced dipoles of the ellipsoids must be taken into account. Following the same thread as outlined in section 1.5.2 for the Bruggeman equation the following integral equation is obtained:[4]

$$\int_0^\phi -\frac{\mathrm{d}\phi'}{1-\phi'} = \int_{\hat{\varepsilon}_\mathrm{M}}^{\hat{\varepsilon}} \frac{3}{\hat{\varepsilon}'(\hat{\varepsilon}' - \hat{\varepsilon}_\mathrm{P})} \Big(\sum_{k=x,y,z} \frac{1}{\hat{\varepsilon}' + (\hat{\varepsilon}_\mathrm{P} - \hat{\varepsilon}') L_k} \Big)^{-1} \mathrm{d}\hat{\varepsilon}' \tag{1.138}$$

The solution of this integral equation is given by

$$1-\phi=\Big(\frac{\hat{\varepsilon}_{\mathrm{M}}-\alpha\hat{\varepsilon}_{\mathrm{P}}}{\hat{\varepsilon}-\alpha\hat{\varepsilon}_{\mathrm{P}}}\Big)^{A}\Big(\frac{\hat{\varepsilon}_{\mathrm{M}}-\beta\hat{\varepsilon}_{\mathrm{P}}}{\hat{\varepsilon}-\beta\hat{\varepsilon}_{\mathrm{P}}}\Big)^{B}\Big(\frac{\hat{\varepsilon}-\hat{\varepsilon}_{\mathrm{P}}}{\hat{\varepsilon}_{\mathrm{M}}-\hat{\varepsilon}_{\mathrm{P}}}\Big)\Big(\frac{\hat{\varepsilon}_{\mathrm{M}}}{\hat{\varepsilon}}\Big)^{3T} \tag{1.139}$$

where

$$A=-\frac{(1-2S-3T)\alpha+2(S-3T)}{2\sqrt{1-3S}} \tag{1.140}$$

$$B=\frac{(1-2S-3T)\beta+2(S-3T)}{2\sqrt{1-3S}} \tag{1.141}$$

$$\alpha=\frac{S-1-\sqrt{1-3S}}{1+S} \tag{1.142}$$

$$\beta=\frac{S-1+\sqrt{1-3S}}{1+S} \tag{1.143}$$

$$S=L_xL_y+L_yL_z+L_zL_x \tag{1.144}$$

$$T=\frac{L_xL_yL_z}{S} \tag{1.145}$$

For spheroids of $R_x=R_y\neq R_z$, eq. (1.139) is simplified to

$$1-\phi=\Big(\frac{\hat{\varepsilon}_{\mathrm{M}}(1+3L)+\hat{\varepsilon}_{\mathrm{P}}(2-3L)}{\hat{\varepsilon}(1+3L)+\hat{\varepsilon}_{\mathrm{P}}(2-3L)}\Big)^{C}\Big(\frac{\hat{\varepsilon}-\hat{\varepsilon}_{\mathrm{P}}}{\hat{\varepsilon}_{\mathrm{M}}-\hat{\varepsilon}_{\mathrm{P}}}\Big)\Big(\frac{\hat{\varepsilon}_{\mathrm{M}}}{\hat{\varepsilon}}\Big)^{3T} \tag{1.146}$$

where $L=L_x=L_y$ and $L_z=1-2L$ and

$$T=\frac{L_xL_yL_z}{L_xL_y+L_yL_z+L_zL_x}=\frac{L(1-2L)}{2-3L} \tag{1.147}$$

$$C=\frac{2(1-3L)^2}{(2-3L)(1+3L)} \tag{1.148}$$

A further considerable simplification is obtained when the k axis of an ellipsoid is parallel to the electric field:

$$1-\phi=\Big(\frac{\hat{\varepsilon}-\hat{\varepsilon}_{\mathrm{P}}}{\hat{\varepsilon}_{\mathrm{M}}-\hat{\varepsilon}_{\mathrm{P}}}\Big)\Big(\frac{\hat{\varepsilon}_{\mathrm{M}}}{\hat{\varepsilon}}\Big)^{L_k} \tag{1.149}$$

Note that this equation, already derived by Boyle,[35] becomes equivalent to the Hanai equation (1.115) for spherical particles, *i.e.* for $L_x=L_y=L_z=1/3$. For $L_x=L_y>L_z$, prolate spheroids (cylinders) are obtained, whereas $L_x=L_y<L_z$ yields oblate (disk-like) spheroids.[4]

1.5.5 The Effective Complex Permittivity of Particles with a Shell

General Remarks

Recent studies have shown that cationic reverse micelles exhibit regions of extreme salinity near the interface as counterions are attracted by the polar surfactant head groups located there.[74] Therefore, it may be assumed that also the dielectric properties of the interfacial regions of the microemulsions studied in this work deviate considerably from those of the water core. Thus, a model assuming a particle of dielectric properties A in a medium of dielectric properties B may be too simplistic to describe reality. Hence, a model accounting for the special properties of the interface will be discussed in this section.

Let us consider a shell ellipsoidal model exhibiting two confocal surfaces that can be written as

$$\frac{x^2}{R_x^2} + \frac{y^2}{R_y^2} + \frac{z^2}{R_z^2} = 1 \tag{1.150}$$

$$\frac{x^2}{R_{\mathrm{i}x}^2} + \frac{y^2}{R_{\mathrm{i}y}^2} + \frac{z^2}{R_{\mathrm{i}z}^2} = 1 \tag{1.151}$$

$$R_{\mathrm{i}k}^2 = R_k^2 - s \tag{1.152}$$

where R_k and $R_{\mathrm{i}k}$ are the semi-axes of the outer and inner surfaces along the k-axis, respectively, and s is a parameter representing a family of confocal surfaces. Assuming the shell-ellipsoid has an inner phase of complex permittivity $\hat{\varepsilon}_1$ and a shell phase of complex permittivity $\hat{\varepsilon}_2$ the electric potential of the medium outside the shell-ellipsoid can be obtained via the Laplace equation taking into account the boundary conditions at the two surfaces:[4]

$$\Phi_{\mathrm{M}} = -\sum_{k=x,y,z} E_k k\Big(1 - \frac{\hat{\varepsilon}_{\mathrm{p}k} - \hat{\varepsilon}_{\mathrm{M}}}{\hat{\varepsilon}_{\mathrm{M}} + (\hat{\varepsilon}_{\mathrm{p}k} - \hat{\varepsilon}_{\mathrm{M}})L_k} L_k'\Big) \tag{1.153}$$

where

$$\hat{\varepsilon}_{\mathrm{p}k} = \hat{\varepsilon}_2\Big(1 + \frac{\zeta(\hat{\varepsilon}_1 - \hat{\varepsilon}_2)}{\hat{\varepsilon}_2 + (\hat{\varepsilon}_1 - \hat{\varepsilon}_2)(L_{\mathrm{i}k} - \zeta L_k)}\Big) \tag{1.154}$$

with

$$L_{\mathrm{i}k} = \frac{R_{\mathrm{i}x}R_{\mathrm{i}y}R_{\mathrm{i}z}}{2}\int_0^\infty \frac{\mathrm{d}s}{(R_{\mathrm{i}k}^2 + s)R_{\mathrm{i}s}} \tag{1.155}$$

$$R_{\mathrm{i}s} = \sqrt{(R_{\mathrm{i}x}^2 + s)(R_{\mathrm{i}y}^2 + s)(R_{\mathrm{i}z}^2 + s)} \tag{1.156}$$

$$\zeta = \frac{R_{\mathrm{i}x}R_{\mathrm{i}y}R_{\mathrm{i}z}}{R_xR_yR_z} \tag{1.157}$$

Comparing eq. (1.153) to eq. (1.122) describing the potential of the medium outside a simple ellipsoid the only difference is that ε_{P} has been replaced by $\varepsilon_{\mathrm{p}k}$. Thus, when substituting $\varepsilon_{\mathrm{p}k}$ for ε_{P} the equations derived for 'normal' ellipsoids can also be used to determine the properties of shell-ellipsoids, where – in the general case – six Debye-type relaxation processes are expected according to eq. (1.137).[4]

In the case of shell-spheres, eq.(1.154) is simplified to

$$\hat{\varepsilon}_{\mathrm{P}} = \hat{\varepsilon}_2 \frac{2(1-\zeta)\hat{\varepsilon}_2 + (1+2\zeta)\hat{\varepsilon}_1}{(2+\zeta)\hat{\varepsilon}_2 + (1-\zeta)\hat{\varepsilon}_1} \tag{1.158}$$

and two Debye-type relaxations are predicted.

Dilute Dispersions of Spherical Particles - The Pauly-Schwan Equation

Following the ideas outlined above Pauly and Schwan developed a model for dilute dispersions of spheres of radius R covered with shells of radius r^*.[154] They obtained for the complex permittivity of the system

$$\hat{\varepsilon} = \frac{\kappa_{\mathrm{M}} A + \mathrm{i}\omega(\kappa_{\mathrm{M}}\mathrm{E} + \varepsilon_0\varepsilon_{\mathrm{M}}\mathrm{A}) + (\mathrm{i}\omega)^2(\kappa_{\mathrm{M}}\mathrm{B} + \varepsilon_0\varepsilon_{\mathrm{M}}\mathrm{E}) + (\mathrm{i}\omega)^3\varepsilon_0\varepsilon_{\mathrm{M}}\mathrm{B}}{\mathrm{i}\omega\varepsilon_0\mathrm{C}(1 + \mathrm{i}\omega(\mathrm{F}/\mathrm{C}) + (\mathrm{i}\omega)^2(\mathrm{D}/\mathrm{C}))} \tag{1.159}$$

with

$$a = (1+2v)\kappa_{\mathrm{P}} + 2(1-v)\kappa_{\mathrm{S}} \tag{1.160}$$

$$b = (1-v)\kappa_{\mathrm{P}} + (2+v)\kappa_{\mathrm{S}} \tag{1.161}$$

$$c = (1+2v)\varepsilon_{\mathrm{P}} + 2(1-v)\varepsilon_{\mathrm{S}} \tag{1.162}$$

$$d = (1-v)\varepsilon_{\mathrm{P}} + (2+v)\varepsilon_{\mathrm{S}} \tag{1.163}$$

$$A = (1+2\phi)\kappa_{\mathrm{s}} a + 2(1-\phi)\kappa_{\mathrm{M}} b \tag{1.164}$$

$$B = ((1+2\phi)\varepsilon_{\mathrm{S}} c + 2(1-\phi)\varepsilon_{\mathrm{M}} d)\varepsilon_0^2 \tag{1.165}$$

$$C = (1-\phi)\kappa_{\mathrm{S}} a + (2+\phi)\kappa_{\mathrm{M}} b \tag{1.166}$$

$$D = ((1-\phi)\varepsilon_{\mathrm{S}} c + (2+\phi)\varepsilon_{\mathrm{M}} d)\varepsilon_0^2 \tag{1.167}$$

$$E = ((1+2\phi)(\varepsilon_{\mathrm{S}} a + \kappa_{\mathrm{S}} c) + 2(1-\phi)(\varepsilon_{\mathrm{M}} b + \kappa_{\mathrm{M}} d))\varepsilon_0 \tag{1.168}$$

$$F = ((1-\phi)(\varepsilon_{\mathrm{S}} a + \kappa_{\mathrm{S}} c) + (2+\phi)(\varepsilon_{\mathrm{M}} b + \kappa_{\mathrm{M}} d))\varepsilon_0 \tag{1.169}$$

$$v = \Big(\frac{R}{R+r^*}\Big)^3 \tag{1.170}$$

where the letters M, S, and P mean 'medium', 'shell' and 'particle', respectively. Note that the frequency-dependence of the permittivities ε_{M}, ε_{S}, ε_{P} and of the conductivities κ_{M}, κ_{S}, κ_{P} is neglected in this approach, and the static values of these quantities are used. As already mentioned before, this model predicts two Debye-type relaxation processes of relaxation times $\tau_1 > \tau_2$

$$\tau_1 = \frac{F + \sqrt{F^2 - 4CD}}{2C} \tag{1.171}$$

and

$$\tau_2 = \frac{2D}{F + \sqrt{F^2 - 4CD}} \tag{1.172}$$

and of amplitudes

$$S_1 = \frac{\varepsilon_0\varepsilon_{\mathrm{M}} - \kappa_{\mathrm{M}}\tau_1}{\varepsilon_0 C(\tau_1 - \tau_2)\tau_1}(A\tau_1^2 - E\tau_1 + B) \tag{1.173}$$

and

$$S_2 = \frac{\varepsilon_0\varepsilon_{\mathrm{M}} - \kappa_{\mathrm{M}}\tau_2}{\varepsilon_0 C(\tau_1 - \tau_2)\tau_2}(-A\tau_2^2 + E\tau_2 - B) \tag{1.174}$$

Extension to Higher Particle Concentrations

The general equations for diluted suspensions of shell-ellipsoids can be extended to higher volume fractions following the thread proposed by Bruggeman; however, the anisotropy of the equivalent complex permittivity of the shell-ellipsoid $\hat{\varepsilon}_{\mathrm{p}k}$ has to be taken into account. Thus, the following integral equation has to be solved:[4]

$$\int_0^{\phi} -\frac{\mathrm{d}\phi'}{1-\phi'} = \int_{\hat{\varepsilon}_{\mathrm{M}}}^{\hat{\varepsilon}} \frac{3}{\hat{\varepsilon}'}\Big(\sum_{k=x,y,z} \frac{\hat{\varepsilon}' - \hat{\varepsilon}_{\mathrm{p}k}}{\hat{\varepsilon}' + (\hat{\varepsilon}_{\mathrm{p}k} - \hat{\varepsilon}')L_k}\Big)^{-1} \mathrm{d}\hat{\varepsilon}' \tag{1.175}$$

For the special case of rotational ellipsoids ($R_x = R_y$) Boned and Peyrelasse reported the following solution of this integral:[28]

$$1 - \phi = \Big(\frac{\hat{\varepsilon}_{\mathrm{M}}}{\hat{\varepsilon}}\Big)^{3d} \cdot \Big(\frac{\hat{\varepsilon}_{\mathrm{M}} - r}{\hat{\varepsilon} - r}\Big)^{3K_1} \cdot \Big(\frac{\hat{\varepsilon}_{\mathrm{M}} - q}{\hat{\varepsilon} - q}\Big)^{3K_2} \tag{1.176}$$

where

$$d = \frac{L(1-2L)}{2-3L} \tag{1.177}$$

$$r = \frac{\hat{\varepsilon}_{\mathrm{P}x}(3L-1) + 3L\hat{\varepsilon}_{\mathrm{P}z} + \sqrt{\Delta}}{2(3L+1)} \tag{1.178}$$

$$q = \frac{\hat{\varepsilon}_{\mathrm{P}x}(3L-1) + 3L\hat{\varepsilon}_{\mathrm{P}z} - \sqrt{\Delta}}{2(3L+1)} \tag{1.179}$$

$$K_1 = \frac{y - xr}{\sqrt{\Delta}} \tag{1.180}$$

$$K_2 = \frac{xq - y}{\sqrt{\Delta}} \tag{1.181}$$

$$\Delta = \hat{\varepsilon}_{\mathrm{P}x}^2(3L-1)^2 + 9L^2\hat{\varepsilon}_{\mathrm{P}z}^2 - 2\hat{\varepsilon}_{\mathrm{P}x}\hat{\varepsilon}_{\mathrm{P}z} \cdot (9L^2 - 3L - 4) \tag{1.182}$$

$$x = \frac{L(9L-5)}{3L-2} \tag{1.183}$$

$$y = \frac{2\hat{\varepsilon}_{\mathrm{P}x}(2L-1)^2 + \hat{\varepsilon}_{\mathrm{P}z}L^2}{3L-2} \tag{1.184}$$

with $L = L_x L_y$. Note that in this ansatz the isotropic rotational ellipsoid covered with a shell has been substituted by an anisotropic rotational ellipsoid of permittivities $\hat{\varepsilon}_{\mathrm{P}x} = \hat{\varepsilon}_{\mathrm{P}y} \neq \hat{\varepsilon}_{\mathrm{P}z}$.

For the special case of concentrated suspensions of shell-spheres, Hanai *et al.* proposed a solution by inserting eq. (1.158) into the Hanai equation (1.115).[102]

1.6 Interpretation Models

1.6.1 Percolation

Dynamic versus Static Percolation

In microemulsions consisting of conducting droplets of a volume fraction ϕ embedded in an insulating medium clusters of droplets will form when ϕ is increased, leading to a percolation transition. In the literature, both a static and a dynamic model exist to describe this percolation phenomenon.

The static model states that as soon as ϕ reaches a critical value ϕ_c an infinite cluster of droplets is formed creating continuous conductive paths through the insulating medium.[159] Consequently, a sharp increase in electrical conductivity κ is expected at the critical volume fraction ϕ_c. Around ϕ_c the following empirical scaling laws for conductivity exist:[159]

$$\kappa \approx (\phi_\mathrm{c} - \phi)^{-s}, \quad \phi < \phi_\mathrm{c} \tag{1.185}$$

$$\kappa \approx (\phi - \phi_\mathrm{c})^{\mu}, \quad \phi > \phi_\mathrm{c} \tag{1.186}$$

with the critical exponents $s \approx 0.7$[71,135] and $\mu \approx 1.9$.[72]

In contrast, the dynamic percolation model assumes that due to attractive interactions between the water droplets, clusters of particles evolve and rearrange continuously. According to this model, conductivity should increase steadily with increasing ϕ, as it is now dominated by interfacial processes. Charge propagation can either take place by charge hopping between adjacent water droplets or by the motion of the droplet itself. Accordingly, the following scaling expression has been developed for conductivity:[99]

$$\kappa(\phi - \phi_c, T_R, \omega) = (\phi - \phi_c)^{-s'} f(\omega T_R, \omega\tau) \tag{1.187}$$

where T_R is the rearrangement time of a cluster, ω is the driving frequency of the dynamic process and $f(\omega T_R, \omega\tau)$ a scaling function.

If $\omega T_R \ll 1$ the rearrangement times are considerably shorter than ω^{-1} so that κ is frequency-independent. In this case, the dynamic model predicts a conductivity behaviour similar to eq. (1.185) below ϕ_c, where $s' \approx 1.2$[159] is somewhat different from the static case. Above ϕ_c, $\mu \approx 1.9$[159] is obtained, as for the static model.

If, in contrast, $\omega T_R \gg 1$ the conductivity is frequency-dependent; near the percolation threshold, the function $f(\omega T_R, \omega\tau)$ yields the following power-law conductivity behaviour:

$$\kappa(\omega) \approx \omega^u \quad \text{with} \quad u = \frac{\mu}{\mu + s'} \tag{1.188}$$

Near the percolation threshold ϕ_c the complex permittivity $\hat{\varepsilon}$ can be expressed as follows:[159]

$$\hat{\varepsilon}(\omega) \approx \omega^{u-1} \tag{1.189}$$

Furthermore, the loss angle $\Delta(\omega)$, defined as $\tan\Delta(\omega) = \varepsilon''(\omega)/\varepsilon'(\omega)$, does not depend on frequency near ϕ_c. From eq. (1.189) the asymptotic value Δ_c of the loss angle can be calculated as:[159]

$$\Delta_c = \frac{\pi}{2}(1 - u) \tag{1.190}$$

The value of the critical exponent u is predicted by the model to be $u \approx 0.61$.[159]

Ponton, Bose and Delbos found the dynamic percolation model to be very suitable for the description of their experimental results for water-in-oil microemulsions.[159] Boned and Peyrelasse investigated electrical conductivity, dielectric relaxation and dynamic viscosity behaviour for a number of very different aqueous and non-aqueous microemulsions based on the surfactants AOT (sodium bis(2-ethylhexyl) sulfosuccinate) and SDS (sodium dodecylsulfate); they always found their results to be in good agreement with the predictions of the dynamic percolation model.[30]

The Disordered Open Connected Model

The Disordered Open Connected (DOC)[10] model was developed in the 1980s as a quantitative description of static percolation. It is based on three geometrical parameters that can be calculated from the volume fraction of the internal phase of the microemulsion, ϕ, the interfacial area per unit volume, Σ, and the packing parameter, v/al; all of these quantities are experimentally accessible.

The DOC model assumes that beyond the percolation threshold the dispersed phase forms a network of spheres and cylinders in the medium. This network is specified by the density of sphere centres in space, n, the average number of cylinders meeting at each sphere, Z, and the sphere radius, R. As the value of the mean curvature should be the same for spheres and cylinders, the cylinder radius r is fixed to $r = R/2$.

The spheres-and-cylinders network described above can be constructed using the following procedure:[10]

- Generation of a random hard-sphere distribution of points in space by a Monte-Carlo procedure. The minimum separation between two points should be $2R + 2l$, *i.e.* two neighbouring spheres should not approach closer than two surfactant tail lengths l. Subsequently, a sphere of radius R is placed at each of these points.
- Determination of the nearest neighbours by constructing Voronoi polyhedra around each point. Two points are neighbours if their Voronoi polyhedra share a face. The resulting list of neighbours is ordered by their separation distance.
- Connection of neighbouring spheres by cylinders. This is done in order of proximity, until the average coordination number of the structure is equal to Z.

Based on these assumptions, the following equations can be derived, relating the parameters n, R and Z to ϕ and Σ:[10]

$$\phi = \left[\frac{4}{3}\pi R^3 - \frac{1}{3}Zr^3(\Omega\rho^3 - \pi\sqrt{\rho^2 - 1})\right]n + \pi r^2 Z\left[\frac{8.15n^{2/3}}{13.4} - nr\sqrt{\rho^2 - 1}\right] \tag{1.191}$$

$$\Sigma = (4\pi - \Omega Z)R^2 n + 2\pi r Z\left[\frac{8.15n^{2/3}}{13.4} - nr\sqrt{\rho^2 - 1}\right] \tag{1.192}$$

where $\rho = R/r$ and $\Omega = 2\pi[1 - \sqrt{1 - 1/\rho^2}]$. For v/al the expression

$$v/al = 1 + Hl + \frac{1}{3}Kl^2 \tag{1.193}$$

is obtained, which comes from differential geometry, using the relationships between the variation of the surface area as the surface is displaced along its normal and the area-averaged mean (H) and Gaussian (K) curvatures, yielding

$$H = \frac{\Sigma_+ - \Sigma_-}{4\delta\Sigma_0} \tag{1.194}$$

and

$$K = \frac{\Sigma_+ + \Sigma_- - 2\Sigma_0}{2\delta^2\Sigma_0} \tag{1.195}$$

where Σ_0 is the interfacial area per unit volume calculated above, and Σ_+ and Σ_- are the areas of parallel surfaces displaced respectively outside and inside the original surface by a small distance δ. Strictly speaking, this method is only valid for smooth surfaces, but it can be used if the cusps are smoothed and the radius of the curvature of the smoothing is allowed to go to zero.[10]

1.6.2 Hydration

Hydration and Dielectric Relaxation

The term 'hydration' comprises all effects of dissolved substances on the structure and dynamics of the solvent water. However, there are fundamental differences between the hydration of a hydrophilic and of a hydrophobic particle.

Solution of hydrophilic ionic compounds causes strong electrostatic interactions between the ions and the neighbouring water molecules. As a result, the water dipoles are aligned in the electric field of the ion so that their ability to rotate is restricted or even completely lost (*irrotational bonding*, IB). Hence, the orientational polarisation $\vec{P}_\mu$ and also the static permittivity ε and the dispersion amplitude S decrease. This effect is called dielectric saturation; the kind of hydration it is based on is sometimes known as *direct hydration*.

On the other hand, there is some evidence that when hydrophobic particles are dissolved this leads to a reinforcement of hydrogen bonds in their vicinity.[164] As the number of options for the establishment of hydrogen bonds is reduced the dynamics of the concerned water molecules is obviously slowed down. As a consequence the bulk-water relaxation is shifted towards lower frequencies or even the splitting of a slow-water process from the main process may be observed.[113,125] This kind of hydration is known as *hydrophobic hydration*.

As the hydrophobic parts of the surfactant molecules are not situated in the aqueous phase of the microemulsions investigated in this work, hydrophobic hydration is not observed in the present study. Therefore, the following discussion will focus on direct hydration.

Dielectric Decrement

Adding a strong electrolyte to the solvent water typically leads to a decrease of the water dispersion amplitude S; the latter is defined as:

$$S(c) = \varepsilon_{\mathrm{H_2O}}(c) - \varepsilon_{\mathrm{H_2O},\infty}(c) \tag{1.196}$$

This effect, known as dielectric depression, can be ascribed to two additive contributions, an equilibrium term and the kinetic depolarisation effect:

$$\Delta\Delta\varepsilon_{H_2O}(c) = S_{H_2O}(0) - S_{H_2O}(c) = \Delta_{eq}\varepsilon_{H_2O}(c) + \Delta_{kd}\varepsilon_{H_2O}(c) \tag{1.197}$$

Equilibrium Term of Dielectric Depression

The equilibrium term $\Delta_{eq}\varepsilon(c)$ itself is again composed of two contributions: one part of it describes the dilution of the water dipoles by non-polar ions ($\varepsilon_{ion} \approx 2$)[42] and the resulting modification of the inner field. The second part accounts for the fact that some water molecules located near ions loose their ability to rotate, which – as already noted – is due to strong electrostatic ion-dipole-interactions. The dipole moment of these water molecules that are unable to rotate cannot be detected.

Kinetic Depolarisation

Kinetic depolarisation is a dynamic effect which is due to the movement of ions in the external electric field. On the one hand this movement forces those dipole molecules located very close to the migrating ion to rotate against the direction of the external field; on the other hand, the dipole alignment in the external field slows down the ion migration.

According to the continuum theory of Hubbard and Onsager[115,117] kinetic depolarisation is proportional to the specific conductivity κ, assuming point-sized ions in an infinitely diluted solution:

$$\Delta_{kd}\varepsilon(c) = \xi\kappa(c) \tag{1.198}$$

The depolarisation factor ξ depends on the dielectric properties of the pure solvent:

$$\xi = p \cdot \frac{\varepsilon(0) - \varepsilon_\infty(0)}{\varepsilon(0)} \cdot \frac{\tau(0)}{\varepsilon_0} \tag{1.199}$$

Note that the hydrodynamic parameter p assumes the values 1 for *stick* and $^2/_3$ for *slip* boundary conditions.

Experimental results often show a proportionality between ΔS and κ; however, in the majority of cases the experimental slope deviates from the values predicted by the Hubbard-Onsager equation. Apart from that, experimental results often feature a dependence of the depolarisation factor ξ on the electrolyte, which contradicts eq. (1.199). Therefore, Hubbard, Colonomos and Wolynes proposed a theory postulating the dependence of the depolarisation factor ξ on the ionic radius;[116] for large ionic radii this theory becomes equivalent to eq. (1.199).

Publications by Chandra *et al.*[49] deny the existence of kinetic depolarisation. However, recent experimental studies[42,190–192] demonstrate that for aqueous electrolyte solutions the Hubbard-Onsager model assuming *slip* boundary conditions is a good approximation.

Apparent Solvent Concentrations and Effective Solvation Numbers

As already mentioned water dipoles that are interacting so strongly with an ion that they loose their ability to rotate cannot be detected by dielectric relaxation spectroscopy. Thus, by analyzing the experimental spectra, it is possible to calculate the apparent solvent concentration $c_{\mathrm{s}}^{\mathrm{app}}$, which should be smaller than the real solvent concentration $c_{\mathrm{s}}^{\mathrm{bulk}}$ as it only takes into account the *detected* water dipoles.

Various approaches to calculate the apparent solvent concentration $c_{\mathrm{s}}^{\mathrm{app}}$ from the equilibrium amplitude of the solvent dispersion S_{eq}

$$S_{\mathrm{eq}} = S(c) + \Delta_{\mathrm{kd}}\varepsilon(c) \tag{1.200}$$

are presented in the literature.[38,125] As can be seen from a comparative discussion,[19] the results obtained for $c_{\mathrm{s}}^{\mathrm{app}}$ strongly depend on the adopted model so that they are not directly comparable. Apart from that it should be kept in mind that some of these models are only valid for infinitely diluted solutions.

The model used in this work is based on the Cavell equation (1.79). Generalized for ellipsoidal reaction fields it can be written as:

$$c_{\mathrm{s}}^{\mathrm{app}}(c) = \frac{3(\varepsilon + (1-\varepsilon)A_i)}{\varepsilon} \cdot \frac{\mathrm{k_B}T\varepsilon_0}{\mathrm{N_A}} \cdot \frac{(1-\alpha_i f_i)^2}{g_i \mu_i^2} \cdot S_{\mathrm{eq}} \tag{1.201}$$

The reaction field factor, f_i, and the geometry parameter, A_i are given in section 1.4.2.

As already outlined in section 1.4.3 the Kirkwood factor g_i is a convenient way to describe the relative orientation of neighbouring water molecules.[27] If the water dipoles show parallel alignment the total dipole moment is reinforced and $g_i > 1$; in turn, for antiparallel alignment $g_i < 1$ is obtained.

The Kirkwood factor is well known for bulk water ($g_{\mathrm{H_2O}} = 2.68$),[41] and it is certainly reasonable to assume g_i^{bulk} as an approximation for dilute aqueous electrolyte solutions. However, this assumption is not valid for water located in the aqueous subphase of a water-in-oil microemulsion. Due to geometric constraints inside these droplets whose radius amounts to only few nanometers, it is even possible that water molecules near the interface show antiparallel alignment, leading to $g_i < 1$. In this case, only the product $g_i c_{\mathrm{s}}^{\mathrm{app}}$ can be determined from the equilibrium amplitude of the solvent dispersion S_{eq}.

For a comparison between the apparent solvent concentration $c_{\mathrm{s}}^{\mathrm{app}}$ and the actual solvent concentration $c_{\mathrm{s}}^{\mathrm{bulk}}$ the effective solvation number Z_{IB} is introduced:

$$Z_{\mathrm{IB}} = \frac{c_{\mathrm{s}}^{\mathrm{bulk}} - c_{\mathrm{s}}^{\mathrm{app}}}{c} \tag{1.202}$$

Note that c is the concentration of the dissolved species. According to eq. (1.202) Z_{IB} is the average number of water molecules per ion that are unable to contribute to the solvent relaxation process at a certain time. Hence, Z_{IB} may be interpreted as a measure of the relative strength of ion-solvent and solvent-solvent interactions.[42] Usually, Z_{IB} does not coincide with the results of scattering experiments or MD simulations, which both determine the number of solvent molecules located in the first coordination sphere of an ion. This is certainly not surprising considering that the factor $gc_{\mathrm{s}}^{\mathrm{bulk}}$ also encompasses effects exerted by an ion on the solvent structure.

1.6.3 The Electrochemical Double Layer

In ionic microemulsions the oil phase and the water phase are separated by a charged interface made up of surfactant ions that can hardly move, due to geometrical constraints. Consequently, this leads to an alignment of counterions in the adjacent aqueous phase. In many respects, this situation appears to be similar to an electrode-solution interface. Thus, it is crucial for the understanding of the structure of the aqueous microemulsion phase to keep in mind the behaviour of electrolyte solutions at a charged interface.

The Helmholtz Model

The first model describing an electrolyte solution at a charged interface was developed by Helmholtz. He proposed that the counterions in solution should reside directly at the interface. Thus, the interface and the counterions should form two layers of charge, having opposite polarity, separated by a distance of molecular order. Helmholtz coined the term 'double layer' to describe this phenomenon.[9] Such a structure corresponds to a parallel-plate capacitor, where the capacity only depends on the dimensions of the capacitor, not on the electric potential. However, this model cannot be reconciled with experimental results, showing a dependence of the capacity on the electrolyte concentration. Thus, it appears that the Helmholtz model can only be used in the limiting case of very concentrated electrolyte solutions; otherwise, a more elaborate model is required.

The Gouy-Chapman Model

In an electrolyte solution close to a charged interface there is a balance between attractive and repellent forces depending on polarity and random Brownian motion. Thus, the Gouy-Chapman model assumes a *diffuse double layer*: as the strongest electrostatic forces are found adjacent to the interface, the electrolyte concentration should reach its maximum there and then gradually decrease with increasing distance from the interface, as thermal processes become more and more important. Thus, charges at the interface and in the solution are separated by an average distance that is dependent on interfacial potential and electrolyte concentration.

Gouy and Chapman independently proposed this idea and developed a statistical mechanical approach for its description.[9] In this approach, the solution is subdivided into laminae of thickness $\mathrm{d}\,x$, parallel to the interface. Although all these laminae are in thermal equilibrium with each other, the ions of any species i are at different energies in different laminae because the electrostatic potential varies. Thus, the ratio of the ion concentrations in two laminae can be expressed by a Boltzmann factor. Considering a reference lamina far from the electrode, where every ion is at its bulk concentration n_i^0, the population in any other lamina is

$$n_i = n_i^0 \exp\Big(\frac{-z_i \mathrm{e}_0 \Phi}{\mathrm{k_B}\, T}\Big) \tag{1.203}$$

where z_i denotes the charge number of the ion i; the potential Φ is measured with respect to the bulk solution. Thus, the total charge per unit volume, ρ, in any lamina can be written as

$$\rho(x) = \sum_i n_i z_i \mathrm{e}_0 = \sum_i n_i^0 z_i \mathrm{e}_0 \exp\Big(\frac{-z_i \mathrm{e}_0 \Phi}{\mathrm{k_B}\, T}\Big) \tag{1.204}$$

for all ionic species i. It is well-known that $\rho(x)$ depends on the potential at distance x as described by the Poisson equation:[9]

$$\rho(x) = -\varepsilon\varepsilon_0 \frac{\partial^2 \Phi}{\partial x^2} \tag{1.205}$$

Inserting eq. (1.204) into eq. (1.205) yields the Poisson-Boltzmann equation

$$\frac{\partial^2 \Phi}{\partial x^2} = -\frac{\mathrm{e}_0}{\varepsilon\varepsilon_0} \sum_i n_i^0 z_i \exp\Big(\frac{-z_i \mathrm{e}_0 \Phi}{\mathrm{k_B} T}\Big) \tag{1.206}$$

which can easily be converted into:

$$\mathrm{d}\Big(\frac{\partial \Phi}{\partial x}\Big)^2 = -\frac{2\mathrm{e}_0}{\varepsilon\varepsilon_0} \sum_i n_i^0 z_i \exp\Big(\frac{-z_i \mathrm{e}_0 \Phi}{\mathrm{k_B} T}\Big)\, \mathrm{d}\,\Phi \tag{1.207}$$

Integrating eq. (1.207) yields:

$$\Big(\frac{\partial \Phi}{\partial x}\Big)^2 = \frac{2\mathrm{k_B} T}{\varepsilon\varepsilon_0} \sum_i n_i^0 \exp\Big(\frac{-z_i \mathrm{e}_0 \Phi}{\mathrm{k_B} T}\Big) + C^{\mathrm{te}} \tag{1.208}$$

The constant C^{te} can be determined by taking into account that at distances far from the interface $\Phi = 0$ and $(\partial\Phi/\partial x) = 0$:

$$\Big(\frac{\partial \Phi}{\partial x}\Big)^2 = \frac{2\mathrm{k_B} T}{\varepsilon\varepsilon_0} \sum_i n_i^0 \Big[\exp\Big(\frac{-z_i \mathrm{e}_0 \Phi}{\mathrm{k_B} T}\Big) - 1\Big] \tag{1.209}$$

For the special case of symmetric electrolytes, eq. (1.209) can be reduced to:

$$\frac{\partial \Phi}{\partial x} = -\Big(\frac{8\mathrm{k_B} T n^0}{\varepsilon\varepsilon_0}\Big)^{1/2} \sinh\Big(\frac{z \mathrm{e}_0 \Phi}{2\mathrm{k_B} T}\Big) \tag{1.210}$$

The Gouy-Chapman-Stern Model

In the Gouy-Chapman model ions are considered to be point charges that can approach the interface arbitrarily closely. However, this assumption does not reflect reality. An ion is certainly unable to approach the surface closer than to its radius. If it is solvated, the radius of the first solvation shell should be added to that radius. Furthermore, there may be a layer of solvent molecules tightly bound to the interface whose thickness has also to be taken into account. Hence, there is a plane of closest approach for the centres of the

ions at a certain distance x_2 from the interface, which is called the *outer Helmholtz plane* (OHP).

The above considerations are negligible for very dilute electrolyte solutions, where the thickness of the diffuse layer is far larger than x_2. However, they are decisive for concentrated electrolytes or larger polarisation, as in these cases the diffuse layer becomes compressed, approaching more and more the limiting case of the Helmholtz model.

The interfacial model presented above has first been suggested by Stern;[9] it can be regarded as an extension of the Gouy-Chapman model, which still remains valid at distances $x \geq x_2$. Now the potential profile in the diffuse layer of a symmetric electrolyte can be written as

$$\int_{\Phi_2}^{\Phi} \frac{\partial \Phi'}{\sinh(z\mathrm{e}_0\Phi'/2\mathrm{k}_\mathrm{B}T)} = -\Big(\frac{8\mathrm{k}_\mathrm{B}Tn^0}{\varepsilon\varepsilon_0}\Big)^{1/2} \int_{x_2}^{x} \partial x' \tag{1.211}$$

where Φ_2 is the potential at x_2 with respect to the bulk solution. The field strength at x_2 is given from eq. (1.209):

$$\Big(\frac{\partial \Phi}{\partial x}\Big)_{x=x_2} = -\Big(\frac{8\mathrm{k}_\mathrm{B}Tn^0}{\varepsilon\varepsilon_0}\Big)^{1/2} \sinh\Big(\frac{z\mathrm{e}_0\Phi}{2\mathrm{k}_\mathrm{B}T}\Big) \tag{1.212}$$

As there are no charges between the OHP and the interface, the charge density is zero at any point within this interval. Thus, according to eq. (1.205) the field strength remains constant so that the potential profile in the compact layer is linear. Consequently, the total potential drop across the double layer is

$$\Phi_0 = \Phi_2 - \Big(\frac{\partial \Phi}{\partial x}\Big)_{x=x_2} x_2 \tag{1.213}$$

Chapter 2

Experimental

2.1 Preparation of Samples

The following abbreviations are used throughout this thesis:

- *DDAB: didodecyldimethylammonium bromide*
- *W: water*
- *D: n-dodecane*

These three components form the microemulsions investigated in this work.

2.1.1 Treatment of Single Components

As the surfactant and the electrolytes used in this work are fairly hygroscopic careful desiccation was essential to avoid concentration errors of the microemulsions. Therefore, all solids were dried extensively under high vacuum ($\sim 10^{-5}$ bar), using P_2O_5 (Sicapent, Merck) as a desiccant. Experimental details are given in Table 2.1.

Table 2.1: Substances Used and Their Purities, Drying Temperatures, T, and Minimum Drying Times, t

substance (source)	purity	T / K	t/h
DDAB (ACROS Organics)	$> 99\%$	313	24
lithium bromide (Merck)	*extra pure* ($> 99\%$)	373	48
sodium bromide (Merck)	*suprapur*	353	48
cesium bromide (Merck)	*suprapur*	353	48
tetramethylammonium bromide (Fluka)	*puriss.* ($> 99\%$)	323	72

Only de-ionized water produced with a MILLIPORE cleaning apparatus has been used in this work; its specific conductivity has always been found to be less than $2 \cdot 10^{-7}$ S cm^{-1}. Water has always been carefully degassed before use.

n-dodecane (Merck, *for synthesis*, $> 99\%$) was used without any further purification.

2.1.2 Preparation of Microemulsions

Detailed studies of the phase diagram of the system DDAB/W/D have been published in the literature.[89,177] A number of different phases has been found to exist; however, there is only one 'solution' phase, commonly labelled 'L_2' in the literature,[89,177] where stable microemulsions are formed. These microemulsions are always of the water-in-oil (W/O) type, *i.e.* water as the dispersed phase is embedded in the medium dodecane.

Thus, when preparing DDAB/W/D microemulsions care has to be taken to choose ratios of the three components that are located in the L_2 phase so that stable microemulsions can form. A phase diagram of DDAB/W/D showing the boundaries of the L_2 region is given in Figure 3.1.

All samples were prepared gravimetrically without buoyancy correction, using a Mettler AE 240 analytical balance. To avoid contamination with air moisture, a certain mass of DDAB was filled into a Schott flask under nitrogen atmosphere. Then, the equivalent amounts of *n*-dodecane and water were added so that a certain point within the L_2 phase of the ternary phase diagram was obtained.

To prepare microemulsions containing co-ions, appropriately concentrated aqueous solutions of LiBr, NaBr, CsBr and $(CH_3)_4NBr$ that had been prepared previously were used instead of pure water.

After approx. 12 h clear microemulsions formed spontaneously for most samples; for the remaining samples, that were still found to be macroscopically heterogeneous, clear microemulsions were obtained after magnetic stirring for less than 1 h.

All microemulsion samples were stored in tightly closed Schott flasks at 25 °C and protected from light. In most cases, measurements were taken not longer than one to two weeks after the preparation of the sample. However, a small fraction of the dielectric measurements in this work – mainly some of the VNA measurements implemented at Murdoch University – were carried out one to two months after the preparation of the sample. As a test spectrum that had been recorded six months after the preparation of the investigated sample was indistinguishable from the spectrum measured immediately after its preparation, this procedure does not appear to be problematic.

2.2 Dielectric Relaxation Spectroscopy

2.2.1 Methods

Dielectric relaxation spectroscopy (DRS) can be performed using different experimental techniques.[17,27,39] Frequency-domain (FD) measurements determine the generalised complex permittivity $\hat{\eta}$ directly as a function of frequency. In contrast, time-domain (TDR) spectroscopy yields the step response function, from which $\hat{\eta}$ can be obtained by Fourier transformation. In order to determine the complex permittivity $\hat{\varepsilon}$ from $\hat{\eta}$ the specific conductivity κ has to be known (see eqs. (1.38) and (1.39)).

For measurements from approx. 1 MHz up to several GHz a time-domain reflectometer (TDR) including a set of cells of different geometry is available at Regensburg University. However, the maximum frequency for which good quality data can be obtained strongly depends on the properties of the investigated sample. In the case of the microemulsions studied in this work, data for $\nu \gtrsim 0.5$ GHz generally appeared to be very noisy and thus were excluded from further processing.

Data in the frequency range $0.2 \lesssim \nu/\text{GHz} \leq 20$ were acquired using a Vector Network Analyzer (VNA) – based on the principle of frequency-domain reflectometry – at the institute of Professor Glenn Hefter, Murdoch University, Australia.

For the frequency range $8.5 \leq \nu/\text{GHz} \leq 89$ four similar frequency-domain interferometers of different size are available at Regensburg University (details are given in Table 2.2). However, as the sample volume for Ku-band and X-band amounts to 7.5 mL and 20 mL, respectively, and as their frequency range is already covered by the VNA measurements only A-band and E-band were used for this work. Thus, the cost of the samples, which was mainly due to the high price of DDAB, could be reduced considerably.

Table 2.2: Overview of the Instruments: Type, Frequency Range and Limiting Frequency ν_g

instrument	type	frequency range/GHz	ν_g/GHz
TDR	coaxial line	0.001 - 5(10)	0
VNA	coaxial line	0.1 - 20.0	0
X-band	rectangular waveguide	8.5 - 12.0	5.260
Ku-band	rectangular waveguide	13.0 - 17.5	9.487
A-band	rectangular waveguide	26.4 - 40.0	21.07
E-band	rectangular waveguide	60.0 - 89.0	48.37

2.2.2 Time-Domain Reflectometry

Principle and Instruments

This method determines the dielectric properties of a system by measuring its impedance.[21,59,86,87,147] In principle, such measurements can be implemented using either transmission or reflection cells.[12] However, as transmission cells have proven to be very sensitive to mechanical stress reflection cells of the cut-off type are used in the Regensburg laboratories; they are immersed into a bath thermostat (Julabo FP 45) keeping the temperature constant to ± 0.04 K. Table 2.3 summarizes the parameters of the cells used in this work; others are described elsewhere.[118,167]

Table 2.3: Cell Name, Mechanical and Electrical Pin Length, l_{mech} and l_{el}, Diameter of the Inner and Outer Conductor, d and D, and Ratio of the Wave Resistances of Empty Cell and Input Line, g

cell	l_{mech} / mm	l_{el} / mm	d / mm	D / mm	g
T1	0.0	≈ 0.350	0.5	3.3	0.4416[5]
T2	0.5	≈ 0.800	0.5	3.3	0.4416[5,167]
T11	1.5	1.890	0.5	3.5	0.42855[167]
TS1	25	26.377	1.5	3.5	0.82258[167]

Although these four cells featuring partly very different geometrical properties were used for test measurements only T2 yielded reasonable results for DDAB/W/D microemulsions. With the remaining cells very noisy data were obtained that could not be employed for further processing. The reasons for this behaviour are unknown. Test measurements with a number of standard solvents performed at the same time did not show any difficulties. The problems observed might be specific to DDAB/W/D mixtures and might be related to the special dielectric properties or, more likely, the high viscosity of this system.

However, T2 yielded convincing data; when the electrical pin length, which is known to depend on the static permittivity,[5,167] was adjusted according to the calibration curve established by Schrödle[167] (*i.e.* $l_{\mathrm{el}} \approx 0.793$ mm for $\varepsilon_{\mathrm{stat}} \approx 20$) the results were found to be in very good agreement with the VNA data, which in turn agreed very well with the interferometer results.

The reflection cells are connected to the two sampling heads (SD24) of a digital sampling scope (TEK 11802; Tektronix). The latter controls the pulse generators located in the sampling heads, which generate a rectangular voltage pulse with a frequency of 200 kHz and a rise time of 17.5 ps. 5120 data points – separated by the time interval Δt – are recorded per measurement. To improve the signal-noise-ratio average values from 256 single measurements are used.

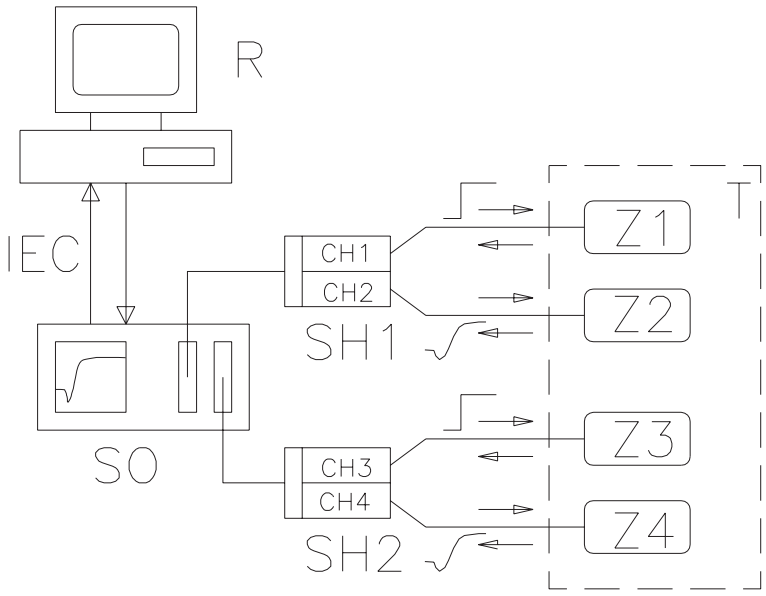

Figure 2.1: Scheme of the time-domain reflectometer at Regensburg University[40] (**SO**: digital sampling oscilloscope; **SH1, SH2**: SD-24 sampling heads; **Z1-Z4**: cut-off cells; **T**: precision thermostat; **R**: personal computer).

Figure 2.1 illustrates the principle of the instrument used in the Regensburg laboratories. A detailed description of the TDR apparatus and the measurement principle can be found in the literature.[16,40]

Data Processing

As a first step of the processing procedure for data obtained by reflection cells, the time-dependent intensities of the initial voltage pulse, $V_0(t)$, and of the signal reflected by the sample, $V_\mathrm{r}(t)$, have to be converted into the frequency domain by Laplace transformation (symbolized by the character $\mathcal{L}$):

$$v_0(\omega) = \mathcal{L}_{\mathrm{i}\omega}\left[\frac{\mathrm{d}}{\mathrm{d}t}V_0(t)\right] = \int_0^\infty \frac{\mathrm{d}}{\mathrm{d}t}V_0(t)\cdot\exp(\mathrm{i}\omega t)\mathrm{d}t \tag{2.1}$$

$$v_\mathrm{r}(\omega) = \mathcal{L}_{\mathrm{i}\omega}\left[\frac{\mathrm{d}}{\mathrm{d}t}V_\mathrm{r}(t)\right] = \int_0^\infty \frac{\mathrm{d}}{\mathrm{d}t}V_\mathrm{r}(t)\cdot\exp(\mathrm{i}\omega t)\mathrm{d}t \tag{2.2}$$

From the Laplace-transformed intensities $v_0(\omega)$ and $v_\mathrm{r}(\omega)$ the absolute reflection coefficient $\hat{\rho}(\omega)$ of the cut-off cell can be calculated:

$$\hat{\rho}(\omega) = \frac{c_0}{\mathrm{i}\omega g l}\cdot\frac{v_0(\omega)-v_\mathrm{r}(\omega)}{v_0(\omega)+v_\mathrm{r}(\omega)} \tag{2.3}$$

where l represents the electrical pin-length, which is determined by calibration. The ratio between the wave resistances of empty cell and feeding line, g, can be calculated from the geometry of the cell according to

$$g = \frac{Z_{\mathrm{L}}}{\frac{1}{2\pi}\sqrt{\frac{\mu_0}{\varepsilon_0}} \cdot \ln(\frac{D}{d})} \tag{2.4}$$

where Z_{L} represents the impedance of the feeding line (normally 50 Ω), d the external diameter of the pin and D the internal diameter of the outer conductor of the cell. Based on the equation

$$\hat{\eta}(\omega) = \hat{\rho}(\omega) \cdot z \cot z \tag{2.5}$$

with

$$z = \frac{\omega l}{c_0}\sqrt{\hat{\eta}(\omega)} \tag{2.6}$$

it is now possible to calculate the generalised complex permittivity $\hat{\eta}(\omega)$ from the absolute reflection coefficient.

However, for this purpose it is necessary to eliminate the signal intensity $V_0(\omega)$ of the wave moving forwards, which cannot be determined exactly by experimental means. Therefore, it is advisable to use a reference substance, whose dielectric properties should be as similar as possible to those of the sample. As its dielectric properties are both very well-known and – at least compared to other possible standard liquids – quite similar to those of DDAB/W/D mixtures, DMA was used as the reference throughout this work.

Thus, a *relative* reflection coefficient $\rho_{\mathrm{xr}}(\omega)$ can be calculated[58,61]

$$\hat{\rho}_{\mathrm{xr}}(\omega) = \frac{c}{\mathrm{i}\omega g l} \cdot \frac{\mathcal{L}_{\mathrm{i}\omega}\left[\frac{\mathrm{d}}{\mathrm{d}t}V_{\mathrm{r}}^{\mathrm{r}}(t)\right] - \mathcal{L}_{\mathrm{i}\omega}\left[\frac{\mathrm{d}}{\mathrm{d}t}V_{\mathrm{r}}^{\mathrm{x}}(t)\right]}{\mathcal{L}_{\mathrm{i}\omega}\left[\frac{\mathrm{d}}{\mathrm{d}t}V_{\mathrm{r}}^{\mathrm{r}}(t)\right] + \mathcal{L}_{\mathrm{i}\omega}\left[\frac{\mathrm{d}}{\mathrm{d}t}V_{\mathrm{r}}^{\mathrm{x}}(t)\right]} \tag{2.7}$$

instead of the absolute one, where $V_{\mathrm{r}}^{\mathrm{x}}(t)$ and $V_{\mathrm{r}}^{\mathrm{r}}(t)$ designate the relative time-dependent reflection intensities of the sample and the reference. It can be shown that the relative reflection coefficient is given by the expression:

$$\hat{\rho}_{\mathrm{xr}} = \frac{\hat{\eta}_{\mathrm{x}} \cdot \hat{z}_{\mathrm{r}} \cot(\hat{z}_{\mathrm{r}}) - \hat{\eta}_{\mathrm{r}} \cdot \hat{z}_{\mathrm{x}} \cot(\hat{z}_{\mathrm{x}})}{\hat{z}_{\mathrm{r}} \cot(\hat{z}_{\mathrm{r}}) \hat{z}_{\mathrm{x}} \cot(\hat{z}_{\mathrm{x}}) + g^2 \cdot \hat{\eta}_{\mathrm{x}}\hat{\eta}_{\mathrm{r}}(\omega l/c)^2} \tag{2.8}$$

Eq. (2.8) is the working equation of time-domain spectroscopy, where the expressions $\hat{z}_{\mathrm{x}}$ and $\hat{z}_{\mathrm{r}}$ are abbreviations containing the complex generalised permittivity of sample and reference, $\hat{\eta}_{\mathrm{x}}$ and $\hat{\eta}_{\mathrm{r}}$, respectively:

$$\hat{z}_{\mathrm{x}} = \frac{\omega l}{c}\sqrt{\hat{\eta}_{\mathrm{x}}} \tag{2.9}$$

$$\hat{z}_{\mathrm{r}} = \frac{\omega l}{c}\sqrt{\hat{\eta}_{\mathrm{r}}} \tag{2.10}$$

In order to obtain the complex permittivity from the relative reflection coefficient eq. (2.8) has to be resolved into $\hat{\eta}_x$. As there is no analytical solution of this problem, either an approximation using a Taylor series expansion of the term $z \cdot \cot z$ or, preferably, a numerical solution based on the Newton-Raphson procedure[112] has to be used.

The complete processing described above can be done at Regensburg University using the processing modules for the EXPLORER system implemented by Hölzl.[113] In the meantime, these modules have been transferred by Schrödle[167] to a PC-based system running under the operating system Linux; recent amendments, especially to improve the processing of conducting samples and/or references, have been implemented by Hunger.[118]

2.2.3 Frequency-Domain Reflectometry

Dielectric data in the frequency range $0.2 \lesssim \nu/\mathrm{GHz} \leq 20$ were acquired using a Hewlett Packard HP85070B coaxial probe and a HP8720D Vector Network Analyzer (VNA) at the institute of Professor Glenn Hefter, Murdoch University (Australia). A scheme of the cut-off cell is given in Figure 2.2. Temperature is controlled by a circulator-thermostat (Hetofrig) to ± 0.02 K, with a NIST-traceable accuracy of ± 0.05 K.

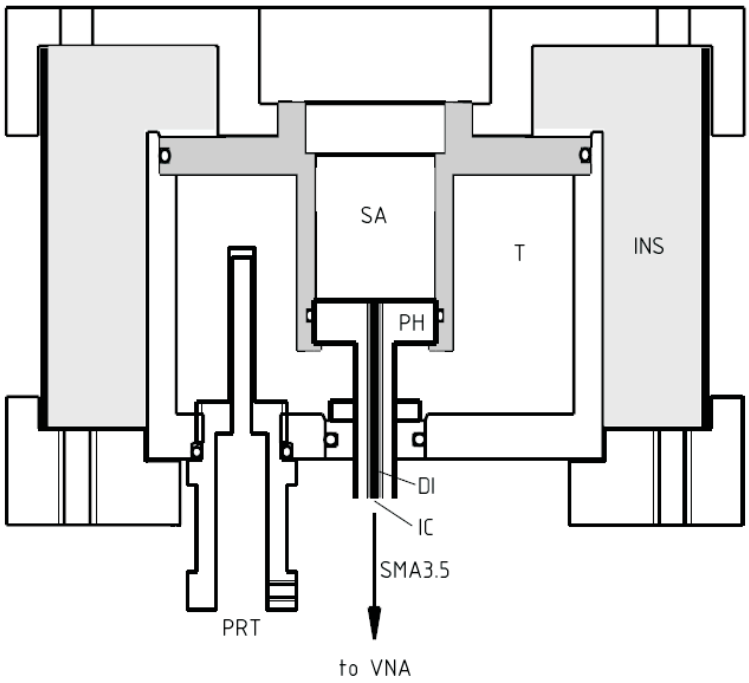

Figure 2.2: Scheme of a VNA cut-off cell for liquid samples.[168] **PH**: HP85070B coaxial probe head; **SA**: sample space; **T**: cleading filled with thermostatting liquid; **PRT**: opening for a platinum resistance temperature probe; **INS**: insulating rubber foam; **IC**: inner conductor of the probe-head; **DI**: dielectric material.

The VNA probes the relative complex reflection coefficient $\hat{\Gamma}_\mathrm{a}$ at the probe-head/sample interface. The relationship between $\hat{\Gamma}_\mathrm{a}$ and the normalised aperture impedance of the probe head, $\hat{Y}$, is given by:

$$\hat{\Gamma}_\mathrm{a} = \frac{1-\hat{Y}}{1+\hat{Y}} \tag{2.11}$$

$\hat{Y}$, in turn, can be used to calculate the complex dielectric properties $\hat{\varepsilon}_\mathrm{m}$ with the help of a simplified coaxial aperture opening model,[25,138] by solving the following equation numerically:

$$\hat{Y} = \frac{\mathrm{i}\hat{k}_\mathrm{m}^2}{\pi\hat{k}_\mathrm{c}\ln(b/a)}\left[\mathrm{i}\Big(I_1 - \frac{\hat{k}_\mathrm{m}^2 I_3}{2} + \frac{\hat{k}_\mathrm{m}^4 I_5}{24} - \frac{\hat{k}_\mathrm{m}^6 I_7}{720} + ...\Big) + \Big(I_2\hat{k}_\mathrm{m} - \frac{\hat{k}_\mathrm{m}^3 I_4}{6} + \frac{\hat{k}_\mathrm{m}^5 I_6}{120} - ...\Big)\right] \tag{2.12}$$

In eq. (2.12), $\hat{k}_\mathrm{c} = \omega\sqrt{\hat{\varepsilon}_\mathrm{c}\varepsilon_0\mu_0}$ and $\hat{k}_\mathrm{m} = \omega\sqrt{\hat{\varepsilon}_\mathrm{m}\varepsilon_0\mu_0}$ represent the propagation constants within the coaxial probe head and the sample, respectively. For the numerical solution of eq. (2.12), the first 28 probe constants I_i, calculated from a theoretical approach and optimised as described in ref.[25], are used.

In order to correct for signal distortions between the reference planes of the probe head and of the VNA, a standard three-point calibration is performed for the reflection coefficient $\hat{\Gamma}_\mathrm{a}$:

$$\hat{\Gamma}_\mathrm{a} = \frac{\hat{\Gamma}_\mathrm{m} - \hat{e}_\mathrm{d}}{\hat{e}_\mathrm{s}(\hat{\Gamma}_\mathrm{m} - \hat{e}_\mathrm{d}) + \hat{e}_\mathrm{r}} \tag{2.13}$$

The complex, frequency-dependent correction constants $\hat{e}_\mathrm{d}$, $\hat{e}_\mathrm{r}$ and $\hat{e}_\mathrm{s}$ are determined by three reference measurements of the uncorrected reflection coefficient $\hat{\Gamma}_\mathrm{m}$ and application of eq. (2.12). Air, a short (mercury) and a liquid whose dielectric properties should be similar to the investigated samples are used as reference standards. In this work, N,N-dimethylacetamide (DMA) has always been used as this third standard because its dielectric behaviour is both well-known and relatively similar to that of DDAB/W/D microemulsions. For a number of samples, measurements using benzonitrile as the third standard have been performed for comparative reasons; however, the results proved to be indistinguishable from those of the DMA calibrations.

VNA spectra used for further processing were obtained by calculating the average value of at least two consistent measurements of independent calibrations.

In previous studies, where the dielectric constant varied considerably between the samples of one series of measurements, a Padé approximation had been successfully applied for further correction of the VNA results.[168,181] Although the dielectric constants of DDAB/W/D microemulsions show only very little variation in the VNA frequency range, this procedure has also been tested for selected samples of this work. However, as the uncorrected data showed excellent agreement with the IFM measurements (which are thought to be very reliable as they are absolute values obtained without using any reference substances for calibration) and as the Padé correction did not yield any noticeable improvements, it was not used for the treatment of the present results.

2.2.4 Interferometry

Principles and Instrumentation

Interferometers work according to a transmission principle: by superposition of two waves, one passing the sample and one passing a reference path, a signal arises whose power is measured. A frequency-stabilised signal source supplies both a measuring and a reference branch. The measuring branch contains a phase shifter and the measuring cell, whereas the reference branch contains several precision attenuators. The measuring cell itself consists of a piece of waveguide filled with the sample, in which a probe is immersed whose position in the z direction is variable and can be determined using a precision gauge. Temperature is controlled by a circulating thermostat (Lauda RK 20) to ± 0.01 K. A block diagram of one of the instruments used in the Regensburg laboratories is given in Figure 2.3.

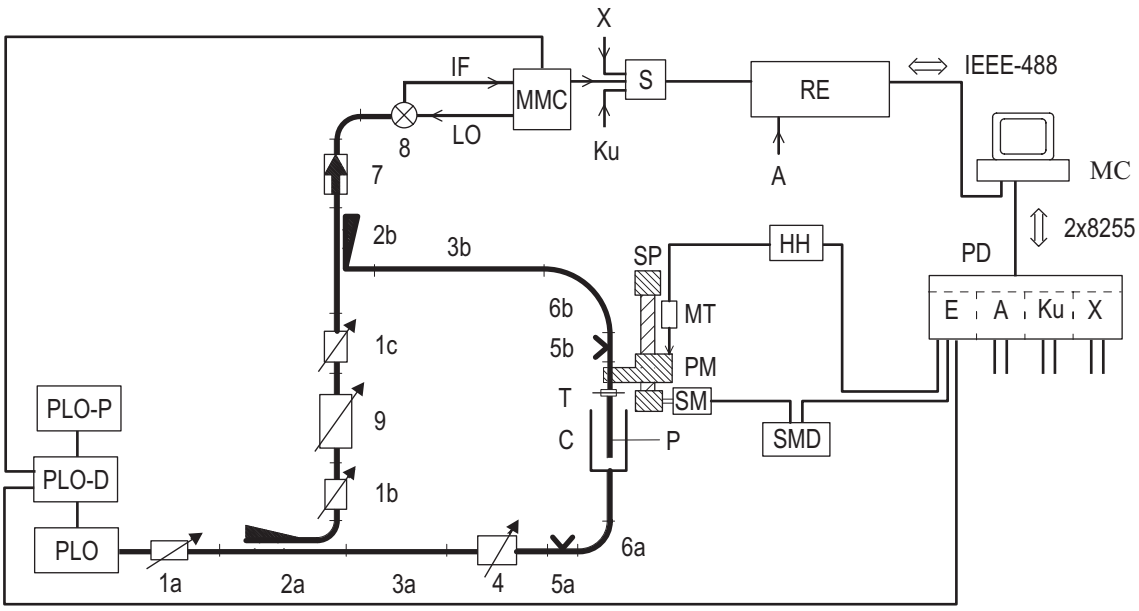

Figure 2.3: Block diagram of the E-band apparatus.[13] **1a,b,c**: variable attenuators; **2a,b**: directional couplers; **3a,b**: waveguide sections; **4**: precision phase shifter; **5a,b**: E/H tuners; **6a,b**: flexible waveguides; **7**: insulator; **8**: harmonic mixer; **9**: variable precision attenuator; **C**: cell; **HH**: bidirectional counter; **MC**: microcomputer; **MMC**: millimeter-wave to microwave converter; **MT**: digital length gauge; **P**: probe; **PD**: parallel interface unit; **PLO**: phase-locked oscillators; **PLO-D**: PLO control unit; **PLO-P**: PLO power supply; **PM**: probe mount; **RE**: precision receiver; **S**: electromechanical switch; **SM**: stepping motor; **SMD**: stepping motor control unit; **SP**: spindle and spindle mount; **T**: tapered transmission; bold lines symbolize semi-rigid microwave cables, normal lines data transfer connections.

More detailed descriptions of the instruments and the measurement principle have been published previously.[13,16,167] The maximum error in ε'' and η'' is 2% relative to the static permittivity ε of the sample.[6]

Solving the Wave Equation for a Rectangular Waveguide

In the frequency domain both the type and the frequency range of waves that can be transmitted are determined by the geometries and the dimensions of the wave-transmitting devices. To avoid signal distortions and mode conversions it is advisable to choose a waveguide geometry that only allows propagation of *one* mode. As the microwave range of the electromagnetic spectrum comprises wavelengths between 1 mm and 1 m and as the corresponding instruments must be of the same dimension several measuring stations are required to cover the complete frequency range.

Considering a harmonically oscillating field propagating in a rectangular waveguide of the width a (along the positive x-axis) and the height b (along the positive y-axis) it is sufficient to solve the wave equation for the z-component of the electric field.[155] The two remaining components can be determined from this with the help of the Maxwell equations (1.1) to (1.4).

Both the tangential component of the electrical field vector and the normal component of the magnetic field vector must be zero at metallic boundaries. Taking into account the particular geometry of a rectangular waveguide the boundary conditions for the solutions of the wave equation are obtained:

$$\text{for } X = 0 \text{ and } X = a : \begin{cases} \hat{E}_y(X, y, z) = 0 \\ \hat{E}_z(X, y, z) = 0 \\ \hat{H}_x(X, y, z) = 0 \end{cases} \tag{2.14}$$

and

$$\text{for } Y = 0 \text{ and } Y = b : \begin{cases} \hat{E}_x(x, Y, z) = 0 \\ \hat{E}_z(x, Y, z) = 0 \\ \hat{H}_y(x, Y, z) = 0 \end{cases} \tag{2.15}$$

The reduced wave equations (1.28) and (1.32) can be solved for harmonically oscillating fields propagating in the z direction using the ansatz functions

$$\hat{H}_z = H_0(x, y) \cdot \exp(\mathrm{i}\omega t - \hat{\gamma} z) \tag{2.16}$$

and

$$\hat{E}_z = E_0(x, y) \cdot \exp(\mathrm{i}\omega t - \hat{\gamma} z) \tag{2.17}$$

In eqs. (2.16) and (2.17) H_0 and E_0 represent the field amplitudes and $\hat{\gamma}$ the complex propagation constant, which is defined as:

$$\hat{\gamma} = \alpha + \mathrm{i}\beta \tag{2.18}$$

The real part α of the complex propagation constant is called the damping coefficient, and the imaginary part $\beta = 2\pi/\lambda_\mathrm{M}$ the phase constant, where λ_M is the medium wavelength.

The damping coefficient α characterizes the attenuation of the amplitude, whereas the phase constant β describes the phase rotation along the propagation direction.

Considering the boundary conditions for a rectangular waveguide as described by eqs. (2.14) and (2.15) the separation ansatzes (2.16) and (2.17) yield the following two field types

$$\hat{H}_z = H_0 \cdot \cos(\frac{m\pi}{a}x) \cdot \cos(\frac{n\pi}{b}y) \cdot \exp(\mathrm{i}\omega t - \hat{\gamma}z) \tag{2.19}$$

and

$$\hat{E}_z = E_0 \cdot \sin(\frac{m\pi}{a}x) \cdot \sin(\frac{n\pi}{b}y) \cdot \exp(\mathrm{i}\omega t - \hat{\gamma}z) \tag{2.20}$$

containing the natural numbers m and n. Taking into account the reduced wave equations (1.28) and (1.32) this yields the following condition for the complex propagation constant:

$$\hat{\gamma}_{mn}^2 = -\hat{k}^2 + (\frac{m\pi}{a})^2 + (\frac{n\pi}{b})^2 \tag{2.21}$$

Hence, for a rectangular waveguide of a given geometry there is an infinite number of solutions of the wave equation, which can be classified into TE (*transversal-electrical*) and TM (*transversal-magnetic*) modes. TM modes do not have any component of the magnetic field in z direction ($H_z = 0$), for TE modes the z component of the electric field is equal to zero ($E_z = 0$). Each mode has a characteristic propagation constant $\hat{\gamma}_{mn}$ and a cut-off wavelength $\lambda_{c,mn}$; the latter is the maximum wavelength that can be transmitted.[15] For measurement the TE_{10} mode is used as this is the only mode for which a frequency range exists where no other mode is able to propagate. For the waveguide geometry $a = 2b$ the technically useful range is given by:

$$0.53 \leq \frac{\lambda}{\lambda_{c,10}} \leq 0.8 \tag{2.22}$$

Linking eq. (2.18) to eq. (2.21) yields for a TE_{10} mode:

$$\hat{\gamma}_{10}^2(\omega) = -\hat{k}^2(\omega) + \left(\frac{\pi}{a}\right)^2 = (\alpha(\omega) - \mathrm{i}\beta(\omega))^2 \tag{2.23}$$

For the complex propagation constant $\hat{k}$ relations (1.30) and (1.33) apply; when these are inserted into eq. (2.23) the following expression is obtained for the generalised complex permittivity:

$$\hat{\eta}(\omega) = \left(\frac{c_0}{\omega}\right)^2 \cdot \left[\left(\frac{\pi}{a}\right)^2 - (\alpha + \mathrm{i}\beta)^2\right] \tag{2.24}$$

Using the medium wavelength $\lambda_\mathrm{M} = 2\pi/\beta$ and the cut-off wavelength for the empty waveguide, $\lambda_{c,10}^\mathrm{vac} = 2a$, it is now possible to calculate the complex permittivity from the

measurable quantities $\alpha(\nu)$, $\lambda_{\mathrm{M}}(\nu)$ and κ, according to eqs. (1.38) and (1.39):

$$\varepsilon'(\nu) = \left[\left(\frac{1}{\lambda_{c,10}^{\mathrm{vac}}}\right)^2 + \left(\frac{1}{\lambda_{\mathrm{M}}(\nu)}\right)^2 - \left(\frac{\alpha(\nu)}{2\pi}\right)^2\right] \cdot \left(\frac{c_0}{\nu}\right)^2 \tag{2.25}$$

$$\varepsilon''(\nu) = \frac{\alpha(\nu)}{\pi\lambda_{\mathrm{M}}(\nu)} \cdot \left(\frac{c_0}{\nu}\right)^2 - \frac{\kappa}{2\pi\nu\varepsilon_0} \tag{2.26}$$

For a coaxial waveguide the wave equation can be solved analogously. However, in this case only TEM (transversal-electromagnetic) waves are able to propagate, *i.e.* waves where the components of *both* the electric and the magnetic field are zero in the direction of propagation. For coaxial waveguides $\lambda_c = \infty$ applies.

Interference Measurements

In an interference measurement, the damping coefficient α and the medium wavelength λ_{M}, which are both necessary to calculate the complex permittivity, are determined simultaneously. For this, first the reference branch is completely closed and the probe is moved to a position of suitable signal amplitude, where the receiver is locked to the frequency that is to be investigated. Next, the instrument is aligned to total destructive interference using the phase shifter and the attenuators. Subsequently, the probe is moved to its starting position – without altering the positions of the phase shifter or the attenuators – and the actual measurement starts. While the probe is travelling across the minimum towards its final position the relative damping is registered and plotted as a function of the probe position.

When harmonically oscillating fields are applied the following relation holds for the reference branch:

$$\hat{E}_1(t) = \hat{E}_0 \exp(\mathrm{i}\omega t) \tag{2.27}$$

When z_0 is introduced as the optical path-length of the measuring branch seen from the minimum and $x = z_0 - z_0'$ as the relative deviation from the reference minimum, we obtain for the measuring branch:

$$\hat{E}_2(t,x) = \hat{E}_0 \, \exp(-\alpha x) \, \exp\Big(\mathrm{i}(\omega t + \pi - \beta x)\Big) \tag{2.28}$$

The summand π in the second exponential term results from the condition of destructive interference; it says that the phase difference $\Delta\varphi$ of the superposing waves must satisfy the equation:

$$\Delta\varphi = (2n+1)\pi, \qquad n \in \mathbb{Z} \tag{2.29}$$

The field arriving at the receiver is a sum of the fields propagating in the measuring and the reference branches:

$$\hat{E}(t,x) = \hat{E}_1(t) + \hat{E}_2(t,x) = \hat{E}_0 \exp(\mathrm{i}\omega t)\Big[1 + \exp(-\alpha x)\exp\big(\mathrm{i}(\pi - \beta x)\big)\Big] \tag{2.30}$$

The power P at the receiver is proportional to the square of the amplitude of the field existing there:

$$P = \hat{E} \cdot \hat{E}^* = E_0^2 \cdot I(x) \tag{2.31}$$

In this equation, I represents the interference function, which is defined as:

$$I(x) = \Big[1 + \exp(-\alpha x)\exp\big(\mathrm{i}(\pi - \beta x)\big)\Big] \cdot \Big[1 + \exp(-\alpha x)\exp\big(\mathrm{i}(\pi - \beta x)\big)\Big] \tag{2.32}$$

$$= 1 + \exp(-2\alpha x) + \exp(-\alpha x) \cdot 2\cos(-\pi + \beta x) \tag{2.33}$$

Only the relative attenuation $A(x)$ present at the receiver is experimentally accessible:

$$A(x) = 10\lg\frac{P(x)}{P_{\mathrm{ref}}} \tag{2.34}$$

As P_{ref} is unknown, it is normalised to the attenuation A_0, for which the relation $P_0 = E_0^2$ is valid:

$$\begin{aligned} A_{\mathrm{rel}}(x) &= A(x) - A_0 \\ &= 10\lg\frac{P(x)}{P_{\mathrm{ref}}} - 10\lg\frac{P_0}{P_{\mathrm{ref}}} \\ &= 10\lg\frac{P(x)}{P_0} \\ &= 10\lg\frac{E_0^2 \cdot I(x)}{E_0^2} \end{aligned} \tag{2.35}$$

This yields the following equation:[13]

$$\begin{aligned} A(z_0 - z_0') = A_0 + 10\lg\Big[1 + \exp\big(-2p\alpha(z_0 - z_0')\big)\Big] \\ - 2\cos\Big[\frac{2\pi}{\lambda_{\mathrm{M}}}(z_0 - z_0')\Big] \cdot \exp(-p\alpha(z_0 - z_0')) \end{aligned} \tag{2.36}$$

with the conversion factor

$$p = \left(20\lg\mathrm{e} \cdot \frac{\mathrm{dB}}{\mathrm{Np}}\right)^{-1} \tag{2.37}$$

The required quantities α and λ_{M} are obtained by a nonlinear fit to eq. (2.36).

2.3 Infrared Spectroscopy

As infrared spectroscopy has been used in this work only as a complementary experimental method to gain some further information for selected samples, this section does not aim to present an extensive discussion of the fundamentals on which this technique is based. For detailed information, the reader may be referred to the literature.[105,166,196] However, a brief summary reviewing the basic principles of infrared spectroscopy will be given on the next pages.

2.3.1 The Bouguer-Lambert-Beer Law

Taking into account eqs. 1.1 and 1.2 the electric field strength $\hat{E}(t,z)$ of a wave travelling a distance z can be expressed as[24]

$$\vec{E} = \vec{E}_0 \exp[\mathrm{i}(\omega t - \hat{\gamma} z)] \tag{2.38}$$

where the propagation coefficient $\hat{\gamma}$ is defined as

$$\hat{\gamma} = \sqrt{\hat{\mu}\mu_0(\hat{\varepsilon}\varepsilon_0\omega^2 - \mathrm{i}\omega\hat{\kappa})} \tag{2.39}$$

When non-magnetic materials like electrolyte solutions are concerned, $\hat{\mu} = 1$, so that eq. (2.39) can be simplified to

$$\hat{\gamma} = \frac{\omega}{c_0}\sqrt{\hat{\eta}(\nu)} \tag{2.40}$$

where c_0 is the vacuum speed of light and $\hat{\eta}(\nu)$ the generalised complex permittivity. Introducing the complex refractive index

$$\hat{n}(\nu) = \sqrt{\hat{\eta}(\nu)} = n(\nu) - \mathrm{i}k(\nu) \tag{2.41}$$

yields the frequency-dependent optical constants of a system, the refractive index $n(\nu)$ and the absorption index $k(\nu)$. Taking into account eqs. (2.40) and (2.41) eq. (2.38) can be expressed as:

$$\vec{E} = \vec{E}_0 \exp\left[-\mathrm{i}\omega\left(t - \frac{nz}{c_0}\right)\right] \exp\left[-\frac{\omega k z}{c_0}\right] \tag{2.42}$$

The intensity of an electromagnetic wave, described by the Poynting vector $\vec{I}$,[77] is directly proportional to the square of the electric field strength $\vec{E}$:

$$|\vec{I}| = \varepsilon_0 c_0 |\vec{E}|^2 \tag{2.43}$$

Inserting eq. (2.42) in eq. (2.43) and combining all terms that do not contain the absorption index k to a constant output intensity I_0 yields the Bouguer-Lambert-Beer law[81]

$$I = I_0 \exp\left[-\frac{2\omega k z}{c_0}\right] = I_0 \exp[-4\pi\bar{\nu} k z] = I_0 \exp[-\alpha(\bar{\nu}) z] \tag{2.44}$$

with the wavenumber $\bar{\nu} = \nu/c_0$ and the absorption coefficient $\alpha(\bar{\nu}) = 4\pi\bar{\nu}k$. In eq. (2.44), the distance z is interpreted as the layer thickness d.

As the energy required to stimulate a molecular vibration is by far larger than that required to stimulate a rotation of a molecule, every vibration spectrum exhibits a superposition of rotation bands. In the gas phase this superposition may be resolved as the rotational fine structure of a vibration band. In condensed phases, due to the interactions of a molecule with its neighbours, a resolution is no longer possible; a broadening of the vibrational bands can be observed instead. Therefore, it is appropriate to introduce the integrated extinction E_{int} as a measure for the intensity I as defined in eq. (2.44):

$$E_{\text{int}} = \ln \frac{I}{I_0} = \int_{band} \alpha(\bar{\nu}) \mathrm{d}\bar{\nu} \cdot c \; d = \epsilon \; c \; d \tag{2.45}$$

where ϵ is the extinction coefficient and c the molar concentration of the sample.

2.3.2 The Attenuated Total Reflectance Method

The attenuated total reflectance (ATR) method, developed by Harrick[104] and Fahrenfort,[80] allows the investigation of samples showing strong absorption in the infrared region.

The use of the attenuated total reflectance method in infrared spectroscopy is based on the interaction of an electromagnetic wave between the crystal, an optically dense medium of refractive index n_1 and the sample (medium 2, $n_2 < n_1$). At the interface between the two media the wave may either be reflected or transmitted, according to the Snell refraction law:

$$n_1 \sin \varphi_1 = n_2 \sin \varphi_2 \tag{2.46}$$

If the angle of incidence φ_1 is larger than the critical angle φ_c

$$\varphi_1 > \varphi_c = \arcsin \frac{n_2}{n_1} \tag{2.47}$$

total reflectance is observed; otherwise transmission with partial reflectance takes place.

Although the angle of reflexion is equal to the angle of incidence the reflected beam will be slightly shifted. This is caused by diffraction at the edges of the incoming beam, leading to a penetration of energy into medium 2 despite total reflectance. Along the interface a surface wave is observed, featuring an exponential decay with increasing distance from medium 1. At a distance d_e, called the penetration depth,

$$d_e = \frac{\lambda}{2\pi n_1 \sqrt{\sin^2 \varphi_1 - \left(\frac{n_2}{n_1}\right)^2}} \tag{2.48}$$

the amplitude of the electric field has decreased to e^{-1} of its initial value. Obviously, d_e – and thus the absorption – depends on the wavelength; this effect is accounted for by an ATR correction of the recorded FTIR spectra. As medium 2 absorbs energy the amount

of energy of the reflected beam will be smaller than that of the incoming beam. Thus, an attenuated total reflection is observed.

Detailed information about the ATR method can be found in the literature.[105,166]

2.3.3 Instrumentation

Infrared spectra were recorded at room temperature (approx. 24 ℃) using a FTIR spectrometer (Jasco, FT/IR-610, resolution 0.5 cm^{-1}) equipped with a standard KBr beam splitter. For all measurements, a commercial single-bounce HATR cell using a ZnSe crystal (Spectra-Tech) that had been equipped with a sample vessel developed in our laboratories was used.[18] Detailed information on the cell is given by Wismeth.[196]

2.4 Additional Measurements

2.4.1 Density

As volume fractions are an essential parameter for the interpretation of the microemulsion structure, density data are required to allow conversion from the masses of the microemulsion and its components. Density measurements were carried out using a digital densitometer (Anton Paar, type DMA 602/mPDS4000 system, accuracy to $5 \cdot 10^{-3}$ kg m^{-3}), whose measuring cell was temperature-controlled to 25.00 ± 0.005 °C with a circulating thermostat. Average values of at least two independent measurements were calculated for each sample.

The density ρ is calculated from the period τ of a vibrating tube filled with the sample according to the following equation:[133]

$$\rho = A^{-1}(\tau^2 - B) \tag{2.49}$$

A and B are parameters specific to the instrument, defined as

$$A = \frac{\tau^2_{H_2O} - \tau^2_{N_2}}{\rho_{H_2O} - \rho_{N_2}} \tag{2.50}$$

and

$$B = \tau^2_{H_2O} - A\,\rho_{H_2O} \tag{2.51}$$

which were determined by calibration with dried nitrogen and degassed Millipore water before every series of measurements. For the density of pure water at 298.15 K the IAPWS-IF97 value of 997.048 kg m^{-3} was used.[183] The density of nitrogen was calculated according to the van-der-Waals equation

$$\left(p + a\frac{\rho^2}{M^2}\right)\left(1 - b\frac{\rho}{M}\right) = \frac{\rho}{M}\mathrm{R}\,T \tag{2.52}$$

where p represents the atmospheric pressure, M the molar mass of nitrogen, R the gas constant and T the cell temperature. For nitrogen, the van-der-Waals coefficients a and b assume the values $a = 0.1370\,\mathrm{Pa\,m^6\,mol^{-2}}$ and $b = 3.87 \cdot 10^{-5}\,\mathrm{m^3\,mol^{-1}}$.[62]

2.4.2 Conductivity

Conductivities of the microemulsions studied in this work were estimated from the low-frequency TDR data. As the dielectric loss ε'' should be equal to zero for very low frequencies (*i.e.* the dipoles are able to follow the electric field without any delay) the conductivity κ was adjusted accordingly. As κ was always found to be less than $0.5\,\mathrm{S\,m^{-1}}$ this procedure, which substantially reduced the cost of the measurements, is justifiable.

2.4.3 Refractive Indices

To calculate the polarisabiliy α of DDAB the refractive indices, n, of DDAB/ethanol mixtures were measured at 298.15 K with an Abbé type refractometer (Carl Zeiss Jena), using the sodium D line. The medium mole refraction $[R]$ of a binary mixture can be calculated using the relation:[33]

$$[R] = \frac{x_1 M_1 + x_2 M_2}{\rho} \cdot \frac{n^2 - 1}{n^2 + 2} \tag{2.53}$$

On the other hand, [R] depends linearly on the partial mole refractions $[R_i]$ of its components

$$[R] = x_1[R_1] + x_2[R_2] \tag{2.54}$$

which, in turn, can be converted into the polarisability α of the component i according to:

$$[R_i] = \frac{4\pi \mathrm{N_A}}{3}\,\alpha_i \tag{2.55}$$

Chapter 3

Data Analysis

3.1 Selection of Samples in the System Didodecyldimethylammonium Bromide / Water / n-Dodecane

Figure 3.1 shows the position of the microemulsion phase, commonly labelled 'L_2' in the literature,[89,177] in the phase diagram of DDAB/W/D at 25 °C as published by Skurtveit and Olsson.[177] As phase diagrams of DDAB/W/D and related systems found in the literature are typically given in mass fractions, w_i, this scale has also be adopted in the present work. Also the compositions of the samples studied in this work are given in mass fractions to facilitate their localisation in the phase diagram. However, care must be taken as mass fractions may be very misleading when considering the molecular ratios in the system DDAB/W/D, since $M_{\mathrm{DDAB}} \gg M_{\mathrm{D}} \gg M_{\mathrm{W}}$. Therefore, the molar ratios, W, are also included in Table 3.1.

The composition of the DDAB/W/D samples investigated in the present study is described by labels of the type

$$z\ y\ x$$

in this work, where

- z designates the D mass fraction (see Table 3.1 and Figure 3.1)
- y designates the DDAB/W ratio (see Table 3.1 and Figure 3.1)
- x designates the co-electrolyte concentration (see Tables 3.4 to 3.7). For $x \neq 0$, the added co-electrolyte is designated by a subsequent letter (L: LiBr, N: NaBr, C: CsBr, T: $(CH_3)_4NBr$).

For example, a sample labelled '22b0' is a DDAB/W/D microemulsion without an added co-electrolyte ($x = 0$), exhibiting a dodecane mass fraction of $w_{\mathrm{D}} = 0.35$ ($z = 2$) and a DDAB/W mass ratio of $w_{\mathrm{DDAB}}/w_{\mathrm{W}} = 0.547$ ($y = 2\mathrm{b}$).

Note, however, that samples labelled by the numbers '1' to '19' are exploration measurements and do not follow this nomenclature; their composition can be seen from Table 3.2.

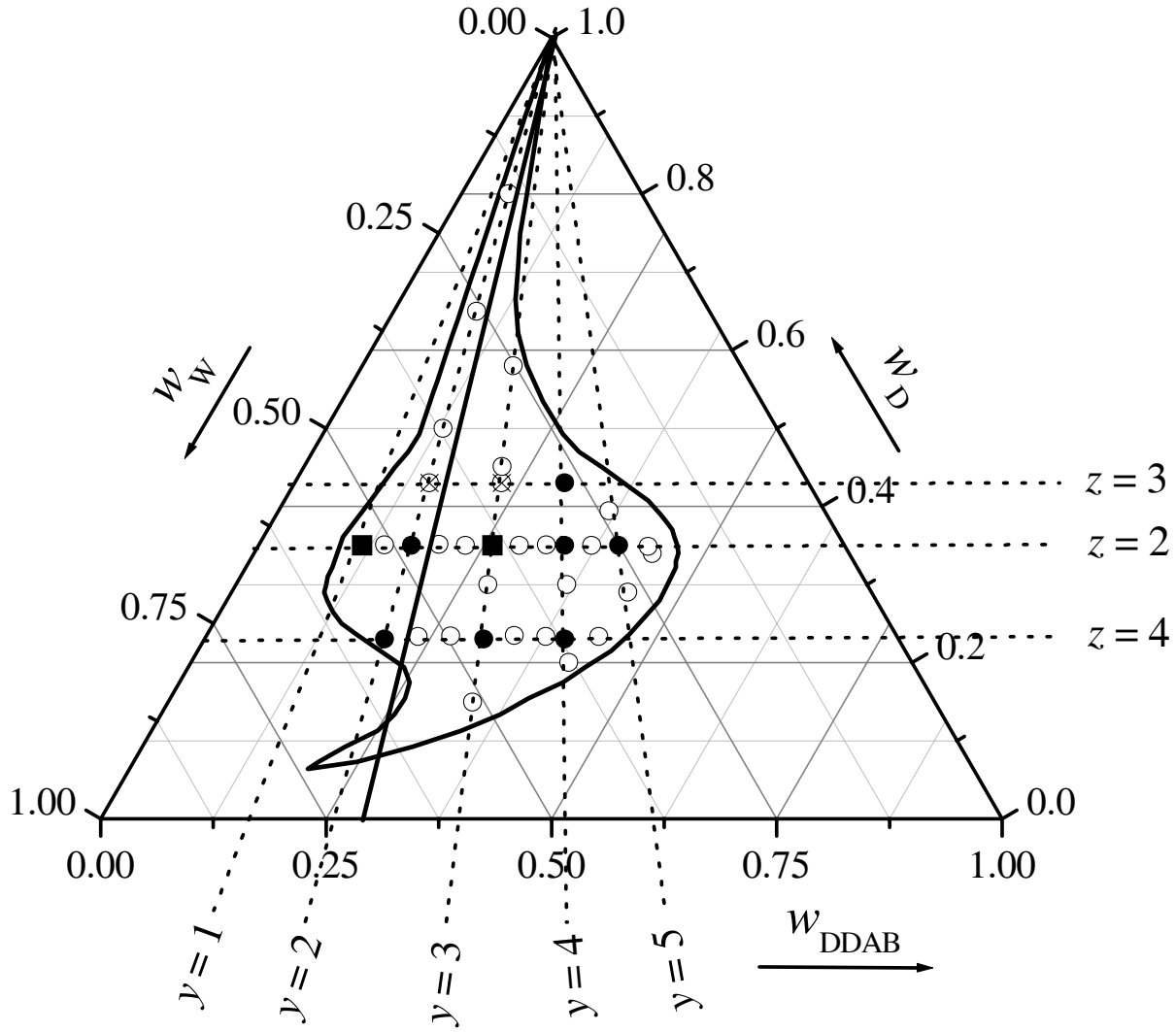

Figure 3.1: Phase diagram[177] showing the microemulsion phase (L_2) of the system DDAB/W/D at 25 °C and samples investigated in this work. ○: DDAB/W/D without co-ions; ⊗: exploration measurements of DDAB/NaBr(aq)/D; ●: DDAB/W/D and exploration measurements of DDAB/NaBr(aq)/D; ■: DDAB/W/D and detailed concentration series of DDAB/LiBr(aq)/D, DDAB/NaBr(aq)/D, DDAB/CsBr(aq)/D and DDAB/$(CH_3)_4$NBr(aq)/D. The full line represents the percolation threshold postulated by Barnes *et al.*[11], dotted lines are given as a visual aid.

Table 3.1: Values of the Variables y and z Used in This Work to Identify Points in the DDAB/W/D Phase Diagram. For Conversion Purposes, Values of the Molar Water/Surfactant Ratio, $W = n_W/n_{DDAB}$, Are Also Included.

y	1	1a	2	2a	2b	3	3a	3b	4	4a	5	5a
w_{DDAB}/w_W	0.216	0.275	0.358	0.443	0.547	0.667	0.806	0.971	1.10	1.32	1.62	2.03
W	119	93.4	71.7	58.0	46.9	38.5	31.9	26.4	23.3	19.5	15.9	12.7
z	2	3	4									
w_D	0.35	0.43	0.23									

Unlike for a binary system, where only the ratio between its two components can be varied, the situation is less straightforward for a ternary system: *a priori*, it is not obvious which 'paths' across L_2 should be chosen for investigation.

In this work, the selection was made on the basis of the structural model of Barnes *et al.*[11] These authors reported a percolation threshold between separated water droplets in oil and a bicontinuous network of channels at a constant W/DDAB mass ratio of 2.5 (full line in Figure 3.1). As it is widely accepted that for dispersed particles coated by a surfactant and embedded in a medium the particle size and shape should only be determined by the dispersed phase/surfactant ratio, only the concentration of the dispersed water droplets, but not their geometrical properties should vary along a dodecane dilution line below the percolation threshold. Above this threshold the number of water channels crossing the medium dodecane should increase with decreasing dodecane content.

Thus, five dodecane dilution lines at different W/DDAB ratios were investigated in this work. However, both dielectric and conductivity results did not show the abrupt changes that were expected from the model of Barnes *et al.*, but rather gradual modifications. At the same time, co-ion exploration measurements throughout the microemulsion phase using NaBr as the co-electrolyte showed a very high co-ion sensitivity for high W/DDAB ratios that was decreasing gradually, but very significantly for decreasing W/DDAB ratios.

Therefore, it was regarded as essential to gain a better understanding of these gradual changes induced by the W/DDAB ratio. Thus, two lines with constant D mass fractions ($z = 2$ and $z = 4$) and varying W/DDAB ratios were thoroughly investigated using a large number of additional samples.

As the co-ion exploration measurements showed a very high sensitivity at very high W/DDAB ratios, point 21 was chosen for detailed investigations using extensive concentration series with the co-electrolytes LiBr, NaBr, CsBr and $(CH_3)_4NBr$. Only univalent bromide ions have been selected in order to confine the co-electrolyte effect to the effect of univalent cations; as the surfactant DDAB already adds a large amount of Br^- anions to the system (approx. 0.5 M - 3.5 M in the aqueous phase, depending on the DDAB/W ratio) , an increase in Br^- concentration of a few mM can be regarded to be negligible.

To allow comparisons, concentration series with the co-electrolytes LiBr, NaBr, CsBr and $(CH_3)_4NBr$ have also been investigated at point 23.

Note that all dielectric measurements of this study were performed at standard temperature ($T = 298.15$ K).

3.2 Studied Phase Points

3.2.1 Data Summary

The compositions, densities and conductivities of the samples investigated in this work are summarised in Tables 3.2 to 3.7. Also included are the volume fractions of the water droplets, ϕ, which are calculated according to

$$\phi = \phi_{\mathrm{W}} + \phi_{\mathrm{DDAB}} \cdot \frac{v_{\mathrm{h}}}{v_{\mathrm{h}} + v_{\mathrm{t}}} \tag{3.1}$$

where $v_{\mathrm{h}} = 120$ Å^3 and $v_{\mathrm{t}} = 704$ Å^3 are the volumes of the DDAB head group and tails, respectively.[53]

Table 3.2: Mass Fractions, w, Conductivity, κ, Density, ρ, and Volume Fraction of the Water Droplets, ϕ, of the DDAB/W/D Microemulsions Investigated in This Work at 25 °C: D Dilution Lines.

sample name	w_{DDAB}	w_{W}	w_{D}	κ / S m^{-1}	ρ / kg m^{-3}	ϕ
420	0.2021	0.5643	0.2336	0.06	918.83	0.549
220	0.1714	0.4786	0.3500	0.05	887.87	0.449
8	0.1319	0.3681	0.5000	0.01	850.39	0.331
9	0.0923	0.2577	0.6500	0	816.60	0.223
10	0.0527	0.1473	0.8000	0		
13	0.3382	0.5127	0.1491	0.50	942.16	0.533
430	0.3068	0.4597	0.2335	0.32	919.11	0.467
14	0.2799	0.4202	0.2999	0.25	900.32	0.418
230	0.2597	0.3907	0.3496	0.24	887.46	0.384
15	0.2198	0.3293	0.4509	0.17	860.44	0.313
16	0.1679	0.2522	0.5799	0.11	830.32	0.232
11	0.4195	0.3805	0.2000	0.46	924.83	0.412
440	0.4021	0.3640	0.2339	0.41	916.27	0.392
12	0.3670	0.3330	0.3000	0.39	897.87	0.350
240	0.3408	0.3091	0.3501	0.37	885.88	0.323
340	0.2998	0.2721	0.4281	0.28		
18	0.4401	0.2701	0.2898	0.40	898.30	0.303
250	0.4025	0.2477	0.3498	0.39	884.08	0.276
19	0.3668	0.2389	0.3943	0.33	872.14	0.258
1	0.4423	0.2181	0.3396	0.38		

Table 3.3: Mass Fractions, w, Conductivity, κ, Density, ρ, and Volume Fraction of the Water Droplets, ϕ, of the DDAB/W/D Microemulsions Investigated in This Work at 25 °C: Series with Constant D Mass Fractions.

sample name	w_{DDAB}	w_{W}	w_{D}	κ / S m^{-1}	ρ / kg m^{-3}	ϕ
210	0.1154	0.5346	0.3500	0	889.29	0.492
21a0	0.1401	0.5095	0.3504	0	891.18	0.475
220	0.1714	0.4786	0.3500	0.05	887.87	0.449
22a0	0.1997	0.4503	0.3500	0.09	889.47	0.428
22b0	0.2300	0.4201	0.3499	0.18	888.13	0.407
230	0.2600	0.3900	0.3500	0.24	887.49	0.384
23a0	0.2900	0.3599	0.3501	0.29	886.78	0.361
23b0	0.3201	0.3297	0.3502	0.34	886.38	0.338
240	0.3410	0.3090	0.3500	0.37	885.92	0.323
24a0	0.3698	0.2802	0.3500	0.36	884.97	0.301
250	0.4025	0.2477	0.3498	0.39	884.08	0.276
25a0	0.4352	0.2147	0.3501	0.37	884.21	0.254
420	0.2019	0.5649	0.2332	0.06	919.91	0.549
42a0	0.2358	0.5307	0.2335	0.19	921.15	0.523
42b0	0.2713	0.4948	0.2339	0.24	920.37	0.495
430	0.3068	0.4598	0.2334	0.32	920.19	0.467
43a0	0.3419	0.4237	0.2344	0.35	918.75	0.439
43b0	0.3772	0.3895	0.2333	0.39	918.40	0.412
440	0.4013	0.3640	0.2347	0.41	917.36	0.392
44a0	0.4363	0.3302	0.2335	0.44	916.36	0.366

Table 3.4: Co-Electrolyte Concentration, c, Mass Fractions, w, and Conductivity, κ, of the DDAB/NaBr(aq)/D Microemulsions Investigated in This Work at 25 °C.

sample name	c_{NaBr}/mM	w_{DDAB}	w_{W}	w_{D}	κ / S m^{-1}
211N	0.05	0.1153	0.5349	0.3498	0.02
212N	0.10	0.1154	0.5342	0.3504	0
213N	0.18	0.1154	0.5344	0.3502	0.01
214N	0.25	0.1154	0.5347	0.3499	0
215N	0.50	0.1152	0.5352	0.3496	0.01
216N	1.0	0.1151	0.5359	0.3490	0
219N	0.65	0.1154	0.5346	0.3500	0
2110N	0.80	0.1154	0.5346	0.3500	0.01
221N	1.0	0.1699	0.4803	0.3498	0.03
222N	7.0	0.1699	0.4803	0.3498	0.02
231N	1.0	0.2600	0.3900	0.3500	0.25
232N	5.0	0.2597	0.3904	0.3499	0.25
234N	10	0.2596	0.3901	0.3503	0.24
241N	1.0	0.3408	0.3091	0.3501	0.34
242N	10	0.3410	0.3091	0.3499	0.32
251N	1.0	0.4031	0.2469	0.3500	0.36
253N	25	0.4027	0.2472	0.3501	0.38
321N	1.0	0.1495	0.4221	0.4284	0
322N	7.0	0.1497	0.4219	0.4284	0
331N	1.0	0.2290	0.3428	0.4282	0.19
332N	10	0.2288	0.3433	0.4279	0.19
341N	1.0	0.2998	0.2721	0.4281	0.30
342N	10	0.3000	0.2719	0.4281	0.27
421N	1.0	0.2003	0.5661	0.2336	0.07
422N	7.0	0.2005	0.5661	0.2334	0.06
431N	1.0	0.3068	0.4597	0.2335	0.29
432N	10	0.3064	0.4602	0.2334	0.32
441N	1.0	0.4021	0.3640	0.2339	0.36
442N	10	0.4018	0.3645	0.2337	0.43

Table 3.5: Co-Electrolyte Concentration, c, Mass Fractions, w, Conductivity, κ, Density, ρ, and Volume Fraction of the Water Droplets, ϕ, of the DDAB/LiBr(aq)/D Microemulsions Investigated in This Work at 25 °C.

sample name	c_{LiBr}/mM	w_{DDAB}	w_{W}	w_{D}	κ / S m^{-1}	ρ / kg m^{-3}	ϕ
211L	0.05	0.1154	0.5337	0.3509	0.01		
212L	0.10	0.1153	0.5349	0.3498	0		
213L	0.18	0.1153	0.5340	0.3507	0		
214L	0.25	0.1155	0.5343	0.3502	0.02	889.54	0.494
215L	0.50	0.1154	0.5347	0.3499	0.01	890.25	0.494
216L	1.0	0.1155	0.5343	0.3502	0.01	890.10	0.494
219L	0.65	0.1152	0.5350	0.3498	0	888.95	0.494
2110L	0.80	0.1154	0.5348	0.3498	0	890.46	0.494
231L	1.0	0.2600	0.3901	0.3499	0.24	886.80	0.384
232L	5.0	0.2597	0.3901	0.3502	0.24	887.09	0.384
233L	7.0	0.2599	0.3898	0.3503	0.24		
234L	10	0.2601	0.3898	0.3501	0.25	887.94	0.383

Table 3.6: Co-Electrolyte Concentration, c, Mass Fractions, w, Conductivity, κ, Density, ρ, and Volume Fraction of the Water Droplets, ϕ, of the DDAB/CsBr(aq)/D Microemulsions Investigated in This Work at 25 °C.

sample name	c_{CsBr}/mM	w_{DDAB}	w_{W}	w_{D}	κ / S m^{-1}	ρ / kg m^{-3}	ϕ
211C	0.05	0.1154	0.5342	0.3504	0		
212C	0.10	0.1155	0.5345	0.3500	0.01	889.67	0.494
213C	0.18	0.1155	0.5345	0.3500	0		
214C	0.25	0.1152	0.5355	0.3493	0	889.65	0.494
215C	0.50	0.1153	0.5350	0.3497	0.01	889.88	0.494
216C	1.0	0.1154	0.5349	0.3497	0	890.46	0.494
219C	0.65	0.1154	0.5345	0.3501	0	889.85	0.494
2110C	0.80	0.1154	0.5345	0.3501	0	889.73	0.494
231C	1.0	0.2598	0.3899	0.3503	0.24	887.32	0.384
232C	5.0	0.2599	0.3900	0.3501	0.22		
233C	7.0	0.2598	0.3901	0.3501	0.24		
234C	10	0.2596	0.3909	0.3495	0.24	887.54	0.384

Table 3.7: Co-Electrolyte Concentration, c, Mass Fractions, w, Conductivity, κ, Density, ρ, and Volume Fraction of the Water Droplets, ϕ, of the DDAB/$(CH_3)_4NBr$(aq)/D Microemulsions Investigated in This Work at 25 °C.

sample name	$c_{(CH_3)_4NBr}$/mM	w_{DDAB}	w_W	w_D	κ / S m^{-1}	ρ / kg m^{-3}	ϕ
211T	0.05	0.1154	0.5348	0.3498	0		
212T	0.10	0.1154	0.5345	0.3501	0.01		
213T	0.18	0.1155	0.5343	0.3502	0.01		
214T	0.25	0.1154	0.5346	0.3500	0.01	890.32	0.494
215T	0.50	0.1153	0.5349	0.3498	0		
216T	1.0	0.1153	0.5350	0.3497	0	889.79	0.494
219T	0.65	0.1153	0.5347	0.3500	0		
2110T	0.80	0.1154	0.5344	0.3502	0		
231T	1.0	0.2600	0.3896	0.3504	0.25	887.02	0.383
232T	5.0	0.2598	0.3903	0.3499	0.22		
233T	7.0	0.2599	0.3900	0.3501	0.21		
234T	10	0.2584	0.3885	0.3531	0.22	886.65	0.382

3.2.2 Density

It is remarkable that the density data for all D dilution lines could be well fitted by the same straight line, $\rho = (974.886 - 250.217 \cdot w_D)$ kg m^{-3}, as can be seen from Figure 3.2. Apparently, ρ is decreasing with an increasing dodecane fraction, whereas its dependence on the water/surfactant ratio, as plotted in Figure 3.3, is very weak. For the co-electrolyte concentration series studied in this work, density measurements have only been performed for selected samples, as the addition of co-electrolytes does not seem to have any significant influence on the density data.

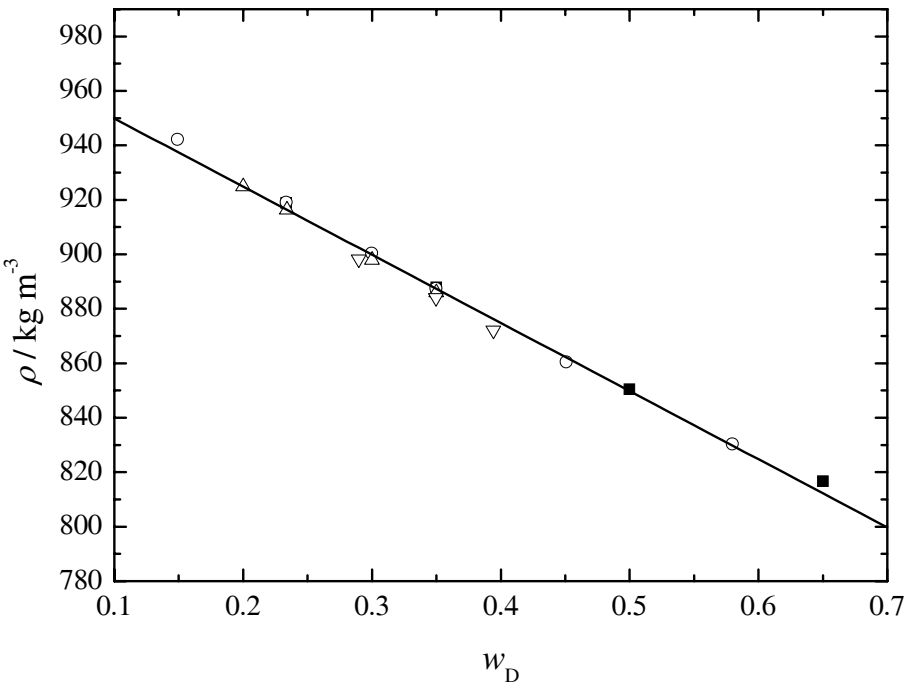

Figure 3.2: Density, ρ, of DDAB/W/D microemulsions as a function of the dodecane mass fraction, w_{D}, at 25 ℃. ■ : $w_{\mathrm{DDAB}}/w_{\mathrm{W}} = 0.358$; ∘ : $w_{\mathrm{DDAB}}/w_{\mathrm{W}} = 0.660$; △ : $w_{\mathrm{DDAB}}/w_{\mathrm{W}} = 1.10$; ▽ : $w_{\mathrm{DDAB}}/w_{\mathrm{W}} = 1.63$.

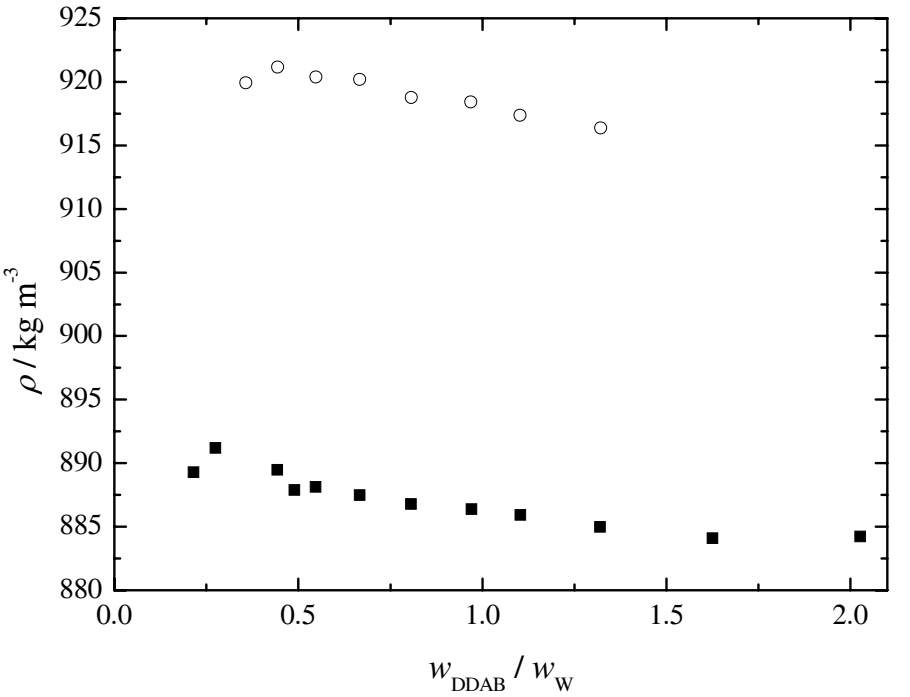

Figure 3.3: Density, ρ, of DDAB/W/D microemulsions as a function of the surfactant/water ratio , $w_{\mathrm{DDAB}}/w_{\mathrm{W}}$, at 25 ℃. ■ : $w_{\mathrm{D}} = 0.35$; ∘ : $w_{\mathrm{D}} = 0.23$.

3.2.3 Conductivity

As can be seen from Figure 3.4 the conductivity κ of the DDAB/W/D microemulsions investigated in this work is increasing steadily with increasing DDAB/water ratio until it reaches a kind of plateau value at $w_{\mathrm{DDAB}}/w_{\mathrm{W}} \gtrsim 1.2$ ($W \lesssim 21$). However, this increase is already beginning well before the percolation threshold as predicted by Barnes *et al.*[11] and proceeds much more smoothly than it would be expected for static percolation.

Considering a dodecane dilution line at a constant surfactant/water ratio, κ is always decreasing with increasing dodecane content (see Figure 3.5). The present results are in good agreement with conductivity measurements by Lenz and Hoffmann, who studied one dodecane dilution line situated very close to one of the lines investigated in this work.[137]

Co-electrolyte additions of the concentrations studied in this work do not show any significant influence on the conductivity data (see Tables 3.2 to 3.7), highlighting the fact that the concentration of mobile ions is determined by the amount of DDAB.

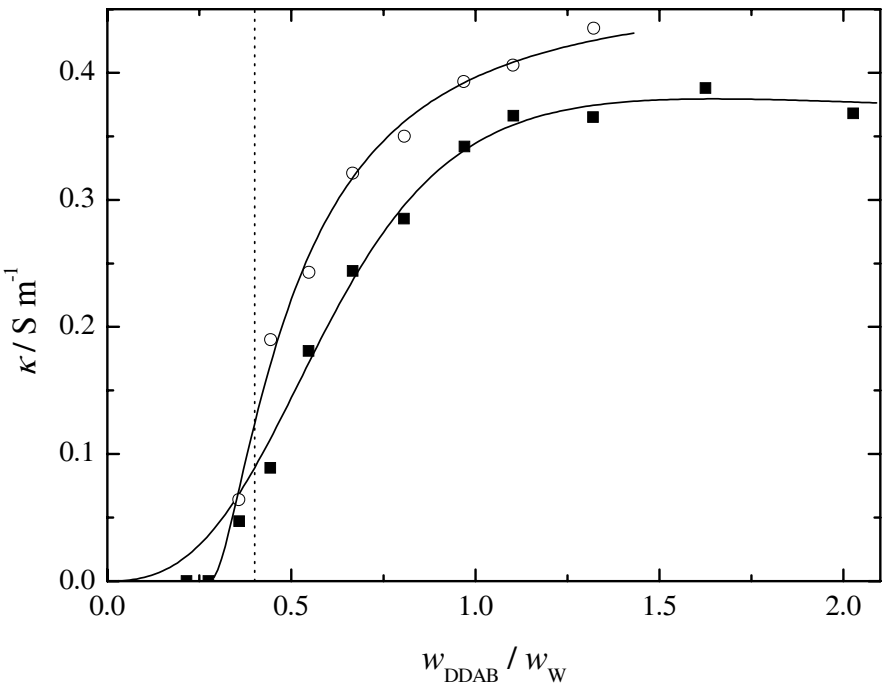

Figure 3.4: Conductivity, κ, of DDAB/W/D microemulsions as a function of the surfactant/water ratio , $w_{\mathrm{DDAB}}/w_{\mathrm{W}}$, at 25 °C. ■ : $w_{\mathrm{D}} = 0.35$; ○ : $w_{\mathrm{D}} = 0.23$. Full lines are only given as a visual aid; dotted line: percolation threshold predicted by Barnes *et al.*[11]

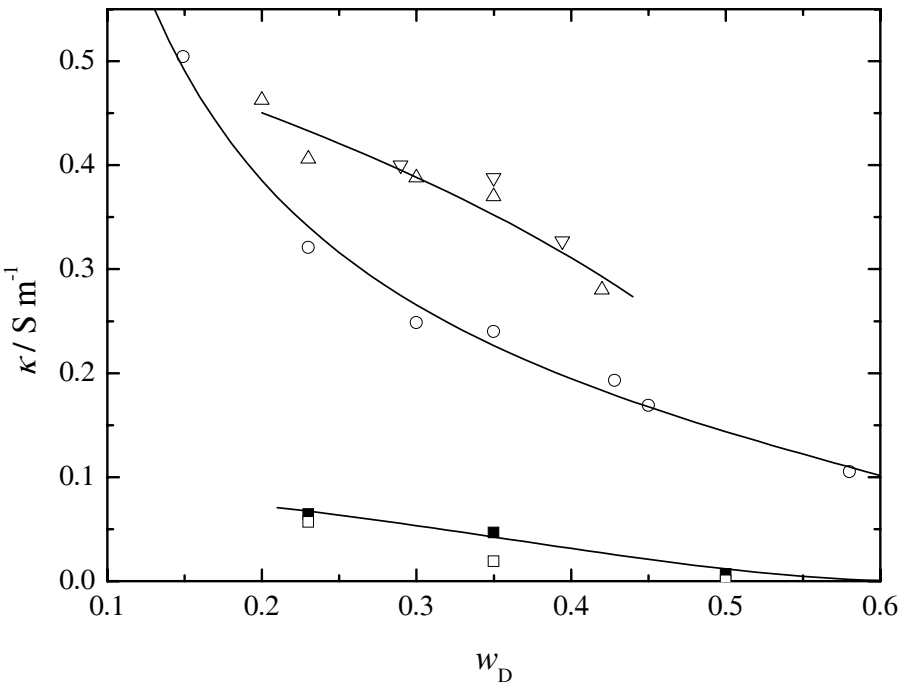

Figure 3.5: Conductivity, κ, of DDAB/W/D microemulsions as a function of the dodecane mass ratio, w_{D}, at 25 ℃. ■ : $w_{\mathrm{DDAB}}/w_{\mathrm{W}} = 0.358$; ∘ : $w_{\mathrm{DDAB}}/w_{\mathrm{W}} = 0.660$; △ : $w_{\mathrm{DDAB}}/w_{\mathrm{W}} = 1.10$; ▽ : $w_{\mathrm{DDAB}}/w_{\mathrm{W}} = 1.63$. Literature values by Lenz and Hoffmann[137] (□ : $w_{\mathrm{DDAB}}/w_{\mathrm{W}} = 0.40$) are also included. Lines are given as a visual aid.

3.3 Dielectric Relaxation Spectroscopy

3.3.1 General Remarks

Knowledge of the frequency-dependence of the complex permittivity is never sufficient to allow conclusions with respect to molecular processes. To do this, the measured data triples $(\nu_i, \varepsilon_i^{'}, \varepsilon_i^{''})$ have to be fitted using one of the relaxation models presented in chapter 1.3. This fit yields the characteristic quantities of dielectric relaxation, ε_i, τ_i and $\varepsilon_{\infty,i}$, and empirical parameters of the relaxation model.

To identify the model which is most suitable for the description of the experimental data the following criteria are applied in order of priority.

1. The values of the fitting parameters must be physically reasonable. For example, negative relaxation times do not have any physical meaning.

2. The value of the error function χ^2 (see eq. (3.2)) of the fit should be as low as possible.

3. When describing a concentration series it should be avoided to use more than one relaxation model. At least, the fitting parameters of a concentration series have to be compatible to each other.

4. The number of fitting parameters should be as small as possible.

As – according to the Kramers-Kronig relation[27] – the real and the imaginary parts of complex permittivity are not independent of each other but may be affected differently by experimental errors both parts must be fitted simultaneously. This has been carried out using the processing software MWFIT, which is based on the Levenberg-Marquardt-procedure;[22,142] the latter is an algorithm minimising the error function

$$\chi^2 = \frac{1}{2\,m - n} \sum_{i=1}^{m} \left[\left(\frac{\varepsilon'_i - \varepsilon'_{i,\mathrm{calc}}}{w(\varepsilon'_i)} \right)^2 + \left(\frac{\varepsilon''_i - \varepsilon''_{i,\mathrm{calc}}}{w(\varepsilon''_i)} \right)^2 \right] \tag{3.2}$$

which measures the quality of the fit. In eq. (3.2), m represents the number of data triples, n the number of fitting parameters, $\hat{\varepsilon}_i$ the measured and $\hat{\varepsilon}_{i,\mathrm{calc}}$ the calculated permittivity. The scale factor $1/(2m - n)$ accounts for the unequal number of experimental values and fitting parameters; w is a weighting factor.

Unweighted fits ($w(\varepsilon'_i) = w(\varepsilon''_i) = 1$) have been used throughout this work. This appeared to make sense because – due to the high precision of the frequency-domain instruments – systematic errors are one order of magnitude larger than stochastical errors;[113] under those circumstances standard deviations fail to be meaningful weighting factors. Hence, the error given by the software MWFIT is not a standard deviation but a measure of uncertainty describing the 'softness' of the relaxation parameter.[180] Detailed information about the mathematical fundamentals of MWFIT is given by Steger.[180]

3.3.2 Salt-Free Microemulsions

All dielectric spectra of DDAB/W/D microemulsions could be very well described by assuming a superposition of six (for $w_{\mathrm{DDAB}}/w_{\mathrm{W}} \lesssim 0.45$, *i.e.* $W \gtrsim 58$) or five (for $w_{\mathrm{DDAB}}/w_{\mathrm{W}} \gtrsim 0.55$, *i.e.* $W \lesssim 47$) Debye processes (6D/5D model); an example for this superposition can be seen in Figure 3.6. It should be emphasized that even the low-amplitude process 4 could always be resolved without fixing any of the relaxation parameters. However, the relaxation parameters of process 1 must be regarded as rough estimates, because only the higher-frequency edge of this process is within the frequency range experimentally accessible with our instruments. Similarly, the parameters of process 2 are not very accurate, due to the poor quality of most of the TDR data in this frequency range.

It is indeed possible to fit also the DDAB/W/D spectra with high water contents ($W \gtrsim 58$) using a 5D model, which yields only slightly worse values for the error function χ^2. However, this leads to a marked discontinuity in τ_4, dropping from $\sim$ 1000 ps for

$w_{\mathrm{DDAB}}/w_{\mathrm{W}} \lesssim 0.45$ to ~ 200 ps for $w_{\mathrm{DDAB}}/w_{\mathrm{W}} \gtrsim 0.55$. Additionally, the values of both the amplitudes S_i and the relaxation times τ_i for the high-frequency processes 5 and 6 are much more scattered than when a 6D model is used.

Other conceivable relaxation models did not yield any convincing results. In particular, no improvements could be achieved when replacing one of the Debye equations by a Cole-Cole or Cole-Davidson equation.

All fitting parameters are given in Tables 3.8 to 3.10; Figures 3.7 to 3.12 compare experimental spectra and their fits.

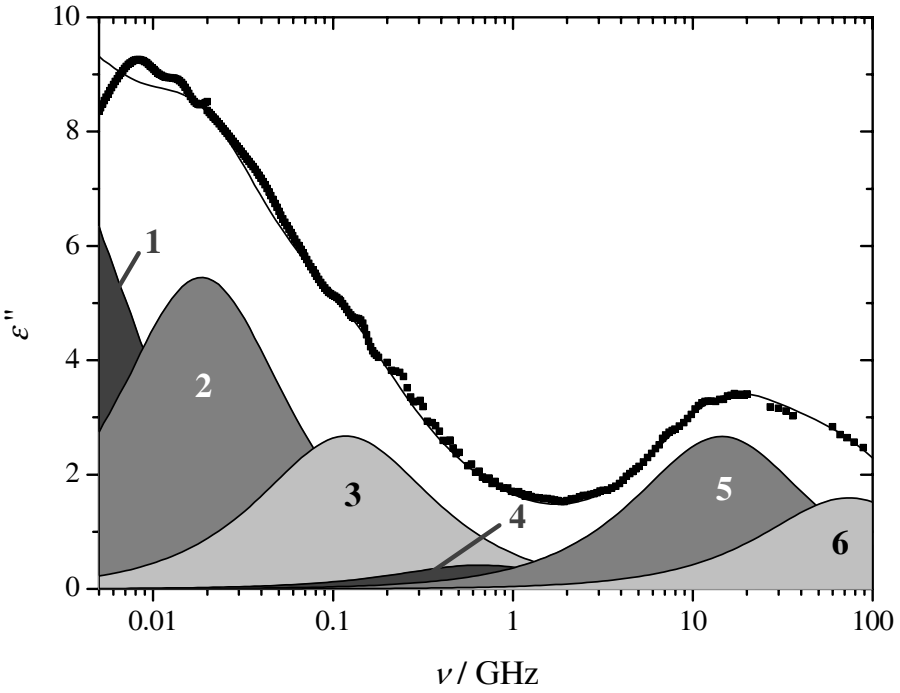

Figure 3.6: Dielectric loss curve for a DDAB/W/D microemulsion (sample 22a0) at 25 °C. Data are fitted by a superposition of six Debye equations.

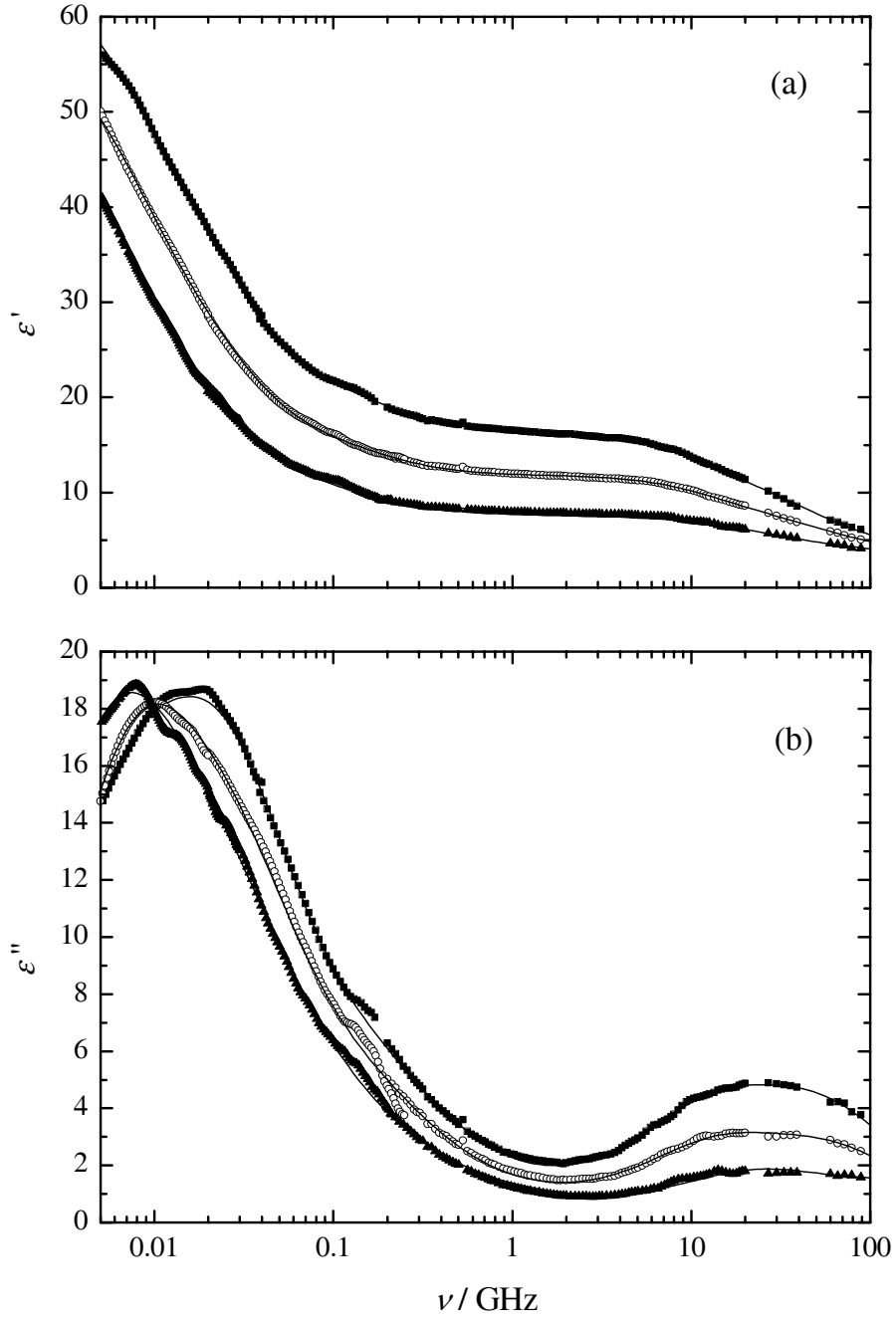

Figure 3.7: Dielectric permittivity (a) and loss (b) spectra for DDAB/W/D microemulsions at 25 ℃. ■ :sample 420; ○: sample 220; ▲: sample 8.

Table 3.8: Dielectric Relaxation Parameters of DDAB/W/D Microemulsions at 25 °C: Dodecane Dilution Lines.

sample	ε_1	τ_1 / ps	ε_2	τ_2 / ps	ε_3	τ_3 / ps	ε_4	τ_4 / ps	ε_5	τ_5 / ps	ε_6	τ_6 / ps	ε_∞	χ^2
420	65.59	24419	45.07	6313	21.00	817	16.48	124	16.11	11.47	9.712	2.687	3.956	0.0253
220	57.76	20520	30.18	5607	15.61	988	12.16	207	11.70	10.88	7.176	2.234	3.544	0.0291
8	54.56	27368	24.79	6952	11.43	1127	7.885	122	7.820	10.18	5.207	1.807	2.972	0.0223
13	149.8	39696	33.62	9489			22.26	284	19.97	13.86	10.06	3.661	3.844	0.1078
430	86.79	47430	24.28	4746			17.53	273	15.54	12.94	7.943	3.061	3.811	0.0530
14	57.31	29568	17.95	2952			15.48	286	13.49	13.03	6.884	2.864	3.606	0.0485
230	57.93	41500	18.75	8738			13.21	163	12.04	12.38	6.247	2.720	3.425	0.0371
15	23.75	14283	12.72	3743			11.13	229	9.789	11.55	4.861	2.130	2.919	0.0516
16	27.40	63599	12.86	8230			8.992	415	7.520	11.36	3.901	1.813	2.628	0.0451
11	130.8	38931	27.20	8486			16.14	129	14.41	13.84	6.867	3.151	3.408	0.0739
12	86.02	39163	16.73	7011			13.67	151	11.91	13.38	5.593	2.592	3.067	0.1065
340	63.44	48556	19.01	12179			11.07	153	9.733	13.24	4.640	2.746	3.082	0.0414
18	99.83	47163	24.10	8996			12.05	95.4	10.45	13.70	4.658	2.401	3.109	0.0742
19	82.72	50410	17.30	11167			10.28	74.3	8.944	12.52	3.980	1.933	2.894	0.0423
1	74.72	41628	13.72	7722			10.09	97.7	8.708	15.51	4.264	2.946	2.982	0.0895

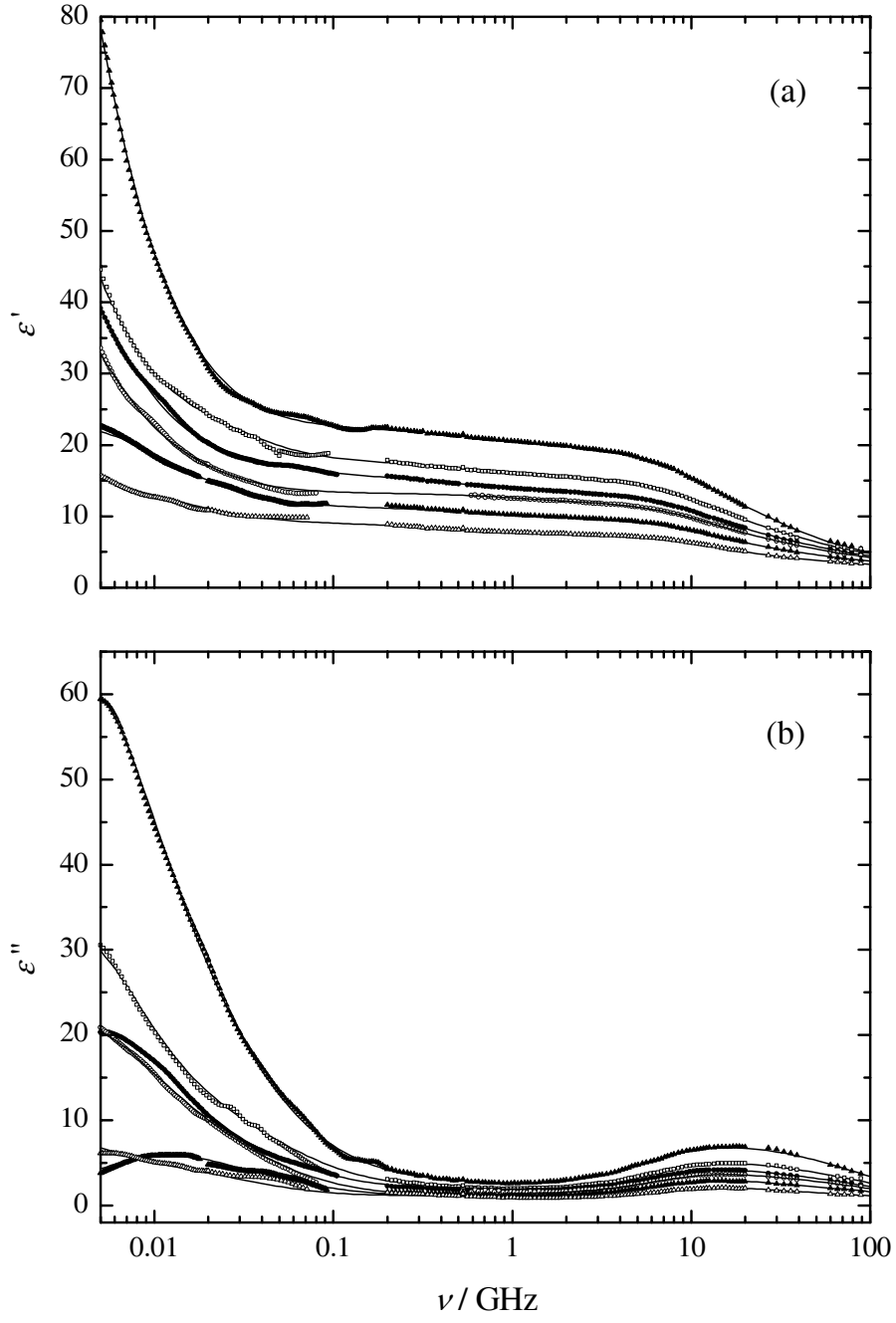

Figure 3.8: Dielectric permittivity (a) and loss (b) spectra for DDAB/W/D microemulsions at 25 ℃. ■ : sample 13; □ : sample 430; •: sample 14; ○: sample 230; ▲: sample 15; △: sample 16.

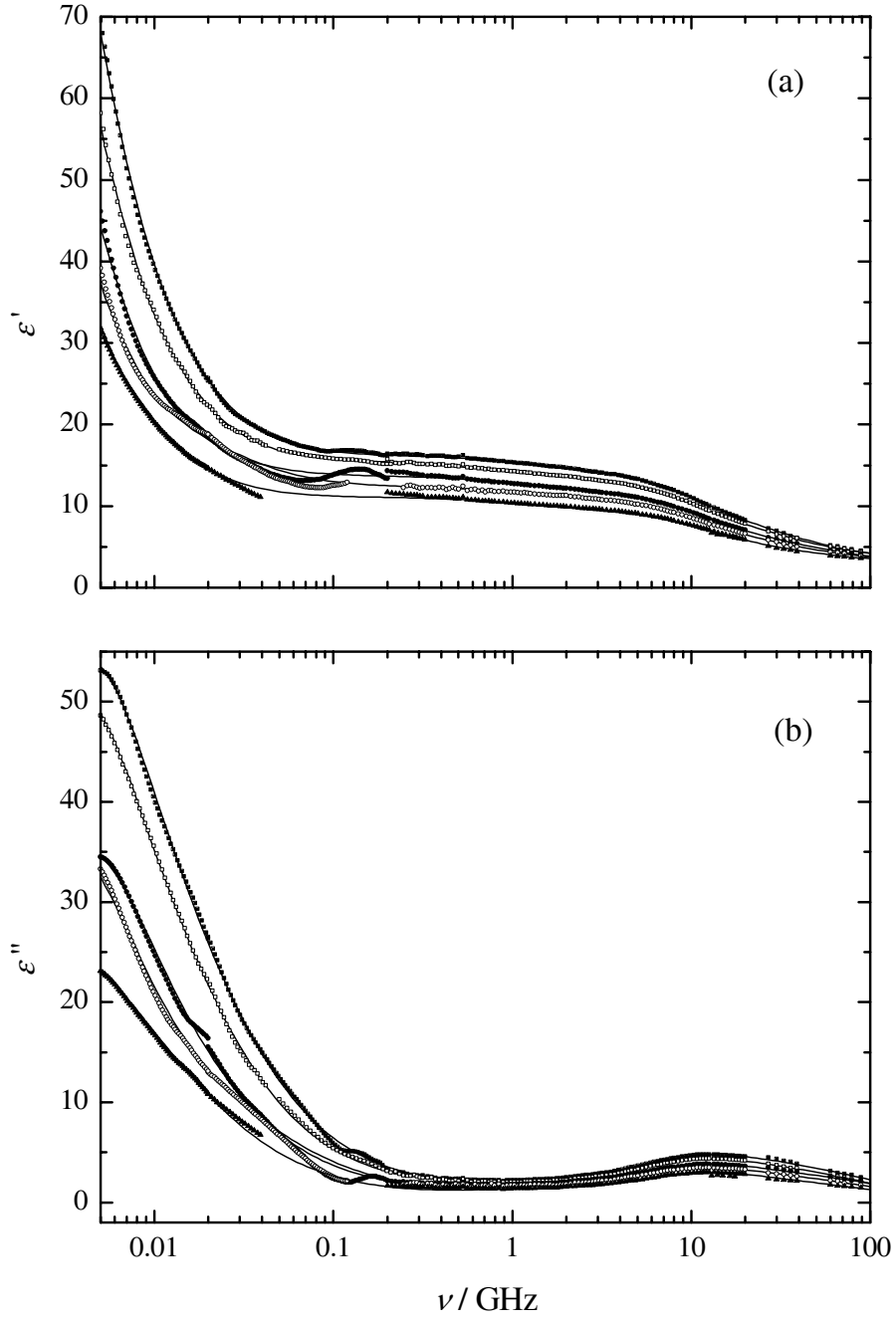

Figure 3.9: Dielectric permittivity (a) and loss (b) spectra for DDAB/W/D microemulsions at 25 ℃. ■ : sample 11; □ : sample 440; ●: sample 12; ○: sample 240; ▲: sample 340.

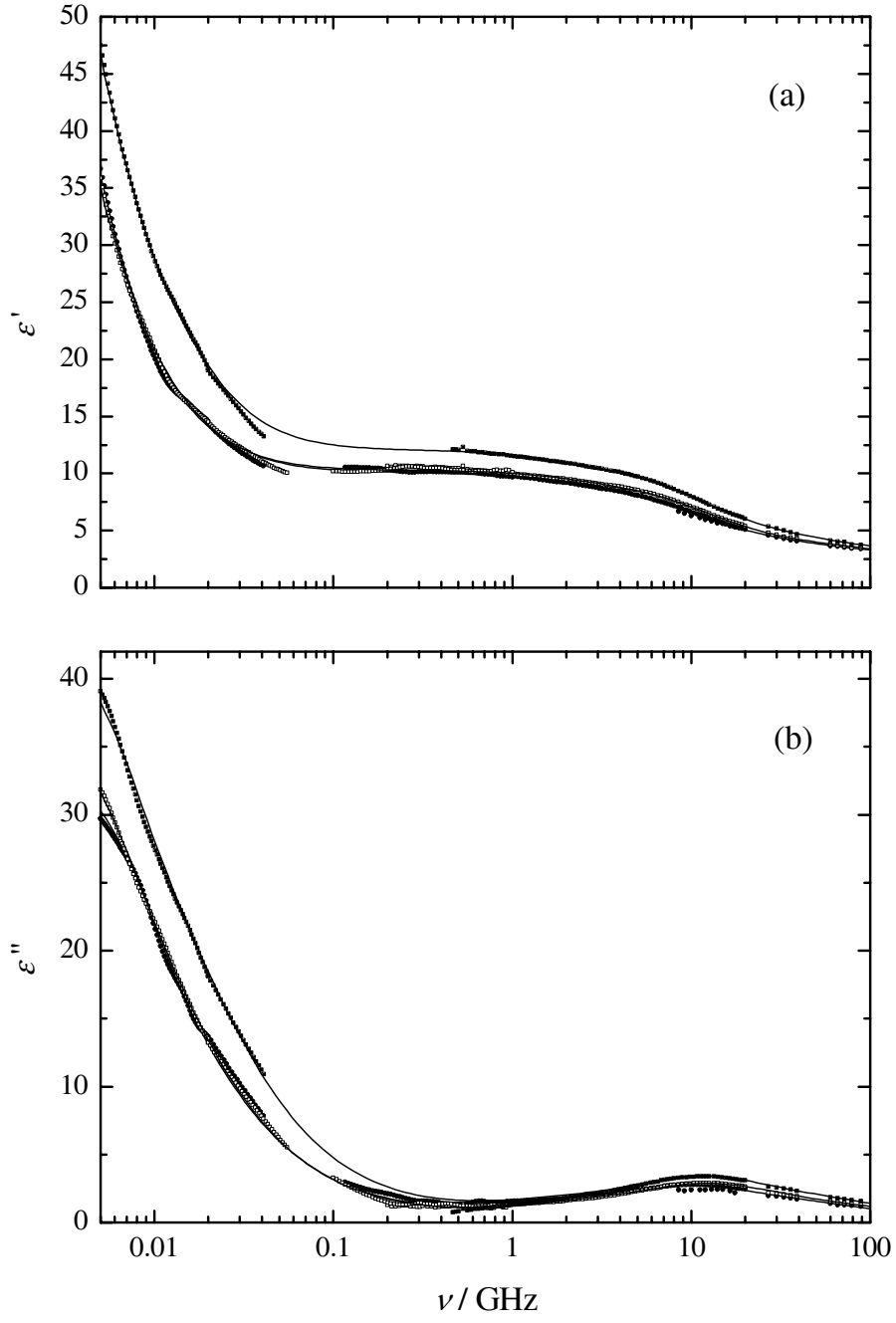

Figure 3.10: Dielectric permittivity (a) and loss (b) spectra for DDAB/W/D microemulsions at 25 ℃. ■ : sample 18; □ : sample 19; •: sample 1.

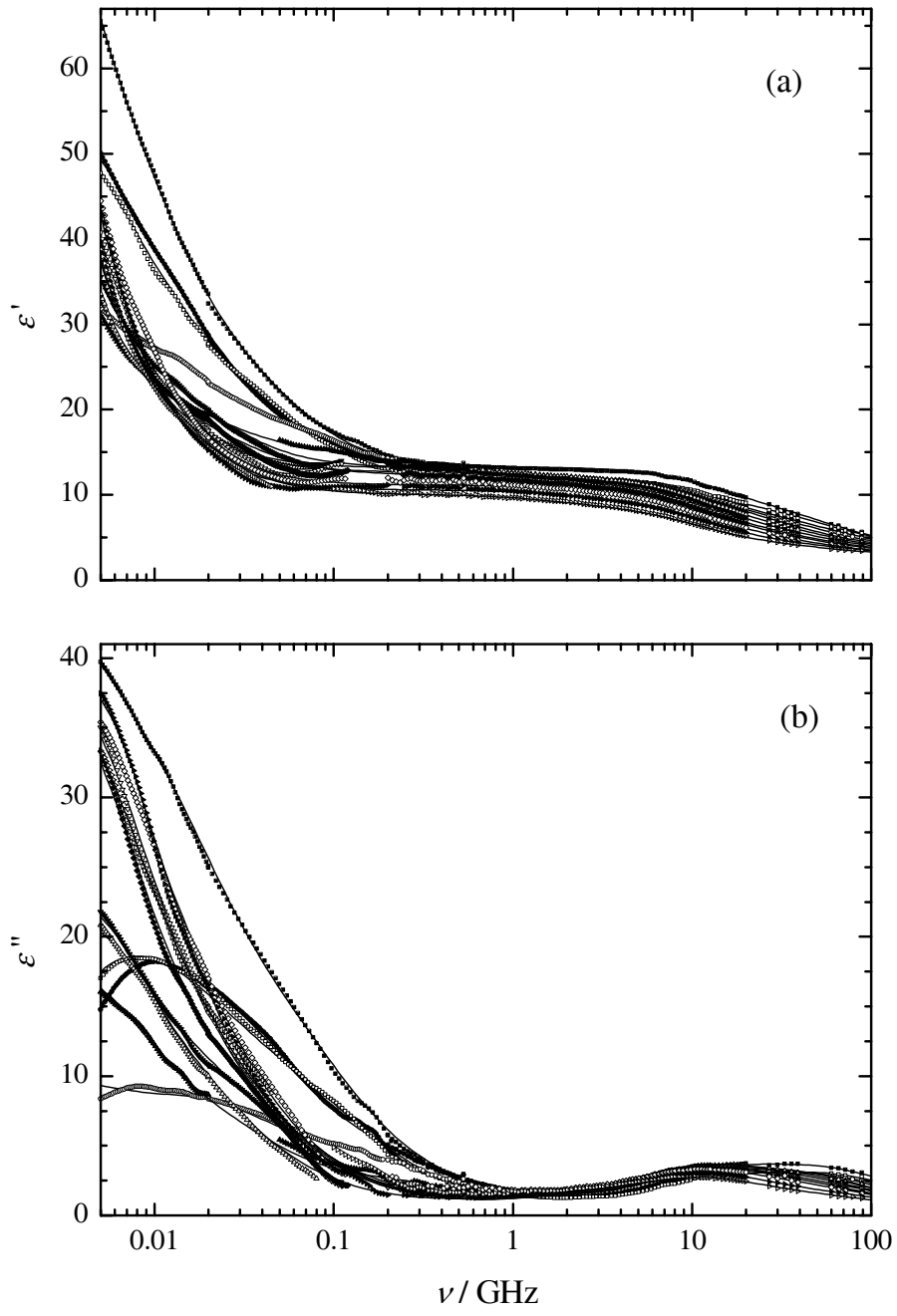

Figure 3.11: Dielectric permittivity (a) and loss (b) spectra for DDAB/W/D microemulsions at 25 ℃. ■ : sample 210; □ : sample 21a0; ●: sample 220; ○: sample 22a0; ▲: sample 22b0; △: sample 230; ▼: sample 23a0; ▽: sample 23b0; ♦: sample 240; ◊: sample 24a0; ►: sample 250; ▷: sample 25a0.

Table 3.9: Dielectric Relaxation Parameters of DDAB/W/D Microemulsions at 25 °C: Constant Dodecane Ratios.

sample	ε_1	τ_1 / ps	ε_2	τ_2 / ps	ε_3	τ_3 / ps	ε_4	τ_4 / ps	ε_5	τ_5 / ps	ε_6	τ_6 / ps	ε_∞	χ^2
210	121.6	58548	55.02	13541	26.36	2995	13.98	559	13.11	10.06	7.960	2.170	3.627	0.0405
21a0	61.29	30095	36.12	10365	21.85	2421	12.20	195	11.74	9.837	7.420	1.925	3.490	0.0462
220	57.76	20520	30.18	5607	15.61	988	12.16	207	11.70	10.88	7.176	2.234	3.544	0.0291
22a0	44.59	61426	29.05	8568	18.15	1352	12.80	242	11.97	10.98	6.638	2.160	3.452	0.0327
22b0	53.09	46531	21.07	7981	15.75	1160	13.14	199	12.07	11.87	6.610	2.659	3.515	0.0091
230	57.93	41500	18.75	8738			13.21	163	12.04	12.38	6.247	2.720	3.425	0.0371
23a0	63.97	45459	21.61	6045			13.26	197	11.83	13.07	5.937	2.823	3.338	0.0304
23b0	89.87	47402	18.76	8638			12.73	163	11.32	13.18	5.405	2.534	3.114	0.0544
240	89.27	51918	18.12	4817			12.39	153	11.05	13.79	5.329	2.871	3.169	0.1102
24a0	88.87	44230	22.70	11355			11.16	56.4	9.993	12.88	4.772	2.564	2.924	0.0801
250	88.47	39878	14.26	8008			10.57	64.2	9.257	12.86	4.216	2.022	2.857	0.0982
25a0	86.59	49074	17.61	7440			10.05	96.3	8.706	14.51	4.061	2.249	2.821	0.0540

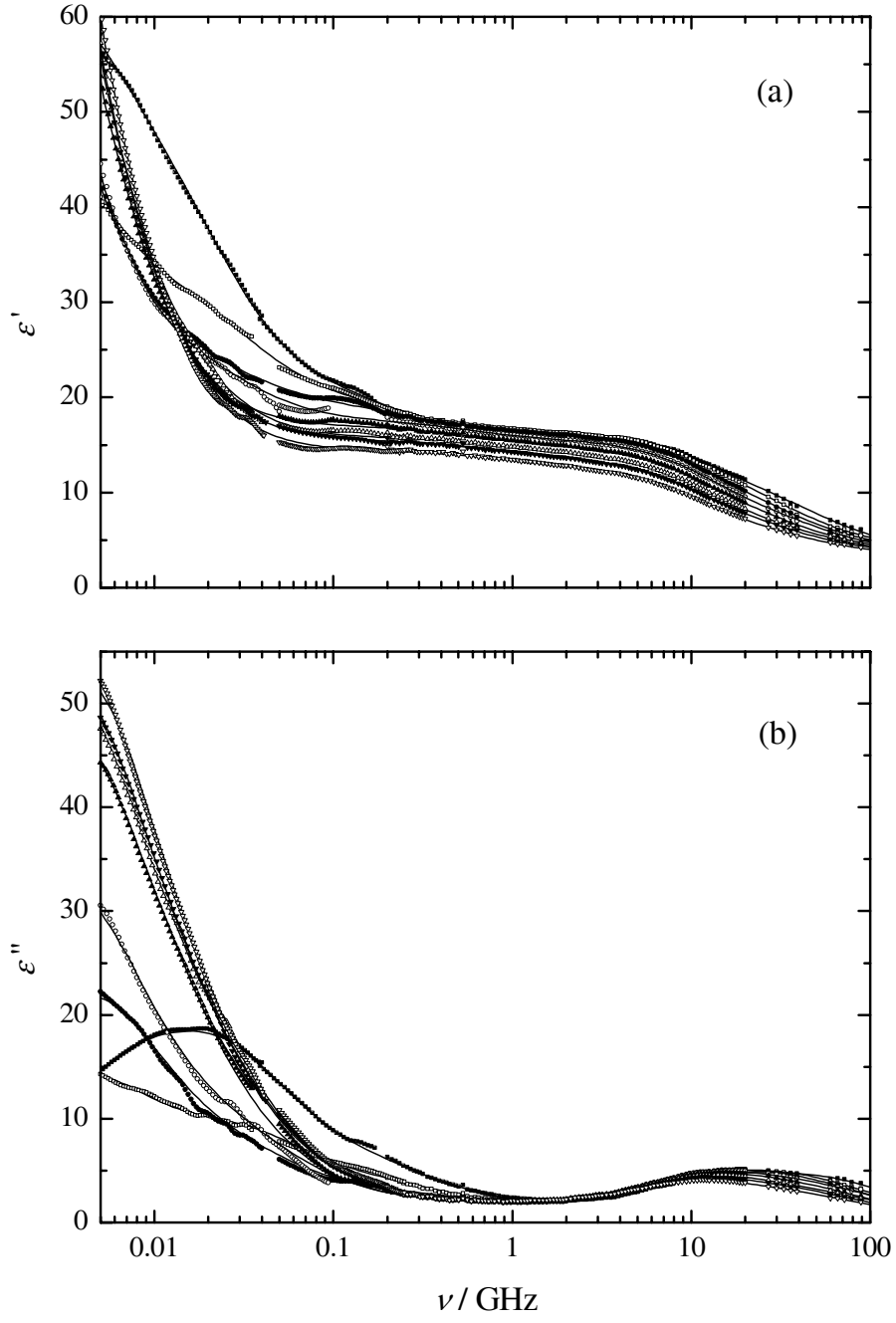

Figure 3.12: Dielectric permittivity (a) and loss (b) spectra for DDAB/W/D microemulsions at 25 ℃. ■ : sample 420; □ : sample 42a0; ●: sample 42b0; ○: sample 430; ▲: sample 43a0; △: sample 43b0; ▼: sample 440; ▽: sample 44a0.

Table 3.10: Dielectric Relaxation Parameters of DDAB/W/D Microemulsions at 25 °C: Constant Dodecane Ratios.

sample	ε_1	τ_1 / ps	ε_2	τ_2 / ps	ε_3	τ_3 / ps	ε_4	τ_4 / ps	ε_5	τ_5 / ps	ε_6	τ_6 / ps	ε_∞	χ^2
420	65.59	24419	45.07	6313	21.00	817	16.48	124	16.11	11.47	9.712	2.687	3.956	0.0253
42a0	57.35	41580	31.77	4788	20.25	790	16.87	152	16.27	12.05	9.348	3.273	4.208	0.0126
42b0	66.26	36406	23.99	4550	19.44	696	16.74	142	15.97	12.08	8.391	3.178	4.064	0.0285
430	86.79	47430	24.28	4746			17.53	273	15.54	12.94	7.943	3.061	3.811	0.0530
43a0	119.0	52365	33.29	15374			16.92	276	14.95	14.04	7.860	3.682	3.877	0.0488
43b0	125.7	49075	28.03	9397			15.74	175	14.06	13.14	6.518	2.839	3.579	0.0767
440	123.9	45939	26.19	10336			15.45	221	13.63	14.70	6.721	3.468	3.618	0.0388
44a0	123.4	40732	22.97	9797			14.36	184	12.68	14.75	6.061	3.344	3.476	0.0760

3.3.3 Microemulsions Containing Co-Electrolytes

Also the spectra of DDAB/XBr(aq)/D microemulsions (X = Li, Na, Cs, $(CH_3)_4N$) could be described best by a 6D or 5D model, depending on the DDAB/W ratio. Note that for some samples of the $21x$ series, process 4 was too small to be detected so that a 5D model had to be used also in these cases. Fitting parameters are given in Tables 3.11 to 3.15; Figures 3.13 to 3.22 compare the experimental spectra to their fits.

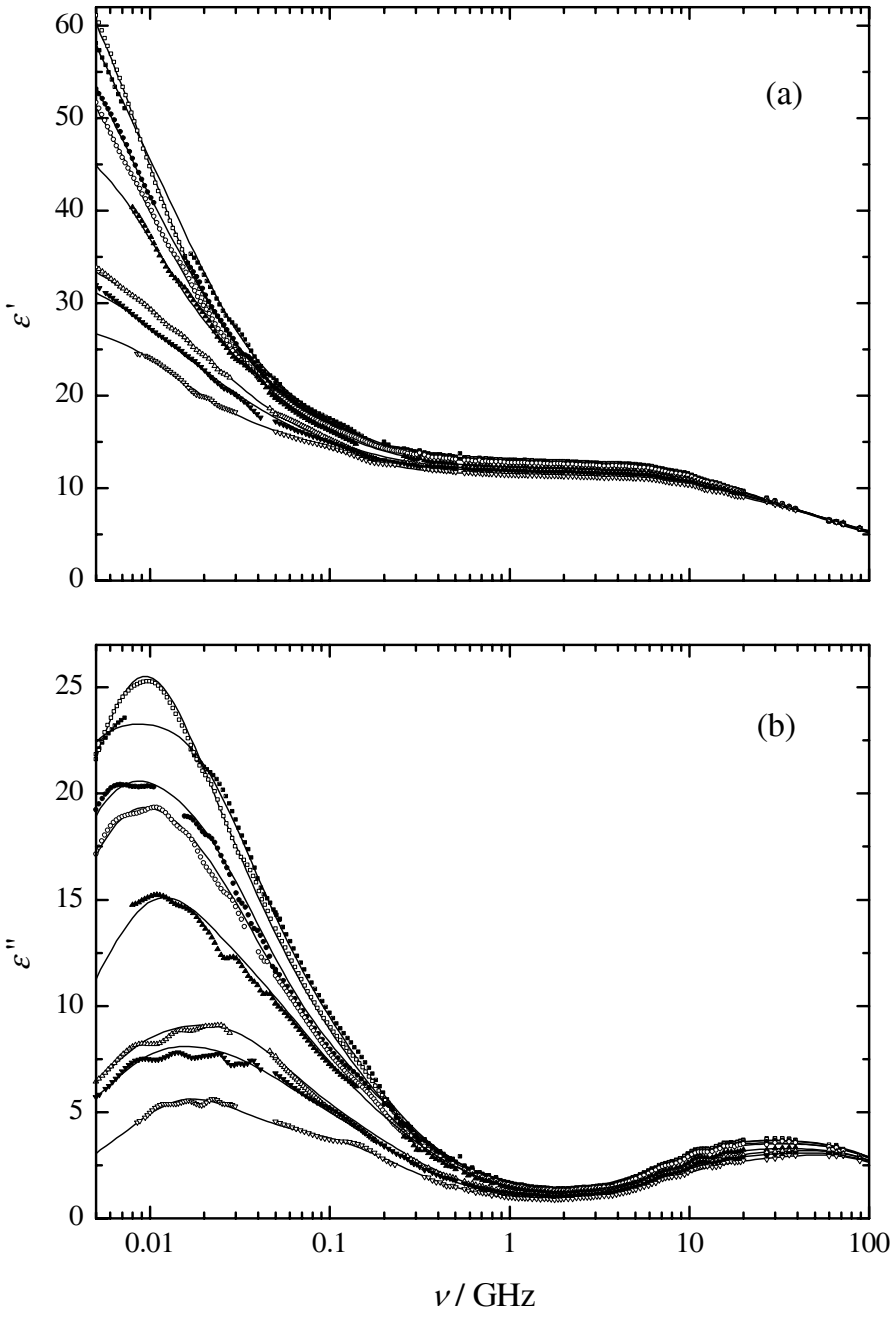

Figure 3.13: Dielectric permittivity (a) and loss (b) spectra for DDAB/LiBr(aq)/D microemulsions at 25 ℃. ■ : sample 211L; □ : sample 212L; •: sample 213L; ○: sample 214L; ▲: sample 215L; △: sample 219L; ▼: sample 2110L; ▽: sample 216L.

Table 3.11: Dielectric Relaxation Parameters of DDAB/LiBr(aq)/D Microemulsions at 25 °C.

sample	ε_1	τ_1 / ps	ε_2	τ_2 / ps	ε_3	τ_3 / ps	ε_4	τ_4 / ps	ε_5	τ_5 / ps	ε_6	τ_6 / ps	ε_∞	χ^2
210	121.6	58548	55.02	13541	26.36	2995	13.98	559	13.11	10.06	7.960	2.170	3.627	0.0405
211L	78.11	38831	47.89	8769	19.54	1663	13.16	196	12.97	9.923	7.947	2.129	3.501	0.0350
212L	72.38	18781	26.29	4500	17.58	1399	12.99	268	12.88	10.06	8.050	2.299	3.584	0.0347
213L	66.80	27084	37.15	7156	17.95	1149	12.85	282	12.81	10.13	8.012	2.120	3.556	0.0371
214L	61.94	23625	33.71	7084	18.19	1479	13.07	311	12.68	10.00	7.979	2.125	3.533	0.0220
215L	50.01	15675	24.35	3432	15.05	887	12.21	64.0	12.20	10.01	7.961	2.110	3.645	0.0500
219L	36.39	19456	26.49	5463	15.52	1230	12.18	219	11.92	9.946	8.058	2.207	3.608	0.0220
2110L	33.54	16474	22.77	4965	15.71	1331	11.89	164	11.75	9.852	7.961	2.019	3.673	0.0307
216L			26.19	9451	15.84	1319	11.53	201	11.36	10.23	8.037	2.046	3.615	0.0240
230	57.93	41500	18.75	8738			13.21	163	12.04	12.38	6.247	2.720	3.425	0.0371
231L	38.03	35402	17.78	6004			14.41	339	12.13	12.72	6.237	2.657	3.439	0.0304
232L	45.24	56089	22.31	11927			14.01	318	11.91	12.62	6.145	2.591	3.422	0.0585
233L	48.01	62344	20.42	8364			14.16	333	11.82	12.27	5.883	2.177	3.245	0.0105
234L	30.71	25226	16.44	5017			13.18	294	11.63	11.62	6.675	3.226	3.624	0.0204

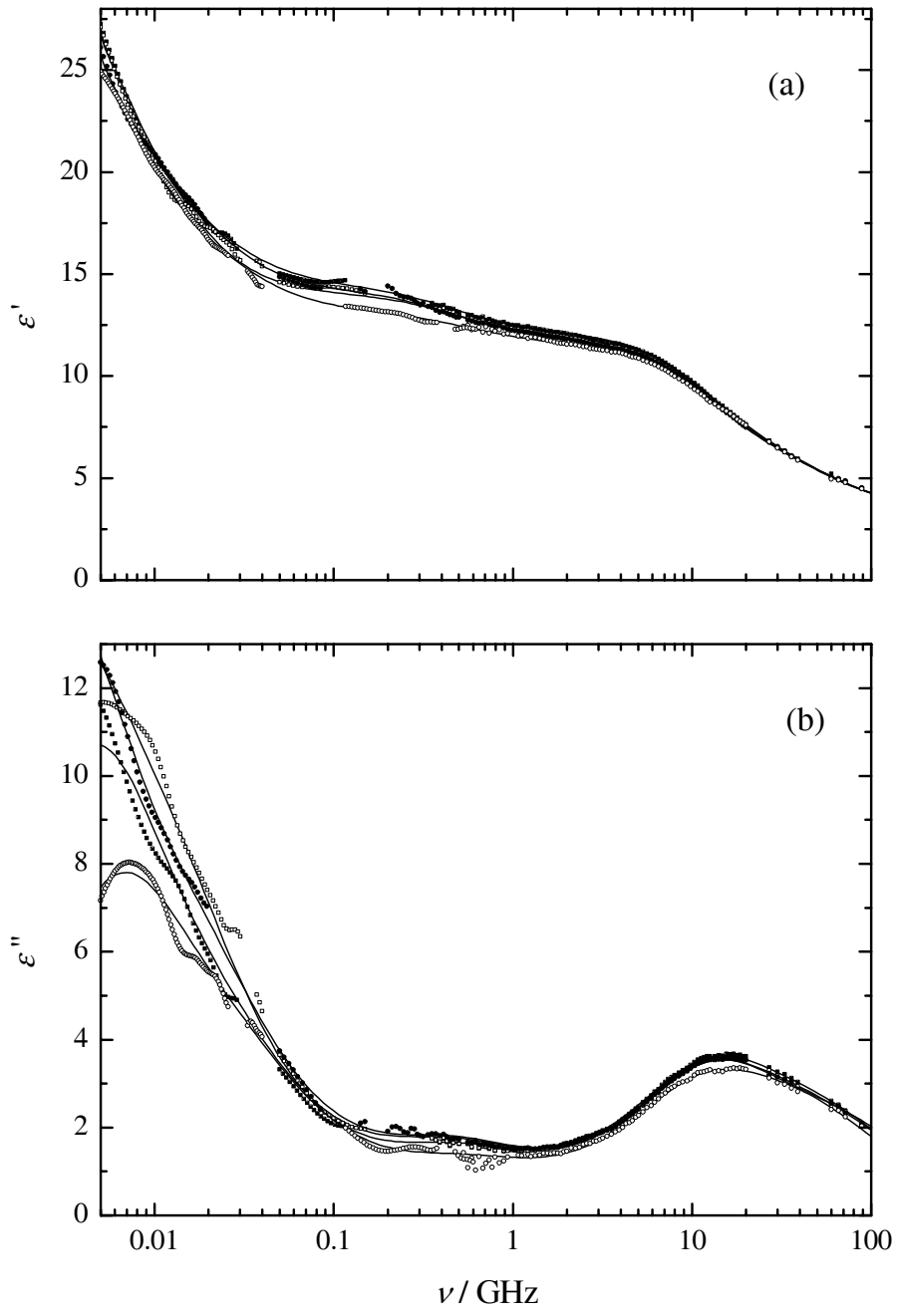

Figure 3.14: Dielectric permittivity (a) and loss (b) spectra for DDAB/LiBr(aq)/D microemulsions at 25 ℃. ■ : sample 231L; □ : sample 232L; •: sample 233L; ○: sample 234L.

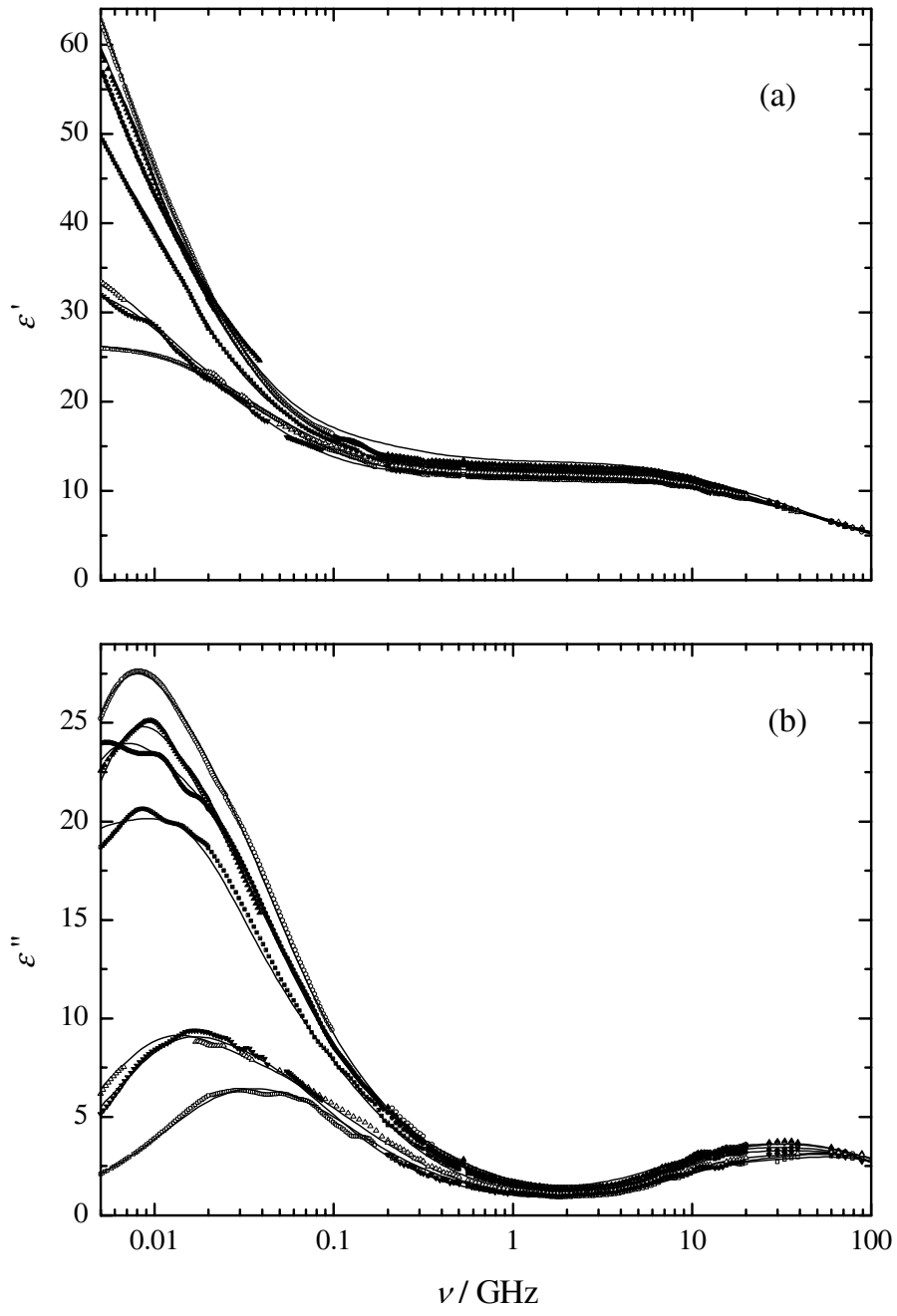

Figure 3.15: Dielectric permittivity (a) and loss (b) spectra for DDAB/NaBr(aq)/D microemulsions at 25 ℃. ■ : sample 211N; □ : sample 212N; ●: sample 213N; ○: sample 214N; ▲: sample 215N; △: sample 219N; ▼: sample 2110N; ▽: sample 216N.

Table 3.12: Dielectric Relaxation Parameters of DDAB/NaBr(aq)/D Microemulsions at 25 °C (Part 1).

sample	ε_1	τ_1 / ps	ε_2	τ_2 / ps	ε_3	τ_3 / ps	ε_4	τ_4 / ps	ε_5	τ_5 / ps	ε_6	τ_6 / ps	ε_∞	χ^2
210	121.6	58548	55.02	13541	26.36	2995	13.98	559	13.11	10.06	7.960	2.170	3.627	0.0405
211N	82.91	37455	43.41	7976	17.16	1396			12.84	9.408	7.522	1.860	3.252	0.0545
212N	80.42	24748	34.47	5729	15.04	951			12.71	9.530	7.830	2.170	3.530	0.0239
214N	75.50	30165	38.23	6456	15.80	1115	12.56	183	12.48	9.711	7.955	2.216	3.720	0.0204
215N	70.33	50203	44.65	10155	18.04	1839			12.20	10.18	8.065	2.208	3.687	0.0611
219N	35.79	14730	20.91	3144	14.35	1156	11.84	131	11.70	9.581	8.052	1.771	3.184	0.0255
2110N	33.74	12278	19.47	2943			11.86	273	11.45	10.89	8.351	2.197	3.523	0.0300
216N			26.54	6604	17.99	2213	12.01	451	11.30	9.944	7.951	1.900	3.478	0.0156
221N	56.71	24464	34.31	6291	16.57	1015	11.74	126	11.43	11.14	7.297	2.231	3.657	0.0543
222N	48.50	19191	23.69	4486			13.10	157	11.97	12.77	6.237	2.230	3.691	0.0432
230	57.93	41500	18.75	8738			13.21	163	12.04	12.38	6.247	2.720	3.425	0.0371
231N	53.48	47140	19.92	7565			14.19	319	12.06	13.03	6.381	2.876	3.464	0.0349
232N	51.66	49882	19.67	11054			14.15	410	11.99	13.65	6.484	2.770	3.355	0.0153
234N	65.46	61880	22.61	11932			13.93	389	11.74	13.41	6.544	2.988	3.364	0.0427
240	89.27	51918	18.12	4817			12.39	153	11.05	13.79	5.329	2.871	3.169	0.1102
241N	81.76	38511	16.49	10921			12.16	99.4	10.82	12.59	4.978	2.404	3.122	0.0505
242N	81.36	34474	14.01	5870			12.19	115	10.83	13.13	5.167	2.681	3.178	0.0397
250	88.47	39878	14.26	8008			10.57	64.2	9.257	12.86	4.216	2.022	2.857	0.0982
251N	72.01	34898	13.68	5420			11.26	120	9.748	14.65	4.719	3.276	3.193	0.1660
253N	73.97	38147	16.68	12950			10.85	94.6	9.379	13.58	4.506	2.978	3.124	0.0454

Table 3.13: Dielectric Relaxation Parameters of DDAB/NaBr(aq)/D Microemulsions at 25 °C (Part 2).

sample	ε_1	τ_1 / ps	ε_2	τ_2 / ps	ε_3	τ_3 / ps	ε_4	τ_4 / ps	ε_5	τ_5 / ps	ε_6	τ_6 / ps	ε_∞	χ^2
321N	59.06	34587	29.09	7717	14.04	1420	9.623	220	9.202	10.89	6.182	2.230	3.482	0.0408
322N	44.02	33355	20.95	5367	11.60	820	8.580	150	8.423	12.59	6.334	2.230	3.485	0.0833
331N	46.89	45216	17.14	6489			11.96	313	10.29	12.68	5.416	2.579	3.177	0.0440
332N	37.21	51954	22.41	16024			12.12	404	10.05	13.43	5.562	2.743	3.232	0.0165
340	63.44	48556	19.01	12179			11.07	153	9.733	13.24	4.640	2.746	3.082	0.0414
341N	94.48	53623	13.50	4390			10.66	96.8	9.474	12.24	4.378	2.192	2.920	0.2240
342N	79.37	62596	23.93	16459			11.28	238	9.770	14.68	5.074	3.258	2.981	0.0245
420	65.59	24419	45.07	6313	21.00	817	16.48	124	16.11	11.47	9.712	2.687	3.956	0.0253
421N	90.02	39635	53.76	7343	22.33	1056	16.67	111	16.15	10.66	8.937	2.230	3.741	0.0361
422N	62.93	25521	40.96	6051	19.68	881	15.12	136	14.58	11.78	9.352	2.230	3.725	0.0334
430	86.79	47430	24.28	4746			17.53	273	15.54	12.94	7.943	3.061	3.811	0.0530
431N	97.32	37110	22.00	6319			17.58	232	15.50	13.14	8.126	3.243	3.826	0.0542
432N	82.84	34769	21.22	5990			17.41	287	15.14	13.73	8.186	3.185	3.847	0.0508
440	123.9	45939	26.19	10336			15.45	221	13.63	14.70	6.721	3.468	3.618	0.0388
441N	263.9	66138	24.05	2356			14.66	102	13.15	12.56	5.761	2.330	3.239	0.4652
442N	151.9	51249	19.91	12804			15.25	161	13.30	13.85	6.375	3.069	3.457	0.1427

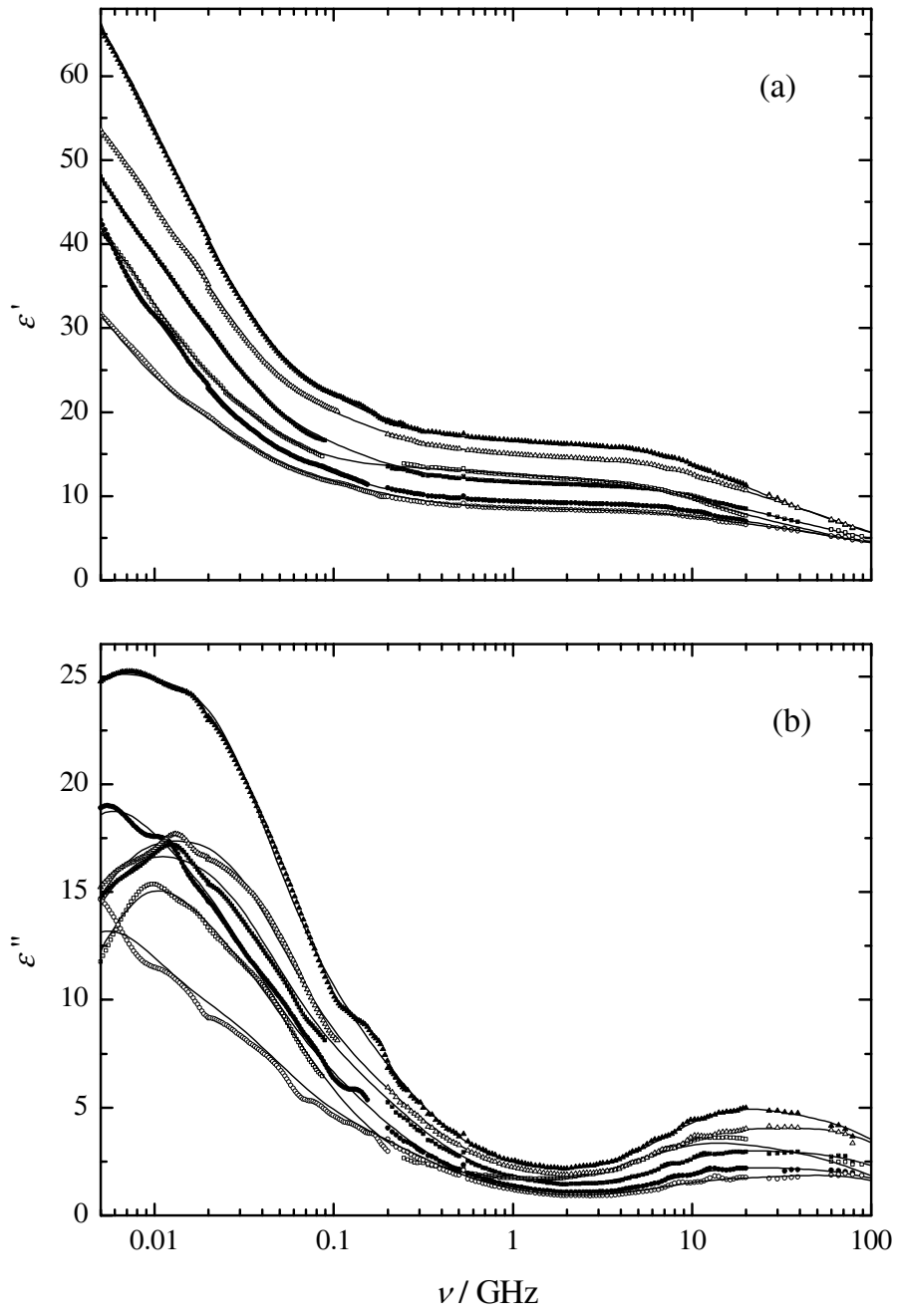

Figure 3.16: Dielectric permittivity (a) and loss (b) spectra for DDAB/NaBr(aq)/D microemulsions at 25 ℃. ■ : sample 221N; □ : sample 222N; •: sample 321N; ○: sample 322N; ▲: sample 421N; △: sample 422N.

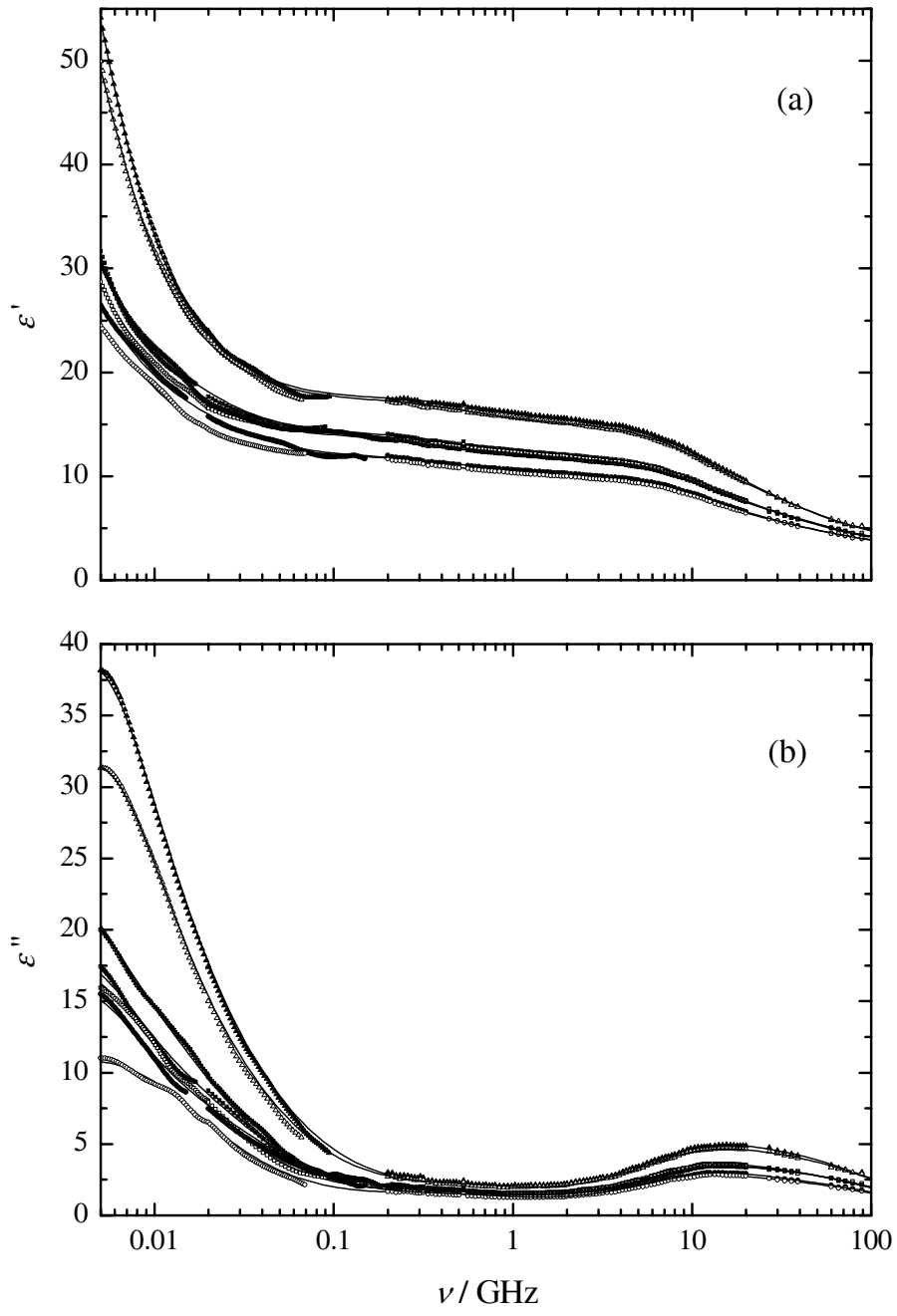

Figure 3.17: Dielectric permittivity (a) and loss (b) spectra for DDAB/NaBr(aq)/D microemulsions at 25 ℃. ■ : sample 231N; □ : sample 232N; ⊠: sample 234N; ●: sample 331N; ○: sample 332N; ▲: sample 431N; △: sample 432N.

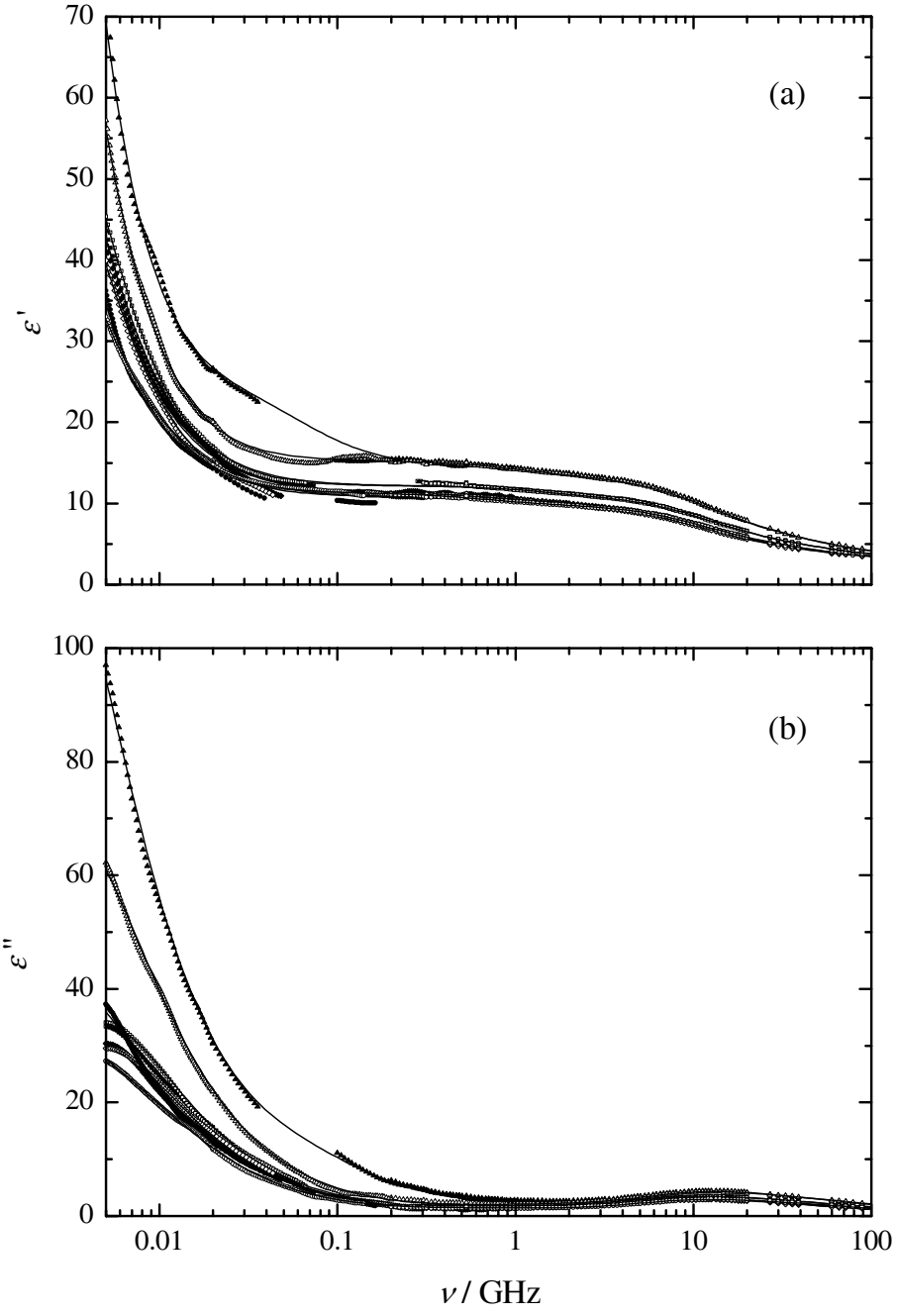

Figure 3.18: Dielectric permittivity (a) and loss (b) spectra for DDAB/NaBr(aq)/D microemulsions at 25 ℃. ■ : sample 241N; □ : sample 242N; ●: sample 341N; ○: sample 342N; ▲: sample 441N; △: sample 442N; ♦: sample 251N; ◇: sample 253N.

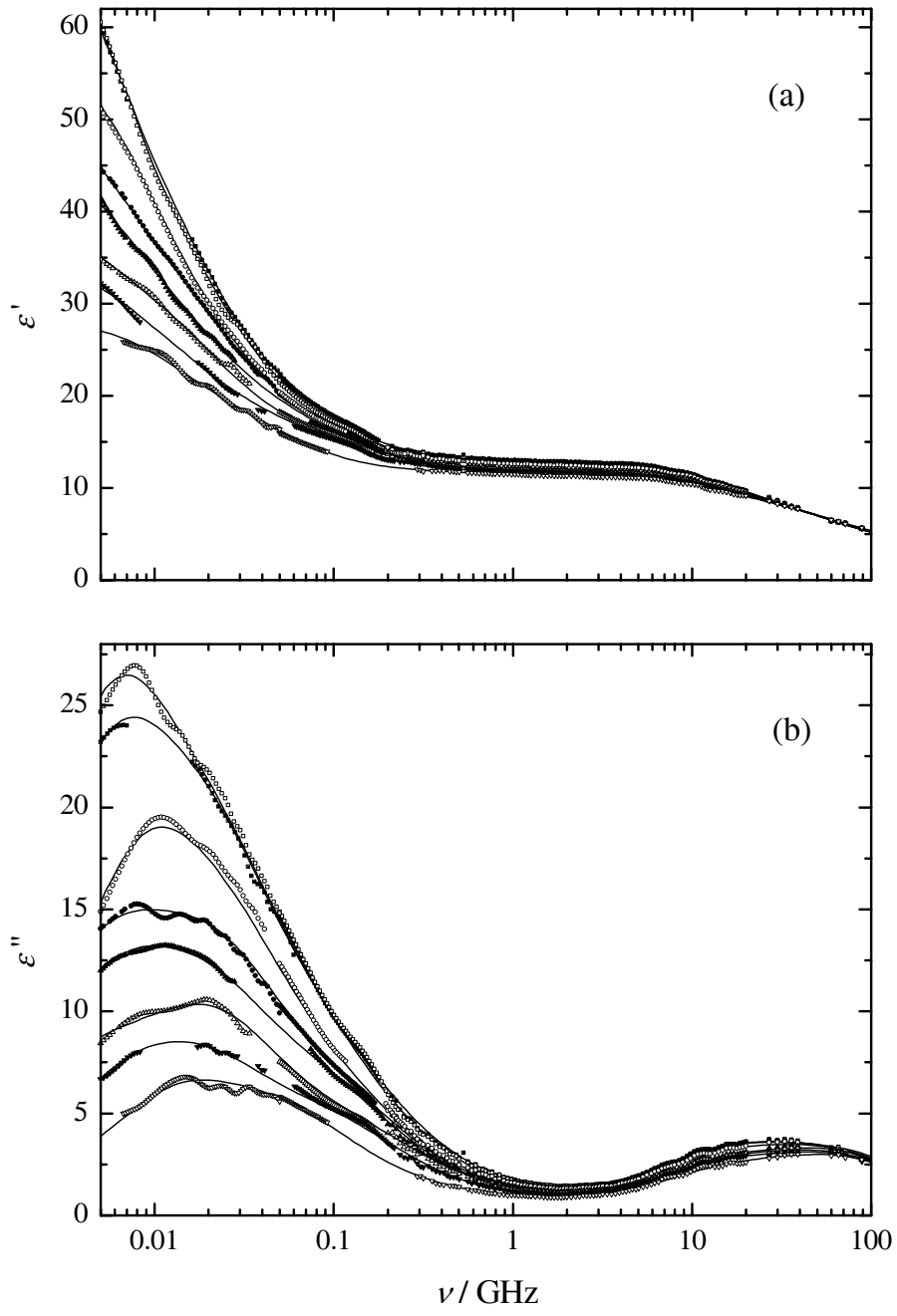

Figure 3.19: Dielectric permittivity (a) and loss (b) spectra for DDAB/CsBr(aq)/D microemulsions at 25 ℃. ■ : sample 211C; □ : sample 212C; ●: sample 213C; ○: sample 214C; ▲: sample 215C; △: sample 219C; ▼: sample 2110C; ▽: sample 216C.

Table 3.14: Dielectric Relaxation Parameters of DDAB/CsBr(aq)/D Microemulsions at 25 °C.

sample	ε_1	τ_1 / ps	ε_2	τ_2 / ps	ε_3	τ_3 / ps	ε_4	τ_4 / ps	ε_5	τ_5 / ps	ε_6	τ_6 / ps	ε_∞	χ^2
210	121.6	58548	55.02	13541	26.36	2995	13.98	559	13.11	10.06	7.960	2.170	3.627	0.0405
211C	77.14	28188	39.75	6949	19.46	1451	12.97	177	12.87	10.18	8.163	2.404	3.830	0.0242
212C	80.29	27704	36.11	6141	18.52	1536			12.79	9.924	7.911	2.110	3.502	0.0642
213C	55.67	31257	35.24	6843	17.86	1331	12.91	219	12.84	9.859	7.979	2.289	3.743	0.0196
214C	59.57	18786	30.05	5445	16.73	1265	12.57	185	12.48	9.886	8.030	2.212	3.575	0.0415
215C	49.31	28574	32.17	7881	19.00	1628	12.23	226	12.03	10.20	8.230	2.245	3.588	0.0191
219C	42.19	37984	31.44	7254	16.17	1012			11.90	10.45	8.247	2.308	3.735	0.0261
2110C	35.38	22615	25.93	7727	17.24	1462	11.82	171	11.72	10.32	8.160	2.237	3.751	0.0193
216C	28.35	11988	18.33	2703			11.78	267	11.35	10.42	8.233	2.169	3.718	0.0247
230	57.93	41500	18.75	8738			13.21	163	12.04	12.38	6.247	2.720	3.425	0.0371
231C	44.44	44109	17.75	6540			14.13	295	12.12	12.59	6.231	2.787	3.512	0.0163
232C	42.95	43269	18.15	4304			13.92	267	11.89	12.30	6.071	2.541	2.541	0.0247
233C	38.59	29801	17.75	4850			13.36	225	11.90	12.91	6.357	2.729	3.432	0.0326
234C	28.63	17755	15.09	1544			12.65	142	11.59	12.30	6.147	2.726	3.514	0.0210

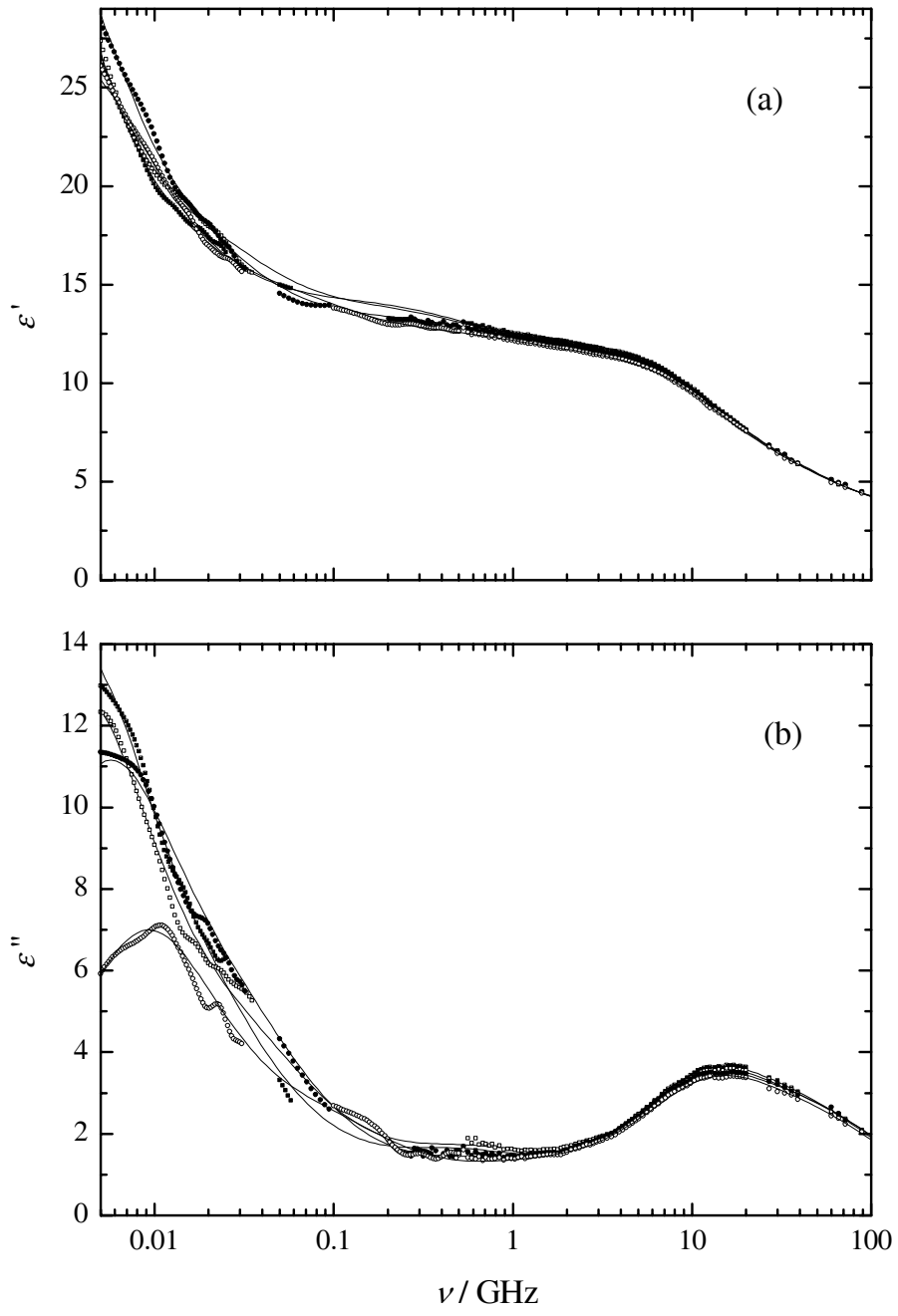

Figure 3.20: Dielectric permittivity (a) and loss (b) spectra for DDAB/CsBr(aq)/D microemulsions at 25 ℃. ■ : sample 231C; □ : sample 232C; •: sample 233C; ○: sample 234C.

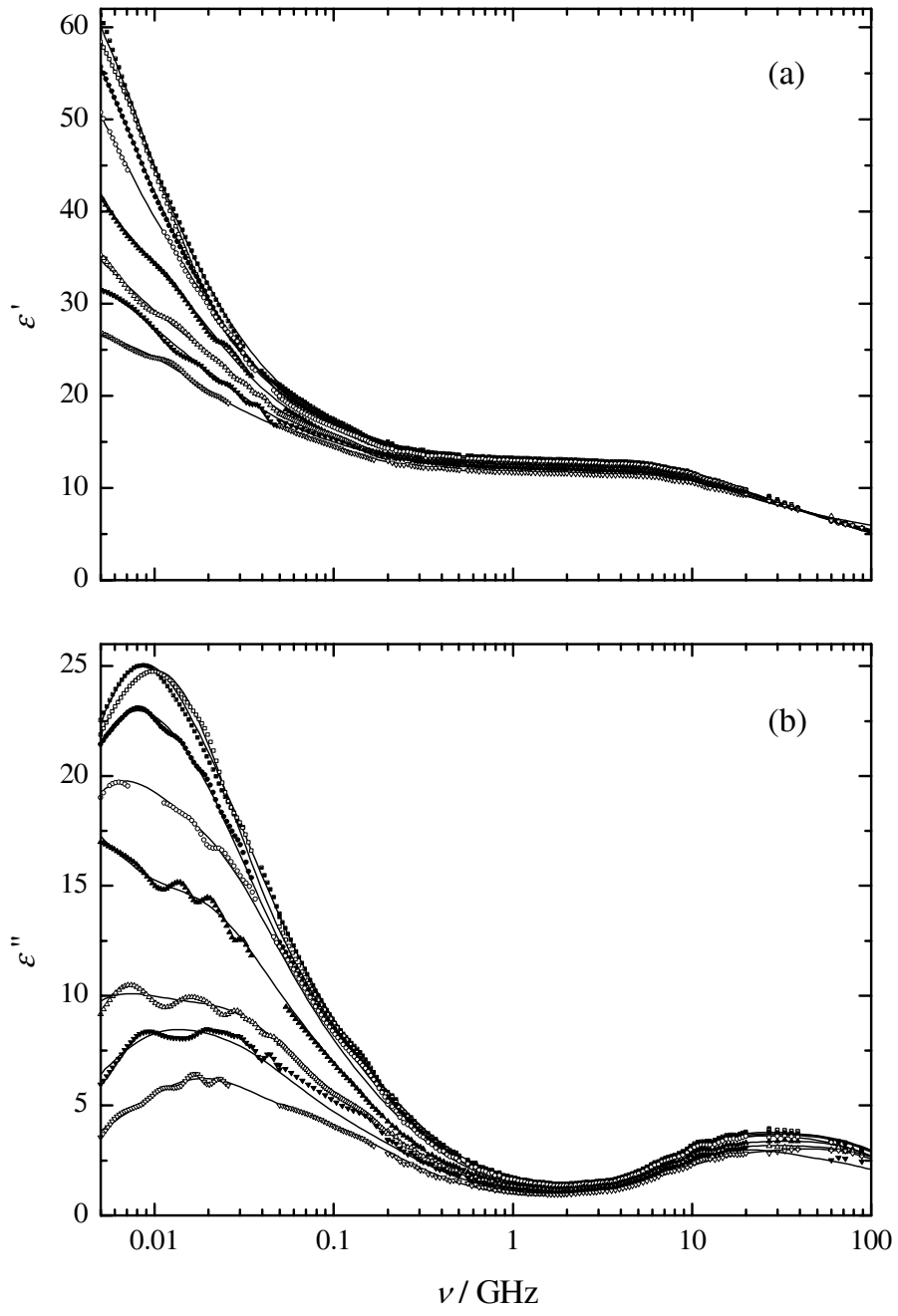

Figure 3.21: Dielectric permittivity (a) and loss (b) spectra for DDAB/$(CH_3)_4NBr$(aq)/D microemulsions at 25 ℃. ■ : sample 211T; □ : sample 212T; •: sample 213T; ○: sample 214T; ▲: sample 215T; △: sample 219T; ▼: sample 2110T; ▽: sample 216T.

Table 3.15: Dielectric Relaxation Parameters of DDAB/$(CH_3)_4NBr$(aq)/D Microemulsions at 25 °C.

sample	ε_1	τ_1 / ps	ε_2	τ_2 / ps	ε_3	τ_3 / ps	ε_4	τ_4 / ps	ε_5	τ_5 / ps	ε_6	τ_6 / ps	ε_∞	χ^2
210	121.6	58548	55.02	13541	26.36	2995	13.98	559	13.11	10.06	7.960	2.170	3.627	0.0405
211T	74.17	21945	32.30	5773	17.55	1144			13.16	10.06	8.075	2.300	3.602	0.0343
212T	73.65	32126	51.43	11664	19.25	1607			12.89	10.31	8.276	2.319	3.446	0.0261
213T	71.49	28036	38.06	8116	18.65	1413			13.03	9.809	7.862	2.079	3.462	0.0178
214T	66.50	31362	35.69	6369	16.84	1271			12.81	9.665	7.873	2.335	3.818	0.0386
215T	67.19	61494	35.89	7915	18.24	1967	12.87	297	12.47	9.775	7.898	2.092	3.696	0.0224
219T	42.85	32146	27.54	5443	15.65	1143	12.21	123	12.15	9.599	7.715	1.922	3.729	0.0240
2110T	34.81	18434	23.06	4907	14.96	997			12.06	9.232	7.167	1.736	4.627	0.0618
216T	28.22	30923	26.34	9356	16.54	1599	11.88	216	11.59	9.809	7.947	2.079	3.756	0.0120
230	57.93	41500	18.75	8738			13.21	163	12.04	12.38	6.247	2.720	3.425	0.0371
231T	52.33	41722	19.35	8002			14.72	387	12.18	13.09	6.482	3.194	3.600	0.0217
232T	57.30	38952	17.62	7595			14.30	335	12.02	12.85	6.315	2.806	3.468	0.0200
233T	47.60	34989	18.77	8888			13.95	301	11.79	12.74	6.317	2.753	3.511	0.0294
234T	51.58	34545	15.76	6950			13.93	517	11.84	15.39	7.176	3.744	3.765	0.0265

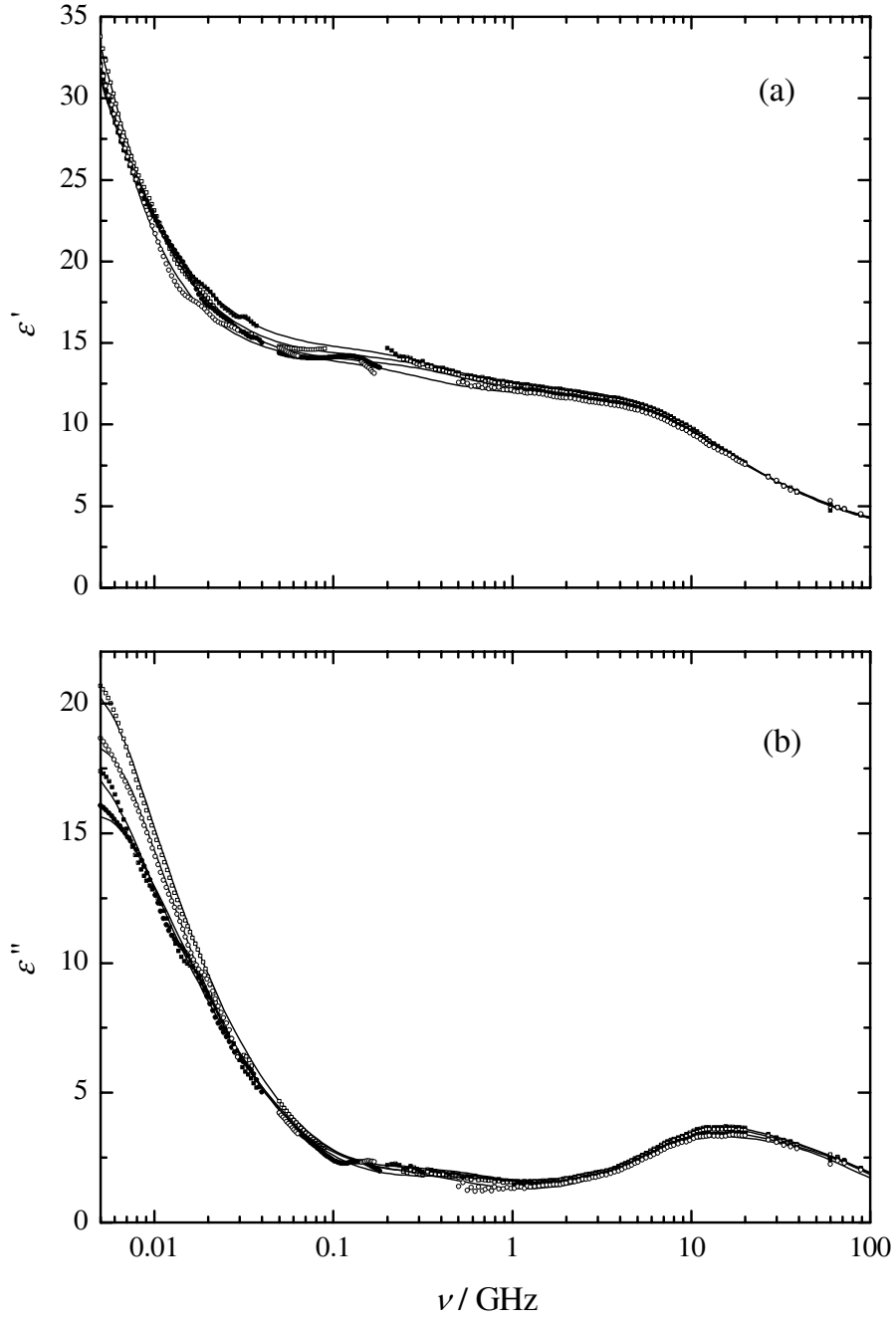

Figure 3.22: Dielectric permittivity (a) and loss (b) spectra for DDAB/$(CH_3)_4NBr$(aq)/D microemulsions at 25 ℃. ■ : sample 231T; □ : sample 232T; •: sample 233T; ○: sample 234T.

3.4 Infrared Measurements

Bands of the O-H stretching vibration present in the infrared spectra of DDAB/W/D and DDAB/NaBr(aq)/D microemulsions (Figures 3.24 to 3.27) were processed using GRAMS^{TM} 386 software (Galactic Industries Corporation, USA). It has been reported previously for aqueous solutions of alkali metal hydroxides[178] that the O-H stretching vibration could be described best by a superposition of four bands, one band being the product of a Gaussian and Lorentzian function and three bands being of merely Gaussian shape. This model proved to be most suitable also for the O-H stretching vibration of the microemulsion studied in this work; an example of this fit can be seen in Figure 3.23. Thus, the peak wavenumbers, $\bar{\nu}_i$, the full widths at half maximum, $\Delta_{1/2,i}$, and the areas, A_i, of the individual bands were obtained as fitting parameters. However, when comparing the areas of the different bands, the variation of intensity as a function of band position must be taken into account. Therefore, the following procedure proposed by Glew and Rath[97,178] was used to obtain corrected peak areas, A^c

$$A_i^c = A_i \cdot \left[1 + \frac{\bar{\nu}_i^0 - \bar{\nu}^g}{3756\ \mathrm{cm}^{-1} - \bar{\nu}^g}\right] \tag{3.3}$$

where $\bar{\nu}_i^0$ is the peak position of a band i and $\bar{\nu}^g$ the gravity centre of the complete O-H stretching vibration. Thus, the corrected relative intensity I_i^c of a band i could be calculated as

$$I_i^c = A_i^c \Big/ \sum_i A_i^c \tag{3.4}$$

All parameters are given in Tables 3.16 and 3.17; the spectra are plotted in Figures 3.24 to 3.27.

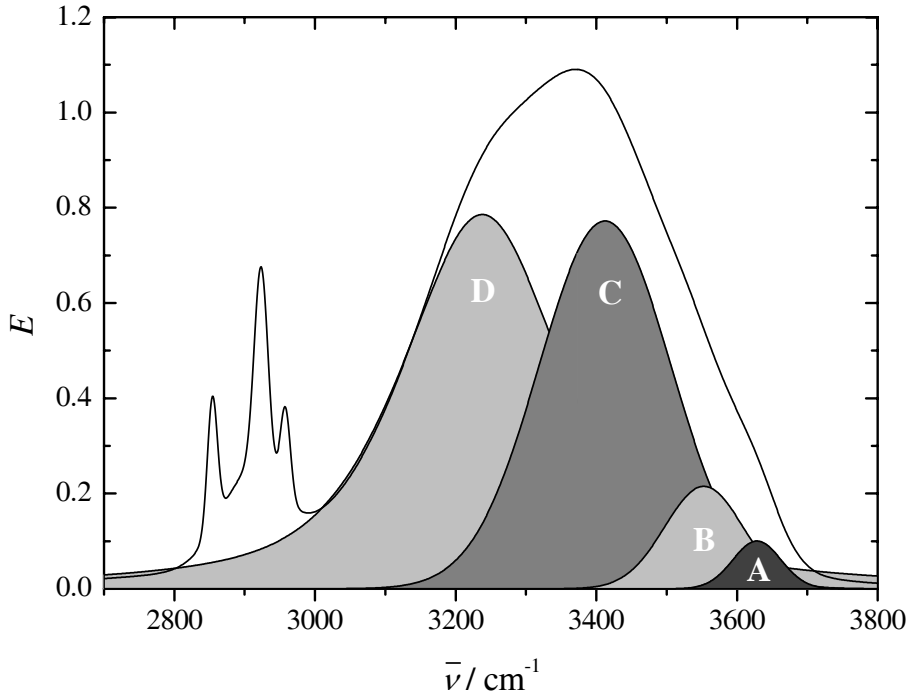

Figure 3.23: Fit of the infrared O-H stretching vibration recorded for a DDAB/W/D microemulsion, sample 210, at $\sim$ 24 °C using four bands. A, B, C: Gaussian bands; D: Gauss-Lorentz product. The C-H stretching vibrations, stemming from D and DDAB, at $2850 \lesssim \bar{\nu}/\mathrm{cm}^{-1} \lesssim 2950$ are not taken into account.

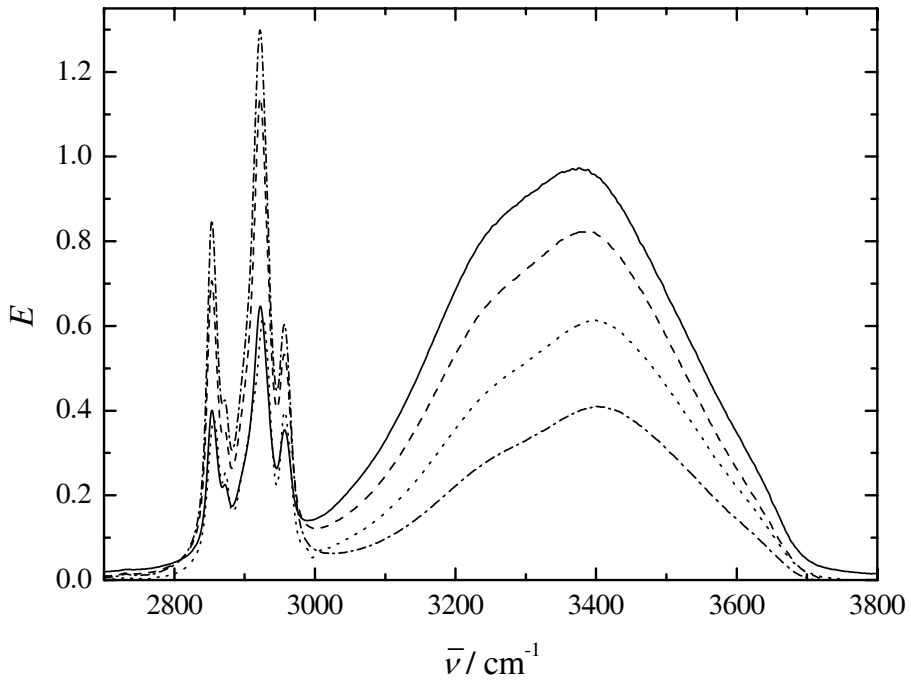

Figure 3.24: Infrared spectra of DDAB/W/D microemulsions at $\sim$ 24 °C. Full line: sample 220; dashed line: sample 8; dotted line: sample 9; dash-dotted line: sample 10.

Table 3.16: Fitting Parameters of the O-H Stretching Vibration in DDAB/W/D Microemulsions at ~ 24 °C (Part 1): Peak Wavenumbers, $\bar{\nu}_i$, Full Widths at Half Maximum, $\Delta_{1/2,i}$, Uncorrected and Corrected Relative Band Intensities, I_i and I_i^c.

sample	$\bar{\nu}_A$ / cm^{-1}	$\Delta_{1/2,A}$ / cm^{-1}	I_A	I_A^c	$\bar{\nu}_B$ / cm^{-1}	$\Delta_{1/2,B}$ / cm^{-1}	I_B	I_B^c
7	3628.4 ± 0.1	80.1 ± 0.1	0.0175	0.0327	3553.8 ± 0.1	133.1 ± 0.3	0.0639	0.105
8	3627.1 ± 1.4	81.3 ± 5.2	0.0153	0.0293	3549.3 ± 2.1	139 ± 12	0.0712	0.119
9	3628.2 ± 1.2	80.3 ± 3.1	0.0191	0.0367	3554.6 ± 1.8	128.8 ± 7.9	0.0661	0.111
10	3626.1 ± 8.0	78 ± 18	0.0193	0.0375	3552 ± 12	127.6 ± 5.2	0.0646	0.109
11	3624.7 ± 0.1	82.9 ± 0.3	0.0176	0.0336	3547.1 ± 0.2	133.6 ± 0.8	0.0672	0.111
12	3625.2 ± 0.9	81.5 ± 2.1	0.0177	0.0341	3549.0 ± 1.1	131.1 ± 5.1	0.0658	0.110
13	3625.2 ± 0.1	81.8 ± 0.1	0.0168	0.0320	3547.3 ± 0.1	134.0 ± 0.3	0.0630	0.105
14	3625.3 ± 1.0	81.5 ± 2.4	0.0173	0.0331	3547.9 ± 1.2	132.2 ± 6.1	0.0642	0.107
15	3625.8 ± 1.0	79.7 ± 2.2	0.0168	0.0323	3549.6 ± 1.3	130.9 ± 6.1	0.0629	0.106
16	3624.9 ± 0.4	79.3 ± 0.9	0.0171	0.0330	3548.8 ± 0.5	129.7 ± 2.5	0.0615	0.103
210	3628.3 ± 0.4	80.8 ± 0.8	0.0176	0.0328	3552.8 ± 0.5	130.7 ± 2.2	0.0610	0.100
213N	3627.3 ± 0.7	81.5 ± 1.6	0.0172	0.0324	3550.6 ± 0.9	132.6 ± 4.3	0.0618	0.103
214N	3626.9 ± 0.3	81.8 ± 0.6	0.0177	0.0336	3549.7 ± 0.3	132.5 ± 1.6	0.0634	0.106
215N	3627.0 ± 0.1	82.1 ± 0.1	0.0180	0.0337	3549.8 ± 0.1	132.5 ± 0.1	0.0630	0.104
216N	3628.1 ± 0.2	80.9 ± 0.4	0.0176	0.0327	3552.5 ± 0.2	130.3 ± 1.1	0.0590	0.0971

Table 3.17: Fitting Parameters of the O-H Stretching Vibration in DDAB/W/D Microemulsions at ~ 24 °C (Part 2): Peak Wavenumbers, $\bar{\nu}_i$, Full Widths at Half Maximum, $\Delta_{1/2,i}$, Uncorrected and Corrected Relative Band Intensities, I_i and I_i^c.

sample	$\bar{\nu}_C$/ cm^{-1}	$\Delta_{1/2,C}$ / cm^{-1}	I_C	I_C^c	$\bar{\nu}_D$ / cm^{-1}	$\Delta_{1/2,D}$ / cm^{-1}	I_D	I_D^c
7	3411.1 ± 0.1	222.3 ± 0.2	0.378	0.468	3236.7 ± 0.1	269.7 ± 0.1	0.540	0.394
8	3409.0 ± 2.0	214.2 ± 7.1	0.385	0.477	3237.8 ± 1.9	268.0 ± 1.0	0.529	0.374
9	3421.0 ± 1.2	213.8 ± 5.1	0.410	0.511	3245.5 ± 1.7	264.0 ± 0.7	0.504	0.341
10	3418.7 ± 8.4	216 ± 29	0.431	0.537	3242.3 ± 8.6	260.7 ± 6.0	0.485	0.316
11	3410.0 ± 0.1	215.6 ± 0.5	0.422	0.521	3236.4 ± 0.1	261.3 ± 0.1	0.493	0.335
12	3412.7 ± 0.9	216.6 ± 3.0	0.420	0.521	3237.5 ± 0.9	259.9 ± 0.5	0.496	0.334
13	3406.5 ± 0.1	220.0 ± 0.2	0.386	0.481	3232.6 ± 0.1	266.6 ± 0.1	0.534	0.382
14	3409.6 ± 1.0	218.0 ± 4.0	0.398	0.495	3235.6 ± 1.1	264.2 ± 0.5	0.520	0.365
15	3412.6 ± 0.9	217.7 ± 3.8	0.412	0.513	3238.0 ± 1.2	264.6 ± 0.5	0.508	0.349
16	3415.5 ± 0.4	213.8 ± 1.4	0.419	0.523	3238.8 ± 0.4	261.6 ± 0.3	0.502	0.340
210	3412.4 ± 0.3	221.0 ± 1.7	0.370	0.459	3237.9 ± 0.6	271.3 ± 0.2	0.551	0.407
213N	3410.7 ± 0.6	219.4 ± 3.0	0.379	0.472	3236.0 ± 0.9	268.5 ± 0.3	0.542	0.393
214N	3409.5 ± 0.2	218.5 ± 1.2	0.374	0.465	3235.7 ± 0.4	268.8 ± 0.1	0.545	0.395
215N	3409.7 ± 0.1	218.9 ± 0.1	0.369	0.457	3236.4 ± 0.1	269.7 ± 0.1	0.550	0.405
216N	3411.9 ± 0.1	222.4 ± 0.8	0.377	0.468	3237.0 ± 0.3	270.7 ± 0.1	0.546	0.402

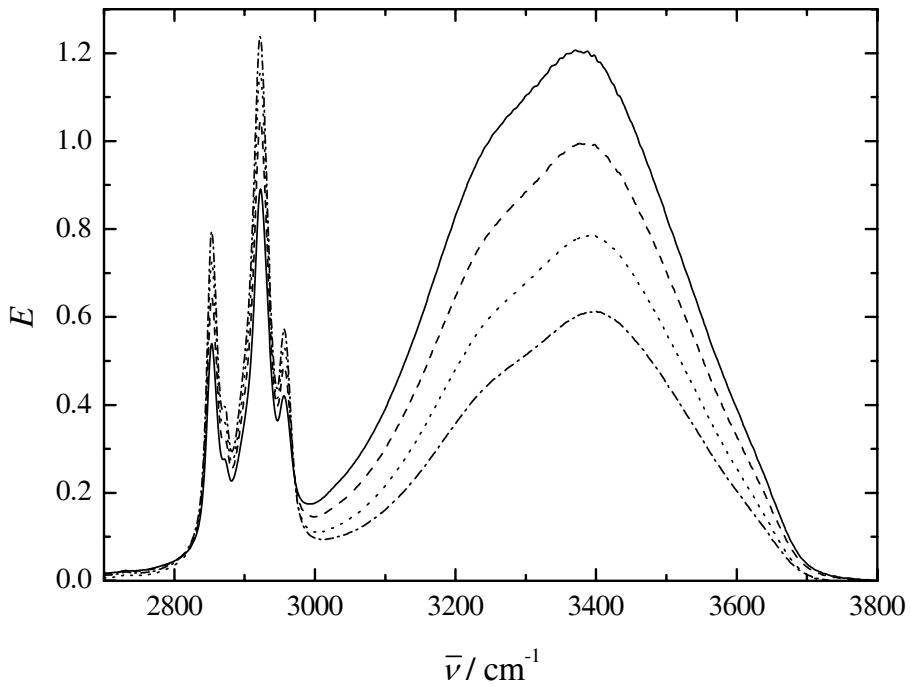

Figure 3.25: Infrared spectra of DDAB/W/D microemulsions at $\sim$ 24 °C. Full line: sample 13; dashed line: sample 14; dotted line: sample 15; dash-dotted line: sample 16.

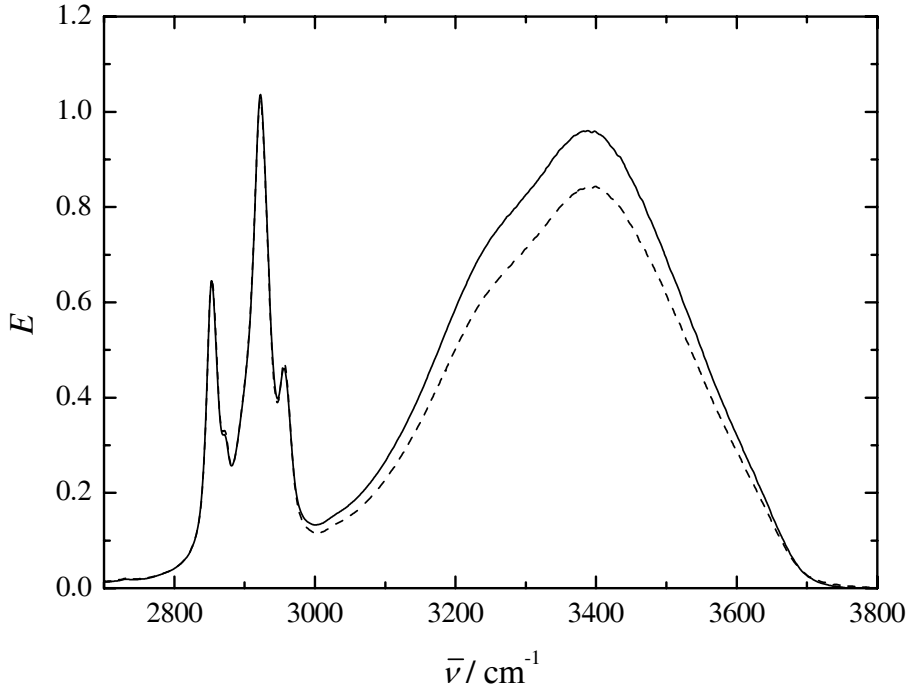

Figure 3.26: Infrared spectra of DDAB/W/D microemulsions at $\sim$ 24 °C. Full line: sample 11; dashed line: sample 12.

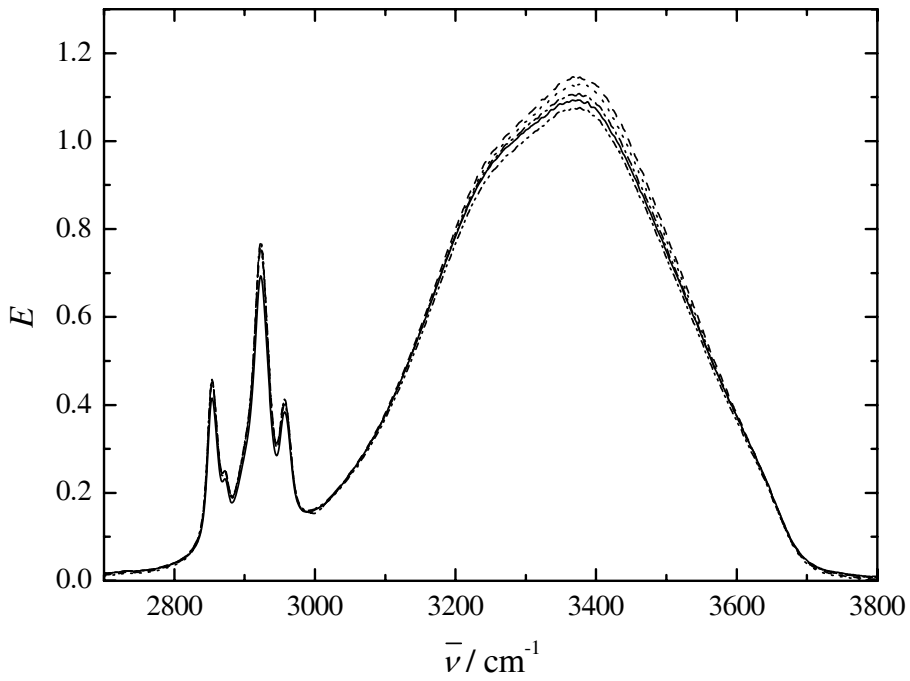

Figure 3.27: Infrared spectra of DDAB/NaBr(aq)/D microemulsions at $\sim$ 24 °C. Full line: sample 210; dashed line: sample 213N; dotted line: sample 214N; dash-dotted line: sample 215N: dash-dot-dotted line: sample 216N.

3.5 Refractive Index of Didodecyldimethylammonium Bromide / Ethanol Mixtures

Values of the refractive indices, n, and the densities, ρ, of the DDAB/ethanol mixtures studied in this work are given in Table 3.18. Using $M_{\mathrm{EtOH}} = 46.07$ g mol^{-1}, $M_{\mathrm{DDAB}} = 462.63$ g mol^{-1} and eq. (2.53) the medium mole refraction, $[R]$, was calculated and plotted as a function of the mole fraction of DDAB. According to eq. (2.54) $[R_{\mathrm{DDAB}}] = 125.9 \cdot 10^{-6}$ m^3 mol^{-1} could be determined as the slope of a linear fit (see Figure 3.28) and thus, the polarisability $\alpha_{\mathrm{DDAB}} = 49.94$ Å^3 was calculated using eq. (2.55).

Table 3.18: Mole Fraction, x_{DDAB}, Refractive Index, n, Density, ρ, and Medium Mole Refraction, $[R]$, of DDAB/Ethanol Mixtures Measured at 25 ℃.

x_{DDAB}	n	ρ / kg m^{-3}	$[R]$ / 10^{-6} m^3 mol^{-1}
0	1.35985	785.25	12.943
0.002000	1.36099	788.46	13.161
0.004001	1.36312	791.57	13.413
0.006000	1.36566	794.63	13.680
0.008002	1.36731	797.53	13.920
0.009990	1.36994	800.25	14.197

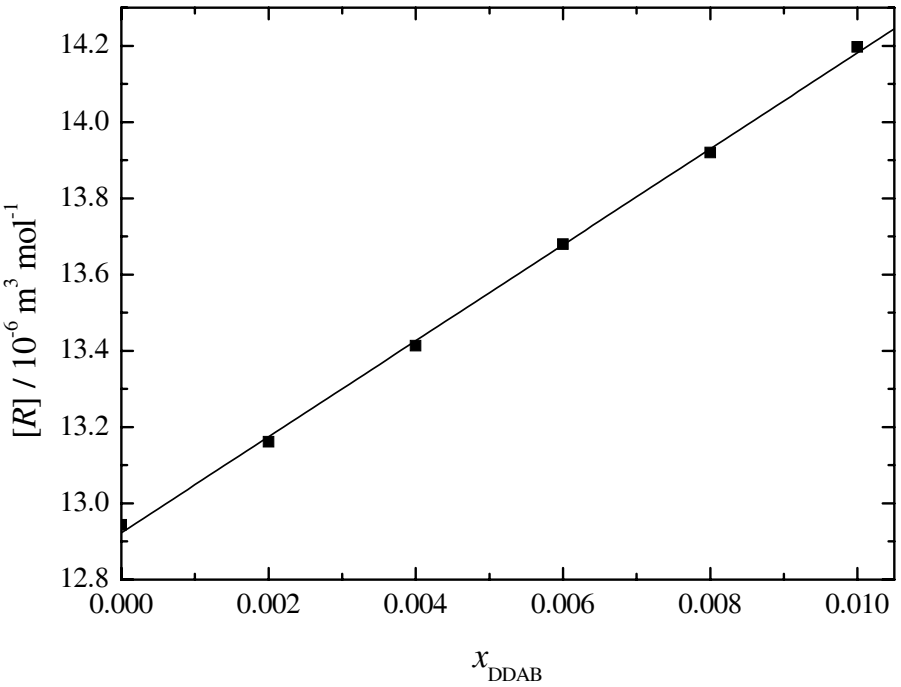

Figure 3.28: Medium mole refraction, $[R]$, of DDAB/ethanol mixtures as function of the mole fraction x_{DDAB} at 25 ℃.

Chapter 4

Discussion Part 1: Didodecyldimethylammonium Bromide / Water / n-Dodecane Microemulsions

4.1 Literature Review

Before starting to discuss the experimental results obtained in this work, it is useful to review existing knowledge about the properties of DDAB/W/D. This system has been investigated by various authors using a number of experimental techniques. However, as can be seen from Figure 4.1, only some NMR self-diffusion studies[89,176] have been conducted over the entire microemulsion phase, commonly labelled 'L_2' in the literature.[89,177] Other techniques have only been applied to a rather small part of L_2, and, in particular, the surfactant-rich area has barely been investigated yet.

When studying the literature dealing with the properties of DDAB/W/D microemulsions only a few facts seem to be well-established. There is no doubt that the equilibrium allowing the formation of microemulsions is extremely delicate; not only the addition of tiny amounts of co-ions,[175] but also variations of the surfactant counterions (*e.g.* chloride or iodide instead of bromide)[52] or of the oil chain length[195] drastically influence the shape of L_2 in the phase diagram. Thanks to NMR self-diffusion measurements it is unambiguous that dodecane represents the continuous phase throughout L_2;[89] thus, the system DDAB/W/D represents a *water-in-oil (W/O) microemulsion*. Furthermore, it is obvious that the surfactant DDAB resides at the water/dodecane interface, as it is very sparingly soluble in both liquids.[11,89]

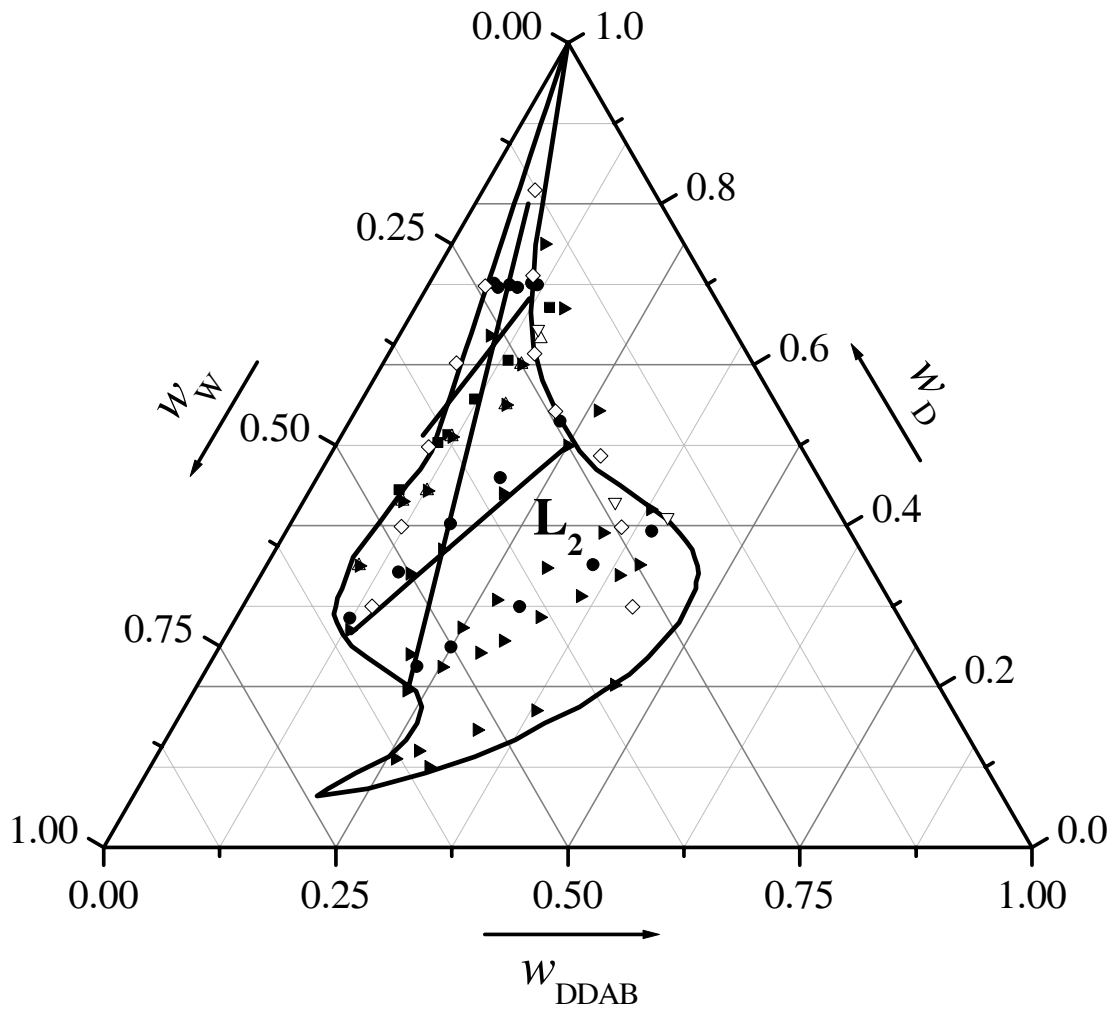

Figure 4.1: Selection of experimental studies of the system DDAB/W/D published in literature. Full lines: Lenz and Hoffmann (flow and electric birefringence, pressure jump relaxation, conductivity);[137] ■: Blum *et al.* (NMR self-diffusion);[26] •: Skurtveit and Olsson (NMR self-diffusion);[176] ►: Fontell *et al.* (NMR self-diffusion);[89] △: Barnes *et al.* (SAXS);[11] ▽: Allen *et al.* (interfacial tension);[1] ◊: Sjöblom and Gestblom (DRS).[175]

In contrast, the structure and geometry of the water 'clusters' dispersed in dodecane are less clear-cut. The only points that are generally accepted are the facts that separated water droplets embedded in oil are expected for very low DDAB/W ratios (see *e.g.* ref.[89]) and that water channels crossing the entire microemulsion phase (*i.e.* a bicontinuous system) will occur for high DDAB/W ratios. The latter phenomenon has been confirmed by interfacial tension measurements, which revealed long-range and extremely strong van der Waals forces that are characteristic of a dielectric of high permittivity and cylindrical shape interacting across a medium of low dielectric constant.[1]

It should be noted in this context that separated W/O droplets are often referred to as 'reverse micelles' in the literature. Strictly speaking, this term is only appropriate for very small droplets ($r \lesssim 0.7$ nm),[73] where all water molecules are strongly affected by the interface and an aqueous core is nonexistent. As a rough estimation of the droplet radii r present in DDAB/W/D microemulsions – according to the semi-empirical relation $r = (1.25W + 2.7)$ Å[47,50] – yields values between $r \approx 2.3$ nm at the surfactant-rich edge ($W = 16$) and $r \approx 15$ nm at the water-rich edge ($W = 119$) of the L_2 phase, we are speaking of 'water droplets' or 'particles' instead of 'reverse micelles' when describing the aqueous subphase of DDAB/W/D microemulsions below percolation in this work. However, as droplet radii of $r \lesssim 5$ nm are fairly small for microemulsions, some results reported in the literature for large reverse micelles of related microemulsion systems are certainly transferable to the system DDAB/W/D. Besides, the term 'reverse micelles' is frequently used in the literature for water particles exhibiting much larger radii than ~ 0.7 nm.

There is a number of competing models trying to explain the transition between separated water droplets in oil and a bicontinuous network. Probably the simplest explanation is the static percolation model proposed by Barnes *et al.*[11] already outlined in section 1.6.1. According to this model, separated water droplets of spherical shape are dispersed in dodecane at low DDAB/W ratios. As their radii are determined by the ratio between volume and interface they are changing as soon as the DDAB/W ratio is altered, but they remain constant along a D dilution line. Thus, the droplets become smaller and smaller with increasing DDAB/W until, at a certain ratio, a bicontinuous channel network becomes energetically more favourable than separated water droplets so that a sudden change of microstructure takes place.

Barnes *et al.* applied the DOC model, presented in section 1.6.1, to predict properties of the systems DDAB/W/*n*-octane and DDAB/W/D. They found their modelled SAXS spectra to be in 'good qualitative agreement with the measured spectra, except in those cases where there is clear evidence of an attractive interaction between aggregates.'[10] Furthermore, they obtained approximate predictions of the phase boundaries. For the percolation transition, the model yielded even values that were in excellent agreement with experimental results from conductivity data.

However, it should be noted that these conductivity measurements[51] have only been carried out in a very small part of L_2 with extremely low DDAB fractions. Lenz and Hoffmann, who investigated the conductivity behaviour of DDAB/W/D over considerably larger parts of L_2 (see Figure 4.1) found a rather gradual increase with increasing DDAB/W ratio. As has been shown in section 3.2.3 their results compare very favourably with the conductivity data obtained in this work. Additionally, a freeze fracture electron microscopy (FFEM) study by Jahn and Strey yielded an image of a DDAB/W/D microemulsion at $w_{\mathrm{DDAB}}/w_{\mathrm{W}} \approx 0.283$ (*i.e.* at $W \approx 91$, far below the percolation threshold predicted by Barnes *et al.*); as can be seen from Figure 4.2, there is already a number of channels linking the droplets, which deviate considerably from spherical geometry.[123] All these observations strongly suggest that percolation already starts at high water fractions and proceeds gradually rather than abruptly.

There is also some evidence questioning the spherical shape of separated water droplets at high water fractions. Lenz and Hoffmann found a large birefringence for DDAB/W/D microemulsions at low DDAB/W ratios, which suggests the particles being of ellipsoidal rather than of spherical shape.[137] Besides, these authors even found some evidence for polydispersity of the water droplets. Skurtveit and Olsson concluded from their NMR self-diffusion data that for very high water fractions rod-like elongated reverse micelles should replace the spherical ones forming at lower water fractions.[176]

Even the concept that the volume of a water droplet should only depend on the DDAB/W ratio is challenged by the water self-diffusion experiments of Skurtveit and Olsson, who reported a volume increase of water droplets along a D dilution line with decreasing D content.[177]

Quite obviously, a variety of microstructures exists between the boundary cases of a bicontinuous network and separated water droplets in oil. Furthermore, there is some evidence that these droplets are polydisperse and that their shapes depend not only on the DDAB/W ratio and deviate considerably from sphericals. Therefore, when using geometrical models like the DOC model it should always be kept in mind that these concepts are quite rough approximations exhibiting inevitably some discrepancies from reality. However, despite their inadequacies, they are still useful tools for the interpretation of microemulsion systems, as it is barely possible to create a model accounting for the variety of microstructures as can be seen, for example, in Figure 4.2.

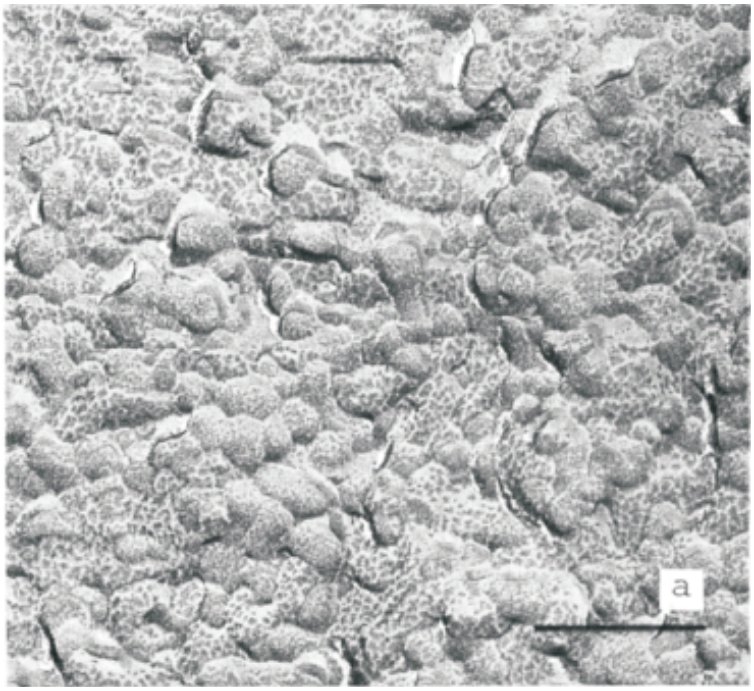

Figure 4.2: FFEM image of DDAB/W/D ($w_{\mathrm{D}} = 0.370$, $w_{\mathrm{DDAB}}/w_{\mathrm{W}} = 0.283$) at 25 °C recorded by Jahn and Strey.[123]

To the best of my knowledge, the only DRS study on DDAB/W/D microemulsions has been conducted by Sjöblom *et al.*[175] investigating the water-rich and the DDAB-rich borderlines of L_2 (see Figure 4.1). However, these authors only recorded data in the frequency ranges $\sim 0.6 \leq \nu/\mathrm{MHz} \leq 1000$ for their water-rich and $\sim 50 \leq \nu/\mathrm{MHz} \leq 1000$ for their surfactant-rich samples, using a TDR instrument. Due to the limited frequency range of the data, they did not detect any water-related processes and did not succeed in finding an appropriate fitting model for their surfactant-rich spectra. In the case of their water-rich spectra, Sjöblom *et al.* had to use one Cole-Cole equation yielding very high values of the distribution parameter α, which they explained by a marked polydispersity of the water droplets. However, this interpretation has to be regarded with caution since the present results show four relaxation processes in the frequency range studied by Sjöblom *et al.*[175]

Many questions remain regarding the structure and properties of DDAB/W/D microemulsions. But given that as many as six relaxation processes may be present in the spectra given in chapter 3 there is a good chance that this work will shed some more light on the system DDAB/W/D. The challenge that has to be met is to gain a physically meaningful interpretation for the relaxations observed in the dielectric spectra.

4.2 General Remarks

Before starting a detailed analysis of the single relaxation processes, it is expedient to have a short look at the static permittivities, ε_s, and conductivities, κ, of the dielectric spectra at a constant dodecane fraction. As Boned and Peyrelasse point out in their review,[29] care must be taken when discussing a curve with varying surfactant/water ratio in a system near the percolation point: percolation may occur at different dodecane contents for different surfactant/water ratios, so that the varying distance of the data points to the percolation threshold may distort the curve. However, there is no evidence from the DRS data (see Table 3.8) that a percolation transition might occur along a dodecane dilution line in this system (unless maybe at very high dodecane fractions, where we lack of experimental data), nor has this been proposed in the literature. Therefore, it makes sense to discuss to data of Figure 4.3.

When considering the present ε_s data obtained in this work (see Figure 4.3), it is crucial to keep in mind that these values are extrapolations. Since ε does not reach its static limit within the studied frequency range, its values are not very reliable. However, it is certainly fair to say that ε_s is increasing until a DDAB/W ratio of 1 where it reaches a plateau value; the conductivity data (see Figure 3.4) show the same pattern. Apparently, at $w_{\mathrm{DDAB}}/w_{\mathrm{W}} \approx 1$ ($W \approx 25$), the percolation threshold has been passed because the conductivity does not rise any more. On the other hand, a maximum in ε_s should be expected when crossing the percolation line.[31,186] Although care must be taken not to over-interpret the present ε_s data, we may conclude that even the surfactant-rich region of L_2 is still quite close to the percolation point. Further support for this view comes from the developing of ε' as a function of the frequency, ν: as outlined by van Dijk *et al.*, the

slope of this function should be constant near the percolation threshold, independent of the composition of the sample.[187] It can easily be seen from Figures 3.11 and 3.12 that this constant slope is observable for a wide range of DDAB/W ratios.

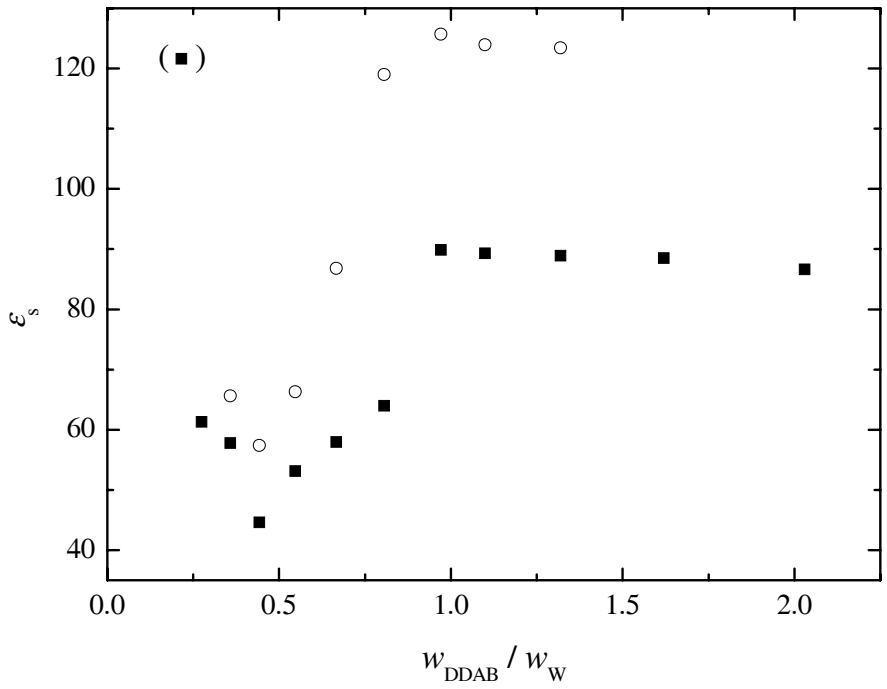

Figure 4.3: Static permittivity, ε_s, of DDAB/W/D microemulsions as a function of the surfactant/water ratio , w_{DDAB}/w_W, at 25 ℃. ■ : $w_D = 0.35$; ∘ : $w_D = 0.23$.

On the water-rich side of L_2, conductivity starts to rise very early, and the shape of the κ curve suggests that also the conductivity values of the first two points ($w_{DDAB}/w_W \lesssim 0.28$) should be larger than zero if they had been determined by a more precise method. Additionally, the fact that the ε_s values are not very low at high water contents, as would be expected for a non-percolating system, supports the view that percolation is starting very early. Note that ε_s is known to be a much more sensitive hint to the beginning of percolation than κ is.[84] Further support for this idea comes from the FFEM image recorded by Jahn and Strey[123] (Figure 4.2), showing already channels between the water droplets at $W \approx 91$ ($w_{DDAB}/w_W \approx 0.283$).

Thus, it may be concluded that in the entire L_2 phase DDAB/W/D microemulsions are quite close to the percolation point. Furthermore, the smooth variations of both the ε_s and κ data strongly question the concept of a sudden structural change in the system. Consequently, models assuming separated water droplets in oil or an abrupt structural change should be applied with great care to DDAB/W/D microemulsions.

4.3 Water in Didodecyldimethylammonium Bromide / Water / n-Dodecane Microemulsions

4.3.1 Preliminary Remarks

Even though there is a variety of microstructures in DDAB/W/D microemulsions, the water 'clusters' present are exposed to geometrical constraints. This phenomenon of 'water under confinement' has created a lot of interest during the last years, not least because of its ubiquitous occurrence in biological processes.[160] A number of authors reported that the properties of water aggregates under confinement are somewhat different from those of bulk water;[34,63,74,94,103,163,197] many of them also stated that the dynamics of water molecules located near the interface differ from those in the core of the water droplets.[63,74,94,103,163] Very recently, Dokter *et al.* conducted a mid-infrared ultrafast pump-probe spectroscopic study of cationic reverse micelles made of cetyltrimethylammonium bromide, water and dichloromethane, a system quite similar to DDAB/W/D. They found regions of extreme salinity near the interface; according to their results, 60 - 90 % of the surfactant counterions should be located in vicinity of the interfacial Stern layer.[74] Further support for this result comes from a chemical trapping study by Cuccovia *et al.*, who analyzed the Br^- distribution in the water pool of hexadecyltrimethylammonium bromide reverse micelles; these authors also found extremely high interfacial Br^- concentrations of up to 6.84 M.[64] These findings are highly important for the interpretation of DDAB/W/D, as this system already contains an overall bromide concentration of approx. 0.5 M - 3.5 M, depending on the DDAB/W ratio. Thus, extremely high electrolyte concentrations should be expected near the interface, strongly suggesting that the water molecules situated there should indeed behave somewhat differently from those located in the core of the water droplets.

In this work, water dynamics in the system DDAB/W/D have been monitored by high-frequency dielectric relaxation spectroscopy. This is one of the first dielectric relaxation studies on microemulsions that extends to the GHz range. As Zhao *et al.* point out in their recent review, water relaxations in microemulsions have barely been investigated.[201] For a selection of samples, the dielectric data of this work have been complemented by FTIR spectra of the O-H stretching vibration. These infrared spectra will be discussed first, as they may provide some useful hints for the interpretation of the dielectric data.

4.3.2 Infrared Data

Components of the O-H Stretching Vibration

As has been outlined in section 3.4, the infrared spectra of the O-H stretching vibration could be described best by a superposition of four bands. This model has been proposed by Śmiechowski and Stangret[178] for pure water; they assigned the highest-wavenumber process A to 'free' O-H oscillators, not forming any H-bonds at all, process B to the H-bonded O-H oscillators of those water molecules having a free O-H oscillator, process C to water molecules situated in a distorted tetrahedral environment (where only less than

four H-bonds per molecule are formed), and process D to water molecules embedded in a tetrahedral ice-like network.

Compared to bulk water, the fractions of ice-like water (process D) are higher and the fractions of free O-H oscillators (processes A and B) are lower for all investigated DDAB/W/D microemulsions. This finding suggests that on the whole, the tetrahedral water network in the water droplets is *strengthened* relative to bulk water. Following a D dilution line at a constant DDAB/W ratio, the fraction of the distorted-tetrahedral water (process C) is increasing with increasing D content at the expense of ice-like water (process D), see Figures 4.4 and 4.5. This is an apparent contradiction to the concept outlined by Barnes *et al.* saying that along a D dilution line only the concentration of H_2O droplets should change, but their geometry should remain constant.[11] This concept is based on the plausible idea that the volume to surface ratio of a droplet in a water-in-oil microemulsion should be governed by the water to surfactant ratio. The fact that it does not seem to apply in this case suggests that we do not observe separated droplets any more, but a structure that is already percolating, making geometrical predictions more complicated.

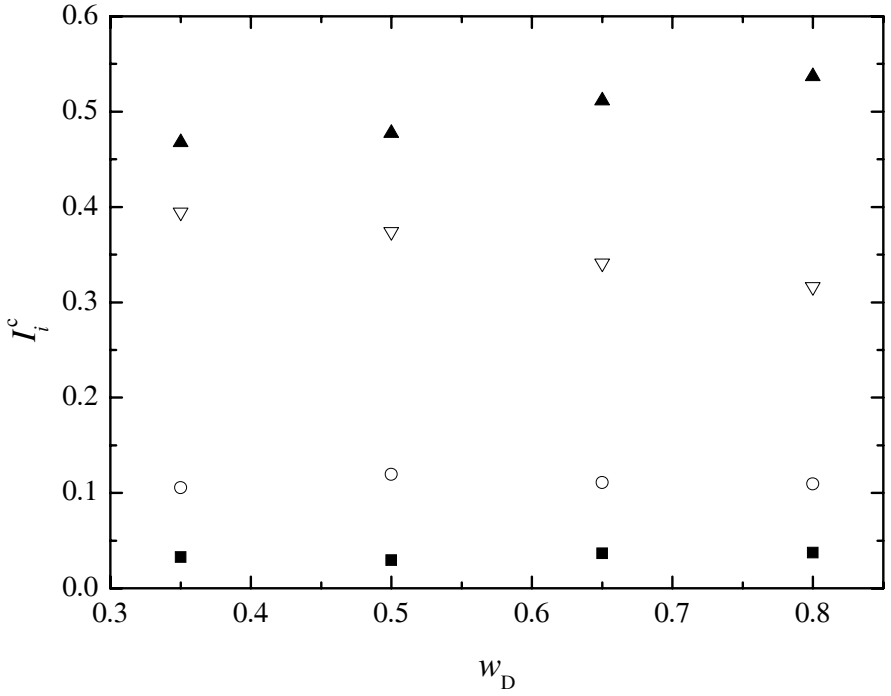

Figure 4.4: Fitting results of the O-H stretching vibration in DDAB/W/D microemulsions: corrected relative band intensities, I_i^c, as a function of the dodecane content, w_D, at $w_{DDAB}/w_W = 0.358$ and 25 ℃. ■: band A; ○: band B; ▲: band C; ▽: band D.

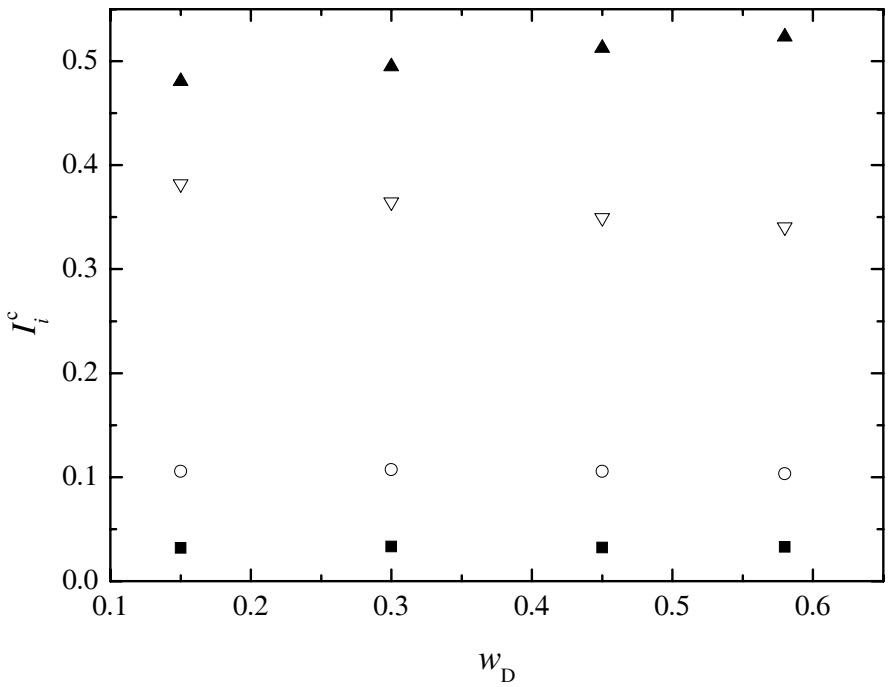

Figure 4.5: Fitting results of the O-H stretching vibration in DDAB/W/D microemulsions: corrected relative band intensities, I_i^c, as a function of the dodecane content, w_D, at $w_{DDAB}/w_W = 0.667$ and 25 ℃. ■: band A; ○: band B; ▲: band C; ▽: band D.

However, the most important finding of this analysis is the increase in process C at the expense of process D with increasing DDAB/W ratio at a constant dodecane fraction. Even though the exact microstructure of the system is not obvious due to increasing percolation effects, the increasing DDAB/W ratio will result in an increasing surface to volume ratio. Consequently, the percentage of water molecules located near the interface will rise at the expense of those water molecules situated in the core. If this transition is accompanied by a decrease in ice-like water and a simultaneous increase in distorted tetrahedral water, it may be concluded that core water contains a higher percentage of ice-like water than interfacial water does. Thus, the tetrahedral water network in the core of water droplets and channels should be stronger than it is at the interface, and it may be expected that this structural difference between the two types of water will also be observable in the dielectric spectra.

It is important to emphasize, though, that all four bands describing the O-H stretching vibration are also present in pure bulk water.[178] Thus, it would be erroneous to equate process D with the core water and process C with the interfacial water of a droplet. The only thing we can deduce from Figure 4.6 is that the *percentage* of ice-like water is higher in the core than it is near the interface.

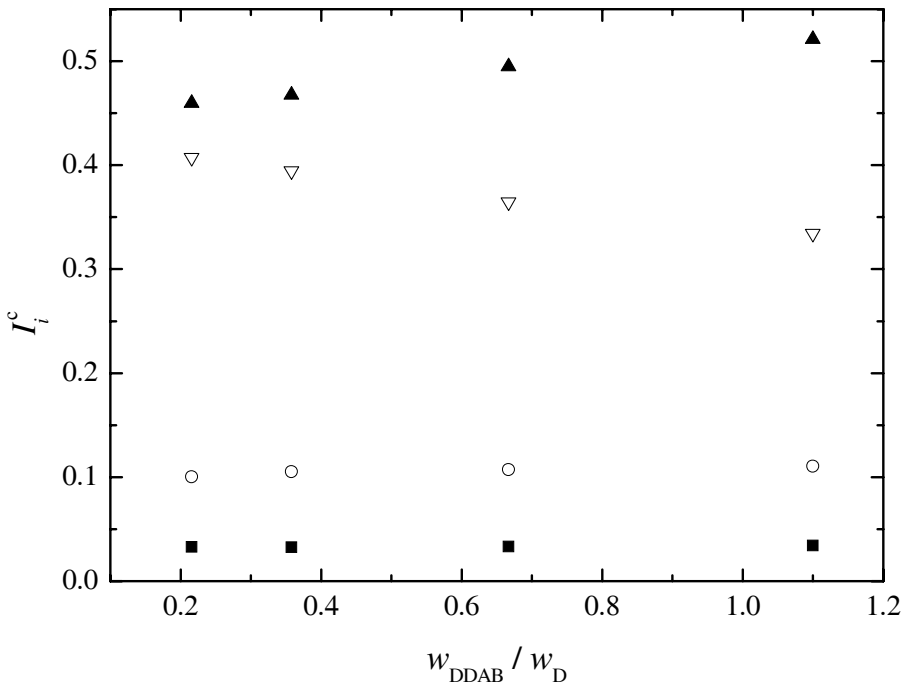

Figure 4.6: Fitting results of the O-H stretching vibration in DDAB/W/D microemulsions: corrected relative band intensities, I_i^c, as a function of the surfactant/water ratio, w_{DDAB}/w_W at $w_D = 0.35$ and 25 ℃. ■: band A; ○: band B; ▲: band C; ▽: band D.

Literature Review

Infrared spectra of water-in-oil microemulsions or related compounds have been recorded by various authors.[36,124,148,149] Jain *et al.* studied reverse micelles made of AOT (sodium bis(2-ethylhexyl) sulfosuccinate), water and isooctane and fitted the O-H stretching vibrations with three Gaussian bands, which they ascribed to trapped water (in the interface), bound water (in the interfacial Stern layer) and free water (in the core of the reverse micelle), respectively.[124] However, this assignment ascribing only one band to bulk water is incompatible with the very recent results of Śmiechowski and Stangret[178] showing that also the O-H stretching vibration of bulk water is composed of four bands.

Onori and Santucci investigated the O-H stretching vibration of AOT/water/CCl_4 microemulsions for different micelle sizes[148] and found the total peak area to increase linearly with the water content, which is consistent with the Bouguer-Lambert-Beer law (see section 2.3.1). Figure 4.7 shows that this also applies to the IR spectra recorded in this work, except for very low dodecane contents. Also Onori and Santucci fitted the total peak using three Gaussian bands so that a comparison with the results of this work is not straightforward. Nevertheless, these authors also observed a distinct decrease of the lowest-frequency band with decreasing droplet size. The quantitative interpretation, however, is somewhat problematic as a 'bulk-water contribution' obtained from the lowest-

frequency band is subtracted from the measured spectra. This processing is questionable in two respects. First, the bulk-water spectrum is composed of several bands, so that it does not make sense to derive a bulk-water contribution only from the lowest-frequency band. Second, as will be outlined later, the DRS results of this work strongly suggest that there is no 'bulk' water present in DDAB/W/D microemulsions: the dynamics of all detected water species exhibit significant differences from bulk water.

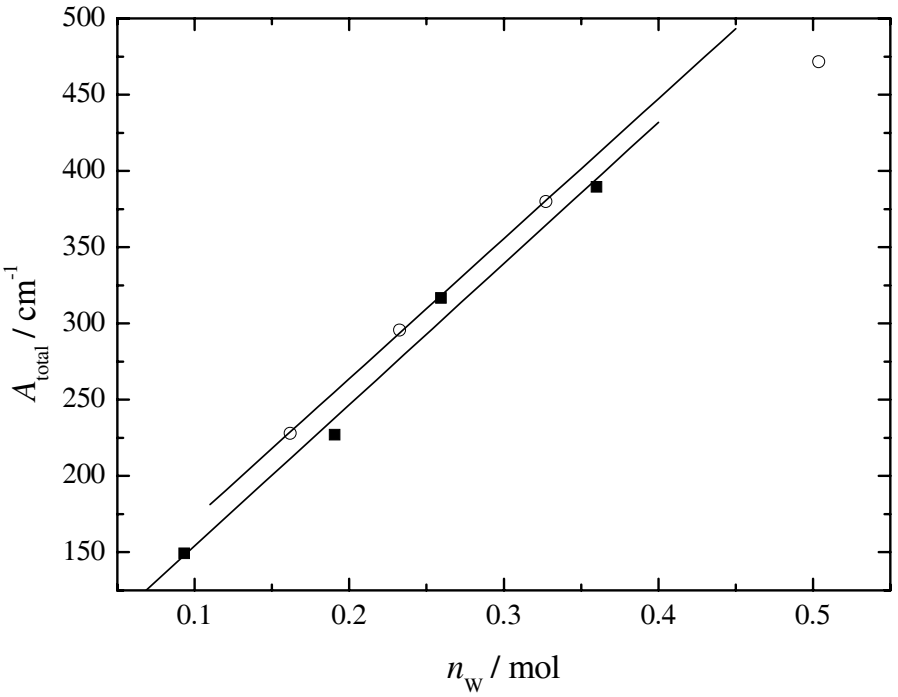

Figure 4.7: Total peak area of the O-H stretching vibration, A_{total}, as a function of the water content, n_{W} of DDAB microemulsions at constant DDAB/W ratio. ■: $w_{\text{DDAB}}/w_{\text{W}} = 0.358$; ○: $w_{\text{DDAB}}/w_{\text{W}} = 0.667$; full lines represent linear fits.

Brubach *et al.* investigated the O-H stretching vibration of non-ionic fluorocarbon reverse micelles.[36] Again, the total peak was fitted using three Gaussian bands, which these authors ascribed to 'almost ice-like network water', 'somewhat connected, but not ice-like' intermediate water and free H_2O oscillators. Consistent with the results of this work, a considerable decrease in the network-water percentage and a simultaneous increase in the intermediate-water percentage were found for increasing surfactant/water ratios. These authors also tried to estimate the thickness of the interfacial water layer by subtracting a bulk-water contribution which was obtained from all three bands. However, also this processing was based on the assumption that water in the core of reverse micelles should behave like bulk water; as outlined previously, the DRS data of this work contradict this assumption.

4.3.3 Dielectric Data

Analysis of Relaxation Times

In the dielectric spectra of DDAB/W/D the two highest-frequency processes 5 and 6 can be ascribed without any doubt to water relaxations. As can be seen from Figures 4.8 and 4.9 both relaxation times ($\tau_5 \approx 12$ ps, $\tau_6 \approx 3$ ps) deviate considerably from the bulk-water value of $\tau_b \approx 8.3$ ps.[41] As water relaxation processes in the dielectric spectrum located in this frequency range are due to the cooperative dynamics of the H-bond network, its relaxation times can be interpreted as the 'dwelling time' a water molecule has to 'wait' until all H-bonds except one are broken so that it can freely rotate.[37] Thus, the unusually long relaxation time τ_5 reflects a strengthening of the H-bond network relative to bulk water. On the other hand, τ_5 is unusually short to be described as *slow water* surrounding a hydrophobic particle. This phenomenon, exhibiting a typical relaxation time of $\tau_{slow} \approx 17.5$ ps, has been observed for aqueous solutions containing large hydrophobic ions such as BPh_4^- and Ph_4P^+,[190] R_4N^+,[43] large carboxylate ions[185] and micellar systems.[7] However, as the hydrophobic parts of the surfactant DDAB should be outside the aqueous subphase of the microemulsion such a slow-water mode is not expected to occur in DDAB/W/D microemulsions.

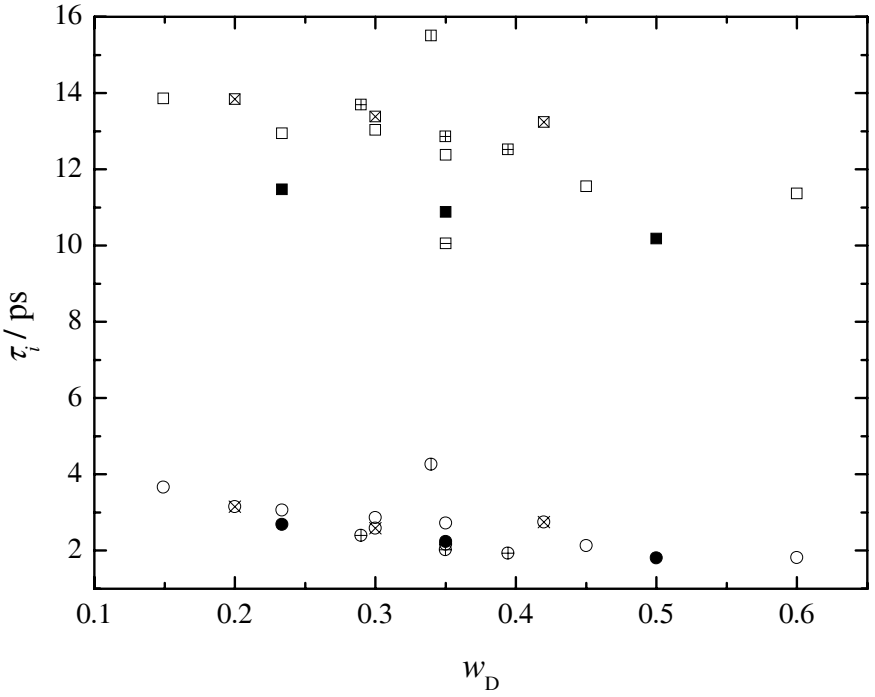

Figure 4.8: Relaxation times τ_5 and τ_6 as a function of the dodecane mass fraction, w_D, at 25 °C. Values given in brackets are the surfactant/water ratios, w_{DDAB}/w_W. ⊟: τ_5 (0.216); ■: τ_5 (0.358); □: τ_5 (0.667); ⊠: τ_5 (1.10); ⊞: τ_5 (1.63); ◫: τ_5 (2.03); ⊖: τ_6 (0.216); ●: τ_6 (0.358); ○: τ_6 (0.667); ⊗: τ_6 (1.10); ⊕: τ_6 (1.63); ⏀: τ_6 (2.03).

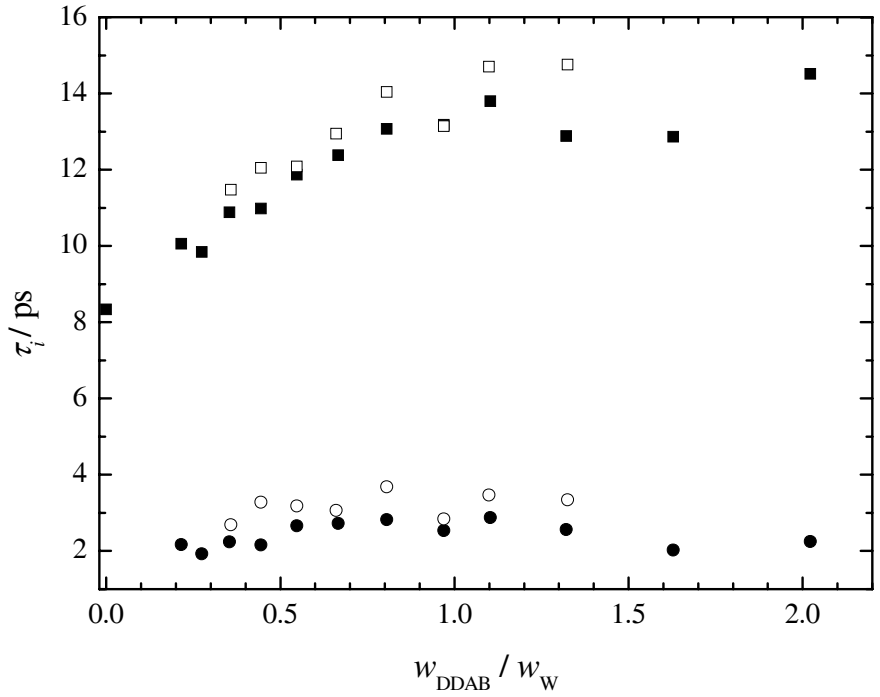

Figure 4.9: Relaxation times τ_5 and τ_6 as a function of the surfactant/water ratio, $w_{\mathrm{DDAB}}/w_{\mathrm{W}}$, at 25 °C. ■: $\tau_5, w_{\mathrm{D}} = 0.35$; □: $\tau_5, w_{\mathrm{D}} = 0.23$; •: $\tau_6, w_{\mathrm{D}} = 0.35$; ○: $\tau_6, w_{\mathrm{D}} = 0.23$.

To the best of my knowledge, the only water process observed so far exhibiting relaxation times similar to τ_6 has been the 'fast water' process in water/dioxane mixtures. This relaxation has been ascribed to those water molecules situated in a dioxane-rich environment where some of the H_2O-H_2O bonds are replaced by the much weaker H_2O-dioxane interactions.[170,171] Similarly, process 6 may be interpreted as the relaxation of water molecules located in a bromide-rich environment. It is known that the addition of low to moderate amounts of NaBr ($c \leq 1.4$ M) already provokes a significant shortening of the bulk-water relaxation times.[189,192] This was interpreted in terms of a *structure-breaking effect* exerted by the Br^- anions on the tetrahedral water network.[189] In this context, it should be kept in mind that 60 to 90 percent of the total amount of surfactant counterions should be located near the interface[74] and that the overall counterion concentration in the aqueous subphase of DDAB/W/D already amounts to 0.5 M - 3.5 M, depending on the DDAB/W ratio.

Further support for this assignment comes from a Raman study by Walrafen, where a breakdown of the three-dimensional water network was observed upon the addition of the larger halide ions.[193] Walrafen concluded that this breakdown is caused by the formation of H-bonds between water molecules and the larger halide anions, which obviously are considerably weaker than H-bonds between two water molecules.

In summary, the relaxation times suggest that process 6 reflects water molecules located near the interface, which would be consistent with the infrared results discussed previously.

Analysis of Relaxation Amplitudes

Even though it may be tempting to accept this assignment on the basis of the preceding reasoning it is essential not to draw any conclusions before a careful analysis of the amplitudes S_5 and S_6 of the two relaxation processes has been done. With the help of the Cavell equation generalised for ellipsoidal reaction fields

$$c_i = \frac{3(\varepsilon + (1-\varepsilon)A_i)}{\varepsilon} \cdot \frac{\mathrm{k_B} T \varepsilon_0}{\mathrm{N_A}} \cdot \frac{(1-\alpha_i f_i)^2}{g_i \mu_i^2} \cdot S_i \tag{4.1}$$

the concentrations c_i of the 'types' of water monitored in processes 5 and 6 can be calculated. Expressions for the reaction field factor, f_i, and the geometry parameter, A_i, are given in section 1.4.2. However, the values of the empirical Kirkwood factors, g_i, are unknown for water confined in the aqueous subphase of a W/O microemulsion.

As has been outlined in section 1.4.3, the Kirkwood factor g accounts for intermolecular interactions. For two neighbouring dipole molecules preferring parallel alignment relative to each other a value of $g > 1$ is observed, antiparallel dipole alignment yields $g < 1$, and statistical alignment $g = 1$.[27] It is well known that considerable dipole-dipole correlations are present in the tetrahedral network of bulk water, yielding a Kirkwood factor of $g \approx 2.8$.[41] However, g is very susceptible to changes in the water structure; for example, for aqueous solutions of electrolytes containing sterically demanding ions like $NaBPh_4$ a significant decrease in g has been observed.[190] Taking into account that the relaxation times of the two water processes 5 and 6 deviate considerably from the bulk-water value, reflecting significant differences in the water structure, the empirical Kirkwood factors g_5 and g_6 are very likely to deviate considerably from the bulk-water value, too. Additionally, since τ_5 and τ_6 imply striking differences in the structure of the water 'regions' monitored by these two relaxations we can assume $g_5 \neq g_6$. It is even possible that due to strong interactions with the interface the dipoles of the interfacial water molecules exhibit antiparallel alignment, yielding $g_i < 1$ (see Figure 4.13).

This problem could be overcome if g_i could be assumed to be constant throughout the L_2 phase. This may be a valid approximation for dodecane dilution lines, where the DDAB/W ratio remains constant and therefore the microstructure is not expected to change drastically. However, when the DDAB/W ratio varies, inducing structural changes from separated water droplets in oil to a network of water channels, it is hard to imagine that this should not affect the Kirkwood factor. In conclusion, there is little prospect of extracting some information about the dependence of c_i on the DDAB/W ratio from the experimental data.

Test of Hypothesis 1: Kirkwood Factor g_5 Remains Constant Throughout L_2

In the following paragraph we will tentatively assume the hypothesis that the changes in g_i with varying DDAB/W ratio are negligible. As changes in c_i obtained from eq. (4.1) are not very meaningful without considering the simultaneous changes in the total water concentration of the microemulsion $c_W = n_W/V_{total}$, $g_i c_i / c_W$ is plotted against the surfac-

tant/water ratio, $w_{\mathrm{DDAB}}/w_{\mathrm{W}}$ (see Figures 4.10 and 4.11). It is conspicuous that $g_5 c_5/c_{\mathrm{W}}$ increases significantly with increasing DDAB/W ratio; hence it is self-evident to speculate that this process may be due to interfacial water because it shares the same characteristics. In order to estimate the fraction of interfacial water relative to the total amount of water in the system, the following geometrical model has been developed on the basis of the geometrical considerations by van Dijk *et al.*[188]

Let us consider first a spherical water droplet of radius R surrounded by n_{DDAB} surfactant molecules; each of them occupies the interfacial area A. The interior of the droplet consists of water molecules of volume v_{W}, surfactant head groups of volume v_{h} and bromide counterions of volume v_{Br}. Then the following relations are valid:

$$n_{\mathrm{DDAB}} A = 4\pi R^2 \tag{4.2}$$

$$n_{\mathrm{DDAB}} \left(\frac{n_{\mathrm{W}}}{n_{\mathrm{DDAB}}} v_{\mathrm{W}} + v_{\mathrm{h}} + v_{\mathrm{Br}} \right) = \frac{4}{3}\pi R^3 \tag{4.3}$$

Eq. (4.2) states that the interfacial area occupied by the surfactant molecules should be equal to the interface of the water droplet, whereas eq. (4.3) equates the total volume of the droplet to the sum of the volumes of its single components. Solving these two equations yields:

$$R = \frac{3}{A} \left(\frac{n_{\mathrm{W}}}{n_{\mathrm{DDAB}}} v_{\mathrm{W}} + v_{\mathrm{h}} + v_{\mathrm{Br}} \right) \tag{4.4}$$

Thus, the radius of a water droplet can be calculated: $v_{\mathrm{W}} = 30.0$ Å^3 is given by the molar mass and the density of water, $v_{\mathrm{h}} = 120$ Å^3 is taken from Chen *et al.*[53] and $v_{\mathrm{Br}} = 50.1$ Å^3 is calculated from the standard partial molar volume $v^{\ominus}_{\mathrm{Br}} = 30.2$ cm^3 mol^{-1} selected by Marcus.[141] The headgroup area A of DDAB as determined from X-ray measurements of the two lamellar phases of DDAB in water is given in the literature;[53] as these measurements yield slightly different results depending on the investigated phase ($A_1 = 60$ Å^2, $A_2 = 68$ Å^2) the average value was used for the calculations done in this work.

With the help of R we are now able to determine the number of water molecules located in the droplet according to:

$$n_{\mathrm{W}} = \frac{\frac{4}{3}\pi R^3 - n_{\mathrm{DDAB}}(v_{\mathrm{h}} + v_{\mathrm{Br}})}{v_{\mathrm{W}}} \tag{4.5}$$

Similarly, the relative fraction of water molecules located near the interface, $n_{\mathrm{W,if}}/n_{\mathrm{W}}$, can be calculated

$$\frac{n_{\mathrm{W,if}}}{n_{\mathrm{W}}} = \frac{\frac{4}{3}\pi R^3 - \frac{4}{3}\pi (R - 2x r_{\mathrm{W}})^3 - n_{\mathrm{DDAB}}(v_{\mathrm{h}} + v_{\mathrm{Br}})}{v_{\mathrm{W}} \cdot n_{\mathrm{W}}} \tag{4.6}$$

where x is the number of water layers belonging to the interfacial area. It is of course arbitrary to draw a borderline between interfacial and core water, but given that the surfactant head groups extend at least 2 Å into the water droplet and given that many of

their nearest neighbours are Br^- ions of the radius $r_{Br^-} = 1.96$ Å[141] the interfacial layer thickness should be equivalent to at least three or possibly four water layers.

Certainly, this model does not account for percolation, which plays a decisive role in DDAB/W/D microemulsions as outlined previously. Therefore it is appropriate to extend this model to cylinders of surface $A = 2\pi rl$ and volume $V = 4\pi r^2 l$, reflecting the structure of a bicontinuous network. Note that the areas of the ends have not been included into A as they are connected to other spheres or cylinders, thus not being a part of the interface. The parameters of this cylindric model can be calculated analogously to eqs. (4.2) to (4.6), assuming a cylinder radius of $r = R/2$, as has been done in the DOC model (see section 1.6.1).

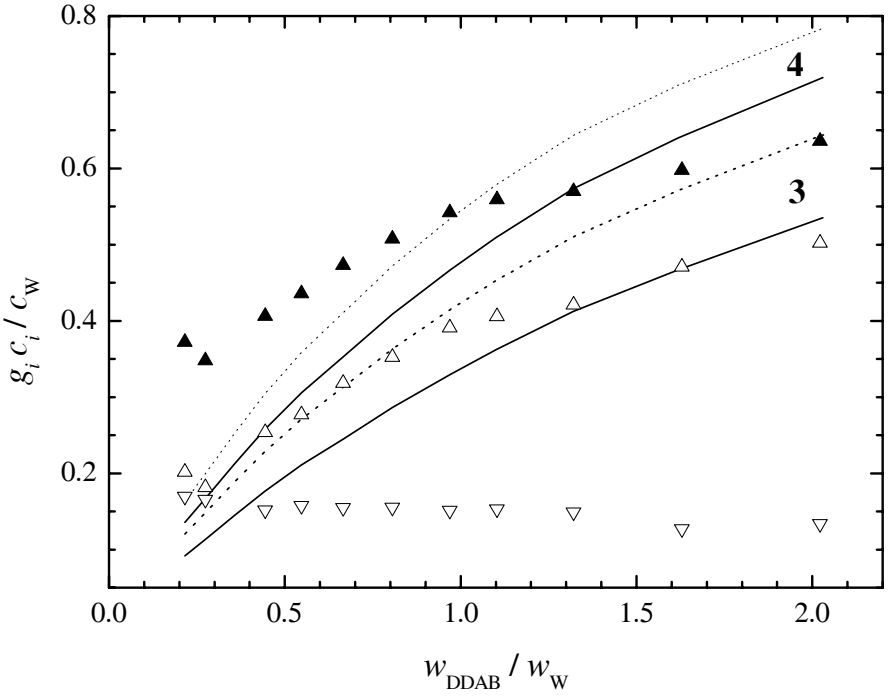

Figure 4.10: Relative water concentrations multiplied by the Kirkwood factor, $g_i c_i/c_W$, as a function of the surfactant/water ratio, w_{DDAB}/w_W, at $w_D = 0.35$ and 25 °C. ▲: $(g_5c_5 + g_6c_6)/c_W$; △: g_5c_5/c_W; ▽: g_6c_6/c_W; full lines: $n_{W,if}/n_W$, spherical droplet model assuming 3 and 4 interfacial W layers; dashed lines: $n_{W,if}/n_W$, cylinder model assuming 3 and 4 interfacial W layers.

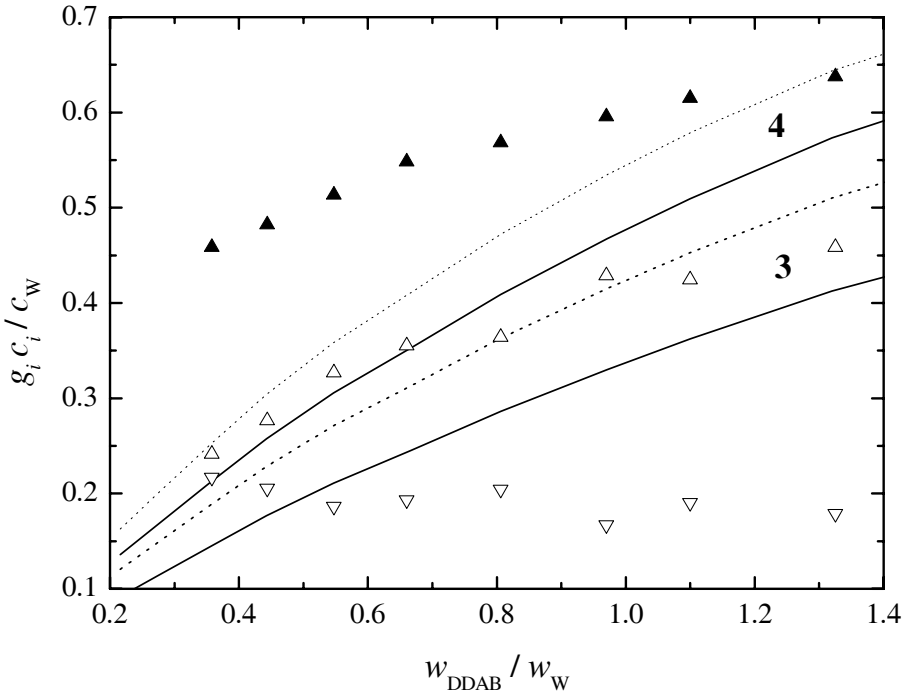

Figure 4.11: Relative water concentrations multiplied by the Kirkwood factor, $g_i c_i/c_W$, as a function of the surfactant/water ratio, w_{DDAB}/w_W, at $w_D = 0.23$ and 25 ℃. ▲: $(g_5c_5 + g_6c_6)/c_W$; △: g_5c_5/c_W; ▽: g_6c_6/c_W; full lines: $n_{W,if}/n_W$, spherical droplet model assuming 3 and 4 interfacial W layers; dashed lines: $n_{W,if}/n_W$, cylinder model assuming 3 and 4 interfacial W layers.

As the actual structure of the microemulsion probably lies in between spherical water droplets and cylinders, the results of both models have been plotted in Figures 4.10 to 4.12, together with the experimental data. As we assume g_5 to be an unknown but constant factor, it is not possible to compare the values of g_5c_5/c_W and $n_{W,if}/n_W$ directly. However, it is noticeable that the dependence of the interfacial water fraction on the DDAB/W ratio does indeed agree very well with that of the experimental g_5c_5/c_W data, which is consistent with the assumption that process 5 can be ascribed to interfacial water. Nevertheless, it should be kept in mind that this assignment is based on the very uncertain hypothesis that the Kirkwood factor g_5 remains constant at varying DDAB/W ratios. Assuming that process 5 is due to interfacial water implies that process 6 can be ascribed to the water in the core of the aqueous subphase. Hence c_6/c_W should decrease significantly with increasing DDAB/W ratio. As the observable decrease in g_6c_6/c_W is only very faint, it must be assumed that g_6 is rising considerably, showing a much stronger dependence on the DDAB/W ratio than g_5 does. This finding is difficult to explain, thus calling our initial hypothesis into question.

If we further assume that g_5 remains constant with varying DDAB/W ratios, it also has to be constant along a dodecane dilution line, where the geometry of the water droplets should change little or not at all. Thus, along a dodecane dilution line g_5c_5/c_W should

either remain constant if the droplet size remains constant, too, or increase with rising dodecane content if the droplet size decreases, leading to an increase in the percentage of interfacial water. However, what can be seen in Figure 4.12 is a *decrease* in g_5c_5/c_W with increasing D content, which cannot be interpreted on the basis of the preceding rationale. In conclusion, our initial hypothesis must be rejected.

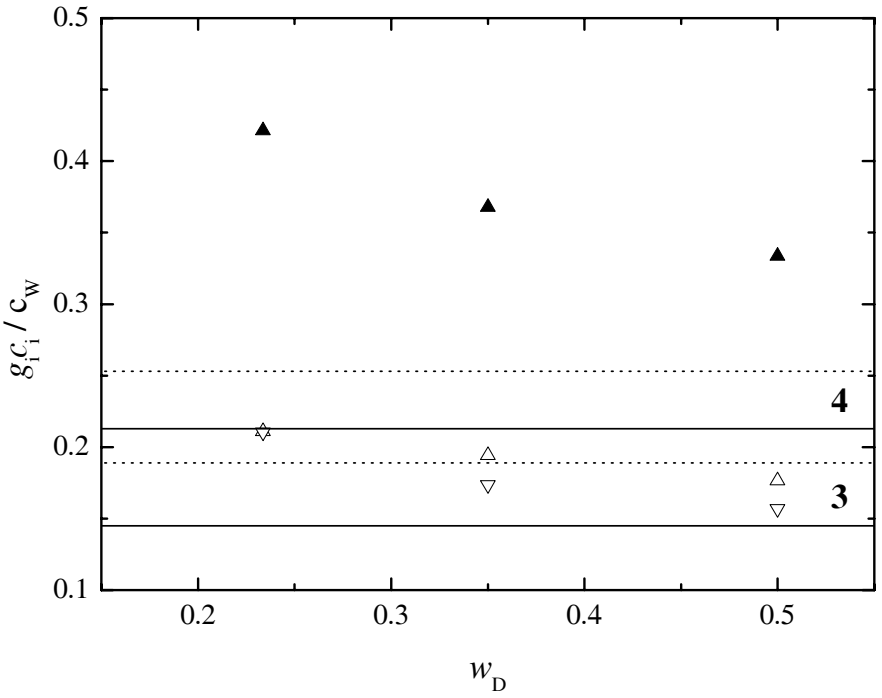

Figure 4.12: Relative water concentrations multiplied by the Kirkwood factor, g_ic_i/c_W, as a function of the dodecane mass fraction, w_D, at $w_\mathrm{DDAB}/w_\mathrm{W} = 0.358$ and 25 °C. ▲: $(g_5c_5 + g_6c_6)/c_\mathrm{W}$; △: g_5c_5/c_W; ▽: g_6c_6/c_W; full lines: $n_\mathrm{W,if}/n_\mathrm{W}$, spherical droplet model assuming 3 and 4 interfacial W layers; dashed lines: $n_\mathrm{W,if}/n_\mathrm{W}$, cylinder model assuming 3 and 4 interfacial W layers.

Test of Hypothesis 2: Kirkwood Factor g_5 Remains Constant Along a Dodecane Dilution Line

There are two possible explications for the result shown in Figure 4.12. First, the Kirkwood factor g_5 is indeed subject to considerable fluctuations depending on the composition of the microemulsion so that our initial hypothesis must be rejected and the complete rationale based on the g_5c_5 data is without significance. Alternatively, we may assume that g_5 remains constant along a D dilution line. This is much more probable than the previous hypothesis as the microstructure of the water droplets or channels should not change considerably at a constant DDAB/W ratio. Then, the decrease in g_5c_5/c_W suggests the assignment that process 5 is due to the water fraction located in the *core* of the aqueous subphase because its percentage decreases with decreasing droplet size.

This assignment is consistent with the experimental data from Figures 4.10 and 4.11. Assuming that process 5 is due to core water its percentage should decrease with increasing DDAB/W ratio. Thus, the fact that $g_5 c_5/c_W$ is increasing means that the Kirkwood factor g_5 must increase, too, to overcompensate the decrease in c_5. This makes sense given the transition from separated spherical water droplets to a bicontinuous network developing with increasing DDAB/W ratio. Due to strong electrostatic interactions with the outer Helmholtz layer of charged counterions, the interfacial water molecules are aligned as sketched in Figure 4.13, leading to an antiparallel orientation of oppositely located dipoles. In the highly ordered geometrical environment of a sphere, this antiparallel alignment of the interfacial water will transmit to the core water dipoles (see Figure 4.13), thus yielding very low g_5 values. In contrast, the more percolation is proceeding, the more this peculiar ordered environment will be lost, and the core water molecules will begin to prefer parallel alignment, similar to bulk water, thus leading to a pronounced increase in g_5.

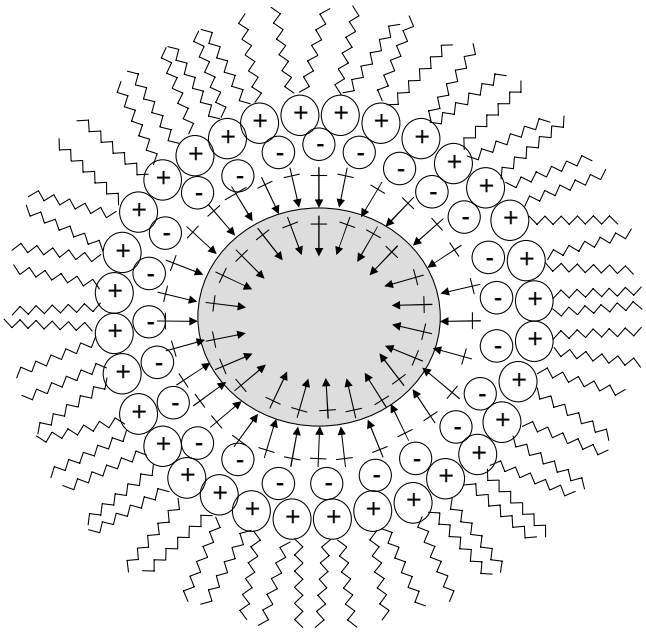

Figure 4.13: Sketch of a spherical water droplet in the system DDAB/W/D according to Overbeek.[152] Surfactant head groups and the outer Helmholtz layer of counterions form the interface, which strongly influences the alignment of the nearby water molecules. This antiparallel dipole alignment of the interfacial water molecules transmits to the orientation of those water molecules located in the core (grey area).

On the other hand, the values of $g_6 c_6/c_W$ are very low compared to the percentage of interfacial water and are even slightly decreasing with a rising DDAB/W ratio although the fraction of interfacial water is increasing simultaneously. Consequently, g_6 must be well below 1, and it has to decrease with increasing DDAB/W ratio. Again, this can be explained considering the strong electrostatic interactions of interfacial water with the interface that are increasing with the rising counterion concentration coming along with an increasing DDAB/W ratio. Thus, antiparallel alignment of the interfacial molecules is even increasing, yielding a decrease in g_6. Note that this 'headgroup-dependent orientation' has also been predicted by a recent MD simulation conducted by Rosenfeld and Schmuttenmaer.[163]

Conclusion: Process Assignment

If there are any conclusions regarding the water process assignment that can be drawn from the $g_i c_i/c_W$ data they support the conclusions coming from a comparison of the relaxation times τ_i with the results of the infrared spectra. Thus, the most probable assignment ascribes process 5 ($\tau_5 \approx 12$ ps) to water in the core of the aqueous subphase, whose dynamics is slowed down due to a very pronounced tetrahedral ice-like structure that may arise from the confinement in a highly geometrically ordered environment. Process 6 ($\tau_6 \approx 3$ ps) is assigned to interfacial water; as outlined in detail previously, its fast relaxation time is due to the scarcity of water caused by the very high bromide concentration in this area, leading to a partial substitution of H-O bonds by the considerably weaker[189,193] H-Br^- bonds.

Irrotationally Bound Water

Besides these two water relaxation processes it is possible that 'irrotationally bound' (IB) water is also present in DDAB/W/D microemulsions. As outlined in section 1.6.2, this term is used to describe water molecules that are bound so tightly by an ion that they cannot rotate on the DRS timescale. As discussed elsewhere, a number of experimental results suggest that the solvation sphere of a chloride anion is very weak, yielding $Z_{IB} = 0$.[42] Given that the hydration of bromide is expected to be even weaker than that of chloride, we can exclude that any irrotational bonding will be due to the counterions.[192] However, it is likely that the cationic surfactant head groups will affect the dynamics of the neighbouring water molecules. It should be noted in this context that micelles made of dodecyltrimethylammonium bromide in aqueous solution exhibit Z_{IB} values of 10.2 ± 0.8.[7] When comparing a series of different alkyltrimethylammonium bromide micelles Z_{IB} increases with increasing chain length, which is equivalent to a *decreasing* distance between neighbouring head groups. Baar *et al.* interpret this apparent paradox in terms of a 'cooperative effect' of the highly positively charged micelle interface, giving rise to a pronounced immobilisation of the nearby water molecules even beyond the first hydration shell.[6,7] Thus, some irrotational bonding should also be expected for the aqueous subphase of DDAB/W/D especially since no 'slow water' surrounding the surfactant head groups has been detected in the dielectric spectra.

Unfortunately, it is not possible to answer this question in a quantitative way. Due to the unknown Kirkwood factors the apparent water concentrations c_5 and c_6 cannot be determined; however, these values are required to calculate Z_{IB} according to eq. (1.202). Nevertheless, the following rough estimation illustrates that it is plausible to assume irrotational bonding. For $w_{\mathrm{DDAB}}/w_{\mathrm{W}} \approx 1.2$, $c_6/c_{\mathrm{W}} \approx 0.6$ is a very high percentage for interfacial water, corresponding to four water layers in a cylindrical model. This assumption implies that the Kirkwood factor $g_6 \approx 1/3$, which is certainly a very low value. However, if the existence of irrotationally-bound water is ruled out, c_5/c_{W} has to be equal to 0.4; as the experimental data yield $g_5 c_5/c_{\mathrm{W}} \approx 0.4$ this means that the Kirkwood factor g_5 must be approximately 1. However, this value is unrealistically low for a phase point located clearly in the bicontinuous part of L_2. In summary, it is likely that irrotational bonding does play a role in DDAB/W/D microemulsions.

Literature Review

In the literature, there are a number of findings which support the conclusions drawn from the high-frequency dielectric data obtained in this work. For example, Hauser *et al.* studied the hydration of AOT reverse micelles combining results from differential scanning calorimetry, ESR spin labelling and ^{2}H NMR.[107] They found a total number of 13 water molecules to be structurally perturbed by one surfactant molecule: two water molecules appeared to be bound very strongly, while the remaining 11 molecules were associated more weakly. A neutron scattering and MD simulation study of AOT reverse micelles by Harpham *et al.* provided significant evidence for the existence of water of reduced mobility near the interface;[103] however, it has to be taken into account that their reverse micelles were considerably smaller than the W/O droplets investigated in this work.

Perhaps the strongest support of the conclusions made in this work comes from a recent MD simulation study of reverse micelles conducted by Rosenfeld and Schmuttenmaer.[163] These authors also detected three types of water, which they call 'trapped', 'bound' and 'bulk-like' water. The trapped water, located directly at the interface, is 'essentially excluded from any bulk-like hydrogen bonding network due to both solvation of the counterions and interaction with the surfactant headgroups'. The bound region, situated adjacent to the trapped water, is 'highly perturbed by the interface and has a headgroup-dependent orientation', yielding a low Kirkwood factor. Furthermore, these authors report that 'in the bound region, the headgroups also partially exclude other waters from accepting hydrogen bonds', thus inducing a weakening of the H-bond network that becomes manifest in a short relaxation time. As can be seen, these results confirm the total number of three regions, each with a different type of water. They are also consistent with the present relaxation times τ_i and Kirkwood factors g_i.

4.4 Ion Pairing

As ion pairs consisting of a cation and an anion exhibit a permanent dipole moment, they can be investigated by dielectric relaxation spectroscopy provided their lifetimes correspond to the range of the experiment. In contrast, 'clusters' of cationic or anionic species do not create a signal in the dielectric spectrum.

Ion pairs have been detected by DRS for a large number of aqueous electrolyte solutions (see *e.g.* refs.[190–192]) and also in the submicellar concentration range of aqueous solutions of ionic surfactants,[8,113] among which was dodecyltrimethylammonium bromide, a molecule very similar to DDAB. Hence, it is very likely that also DDAB is able to form ion pairs; what makes the situation more complicated in the case of DDAB/W/D microemulsions are the geometrical constraints at the interface the surfactant molecules are subject to, strongly restraining their rotatability. Therefore, ion pairs have not been expected to be observed in this system.

However, as can be seen from Figures 4.14 and 4.15, process 4 of the present dielectric spectra exhibits relaxation times of $60 \lesssim \tau_4 \text{ / ps} \lesssim 270$, a range which is typical of ion-pair relaxations. The large scattering of τ_4 is very likely to reflect fitting uncertainties, arising because S_4 is extremely small compared to the amplitudes of the neighbouring processes, although it is remarkable that no fitting parameters had to be fixed to resolve process 4. Considering both the relaxation times and the notably small amplitudes, it appears promising to process these data assuming they reflect the presence of ion pairs.

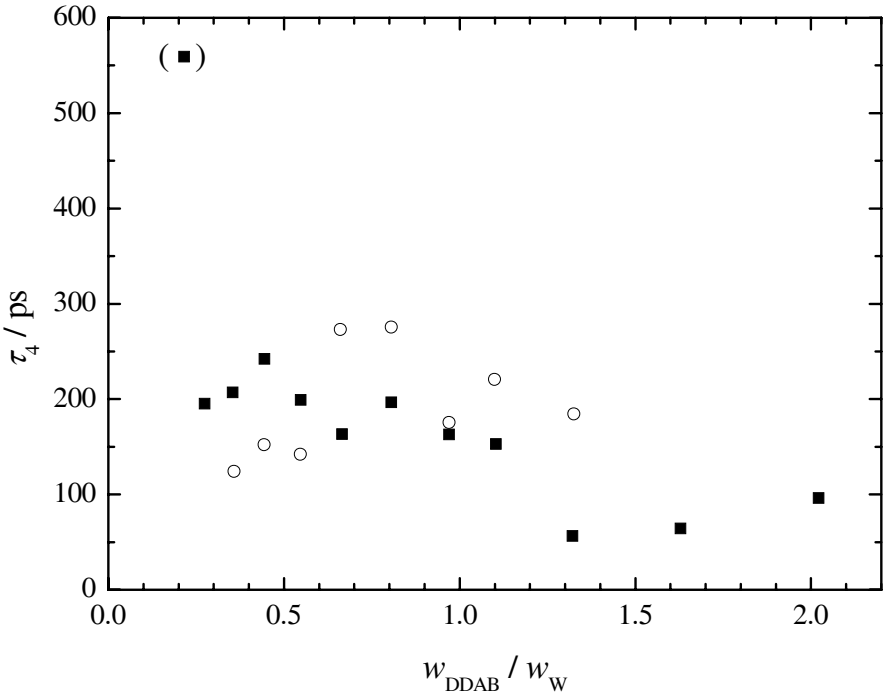

Figure 4.14: Relaxation times of process 4, τ_4, as a function of the surfactant/water ratio, w_{DDAB}/w_W, at 25 °C. ■: $w_D = 0.35$; ○: $w_D = 0.23$.

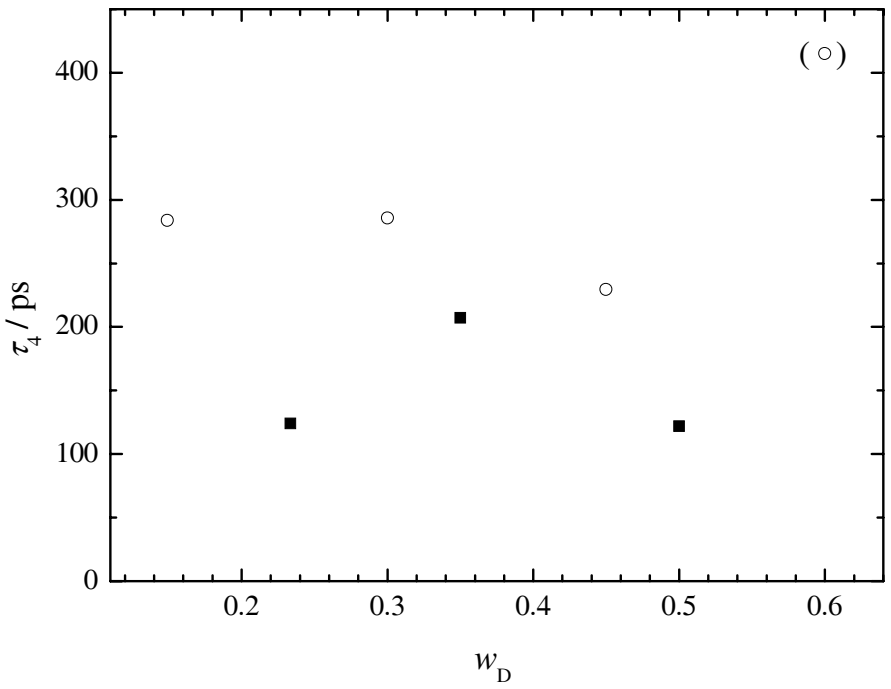

Figure 4.15: Relaxation times of process 4, τ_4, as a function of the dodecane mass fraction, w_D, at 25 °C. ■: $w_{DDAB}/w_W = 0.358$; ○: $w_{DDAB}/w_W = 0.667$.

Ion-pair concentrations, c_{IP}, can be obtained from the relaxation amplitude S_i, via the modified Cavell equation (1.79), where the effective dipole moment, μ_{eff}, is given by the Rittner equation:[162]

$$\mu_{eff} = \mu_0 - \mu_{ind} - n \cdot \mu_{H_2O} \tag{4.7}$$

This equation states that the dipole moment μ_0, defined according to

$$\mu_0 = z\, e_0\, d \tag{4.8}$$

by the valence z, the elementary charge e_0 and the cation-anion distance d, has to be corrected by two factors. First, the induced dipole moment, μ_{ind}, which is caused by the ionic polarisability α and expressed by the equation

$$\mu_{ind} = \frac{(4\pi\varepsilon_0)d^4\, e_0(|z_-|\alpha_+ + z_+\alpha_-) + 2d\alpha_+\alpha_- e_0(|z_-| + z_+)}{(4\pi\varepsilon_0)^2 d^6 - 4\alpha_+\alpha_-} \tag{4.9}$$

has to be taken into account. Additionally, for solvent-shared (SIP, n=1) and solvent-separated (2SIP, n=2) ion pairs the antiparallel dipole moment of the water molecule, $\mu_{H_2O} = 1.834$ D,[106] has to be included; for contact ion pairs (CIP), $n = 0$ applies.

Before these equations can be used to calculate ion-pair concentrations, some assumptions regarding the shape of the ion pair have to be made. As pointed out in ref.[8] for

alkyltrimethylammonium bromide, there are three different possibilities how the alkyl chain can participate in the rotation, which are illustrated in Figure 4.16. Model 1 assumes a rotation axis perpendicular to the fully extended chain; in principle, this is also possible for DDAB when the rotation axis is between the two dodecyl chains. This geometry can be approximated by a rotational ellipsoid as described in eq. (1.82), where the semi-axes $a > b = c$ are given as

$$a = r_- + nr_\mathrm{W} + r_\mathrm{h} + l/2 \tag{4.10}$$

and

$$b = r_\mathrm{h} \tag{4.11}$$

Note that r_-, r_W and r_h are the radii of an anion ($r_{\mathrm{Br}^-} = 196$ pm[141]), a water molecule ($r_\mathrm{W} = 142.5$ pm[95]) and the surfactant head group, respectively, whereas l represents the dodecyl chain length ($l = 1440$ pm[53]). The radius of the surfactant head group, r_h, has been estimated from both the volume ($V = 120$ Å^3[53]) and the surface area ($A = 60$ Å^2 or $A = 68$ Å^2, depending on the lamellar phase considered[53]) assuming a spherical shape; as there was no reason that would justify to prefer one of these estimates, the average value 266 pm was used.

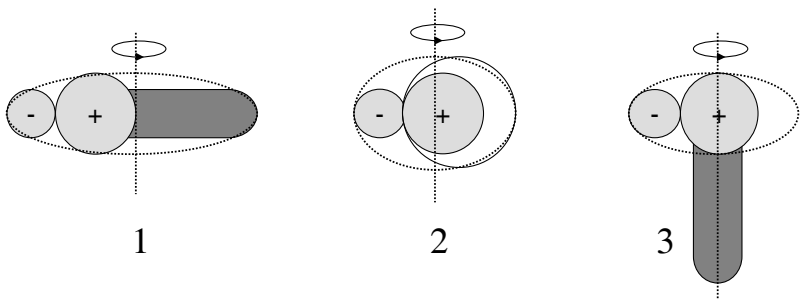

Figure 4.16: Sketch illustrating the three possible mechanisms of surfactant ion-pair rotation.[7] Dotted ellipses indicate the effective rotational volumes approximated by ellipsoids in the calculations.

Model 2 of ref.[8] is similar to model 1, but supposing the alkyl chain is completely folded around the surfactant head group; this is a very unlikely case for a molecule containing *two* dodecyl chains, so that it can be ruled out for DDAB. Model 3, however, assumes rotation of the counterion and the surfactant head group around an axis running along the alkyl chain. The chain is assumed to be 'fixed' in the solution so that the semi-axes a and b can be determined as

$$a = 2r_- + nr_\mathrm{W} + r_\mathrm{h} \tag{4.12}$$

and

$$b = r_\mathrm{h} \tag{4.13}$$

This model has already been proposed for the rotation of surfactant molecules in aqueous micellar solutions;[174] it is evident that it is the only conceivable mechanism for an ion-pair rotation at the interface of a W/O microemulsion.

To get a feeling which of these models is in principle suitable to explain the experimental data of process 4 it is useful to compare the experimental relaxation times τ_4 with estimates coming from the Stokes-Debye-Einstein equation, providing rotational correlation times, τ', for model ion pairs according to[76]

$$\tau' = \frac{3V f_\perp C \eta}{k_B T} \tag{4.14}$$

where V is the ion-pair volume, η the solution viscosity, $f_\perp$ a shape factor that can be calculated from the ion-pair dimensions, and C is a parameter describing the boundary conditions for rotational diffusion ($C = 1$ for *stick*, $C = 1 - f_\perp^{-2/3}$ for *slip* boundary conditions).[76] For rotation on a molecular scale, hydrodynamic boundary conditions are likely to be close to *slip*.[75,76] Again the value of V can be approximated as a prolate ellipsoid as outlined above.

As a result, model 1 yields τ'_{slip} values of 402 ps for CIP, 595 ps for SIP and 838 ps for 2SIP, respectively, assuming *slip* boundary conditions; for *stick* boundary conditions, the rotational correlation times are considerably higher. As these values are not in the same range as the experimental τ_4 data (see Tables 3.8 to 3.10) model 1 does not seem to be an adequate description of the phenomenon monitored in process 4. This is not surprising given that model 1 has already proven to be very unlikely for aqueous solutions of alkyltrimethylammonium bromides,[6] where the geometrical constraints are much less pronounced than in a microemulsion system.

Table 4.1: Semi-Axes a and b, Cation-Anion Distance d, Polarisability α_{IP} and Effective Dipole Moment μ_{eff} of DDAB Ion Pairs at 25 °C. Molecular Volumes, V, Shape Factors, $f_\perp$, and Rotational Correlation Times, τ'_{slip} and τ'_{stick}, as Obtained from the Stokes-Debye-Einstein Equation Are Also Included.

type	a / pm	b / pm	d / pm	α_{IP} [a] / Å^3	μ_{eff} / D	V / Å^3	$f_\perp$	τ'_{slip} / ps	τ'_{stick} / ps
CIP	6.58	2.66	4.62	49.9	7.508	195	1.87	90.7	266
SIP	8.01	2.66	7.47	51.3	29.54	237	2.35	176	406
2SIP	9.43	2.66	10.3	52.8	43.61	279	2.89	299	589

[a] $\alpha_{DDAB} = 49.9$ Å^3 was determined in this work (see section 3.5); $\alpha_{H_2O} = 1.44$ Å^3 was taken from ref.[106]

In contrast, the τ'_{slip} values obtained by model 3 (see Table 4.1) assuming CIP or SIP compare favourably with τ_4. For 2SIP, τ'_{slip} is somewhat higher than the experimental τ_4 values. Additionally, given the high salinity[74] and the resulting scarcity of water near the interface, the 2SIP model appears to be very unlikely so that it can be excluded.

Consequently, model 3 was used to calculate ion-pair concentrations, c_{IP}, as outlined above, assuming CIP and SIP. Parameters used for this calculation are given in Table 4.1; the results are plotted in Figures 4.17 to 4.20.

As can be seen, the CIP model yields relative ion-pair concentrations of $\lesssim 0.2$ at constant dodecane ratios (Figure 4.17) and of $\lesssim 0.12$ and < 0.5 at two dodecane dilution lines, respectively. There is no doubt that this degree of association of surfactant molecules situated at the water/oil interface is realistic, given that theoretical studies predict a counterion binding degree of ≥ 0.8[127] or even of ≥ 0.98.[132] However, as the packing parameter v/al of DDAB in lamellar phases is reported to be close to 1,[53] neighbouring surfactant head groups should approach quite closely also at the water/oil interface; thus, it is not obvious how this large percentage of surfactant ion pairs should be able to rotate. Yet, it has to be kept in mind that the accuracy of the relative ion-pair concentrations as given in Figures 4.17 to 4.20 should not be overestimated. These values – calculated from the relaxation amplitudes S_4 – are prone to errors, as the low-amplitude process 4 embedded between two much more intense adjacent relaxations is extremely difficult to fit.

As an alternative to the CIP model, the SIP model yields significantly lower relative ion-pair concentrations: values of c_{IP}/c_{DDAB} are always found between 0.01 and 0.03, *i.e.* 1 - 3 % of the DDAB molecules present in the system rotate as ion pairs. Although this appears to be a more plausible range, the applicability of the SIP model to the present system seems to be very questionable, given the scarcity of water near the interface and the inability of the ions (especially of Br^-) to fix a water molecule in their coordination spheres. Additionally, according to eqs. 4.10 and 4.12 the rotating radius of a SIP is considerably larger than that of a CIP, thus requiring even more space in the interfacial surfactant layer.

It is known from a DRS study of 'normal' alkyltrimethylammonium bromide micelles in aqueous solution that the assumption of rotating surfactant ion pairs did not yield meaningful results.[6]

In contrast, the idea of ion pairing in water-in-oil microemulsions is supported by a DRS investigation of AOT/water/CCl_4 and AOT/water/*n*-heptane microemulsions conducted by Camardo *et al.* This study also yielded a relaxation process at ~ 200 ps, which was interpreted as an AOT ion-pair relaxation.[45] From the relaxation amplitude, these authors calculated the dipole moment of the ion pair, which was found to be in excellent agreement with the literature value. Hence, they concluded that 'as the water content increases inside the micelle, an increasing number of AOT ion pairs could achieve a sufficient mobility to re-orientate independently from the whole microaggregate'. This finding is even more interesting as the *largest* AOT micelles studied by these authors had a water/surfactant molar ratio of $W \leq 16$, which is equivalent to the *smallest* water droplets investigated in this work.

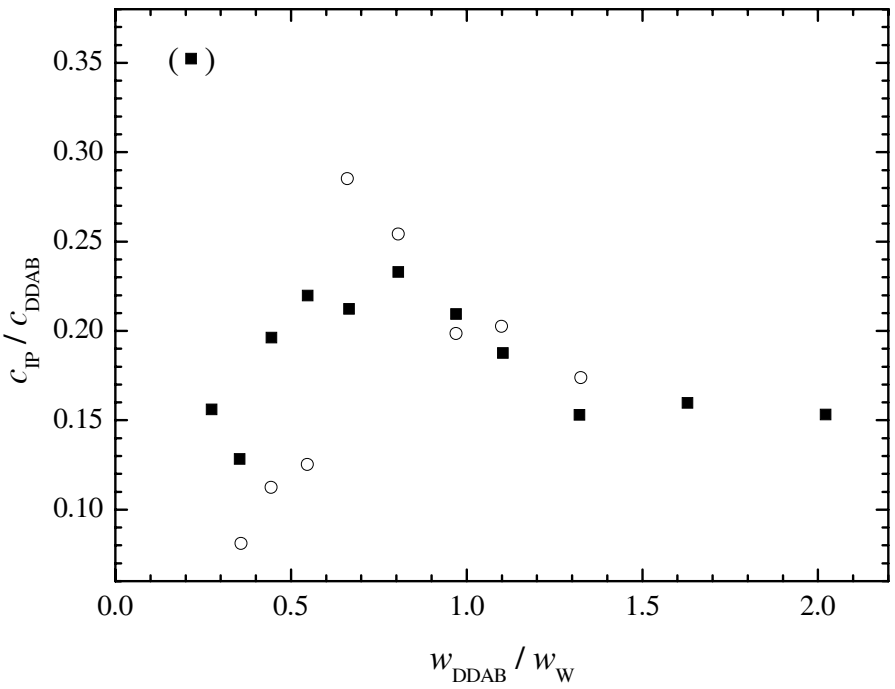

Figure 4.17: Relative ion-pair concentration, c_{IP}/c_{DDAB}, as a function of the surfactant/water ratio, w_{DDAB}/w_W, at 25 °C assuming the CIP model. ■: $w_D = 0.35$; ○: $w_D = 0.23$.

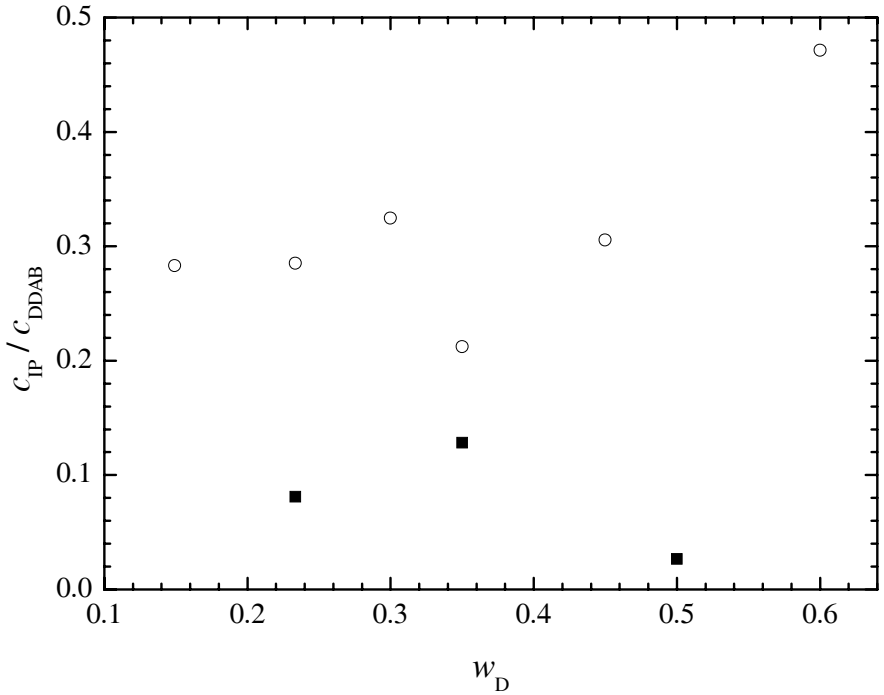

Figure 4.18: Relative ion-pair concentration, c_{IP}/c_{DDAB}, as a function of the dodecane mass fraction, w_D, at 25 °C assuming the CIP model. ■: $w_{DDAB}/w_W = 0.358$; ○: $w_{DDAB}/w_W = 0.667$.

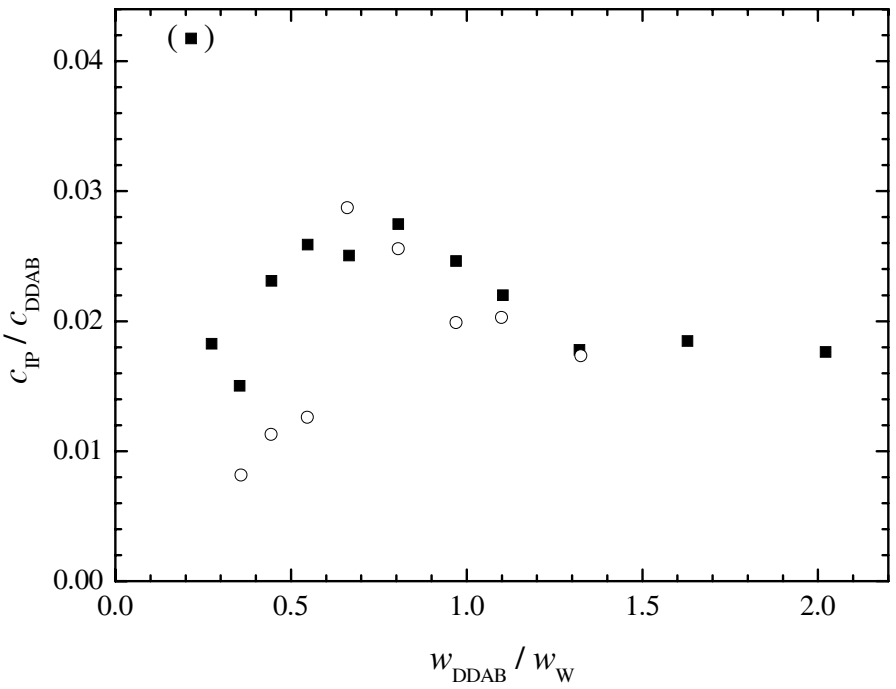

Figure 4.19: Relative ion-pair concentration, c_{IP}/c_{DDAB}, as a function of the surfactant/water ratio, w_{DDAB}/w_W, at 25 °C assuming the SIP model. ■: $w_D = 0.35$; ○: $w_D = 0.23$.

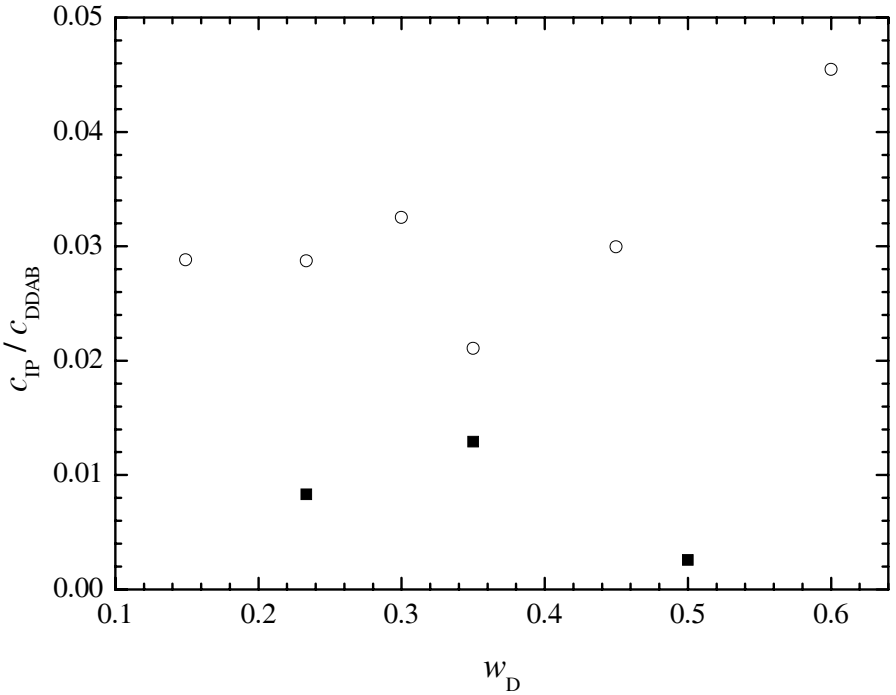

Figure 4.20: Relative ion-pair concentration, c_{IP}/c_{DDAB}, as a function of the dodecane mass fraction, w_D, at 25 °C assuming the SIP model. ■: $w_{DDAB}/w_W = 0.358$; ○: $w_{DDAB}/w_W = 0.667$.

Furthermore, the initial increase in $c_{\mathrm{IP}}/c_{\mathrm{DDAB}}$ with rising DDAB/W ratio seems to be plausible assuming DDAB ion-pair rotation at the surface of the water droplets. At the beginning the ion-pair percentage increases, as the breakdown of the highly ordered geometry of water droplets in oil allows the interfacial surfactant molecules more freedom to rotate. For $w_{\mathrm{DDAB}}/w_{\mathrm{W}} \gtrsim 0.7$ ($W \lesssim 37$), however, the ion-pair fraction decreases again, as the rising DDAB/W ratio leads to an increased packing density of the surfactant molecules, thus reducing their mobility.

Alternatively, it may be assumed that the DDA^+ ions forming the ion pairs observed are no longer located at the water/oil interface, but embedded in the aqueous subphase, where ion pairs can rotate without any difficulties. As in this case an excessive amount of water is present in proximity, we may assume that SIPs will be formed, yielding a DDA^+ concentration in the aqueous phase of $0.01 \lesssim c_{\mathrm{IP}}/\mathrm{M} \lesssim 0.08$. However, this idea still appears to be questionable, as it is not clear how even a small amount of DDA^+ ions containing two non-polar dodecyl chains could be dissolved in a polar medium like water.

An alternative interpretation of process 4 is to ascribe this relaxation to small uncorrelated motions of the counterions in the water droplets, as illustrated in Figure 4.21. On average, the counterions are distributed symmetrically over the aqueous subphase, leading to a mutual cancellation of the single dipole moments present in the system, so that the total dipole moment of the droplet will be equal to zero. However, every single counterion in the diffuse double layer is mobile and thus able to exchange positions with its neighbouring molecules. As these rearrangements are statistical processes they are not correlated over the entire droplet. Thus, for a short moment, the charge distribution will not be symmetrical any more, giving rise to a small total dipole moment.

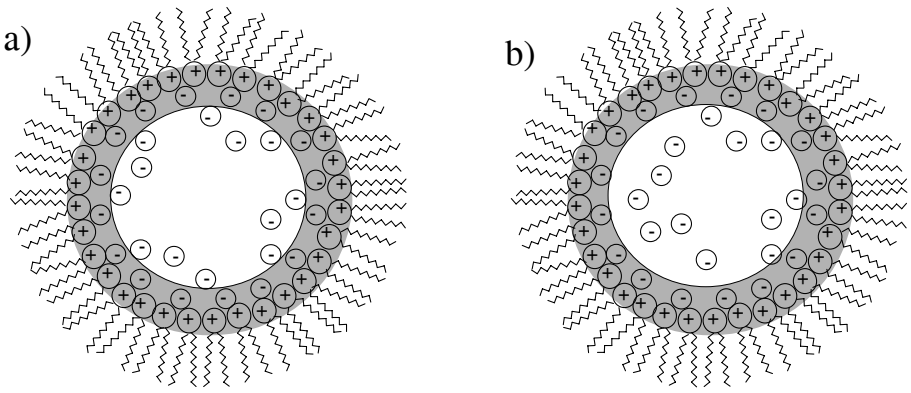

Figure 4.21: Sketch illustrating small uncorrelated motions of counterions in a water droplet:[152] a) average counterion distribution in the diffuse double layer ($\vec{\mu} = 0$); b) snapshot of an instantaneous counterion distribution ($\vec{\mu} > 0$).

This effect has been studied in a MD simulation of a reverse micelle by Tobias and Klein.[184] These authors considered a reverse micelle exhibiting a diameter of 41 Å (which is a bit smaller than the smallest water droplets investigated in this work) and found an average micellar dipole moment of approximately 20 D.

As a result, the mechanism to which process 4 should be ascribed is not obvious, but it is certainly fair to say that this relaxation is related to uncorrelated movements of ionic species present in the system.

4.5 Low-Frequency Processes

When analyzing the low-frequency part of the dielectric spectra obtained in this work, the most striking feature is the pronounced increase in the permittivity, ε', with decreasing frequency, ν. However, this behaviour is well-known in the literature for related systems (see *e.g.* refs.[132,159,187]); as pointed out by Feldman *et al.*, it reflects that the system is close to the percolation threshold.[83] Below the percolation onset dielectric spectra are dominated by fast relaxation processes exhibiting relaxation times of less than 1000 ps, which are due to the dynamics of single components of the system and interfacial polarisation. In the percolation range, however, additional relaxations can be observed on at least two different timescales. Slow processes, whose characteristic relaxation times are greater than 10^6 ps, can be ascribed to the rearrangements of a whole percolation cluster, as assumed in the dynamic percolation theory.[44,46,99] Intermediate processes, exhibiting relaxation times between several hundreds of picoseconds and up to several hundreds of nanoseconds,[84] reflect a cooperative relaxation caused by the transfer of excitation along a percolation cluster. This excitation is due to the transport of charge carriers, giving rise to a fluctuation of the dipole moment of the droplets.[85,122,199]

For the present spectra, the low-frequency range could be fitted assuming three Debye relaxations. Whereas the lowest-frequency process 1 ($\tau_1 \approx 40$ ns) can certainly be ascribed to a charge transport phenomenon arising from percolation, processes 2 and 3 can be well interpreted in the framework of interfacial polarisation, as will be shown in the subsequent section.

4.5.1 Interfacial Polarisation

Surface and Radial Counterion Diffusion

Amplitudes S_i and relaxation times τ_i of processes 2 and 3 are plotted in Figures 4.22 to 4.26. The pronounced scattering of the relaxation parameters especially of process 2 is caused by the obvious difficulties in fitting the lowest-frequency process 1. As the latter is only partly located inside the frequency range which is experimentally accessible to our instruments, it cannot be fitted adequately. Hence, errors arising from that propagate to the quality of the fit of the neighbouring relaxation processes.

The most puzzling feature of the present data is of course the gradual decrease and the subsequent complete disappearance of process 3 with increasing DDAB/W ratio. As can be seen from the relaxation times, both processes 2 and 3 are in a range which in principle could be ascribed either to the transport of charge carriers or to interfacial polarisation. However, in their DRS study of AOT/water/hexane and AOT/water/decane microemulsions Kozlovich *et al.* detected two relaxation processes very similar to those of this work, which these authors interpreted successfully using an interfacial polarisation model.[132] As will be illustrated now, this model appears to be well suited to describe the present spectra, too.

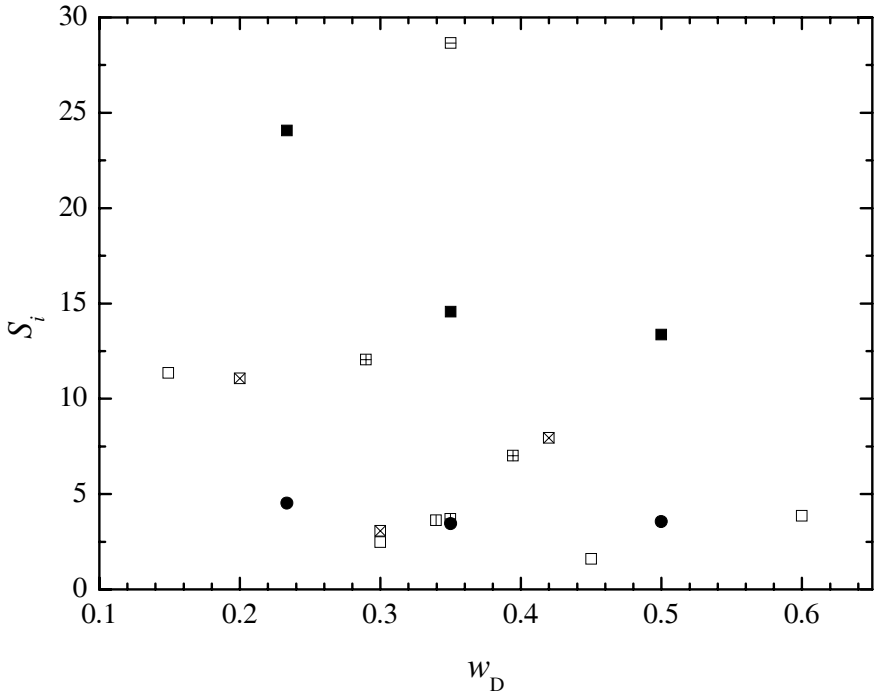

Figure 4.22: Relaxation amplitudes, S_2 and S_3, as a function of the dodecane mass fraction, w_D, at 25 ℃. Values given in brackets are the surfactant/water ratios, w_{DDAB}/w_W. ⊟: S_2 (0.216); ■: S_2 (0.358); □: S_2 (0.667); ⊠: S_2 (1.10); ⊞: S_2 (1.63); ◫: S_2 (2.03); •: S_3 (0.358).

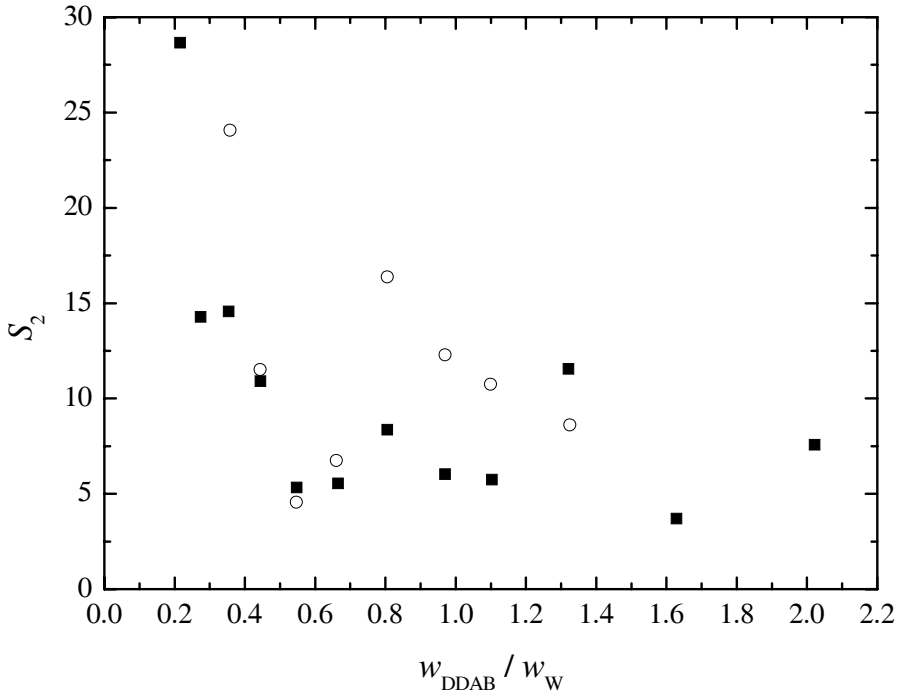

Figure 4.23: Relaxation amplitudes S_2 as a function of the surfactant/water ratio, $w_{\mathrm{DDAB}}/w_{\mathrm{W}}$, at 25 ℃. ■: $w_{\mathrm{D}} = 0.35$; ○: $w_{\mathrm{D}} = 0.23$.

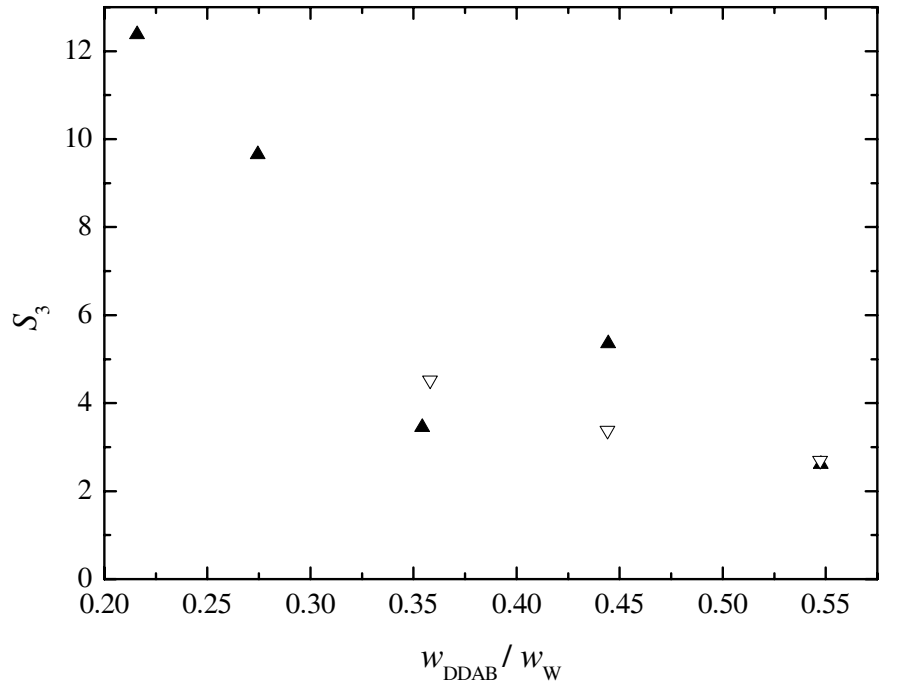

Figure 4.24: Relaxation amplitudes, S_3, as a function of the surfactant/water ratio, $w_{\mathrm{DDAB}}/w_{\mathrm{W}}$, at 25 ℃. ▲: $w_{\mathrm{D}} = 0.35$; ▽: $w_{\mathrm{D}} = 0.23$.

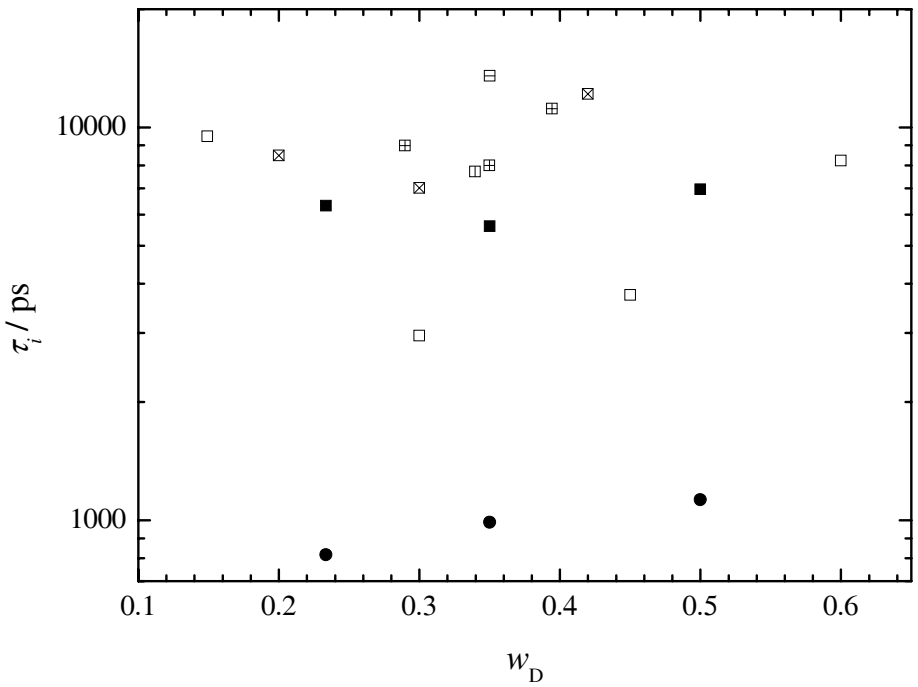

Figure 4.25: Relaxation times, τ_2 and τ_3, as a function of the dodecane mass fraction, w_D, at 25 ℃. Values given in brackets are the surfactant/water ratios, w_{DDAB}/w_W. ⊟: τ_2 (0.216); ■: τ_2 (0.358); □: τ_2 (0.667); ⊠: τ_2 (1.10); ⊞: τ_2 (1.63); ◫: τ_2 (2.03); ●: τ_3 (0.358).

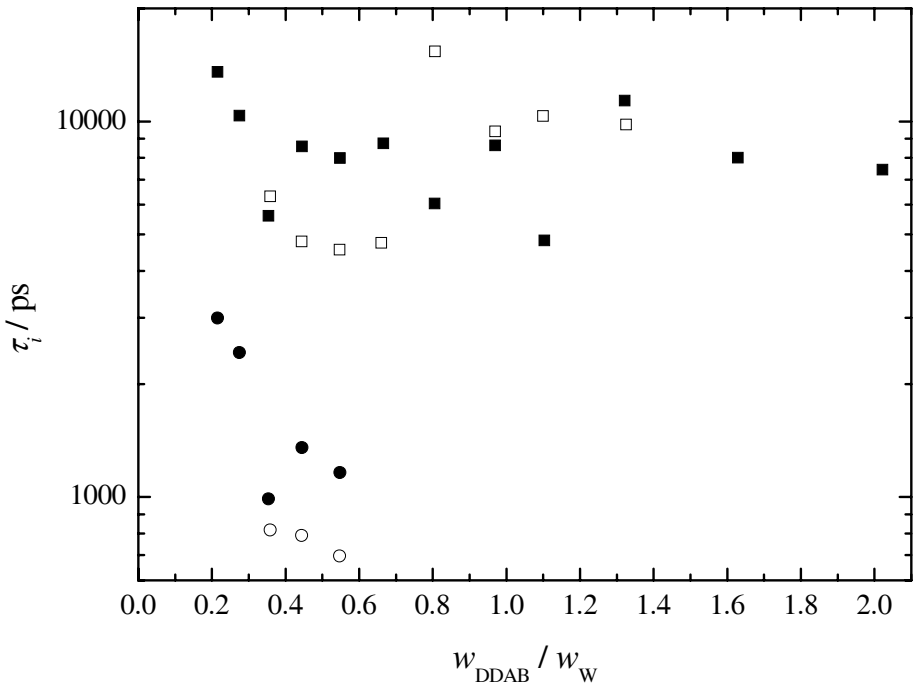

Figure 4.26: Relaxation times, τ_2 and τ_3, as a function of the surfactant/water ratio, w_{DDAB}/w_W, at 25 ℃. ■: $\tau_2, w_D = 0.35$; □: $\tau_2, w_D = 0.23$; ●: $\tau_3, w_D = 0.35$; ○: $\tau_3, w_D = 0.23$.

As has been mentioned repeatedly, a very large fraction of the counterions of the aqueous subphase is located in the vicinity of the (oppositely charged) interface, which is formed by the surfactant ions.[74] It is well known, and has been outlined in section 1.6.3, that the counterions located closest to the charged interface form a layer called the *outer Helmholtz plane* (OHP); due to a high potential barrier they are reluctant to exchange positions with the remaining counterions, located in a diffuse double layer as described by the Gouy-Chapman model. For very large water droplets, the counterions can be regarded as a thin layer near the surface, and the differences between the OHP and the diffuse double layer may be negligible. In contrast, they are decisive for intermediate-sized droplets as they are present in DDAB/W/D. As illustrated in Figure 4.27, counterions located in the OHP preferably move along the surface, whereas those situated in the diffuse double layer exhibit radial diffusion due to concentration polarisation effects. Thus, interfacial polarisation should give rise to two different relaxation processes.

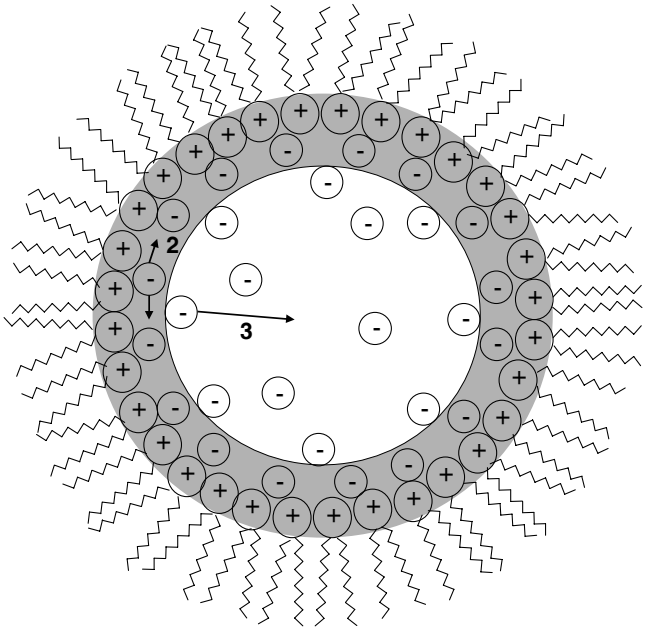

Figure 4.27: Sketch of interfacial polarisation mechanisms occurring in a spherical W/O droplet[152] in the system DDAB/W/D: surface counterion diffusion in the OHP (grey area, process 2) and radial counterion diffusion in the diffuse double layer (process 3).

A ^{23}Na counterion spin relaxation study of AOT/water/isooctane microemulsions revealed that for water/surfactant ratios of $10 < W < 70$ counterion diffusion is in fact three-dimensional rather than two-dimensional.[114] Using the diffusion coefficients determined in that study for a water droplet of $W = 26.3$, relaxation times of ~ 12 ns and ~ 1 ns could be determined for surface and radial counterion diffusion, respectively. These values were

found to be in very good agreement with the relaxation times of the two low-frequency processes detected by Kozlovich *et al.* for AOT/water/decane,[132] but they also agree very well with the relaxation times τ_2 and τ_3 determined in this work for DDAB/W/D.

Thus, it appears to be plausible to ascribe processes 2 and 3 to the surface counterion diffusion in the OHP and the radial counterion diffusion in the diffuse double layer, respectively, caused by interfacial polarisation. In this context, it is also possible to account for the dramatic decrease of S_3 with increasing surfactant/water ratio. With increasing percolation, water droplets are more and more replaced by channels of a much smaller diameter; as the counterion concentration in the aqueous phase is rising simultaneously, the diffuse double layer will cover almost the whole aqueous phase so that concentration polarisation effects will become much less important.

Modelling of Surface Counterion Diffusion: Spherical Water Droplets

Since process 2 can be ascribed to an interfacial polarisation effect along the surface, it should easily be modelled using the Maxwell-Wagner approach. As presented in section 1.5 a number of models based on this approach exist in the literature, which have been proven to be useful tools for the interpretation of dielectric relaxation processes (see *e.g.* ref.[198]). However, all these models assume non-percolating systems, which is certainly a questionable premise when discussing DDAB/W/D microemulsions. Nevertheless, the applicability of various Maxwell-Wagner models to the present spectra was tested.

First, as a very simplistic model, a concentrated solution of water particles in oil was assumed, according to the Hanai equation (1.115). However, for the whole range of volume fractions ϕ located in the L_2 phase the static permittivities were considerably too low, whereas the imaginary part of $\hat{\varepsilon}$ either assumed negative or unreasonably high values. This result was not unexpected, as the charged water/oil interface, which is not accounted for in the Hanai equation, should influence the dielectric properties of the system.

Therefore, as a next step, models describing spherical particles with a shell were considered. Even though the Pauly-Schwan model (see section 1.5.5) is only applicable to dilute solutions, its ability to describe the present microemulsion system was tested. Not surprisingly, this model was found to be inadequate. The static permittivities predicted were far too low, the dispersion step considerably too small ($S \approx 1$), the two relaxation times $\tau_1 \approx 100$ ns and $\tau_2 \approx 1$ ns deviated manifestly from the experimental values, and the imaginary part of $\hat{\varepsilon}$ assumed unreasonably high values.

However, the model proposed by Hanai *et al.* for concentrated solutions of shell-spheres[102] (see section 1.5.5) – which in theory should be an ideal description of the present microemulsion system – did not yield convincing results either. Again the static permittivity values were distinctly too low, and again unrealistically high values for the imaginary part of $\hat{\varepsilon}$ were obtained. Quite obviously, any model assuming spherically-shaped particles is unable to explain the data obtained experimentally for process 2.

Modelling of Surface Counterion Diffusion: Ellipsoidal Water Droplets

Consequently, models assuming rotational ellipsoids of semi-axes $R_x = R_y \neq R_z$ were tested subsequently. First, a simple model describing concentrated solutions of spheroidal water particles in oil according to eq. (1.146) as proposed by Asami[4] was considered, which in the following will be called *'model A'*. For the static permittivity of the medium, the value $\varepsilon_M = 2.02$ obtained for pure dodecane[65] was used, whereas κ_M was set to 10^{-9} S m^{-1} to account for the non-conductivity of the medium. However, the appropriate values of the dielectric properties of the droplet are by far less obvious. Assuming these properties are determined by the two water relaxation processes observable in the system and thus equating $\varepsilon'_P = \varepsilon_5$ yields unrealistically low values of ε_∞, *e.g.* $\varepsilon_\infty = 5.04$ (instead of the experimental value of 21.85) for sample 21a0. As can be seen from Table 4.2, better agreement with the experimental data could be achieved by inserting the static permittivities of NaBr(aq) solutions (determined in ref.[189]) of $c_{NaBr} = c_{DDAB}/2$ for ε'_P; this concentration correction has been applied as only the Br^- counterions, but not the DDA^+ cations, are expected to be part of the aqueous subphase. Similarly, $\kappa_P = \kappa_{NaBr(aq)}/2$ was used for the conductivity of the particle; yet, it should be noted that the conductivity values inserted have virtually no influence on the results obtained by this model.

Using model A as outlined above, the predicted values of $\hat{\varepsilon}(\nu)$ were found to agree favourably with the experimental data. By adjusting L, values of the static permittivity could be modelled very well, except for very high volume fractions of the dispersed phase, ϕ; yet, the ε_∞ values provided by this model were found to be systematically low. In contrast, the imaginary part, ε'', agreed well with the experimental results, yielding relaxation times of ~ 3.5 ns. An extension of the model to ellipsoids exhibiting three different semi-axes ($R_x \neq R_y \neq R_z$) according to eq. (1.139) did not lead to any improvement.

As a next step, the model proposed by Boned and Peyrelasse[28] to describe spheroidal particles surrounded by a shell (see section 1.5.5) was tested (*'model B'*). Using the same assumptions as outlined for model A (again, assuming $\varepsilon'_P = \varepsilon_5$ did not yield meaningful results), even the data of those samples exhibiting large internal volume fractions, ϕ, could be fitted with model B. Apart from that, the quality of the results provided by this model was found to be very similar to model A, as can be seen from Table 4.2.

The fact that a model assuming *rotational ellipsoids* is required to account for the experimental results of process 2 may be interpreted in two different ways. Evidently, it may be regarded as an indication that below the percolation threshold, the water particles are indeed of ellipsoidal rather than of spherical shape, supporting the birefringence results of Lenz and Hoffmann.[137] As an alternative conclusion, it may be assumed that a certain degree of percolation is present throughout the L_2 phase (maybe except for the very dodecane-rich region, which has not been investigated in this work), thus leading to spheroidally-shaped aggregates.

Table 4.2: Sample Name, Volume Fraction of the Internal Phase, ϕ, Experimental Values of Static and Infinite-Frequency Permittivities, ε_s^{exp} and ε_∞^{exp}, and Fitting Results for the Permittivities, ε_s and ε_∞, and the Depolarisation Factors, L, Yielded by the Spheroidal Models Proposed by Asami[4] and Boned and Peyrelasse.[28] Values of ε'_P and κ_P Used for the Calculations Are Also Included.

sample	ϕ	ε_s^{exp}	ε_∞^{exp}	ε_s^a	ε_∞^a	L^a	ε_s^b	ε_∞^b	L^b	ε'_P [d]	κ_P [e]
21a0	0.475	36.12	21.85	36.2	13.3	0.444	36.0	13.6	0.410	74.8	2.9
22a0	0.428	29.05	18.15	28.7	11.3	0.449	29.1	11.7	0.394	72.3	4.7
230	0.384	18.75	13.21	18.6	9.19	0.446	18.9	9.46	0.402	69.8	6.4
23b0	0.338	18.76	12.73	18.9	8.24	0.458	18.8	8.60	0.366	66.5	8.7
24a0	0.301	22.70	11.16	23.0	7.61	0.469	22.8	8.24	0.324	62.1	11.6
25a0	0.254	17.61	10.05	17.5	6.15	0.472	17.6	6.61	0.309	54	16
42a0	0.523	31.77	20.25	45.6	15.1	0.438[c]	31.9	14.3	0.460	72.3	4.7
430	0.467	24.28	17.53	28.6	12.0	0.438[c]	24.4	11.6	0.442	69.8	6.4
43b0	0.412	28.03	15.74	27.9	10.5	0.452	28.0	10.8	0.386	66.5	8.7
44a0	0.366	22.97	14.36	23.0	8.85	0.457	23.2	9.24	0.369	62.1	11.6
13	0.533	33.62	22.26	49.8	15.4	0.438[c]	33.6	13.2	0.463	69.8	6.4
15	0.313	12.72	11.13	12.9	7.25	0.452	12.8	7.08	0.387	69.8	6.4
16	0.232	12.86	8.99	12.7	6.05	0.470	13.0	6.17	0.317	69.8	6.4

[a] values calculated assuming rotational ellipsoids without shells as proposed by Asami;[4] [b] values calculated assuming rotational shell-ellipsoids as proposed by Boned and Peyrelasse;[28] [c] for lower values of L, the model did not yield physically reasonable results; [d] values taken or interpolated, respectively, from ref.[189]; [e] units: S m^{-1}, values taken or interpolated, respectively, from ref.[119].

When comparing the two models presented above, there are some differences concerning the depolarisation factor L. For model A, the values of L are always $> 1/3$, which corresponds to prolate spheroids, and increase with increasing DDAB/W ratio. This developing appears to be plausible given that the aggregates of water droplets should become more and more cylindrical with increasing percolation, as it is postulated *e.g.* in the DOC model (see section 1.6.1). On the other hand, the L values yielded by model A are extremely high (as can be seen from Table 4.2, the minimum value required to obtain physically reasonable fitting results is $L = 0.438$) and very close to 1/2; thus, this model postulates thin W/O 'needles' or micellar aggregates already for very low DDAB/W ratios, which is probably not realistic.

In contrast, the L values as obtained from model B are considerably lower and much closer to $L = 1/3$ required for spherically-shaped particles. From this point of view, model B appears much more trustworthy; however, using this approach L is *decreasing* with increasing DDAB/W ratio, which means the water droplets or their aggregates should become more spherically-shaped with increasing percolation, which is certainly hard to imagine.

Given the scattering of the experimental relaxation parameters of process 2 it is impossible to decide on the basis of the present data which model is more appropriate to describe DDAB/W/D microemulsions. However, the fact that only models assuming ellipsoidal water droplets or aggregates thereof are able to provide a physically meaningful description of this relaxation process is a strong indication that percolation does play a decisive role in the present system. Furthermore, as both model A and B yield systematically low values of ε_∞ we have to be aware that the concept of ellipsoidal water particles in oil is only a very rough approximation of the microstructure of the system; as the FFEM image shown in Figure 4.2 strongly suggests the latter is likely to be much more complex.

4.5.2 Transport of Charge Carriers

Amplitudes, S_1, and relaxation times, τ_1, of process 1 are presented in Figures 4.28 to 4.31. As can be seen, the values of τ_1 are in a range of several tens of nanoseconds, which is typical of the transport of charge carriers between adjacent water droplets or along a percolation cluster, thus giving rise to a variation in the fluctuation of the droplets' dipole moments.[85,122,199] However, as only a minor part of process 1 is located inside the frequency range experimentally accessible to our instruments (see Figure 3.6), the quality of the fitting results is somewhat deficient. Therefore, we will abstain from a quantitative analysis of these data.

It may be noteworthy that a similar relaxation process has already been observed in a low-frequency dielectric study by Schrödle *et al.* investigating non-ionic microemulsions made of water / *n*-octane / penta(ethylene glycol) dodecyl ether.[169] In this study, this relaxation has also been ascribed to the exchange of charges between neighbouring water particles; as a mechanism, the authors proposed the 'hopping' of surfactant ions or – more probably – the much more mobile counterions.[46] Accordingly, the probability of charge hopping should strongly increase with increasing aggregation of water droplets, and indeed a pronounced maximum in the amplitude was observed at the percolation threshold. A similar feature can be seen in Figure 4.29, where the amplitudes S_1 reach a plateau value at $w_{\mathrm{DDAB}}/w_{\mathrm{W}} \gtrsim 1.0$ ($W \lesssim 26$). Even though being well aware of the limited significance of the fitting results of process 1, the fact that only a plateau value, but not a maximum can be observed for S_1 may be a further indication that the entire L_2 phase of DDAB/W/D is close to the percolation point.

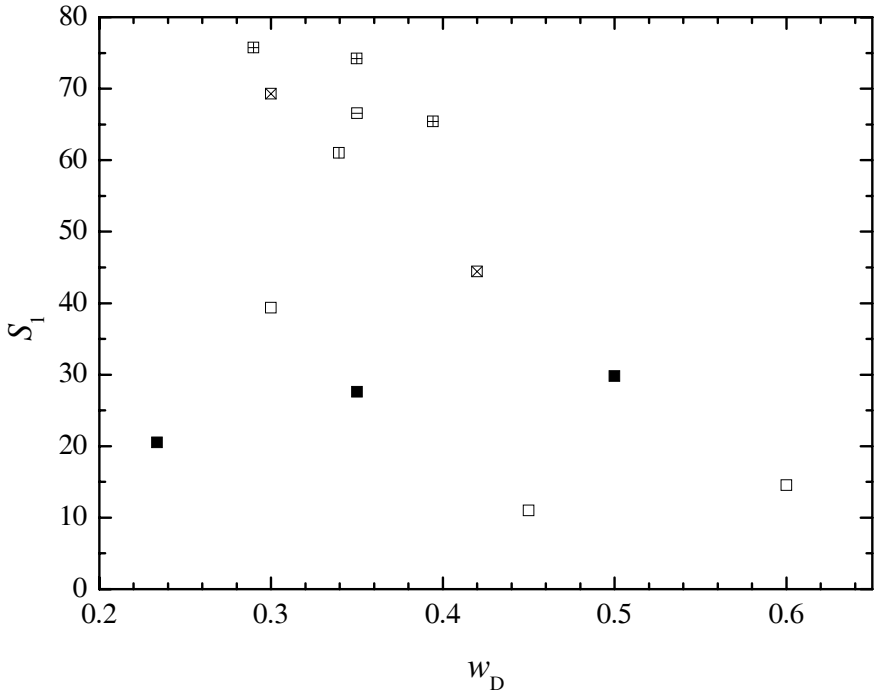

Figure 4.28: Relaxation amplitudes, S_1, at surfactant/water ratios, w_{DDAB}/w_W, as a function of the dodecane mass fraction, w_D, at 25 ℃. ⊟: 0.216; ■: 0.358; □: 0.667; ⊠: 1.10; ⊞: 1.63; ◫: 2.03.

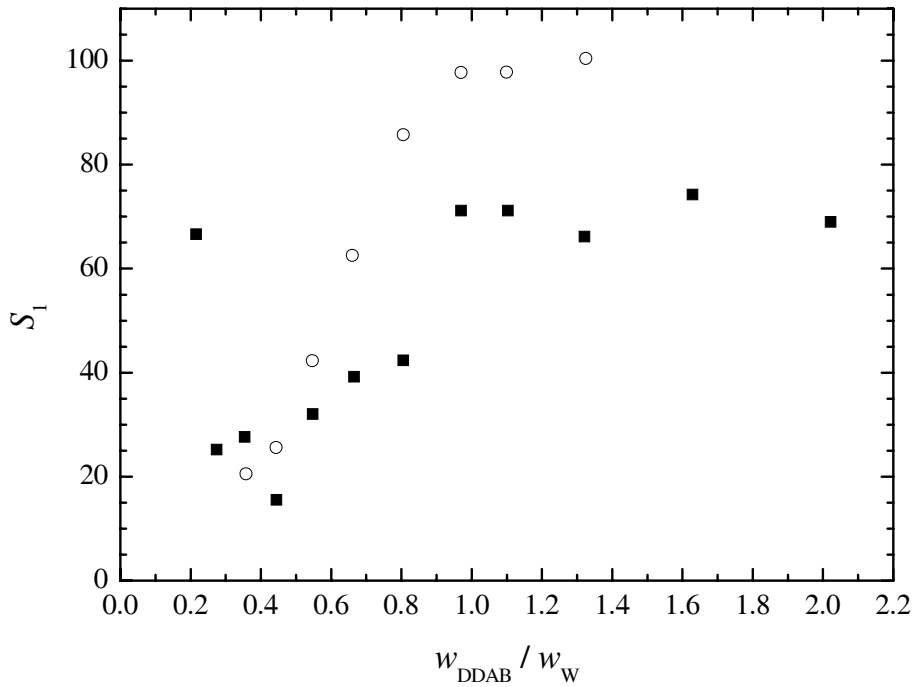

Figure 4.29: Relaxation amplitudes, S_1, at dodecane mass fractions, w_D, as a function of the surfactant/water ratio, w_{DDAB}/w_W, at 25 ℃. ■: 0.35; ○: 0.23.

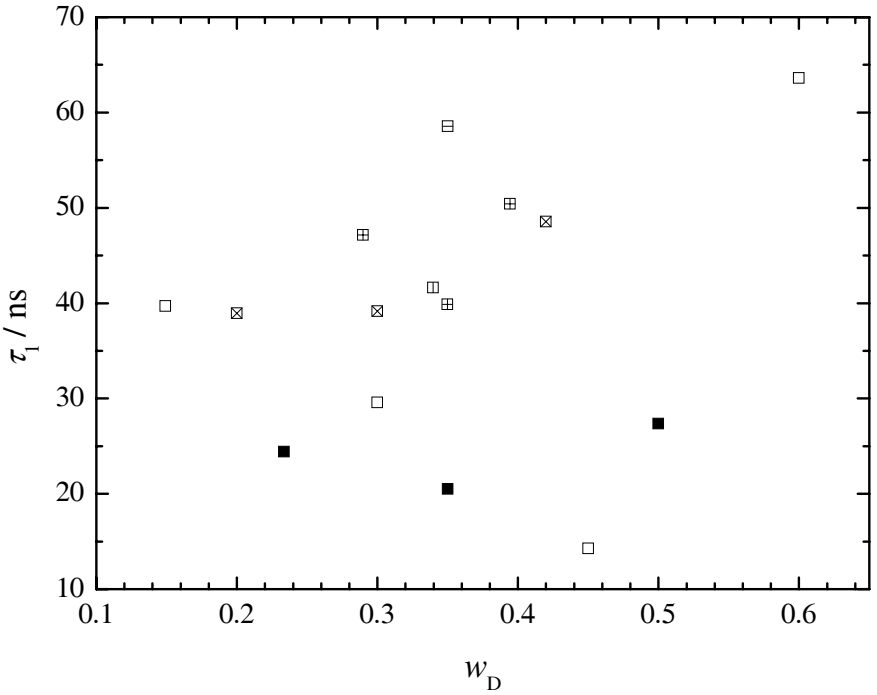

Figure 4.30: Relaxation times, τ_1, at surfactant/water ratios, w_{DDAB}/w_W, as a function of the dodecane mass fraction, w_D, at 25 ℃. ⊟: 0.216; ■: 0.358; □: 0.667; ⊠: 1.10; ⊞: 1.63; ◫: 2.03.

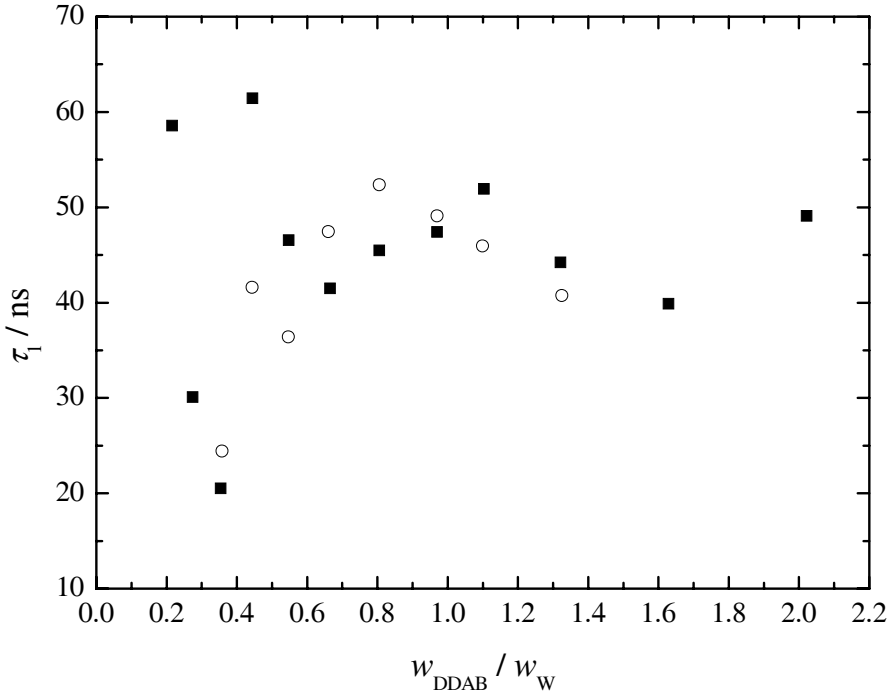

Figure 4.31: Relaxation times, τ_1, at dodecane mass fractions, w_D, as a function of the surfactant/water ratio, w_{DDAB}/w_W, at 25 ℃. ■: 0.35; ○: 0.23.

Chapter 5

Discussion Part 2: The Co-Ion Effect

5.1 The Co-Ion Effect in Didodecyldimethylammonium Bromide / Water / n-Dodecane Microemulsions

5.1.1 Motivation

As pointed out earlier in this work, the equilibrium allowing the formation of microemulsions in the system DDAB/W/D is extremely delicate. Not only does the shape of the microemulsion phase L_2 strongly depend on the surfactant counterion[52] and on the oil-chain length,[195] but even tiny amounts of co-electrolytes added to the aqueous subphase strongly reduce the microemulsion stability. Sjöblom *et al.* reported that replacing water by 1.36 mM NaBr(aq) resulted in a noticeable shrinkage of L_2 at its water-rich boundary.[175] According to these authors, this effect becomes much more pronounced upon increasing the NaBr(aq) concentration to 6.83 mM; with 27.2 mM NaBr(aq) L_2 is reduced to a narrow island, which is located at the surfactant-rich boundary of the large L_2 region observed for a 'salt-free' DDAB/W/D microemulsion (*i.e.* without added co-electrolytes). Similar results were obtained when replacing NaBr(aq) by Na_2SO_4(aq) solutions.[175]

The fact that additions of such tiny amounts of electrolytes give rise to these dramatic effects in microemulsion stability is perplexing and counterintuitive from the electrostatic point of view. As a large amount of bromide anions stemming from the surfactant DDAB is already present in the aqueous subphase ($0.5 \lesssim c_{Br^-}/M \lesssim 4.3$) its concentration is barely increased by adding the co-electrolyte NaBr. Hence, the observed *co-electrolyte effect* must be a *co-ion effect* due to the Na^+ cations. But how can a few millimoles per liter of sodium ions added to aqueous solutions rich in charge carriers evoke such enormous effects?

What makes the situation even more puzzling is the fact that this behaviour is peculiar even amongst ionic microemulsions. An infrared study by MacDonald *et al.* showed that replacing pure water by NaCl(aq) solutions of 1 to 8 mass percent had no effect on the O-H stretching vibration of AOT/H_2O/heptane microemulsions.[140] Gestblom and Sjöblom found virtually no difference between the dielectric spectra of a sodium octanoate/decanol/water and a sodium octanoate/decanol/KCl(aq) microemulsion ($c_{KCl} = 0.2$ M).[92]

Quite obviously, the co-ion effect on DDAB/W/D microemulsions is a conundrum. An aim of this work is to shed some light on this obscure phenomenon from the dielectric point of view. The spectra of salt-free DDAB/W/D microemulsions discussed in the previous chapter will be compared to those of the systems DDAB/LiBr(aq)/D, DDAB/NaBr(aq)/D, DDAB/CsBr(aq)/D and DDAB/$(CH_3)_4$NBr(aq)/D to identify similarities and differences. Only 1:1 electrolytes containing the anion Br^- have been investigated to reduce the co-electrolyte effect to a co-ion effect of cations which are all univalent, but different in charge density and geometrical shape.[141] It is certainly legitimate to expect that this comparison will contribute to a better understanding of the way co-ions influence the system DDAB/W/D.

5.1.2 Literature Review

Before discussing the dielectric spectra obtained in this work, it is useful to review existing knowledge of the co-ion effect in the system DDAB/W/D. Although not many studies have been carried out up to now valuable information is available that may be helpful when interpreting the dielectric relaxation parameters.

There are a number of hints indicating that the co-ion effect is negligible at high surfactant/water ratios. As already mentioned, Sjöblom *et al.* found that a small island of L_2, located at the surfactant-rich boundary of this phase, remained unaffected by the addition of NaBr and Na_2SO_4.[175] A similar result was obtained by Murgia *et al.* who investigated the influence of LiBr, NaBr, CsBr and $(CH_3)_4$NBr and of a number of different sodium salts on the L_2 phase of DDAB/W/*decane* microemulsions. In the surfactant-rich region, none of these electrolytes affected the shape of L_2.[144]

A NMR self-diffusion study by Skurtveit and Olsson found that the diffusion coefficient of water, D_W, in the system DDAB/W/D was insensitive to the addition of co-electrolytes in the surfactant-rich area of the L_2 phase.[176] For the water-rich part of L_2, these authors found a moderate decrease in D_W, suggesting a loss of connectivity between the water droplets. However, no dramatic change in D_W was observed upon co-electrolyte addition throughout L_2, leading to the conclusion that the microstructure of the system does not alter substantially.

The view that the addition of electrolytes reduces the degree of interactions between the water droplets is confirmed in the review by Onori and Santucci dealing with AOT microemulsions.[149] However, these authors were considering co-electrolyte concentrations of ~ 0.5 M, which are about twenty times higher than these added to DDAB/W/D by Sjöblom *et al.*[175]

Murgia *et al.* compared the co-ion effect exerted by different bromide salts on water-rich DDAB/W/decane microemulsions and found that its strength varied considerably with the cations involved, in the order $Cs^+ \gg Na^+ > Li^+ > (CH_3)_4N^+$.[144] Up to now, this result – stating ion specificities similar to those observed in the Hofmeister series – has neither been confirmed nor questioned in the literature.

In a recent NMR study of the system DDAB/D_2O/decane, Murgia *et al.* added very low concentrations of NaBr to the aqueous phase and subsequently investigated the position

of the Na^+ co-ions in the water droplets.[145] Their experimental results – especially the quadrupolar splitting of the ^{23}Na band – strongly suggest that the Na^+ co-ions reside within a distance of 5 to 6 Å from the interface. At first glance, this result appears to be difficult to explain; as has been discussed repeatedly in this work, the electrolyte concentration near the interface is known to be extraordinarily high,[74] whereas it is quite low in the core of the aqueous subphase. Accordingly, co-ions should be expected in the core, where the dielectric constant is higher and a much larger amount of water molecules is available to ensure complete hydration especially of the Na^+ ion. However, Murgia *et al.* explain their result by assuming dispersion forces of quantum-mechanical origin, which can be the dominating effect in a solution of high electrolyte concentrations.

Furthermore, these authors describe another very instructive experiment: they prepared a DDAB/NaBr(D_2O)/decane sample at a ratio where a biphasic system is formed. After allowing one week for complete phase separation the two phases – a water-in-oil microemulsion made of separated reverse micelles in the upper phase and an emulsion in the lower phase – were analyzed by ^{23}Na NMR spectroscopy. Interestingly, almost all Na^+ ions were found to be in the emulsion phase. As a result, we may conclude that Na^+ co-ions are expelled from water droplets when this is possible; otherwise the stability of the droplets is strongly affected, leading to the disappearance of the microemulsion phase in water-rich areas as observed by Sjöblom *et al.*[175]

In a series of recent papers[134,144,145] Ninham *et al.* speculate about the mechanism how such tiny amounts of added co-ions can evoke these dramatic effects. Quite clearly, the number of co-ions is far too small to cause changes in the ionic activities in the bulk or at the surface; likewise, a change of the local curvature of the water droplet can also be ruled out. Hence, these authors suggest that the co-ions are adsorbed at the interface where they act as 'defects'. Ninham *et al.* describe the interface of a W/O droplet as a highly cooperative system, similar to a quasi crystal. They suppose that defects as induced by co-ions into this highly ordered structure will result in a phase transition comparable to the austensite-martensite transition in steel[144] and besides will modify the interfacial water structure.[134]

The only DRS study investigating the influence of co-electrolytes on the system DDAB/W/D appears to have been that of Sjöblom *et al.*[175] These authors observed a pronounced decrease in both the static permittivity, ε_s, and the relaxation time, τ, for water-rich samples upon the addition of NaBr to the aqueous subphase of the microemulsion. As can be seen from Figure 5.1, a decrease in ε_s upon co-ion addition has also been observed in the present data, regardless of the DDAB/W ratio.

The reported decrease in τ cannot be easily verified, as Sjöblom *et al.* only used one Cole-Cole equation to fit their dielectric spectra. However, it is known from the data analysis in chapter 3 that either three or four relaxation processes are present in the frequency range $\sim 0.6 \leq \nu/\mathrm{MHz} \leq 1000$ investigated by these authors. Hence, the relaxation time τ obtained from a Cole-Cole fit is hardly meaningful. This is also true for the Cole-Cole parameter α, which has been reported to decrease.[175] Yet, the data of Sjöblom *et al.* clearly show that the dielectric spectra of DDAB/W/D microemulsions located in the water-rich part of L_2 are indeed affected by the addition of co-electrolytes.

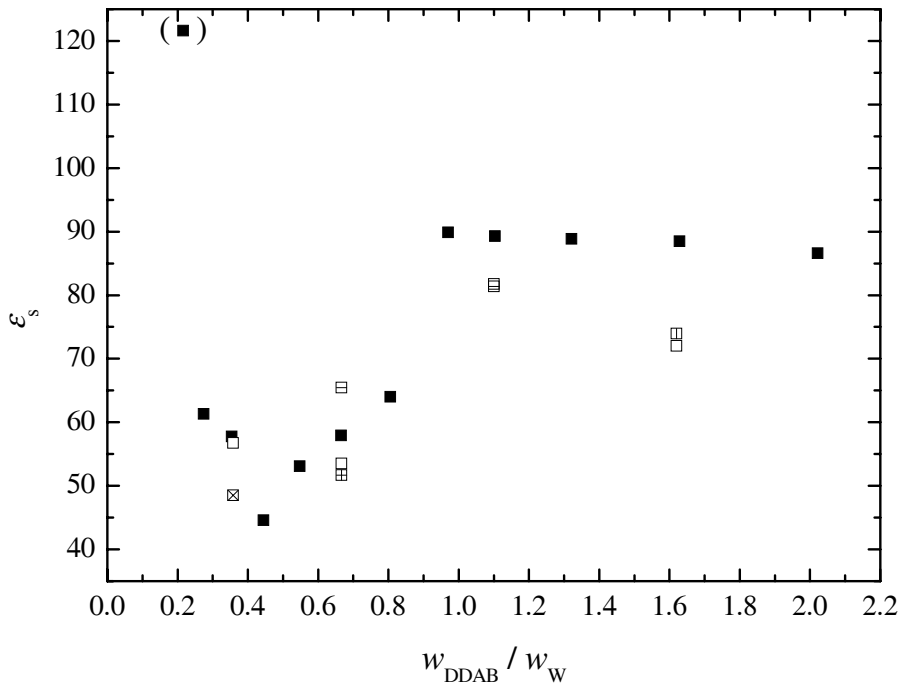

Figure 5.1: Static permittivities, ε_s, of DDAB/NaBr(aq)/D microemulsions as a function of the surfactant/water ratio, w_{DDAB}/w_W, at $w_D = 0.35$, co-electrolyte concentration c and 25 ℃. ■: $c = 0$; □: $c = 1$ mM; ⊞: $c = 5$ mM; ⊠: $c = 7$ mM; ⊟: $c = 10$ mM; ◫: $c = 25$ mM.

5.2 The Co-Ion Effect Monitored by Dielectric Spectroscopy

5.2.1 General Remarks

When monitoring the co-ion effect on the DDAB/W/D system by dielectric relaxation spectroscopy the first striking result is the pronounced dependence of this effect on the DDAB/W ratio. It can be seen readily from Figures 3.15 to 3.18 that replacing water by an aqueous solution containing a co-electrolyte of concentration c evokes a pronounced decrease in both ε' and ε'' in the water-rich region of L_2 ($60 \lesssim W \lesssim 120$), even for concentrations as low as $c \leq 1$ mM. This is an extraordinary and fascinating result, given that DR spectra of aqueous electrolyte solutions can hardly be distinguished from that of pure water for $c \lesssim 50$ mM (see *e.g.* supporting information of ref.[192]). On the other hand, almost no difference can be observed between $c_{NaBr} = 0$, $c_{NaBr} = 1$ mM or $c_{NaBr} = 25$ mM at point $25x$ ($W = 12.7$) in the surfactant-rich part of L_2. It should be emphasized in this context that the decrease in sensitivity towards co-electrolyte addition as shown in Figures 3.15 to 3.18 is a *gradual* effect; there are no indications of a sudden change in sensitivity between two neighbouring samples, as would be expected from the static percolation model by Barnes *et al.*[11]

It may of course be assumed that the dielectric spectra of DDAB/W/D microemulsions are only sensitive to the addition of co-electrolytes immediately before the breakup of the microemulsion phase. It is known from the phase diagram studies conducted by Sjöblom *et al.*[175] that L_2 does not exist any more at point $21x$ for $c_{NaBr} = 1.36$ mM; hence the strong co-ion sensitivity shown in Figure 3.15 may be due to the fact that the investigated concentrations ($c_{NaBr} \leq 1$ mM) are immediately below the phase boundary at this point. In contrast, at point $23x$, where the co-ion sensitivity investigated at $c_{NaBr} \leq 10$ mM is considerably lower (see Figure 3.17), it is only known from the literature that L_2 disappears at $c_{NaBr} = 27.2$ mM.[175] Thus, it cannot be excluded that the co-electrolyte concentrations studied at this point are just too far away from the phase boundary to show a pronounced effect.

To check this hypothesis, a series of DDAB/NaBr(aq)/D samples of $c_{NaBr} \geq 10$ mM was made up at point $23x$ to determine the co-ion concentration required to induce a phase transition. However, even at $c_{NaBr} = 11.5$ mM, no optically clear microemulsion could be formed any more. For $c_{NaBr} = 11.0$ mM a VNA spectrum was measured that was indistinguishable from that obtained for $c_{NaBr} = 10$ mM. It can be concluded that the co-ion effect is indeed less significant at point $23x$ than it is at point $21x$.

How can these substantial differences in co-ion sensitivity be explained? It is noteworthy that there is another physical property of DDAB/W/D microemulsions determined in this work that shares the characteristics of the co-ion effect on the dielectric data. As can be seen in Figure 3.4, the conductivity data display the same gradual development with varying w_{DDAB}/w_W that we observe for the co-ion sensitivity of the dielectric spectra. For $w_{DDAB}/w_W \gtrsim 1.0$ (*i.e.* $W \lesssim 26$) κ reaches a plateau value, while the dielectric data are almost insensitive towards the addition of co-ions (Figure 3.18).

This apparent analogy suggests that the co-ion effect on the dielectric data and the developing of the conductivity data are linked phenomena. It is plausible and widely accepted that in microemulsion systems the conductances are a measure of percolation. As soon as water particles aggregate κ increases until it reaches a plateau value when a bicontinuous network is formed. Thus, we may conclude that the co-ion effect is only important for non-percolating systems. It decreases gradually with increasing percolation until it vanishes completely when a bicontinuous network is formed in the L_2 phase. This conclusion is in good agreement with the NMR self-diffusion study by Skurtveit and Olsson[176] presented above.

After this general discussion of the dielectric data, we now analyze the influence of co-ions on each of the relaxation processes described in the previous chapters.

5.2.2 Influence on Water Relaxation

As discussed in chapter 4, processes 5 and 6 of the present spectra can be ascribed to the relaxations of water located in the core and near the interface of the aqueous subphase, respectively. Thus, variations in the relaxation parameters of these processes will contribute to a better understanding of the way these types of water are affected by the addition of co-ions.

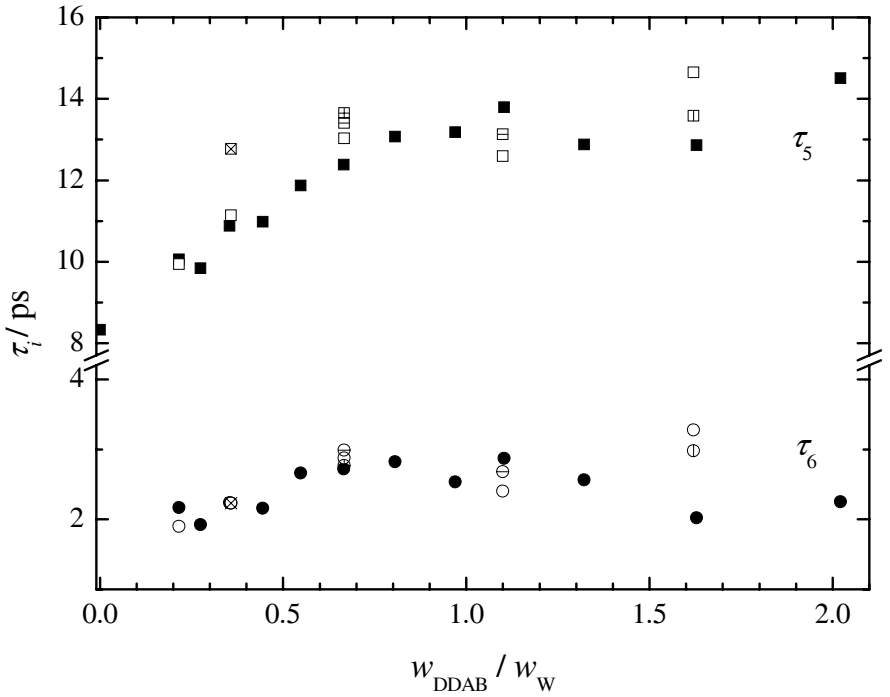

Figure 5.2: Relaxation times, τ_5 and τ_6, of DDAB/NaBr(aq)/D microemulsions as a function of the surfactant/water ratio, $w_{\mathrm{DDAB}}/w_{\mathrm{W}}$, at $w_{\mathrm{D}} = 0.35$, co-electrolyte concentration c and 25 ℃. ■: $\tau_5, c = 0$; □: $\tau_5, c = 1$ mM; ⊞: $\tau_5, c = 5$ mM; ⊠: $\tau_5, c = 7$ mM; ⊟: $\tau_5, c = 10$ mM; ◫: $\tau_5, c = 25$ mM; •: $\tau_6, c = 0$; ○: $\tau_6, c = 1$ mM; ⊕: $\tau_6, c = 5$ mM; ⊗: $\tau_6, c = 7$ mM; ⊖: $\tau_6, c = 10$ mM; ⏀: $\tau_6, c = 25$ mM.

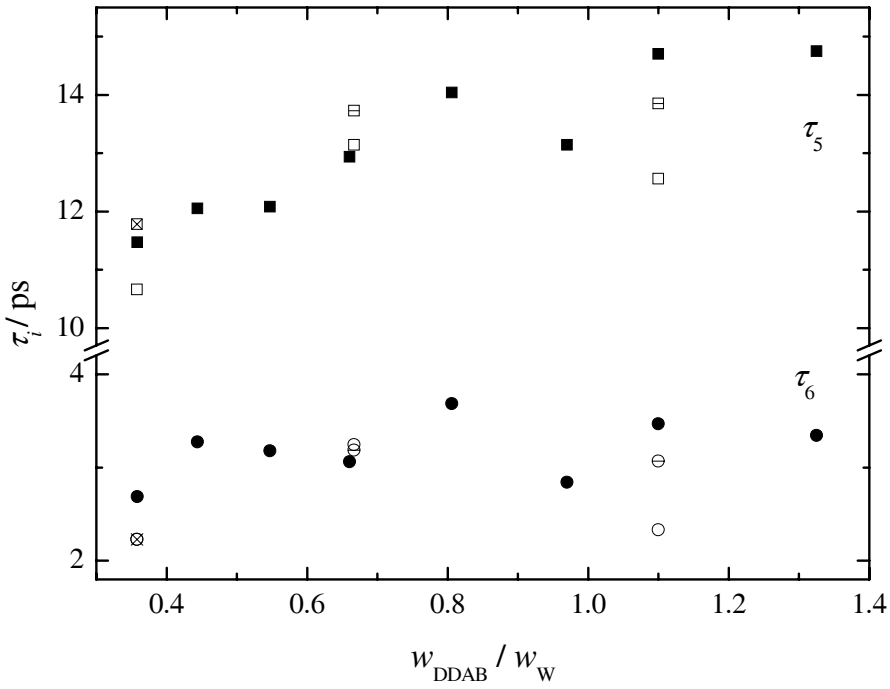

Figure 5.3: Relaxation times τ_5 and τ_6 of DDAB/NaBr(aq)/D microemulsions as a function of the surfactant/water ratio, $w_{\mathrm{DDAB}}/w_{\mathrm{W}}$, at $w_{\mathrm{D}} = 0.23$, co-electrolyte concentration c and 25 ℃. ■: $\tau_5, c = 0$; □: $\tau_5, c = 1$ mM; ⊠: $\tau_5, c = 7$ mM; ⊟: $\tau_5, c = 10$ mM; •: $\tau_6, c = 0$; ○: $\tau_6, c = 1$ mM; ⊗: $\tau_6, c = 7$ mM; ⊖: $\tau_6, c = 10$ mM.

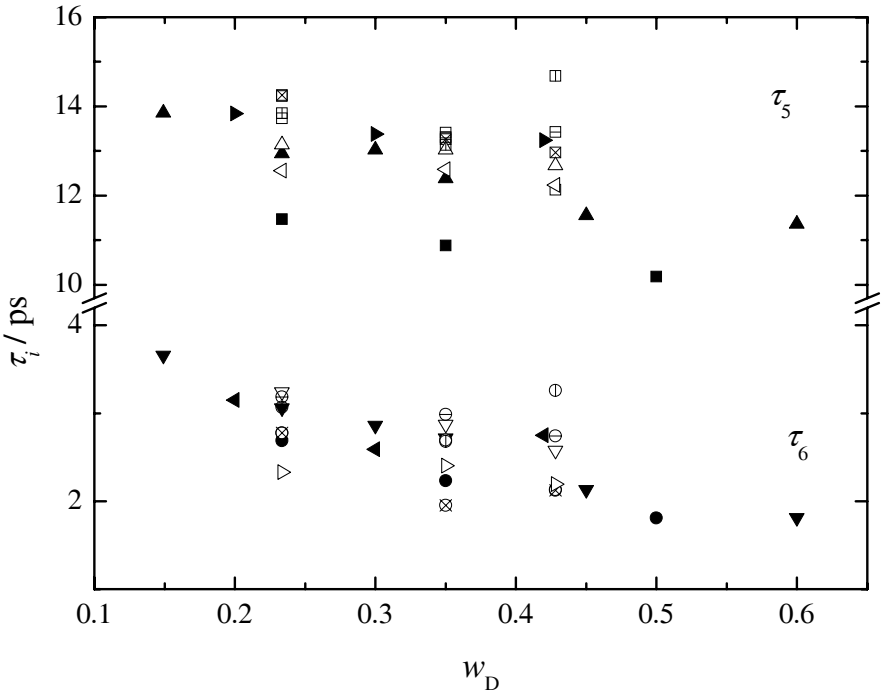

Figure 5.4: Relaxation times τ_5 and τ_6 of DDAB/NaBr(aq)/D microemulsions as a function of the dodecane mass fraction, w_D, at co-electrolyte concentration c and 25 ℃. Values given in brackets are the surfactant/water ratios, w_{DDAB}/w_W. ■: τ_5 (0.358), $c = 0$; □: τ_5 (0.358), $c = 1$ mM; ⊠: τ_5 (0.358), $c = 7$ mM; ▲: τ_5 (0.667), $c = 0$; △: τ_5 (0.667), $c = 1$ mM; ⊟: τ_5 (0.667), $c = 10$ mM; ◀: τ_5 (1.10), $c = 0$; ◁: τ_5 (1.10), $c = 1$ mM; ◫: τ_5 (1.10), $c = 10$ mM; ●: τ_6 (0.358), $c = 0$; ○: τ_6 (0.358), $c = 1$ mM; ⊗: τ_6 (0.358), $c = 10$ mM; ▼: τ_6 (0.667), $c = 0$; ▽: τ_6 (0.667), $c = 1$ mM; ⊖: τ_6 (0.667), $c = 10$ mM; ▶: τ_6 (1.10), $c = 0$; ▷: τ_6 (1.10), $c = 1$ mM; ⦶: τ_6 (1.10), $c = 10$ mM.

Obviously, the relaxation times τ_5 and τ_6 are barely influenced by the addition of co-ions. Figures 5.2, 5.3 and 5.4, covering the complete range of L_2, show some scattering, but no systematic deviations between the salt-free systems and those with added NaBr. A comparison of the co-electrolytes LiBr, NaBr, CsBr and $(CH_3)_4NBr$ at two different points within the L_2 phase (see Figures 5.5 and 5.6) did not reveal any ion-specific effects. As dielectric relaxation times of cooperative water relaxations reflect the strength of the H-bond network[43] these results suggest that the structures of both the core and interfacial water are not modified by the addition of co-ions.

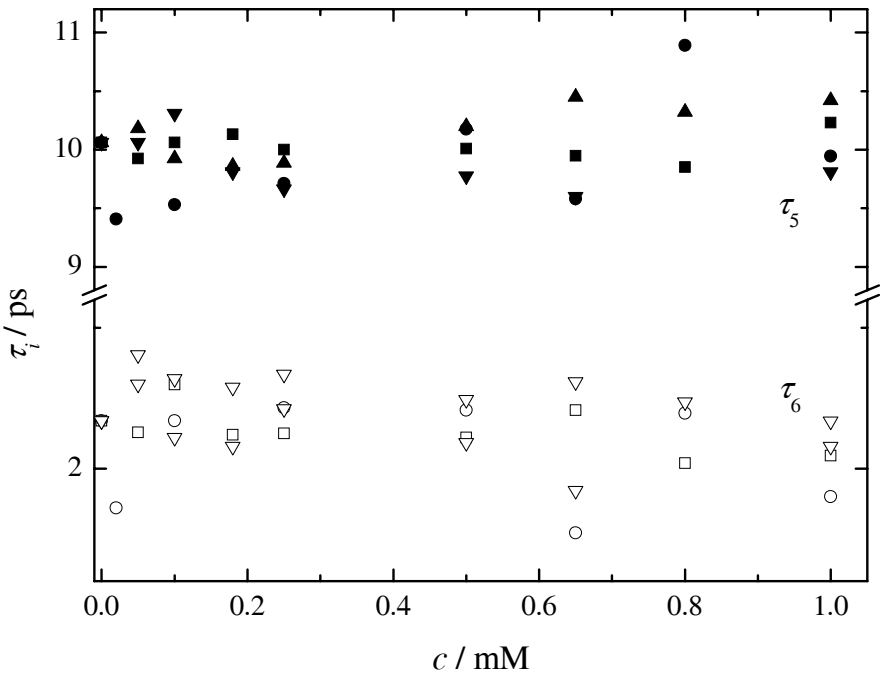

Figure 5.5: Relaxation times τ_5 and τ_6 of DDAB/XBr(aq)/D microemulsions as a function of the co-electrolyte concentration, c, at $w_D = 0.35$, $w_{DDAB}/w_W = 0.216$ (point 21x) and 25 °C. ■: τ_5, LiBr; ●: τ_5, NaBr; ▲: τ_5, CsBr; ▼: τ_5, $(CH_3)_4NBr$; □: τ_6, LiBr; ○: τ_6, NaBr; △: τ_6, CsBr; ▽: τ_6, $(CH_3)_4NBr$.

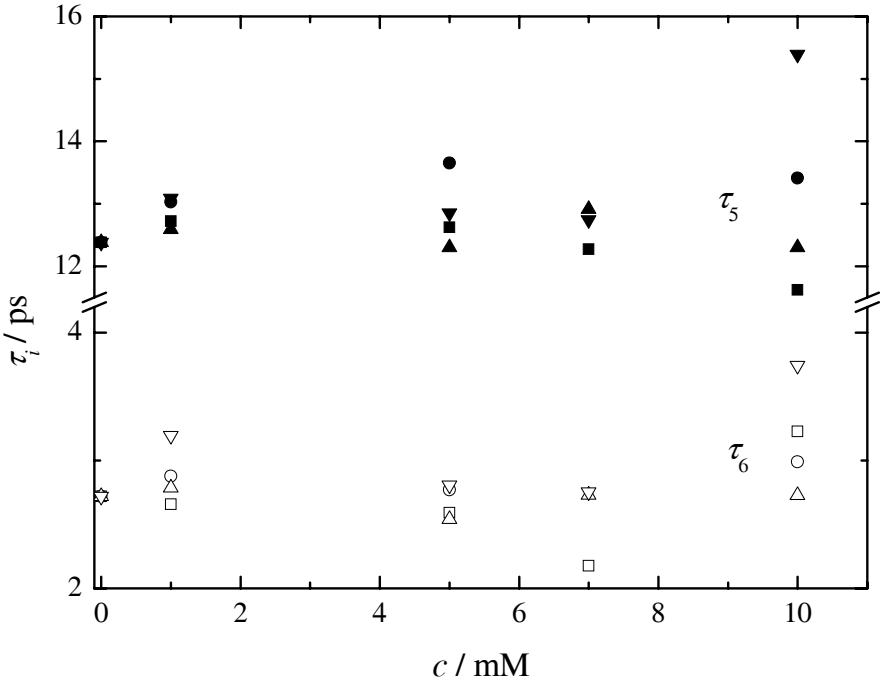

Figure 5.6: Relaxation times τ_5 and τ_6 of DDAB/XBr(aq)/D microemulsions as a function of the co-electrolyte concentration, c, at $w_D = 0.35$, $w_{DDAB}/w_W = 0.667$ (point 23x) and 25 °C. ■: τ_5, LiBr; ●: τ_5, NaBr; ▲: τ_5, CsBr; ▼: τ_5, $(CH_3)_4NBr$; □: τ_6, LiBr; ○: τ_6, NaBr; △: τ_6, CsBr; ▽: τ_6, $(CH_3)_4NBr$.

From the relaxation amplitudes S_5 and S_6 the relative water concentrations multiplied by the Kirkwood factor, $g_i c_i/c_W$, were calculated as described in section 4.3. As can be seen from Figures 5.7 and 5.8, there is a general trend towards lower $g_5 c_5/c_W$ and higher $g_6 c_6/c_W$ values upon addition of NaBr throughout the L_2 phase; however, Figure 5.9 shows that these values are rather scattered. Perhaps the most eye-catching feature of the water relaxation parameters is the pronounced decrease in $g_5 c_5/c_W$ upon addition of co-electrolytes (Figures 5.10 and 5.13). At first glance, this finding is surprising: why should the fraction of bulk water in the system decrease to such an extent? However, if we take into account Figure 5.11, showing the fitting results of the O-H stretching vibration of DDAB/NaBr(aq)/D at point $21x$, it becomes evident that the relative fractions of ice-like and distorted tetrahedral water do not vary upon increasing co-ion addition. Thus, the only possibility to explain the decrease in $g_5 c_5/c_W$ is to assume a decrease in the Kirkwood factor, g_5. This assumption appears plausible in the context of the results by Skurtveit and Olsson[176] and by Onori and Santucci,[149] both suggesting a reduction of interactions between the water droplets upon addition of a co-electrolyte. This 'loss of connectivity' is likely to be accompanied by a transition from ellipsoidal to rather spherical droplet shapes, which in turn gives rise to an increased antiparallel orientation of the core water dipoles, as discussed in section 4.3.3 (see Figure 4.13). Thus, a decrease in g_5 may be expected.

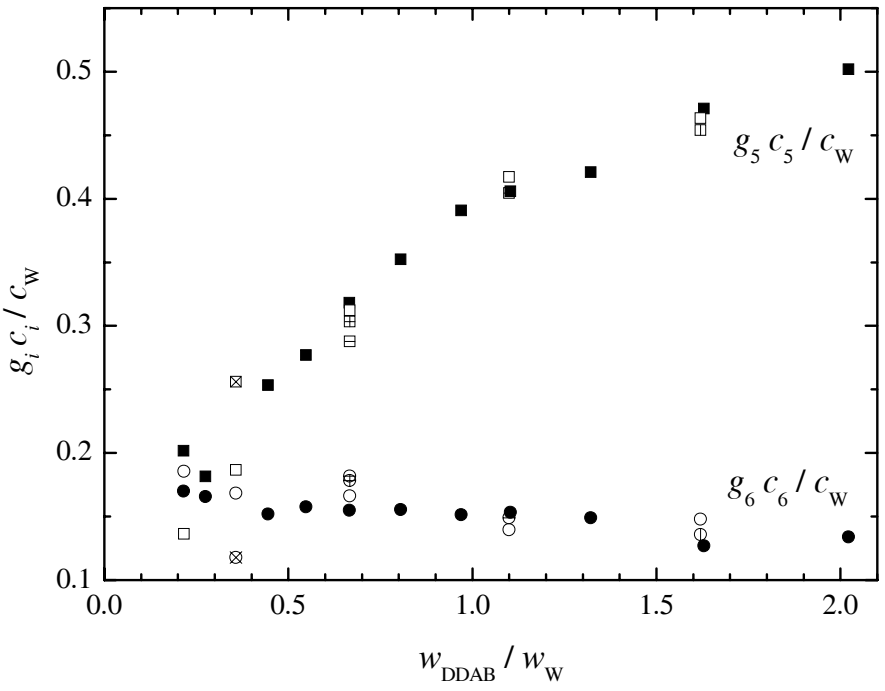

Figure 5.7: Relative water concentrations multiplied by the Kirkwood factor, $g_i c_i/c_W$, of DDAB/NaBr(aq)/D microemulsions as a function of the surfactant/water ratio, w_{DDAB}/w_W, at $w_D = 0.35$, co-electrolyte concentration c and 25 °C. ■: $g_5 c_5/c_W$, $c = 0$; □: $g_5 c_5/c_W$, $c = 1$ mM; ⊞: $g_5 c_5/c_W$, $c = 5$ mM; ⊠: $g_5 c_5/c_W$, $c = 7$ mM; ⊟: $g_5 c_5/c_W$, $c = 10$ mM; ◫: $g_5 c_5/c_W$, $c = 25$ mM; •: $g_6 c_6/c_W$, $c = 0$; ○: $g_6 c_6/c_W$, $c = 1$ mM; ⊕: $g_6 c_6/c_W$, $c = 5$ mM; ⊗: $g_6 c_6/c_W$, $c = 7$ mM; ⊖: $g_6 c_6/c_W$, $c = 10$ mM; ⊙: $g_6 c_6/c_W$, $c = 25$ mM.

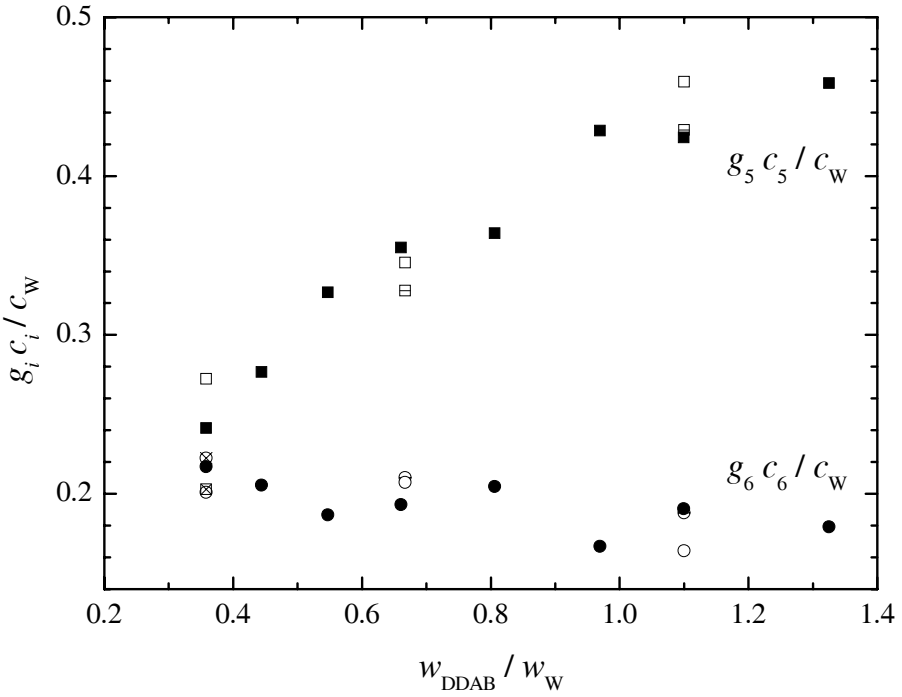

Figure 5.8: Relative water concentrations multiplied by the Kirkwood factor, $g_i c_i/c_W$, of DDAB/NaBr(aq)/D microemulsions as a function of the surfactant/water ratio, w_{DDAB}/w_W, at $w_D = 0.23$, co-electrolyte concentration c and 25 °C. ■: g_5c_5/c_W, $c = 0$; □: g_5c_5/c_W, $c = 1$ mM; ⊠: g_5c_5/c_W, $c = 7$ mM; ⊟: g_5c_5/c_W, $c = 10$ mM; •: g_6c_6/c_W, $c = 0$; ∘: g_6c_6/c_W, $c = 1$ mM; ⊗: g_6c_6/c_W, $c = 7$ mM; ⊖: g_6c_6/c_W, $c = 10$ mM.

The relative concentrations of core water multiplied by the Kirkwood factor, g_6c_6/c_W, appear to be almost constant upon co-ion addition at point $21x$ (Figure 5.12), whereas they show significant scattering and in most cases an increase with increasing co-electrolyte concentration at point $23x$ (Figure 5.14). Although the added co-ions are known to cause irrotational bonding of the surrounding water molecules (*e.g.* $8 \lesssim Z_{IB}(Li^+, c = 0) \lesssim 12$,[191] $Z_{IB}(Na^+, c = 0) = 4.2 \pm 0.3$[42]) this cannot explain a change in c_6 as the co-electrolyte concentration only amounts to ≤ 10 mM. As c_5 remains constant, too, it is reasonable to assume that the scattering of g_6c_6/c_W is caused by fluctuations in the Kirkwood factor, g_6. The added co-ions apparently exert some influence on the interface, leading to some disorder in the antiparallel alignment of the water molecules located there; this is reflected by an increase in g_6, as can be observed for most data points in Figure 5.14. Given the often large differences in g_6c_6/c_W at equal co-electrolyte concentrations, the co-ion effect on the interface may well be ion-specific. However, the number of data points in Figure 5.14 is not sufficient to prove this.

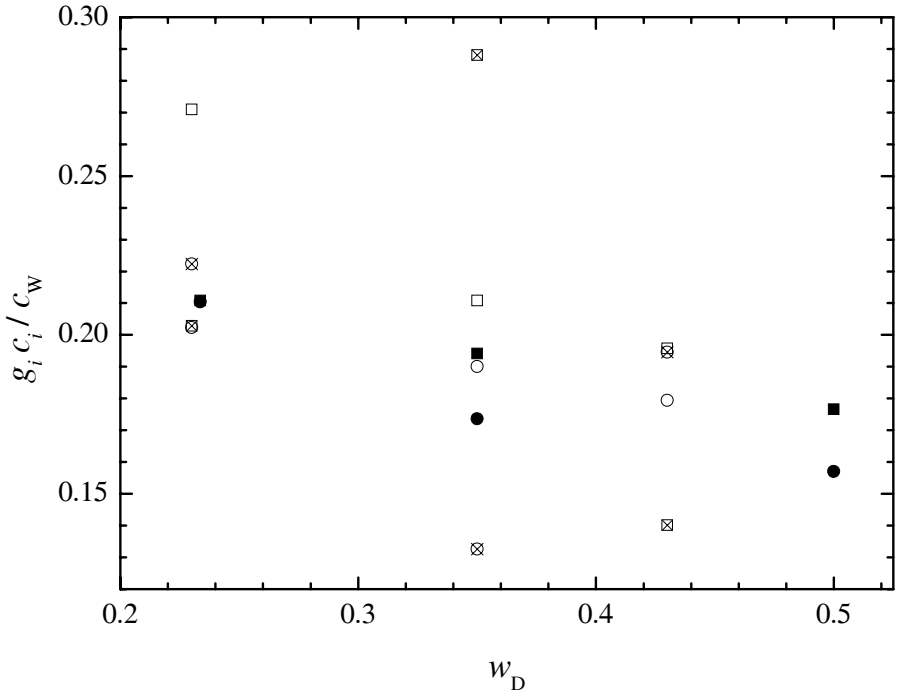

Figure 5.9: Relative water concentrations multiplied by the Kirkwood factor, $g_i c_i / c_W$, of DDAB/NaBr(aq)/D microemulsions as a function of the dodecane mass fraction, w_D, at $w_{DDAB}/w_W = 0.358$, co-electrolyte concentration c and 25 ℃. ■: $g_5 c_5 / c_W$, $c = 0$; □: $g_5 c_5 / c_W$, $c = 1$ mM; ⊠: $g_5 c_5 / c_W$, $c = 7$ mM; ●: $g_6 c_6 / c_W$, $c = 0$; ○: $g_6 c_6 / c_W$, $c = 1$ mM; ⊗: $g_6 c_6 / c_W$, $c = 7$ mM.

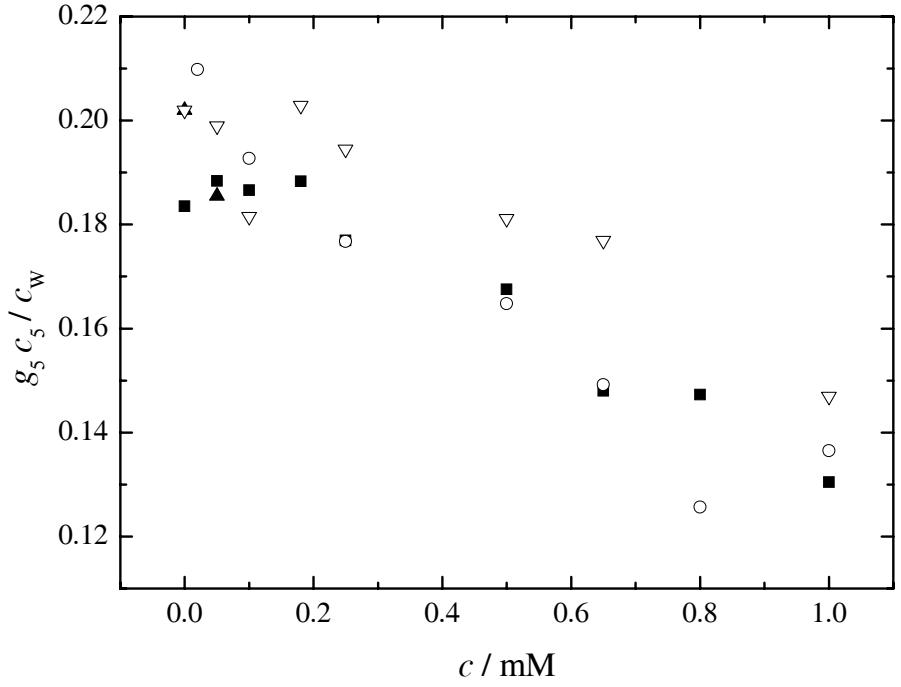

Figure 5.10: Relative water concentrations multiplied by the Kirkwood factor, $g_5 c_5 / c_W$, of DDAB/XBr(aq)/D microemulsions as a function of the co-electrolyte concentration, c, at $w_{DDAB}/w_W = 0.216$, $w_D = 0.35$ (point 21x) and 25 ℃. ■: LiBr; ○: NaBr; ▲: CsBr; ▽: $(CH_3)_4NBr$.

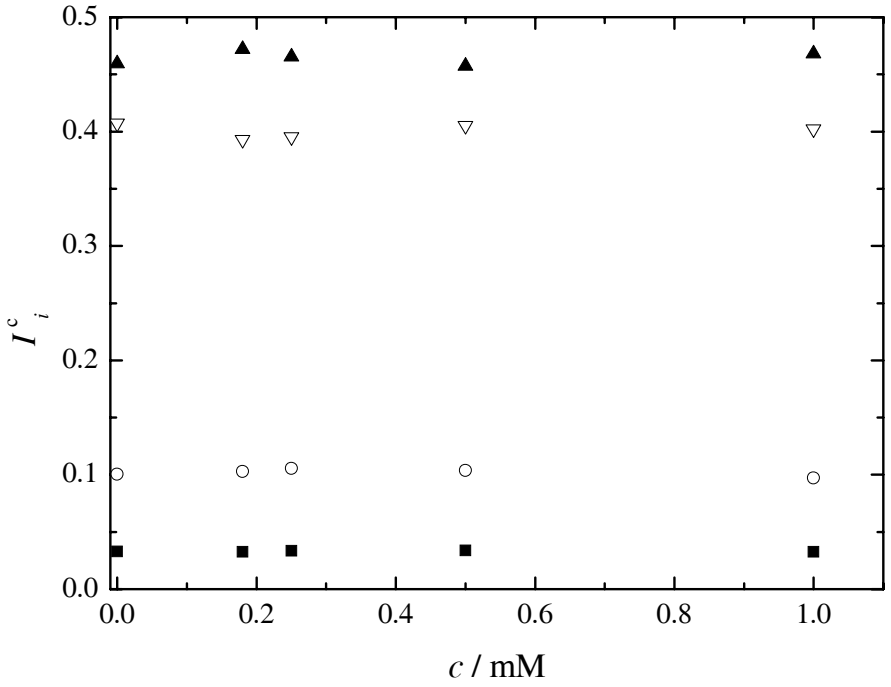

Figure 5.11: Fitting results of the O-H stretching vibration in DDAB/NaBr(aq)/D microemulsions: corrected relative band intensities, I_i^c, as a function of the NaBr concentration, c, at $w_D = 0.35$, $w_{DDAB}/w_W = 0.216$ (point 21x) and $\sim$ 24 ℃. ■: band A; ○: band B; ▲: band C; ▽: band D.

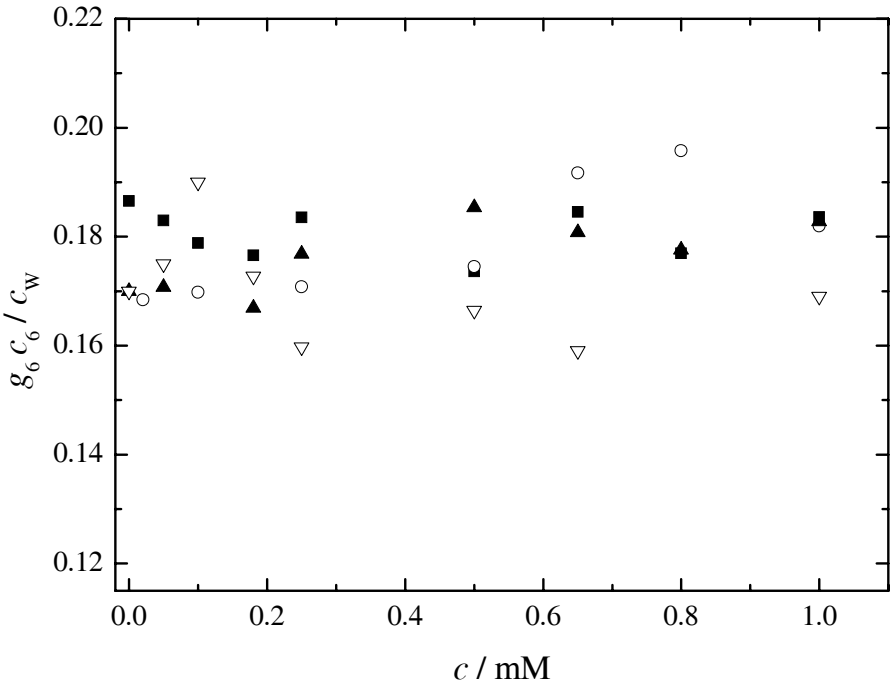

Figure 5.12: Relative water concentrations multiplied by the Kirkwood factor, $g_6 c_6/c_W$, of DDAB/XBr(aq)/D microemulsions as a function of the co-electrolyte concentration, c, at $w_{DDAB}/w_W = 0.216$, $w_D = 0.35$ (point 21x) and 25 ℃. ■: LiBr; ○: NaBr; ▲: CsBr; ▽: $(CH_3)_4NBr$.

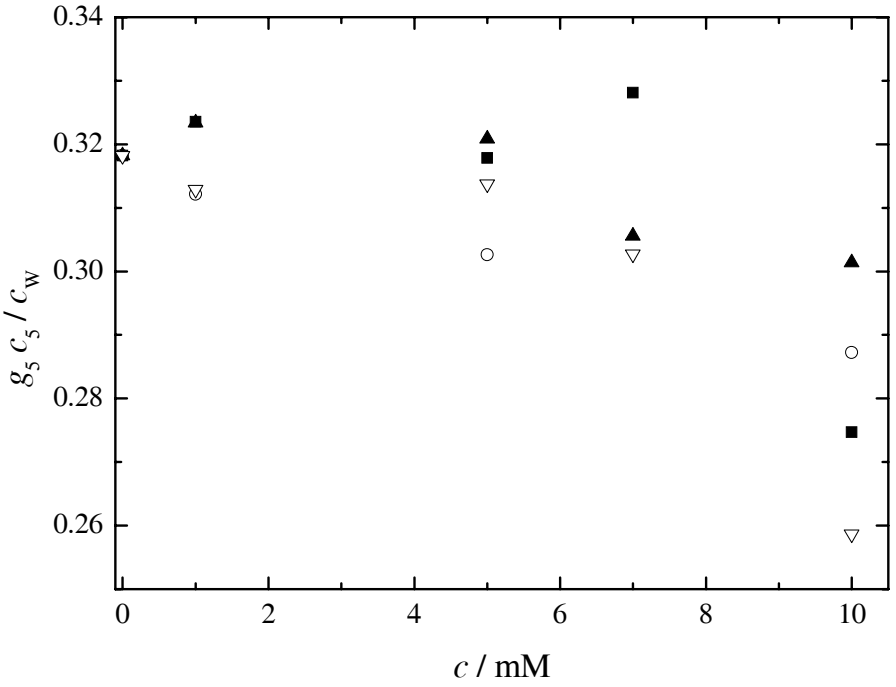

Figure 5.13: Relative water concentrations multiplied by the Kirkwood factor, $g_5 c_5 / c_W$, of DDAB/XBr(aq)/D microemulsions as a function of the co-electrolyte concentration, c, at $w_{DDAB}/w_W = 0.667$, $w_D = 0.35$ (point 23x) and 25 °C. ■: LiBr; ○: NaBr; ▲: CsBr; ▽: $(CH_3)_4NBr$.

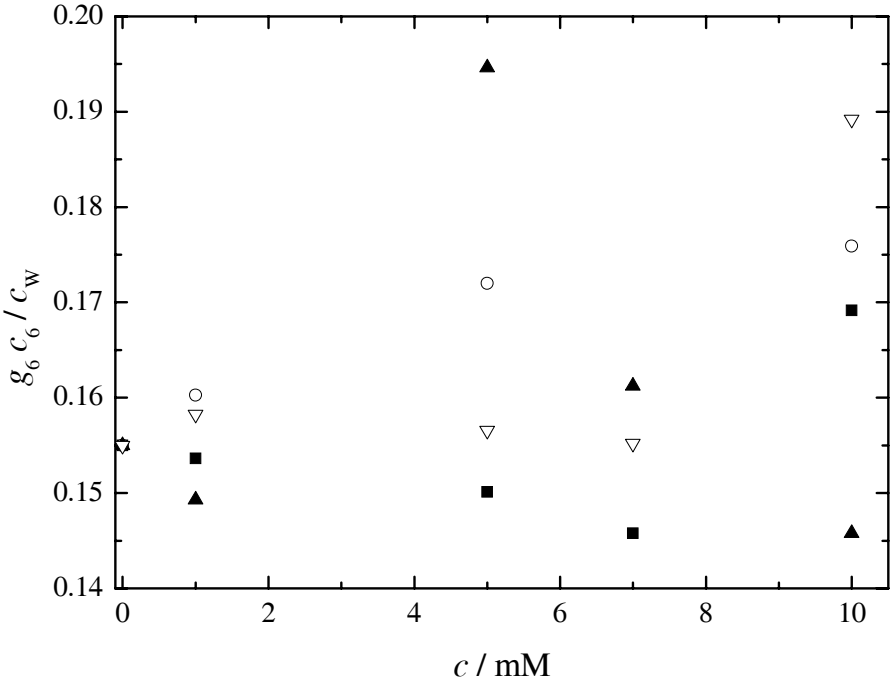

Figure 5.14: Relative water concentrations multiplied by the Kirkwood factor, $g_6 c_6 / c_W$, of DDAB/XBr(aq)/D microemulsions as a function of the co-electrolyte concentration, c, at $w_{DDAB}/w_W = 0.667$, $w_D = 0.35$ (point 23x) and 25 °C. ■: LiBr; ○: NaBr; ▲: CsBr; ▽: $(CH_3)_4NBr$.

5.2.3 Influence on Ion-Pairing Rotation

Figures 5.15 to 5.17 compare the relaxation times τ_4 of the systems DDAB/W/D and DDAB/NaBr(aq)/D. These data are somewhat scattered, probably due to the difficulties in resolving this low-amplitude process correctly, as has been outlined in section 4.4. Beyond this, no significant trends can be observed. This is also the case for the τ_4 values obtained upon addition of different co-electrolytes to the system DDAB/W/D at point $21x$ (Figure 5.18). The value for $c = 0$ appears to be an outlier. In contrast, at point $23x$ (Figure 5.19) τ_4 is distinctly different between the salt-free microemulsion system and samples containing co-electrolytes. After a quick rise for $c = 1$ mM, τ_4 decreases significantly for the co-electrolyte CsBr and moderately for $(CH_3)_4NBr$, whereas it increases for NaBr and remains roughly constant for LiBr. Although being well aware that the relaxation parameters of process 4 are prone to errors, we may regard this finding as an indication of an ion-specific effect.

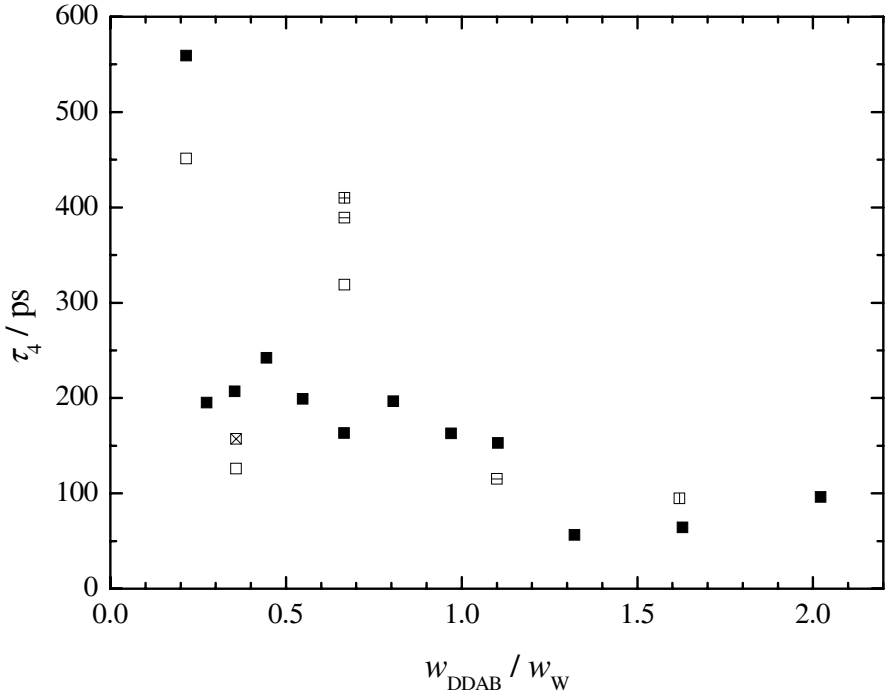

Figure 5.15: Relaxation times τ_4 of DDAB/NaBr(aq)/D microemulsions as a function of the surfactant/water ratio, w_{DDAB}/w_W, at $w_D = 0.35$, co-electrolyte concentration, c, and 25 °C. ■: $c = 0$; □: $c = 1$ mM; ⊞: $c = 5$ mM; ⊠: $c = 7$ mM; ⊟: $c = 10$ mM; ◫: $c = 25$ mM.

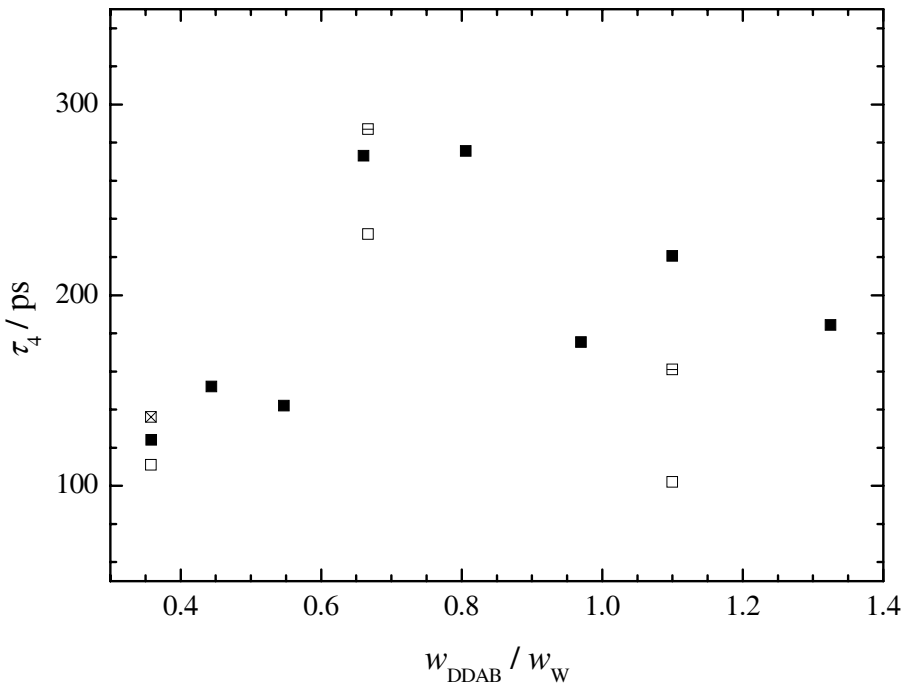

Figure 5.16: Relaxation times τ_4 of DDAB/NaBr(aq)/D microemulsions as a function of the surfactant/water ratio, w_{DDAB}/w_W, at $w_D = 0.23$, co-electrolyte concentration, c, and 25 °C. ■: $c = 0$; □: $c = 1$ mM; ⊠: $c = 7$ mM; ⊟: $c = 10$ mM.

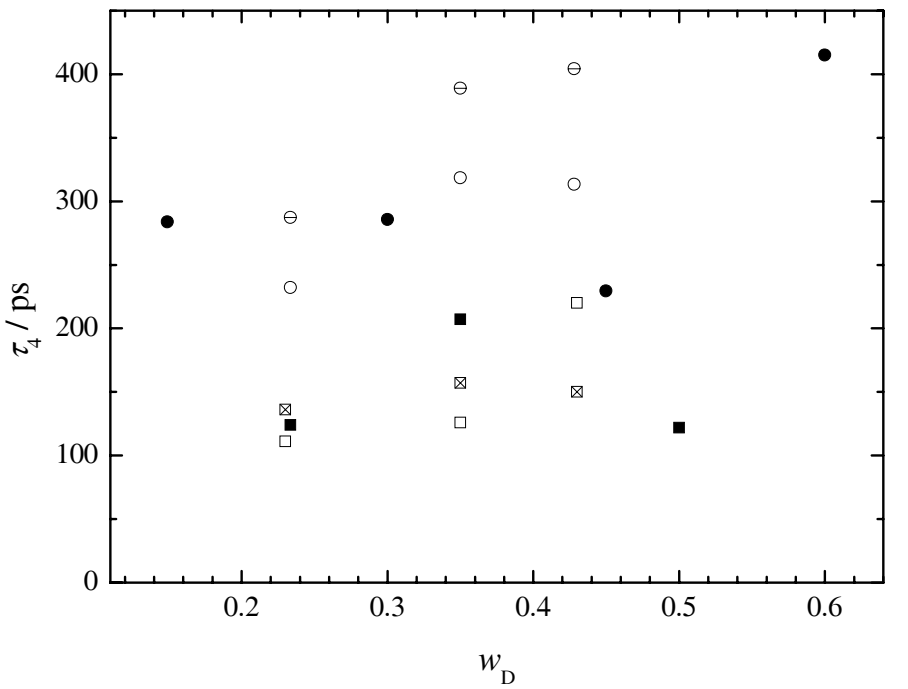

Figure 5.17: Relaxation times τ_4 of DDAB/NaBr(aq)/D microemulsions as a function of the dodecane mass fraction, w_D, at co-electrolyte concentration, c, and 25 °C. Values given in brackets are the surfactant/water ratios, w_{DDAB}/w_W. ■: (0.358), $c = 0$; □: (0.358), $c = 1$ mM; ⊠: (0.358), $c = 7$ mM; ●: (0.667), $c = 0$; ○: (0.667), $c = 1$ mM; ⊖: (0.667), $c = 10$ mM.

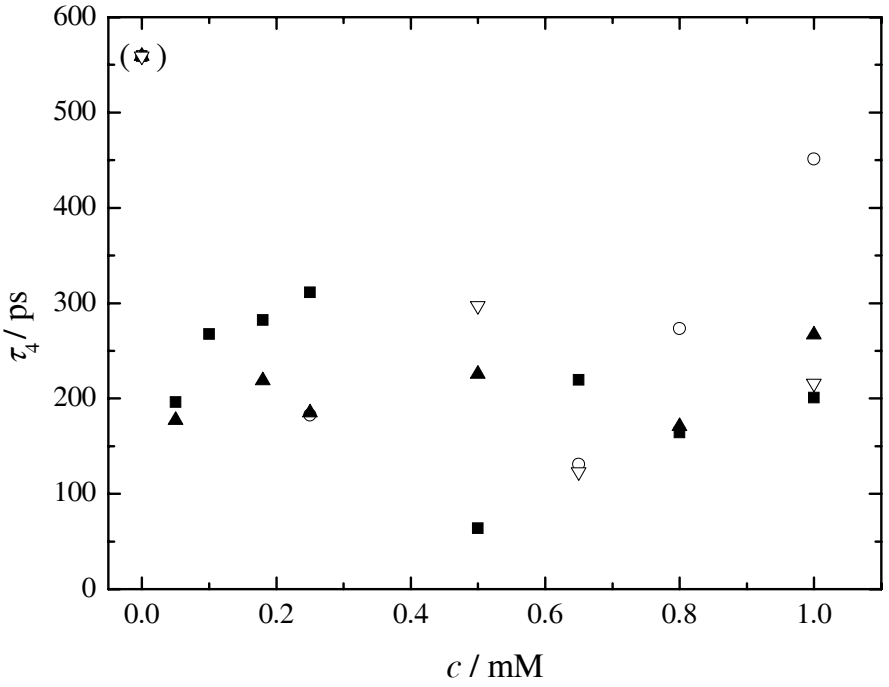

Figure 5.18: Relaxation times τ_4 of DDAB/XBr(aq)/D microemulsions as a function of the co-electrolyte concentration, c, at $w_{\mathrm{DDAB}}/w_{\mathrm{W}} = 0.216$, $w_{\mathrm{D}} = 0.35$ (point 21x) and 25 ℃. ■: LiBr; ○: NaBr; ▲: CsBr; ▽: $(CH_3)_4NBr$.

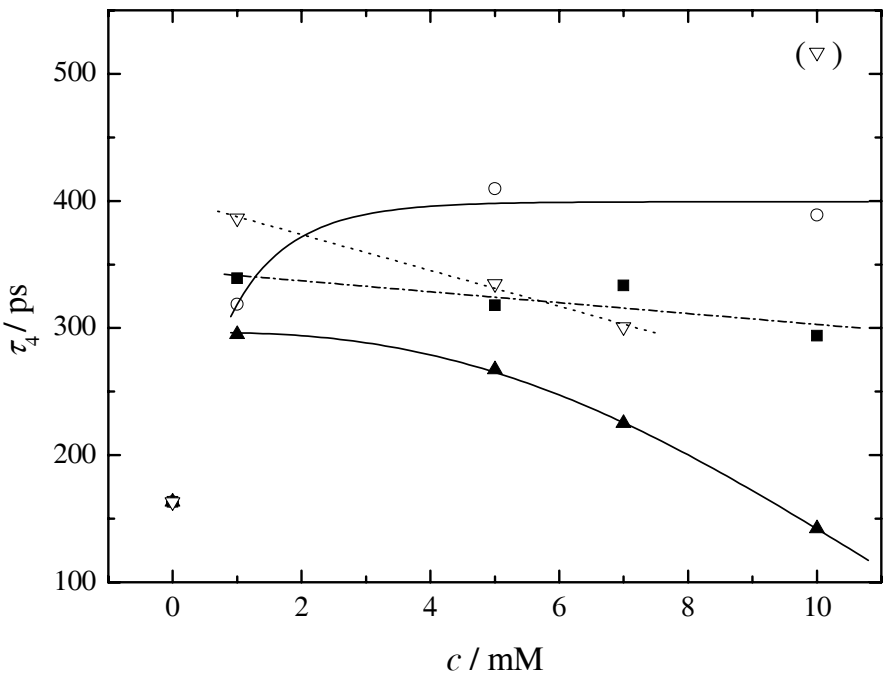

Figure 5.19: Relaxation times τ_4 of DDAB/XBr(aq)/D microemulsions as a function of the co-electrolyte concentration, c, at $w_{\mathrm{DDAB}}/w_{\mathrm{W}} = 0.667$, $w_{\mathrm{D}} = 0.35$ (point 23x) and 25 ℃. ■: LiBr; ○: NaBr; ▲: CsBr; ▽: $(CH_3)_4NBr$; lines are only given as a visual aid.

Following the procedure outlined in section 4.4, relative DDAB ion-pair concentrations, c_{IP}/c_{DDAB}, have been calculated for the co-electrolyte samples using the CIP model (Figures 5.20 to 5.24). Comparing the systems DDAB/W/D and DDAB/NaBr(aq)/D over the entire L_2 phase (Figures 5.20 to 5.22), no significant trends are apparent. However, comparing the influence of different co-electrolytes at point $21x$ ($W = 119$, Figure 5.23) it becomes evident that the fraction of DDAB ion pairs is significantly lower relative to the salt-free system. There are no obvious differences between the co-electrolytes, except for the pronounced increase in c_{IP}/c_{DDAB} for NaBr at $c \geq 0.65$ mM. Surprisingly, comparing the effects of the same co-electrolytes at point $23x$ ($W = 39$, Figure 5.24) leads to a very different result. In this case, the relative DDAB ion-pair concentrations *increase* significantly in the order $(CH_3)_4NBr$ > LiBr > NaBr > CsBr for low co-electrolyte additions ($c = 1$ mM). When c is increased c_{IP}/c_{DDAB} decreases for CsBr (strongly) and $(CH_3)_4NBr$ (moderately) or remains constant for NaBr, but decreases suddenly at $c = 10$ mM for LiBr.

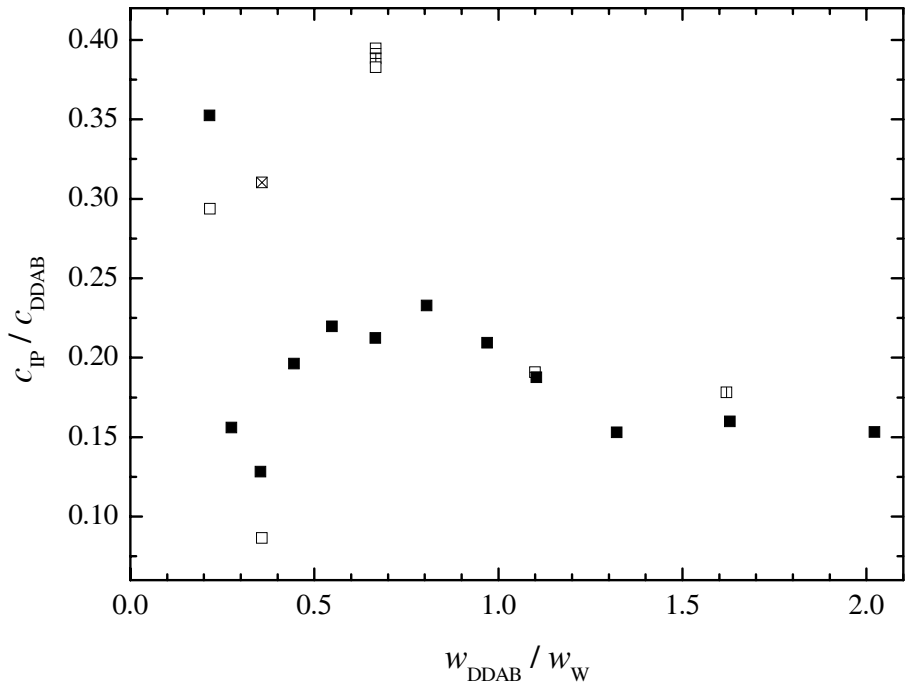

Figure 5.20: Relative ion-pair concentration, c_{IP}/c_{DDAB}, of DDAB/NaBr(aq)/D microemulsions as a function of the surfactant/water ratio, w_{DDAB}/w_W, at $w_D = 0.35$, co-electrolyte concentration, c, and 25 °C assuming the CIP model. ■: $c = 0$; □: $c = 1$ mM; ⊞: $c = 5$ mM; ⊠: $c = 7$ mM; ⊟: $c = 10$ mM; ◫: $c = 25$ mM.

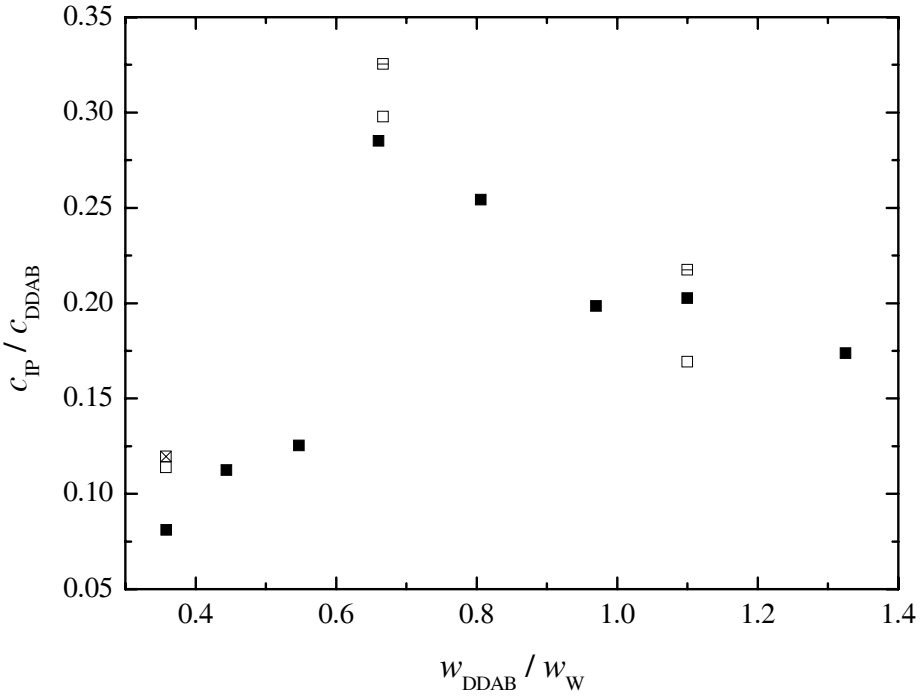

Figure 5.21: Relative ion-pair concentration, c_{IP}/c_{DDAB}, of DDAB/NaBr(aq)/D microemulsions as a function of the surfactant/water ratio, w_{DDAB}/w_W, at $w_D = 0.23$, co-electrolyte concentration, c, and 25 °C assuming the CIP model. ■: $c = 0$; □: $c = 1$ mM; ⊠: $c = 7$ mM; ⊟: $c = 10$ mM.

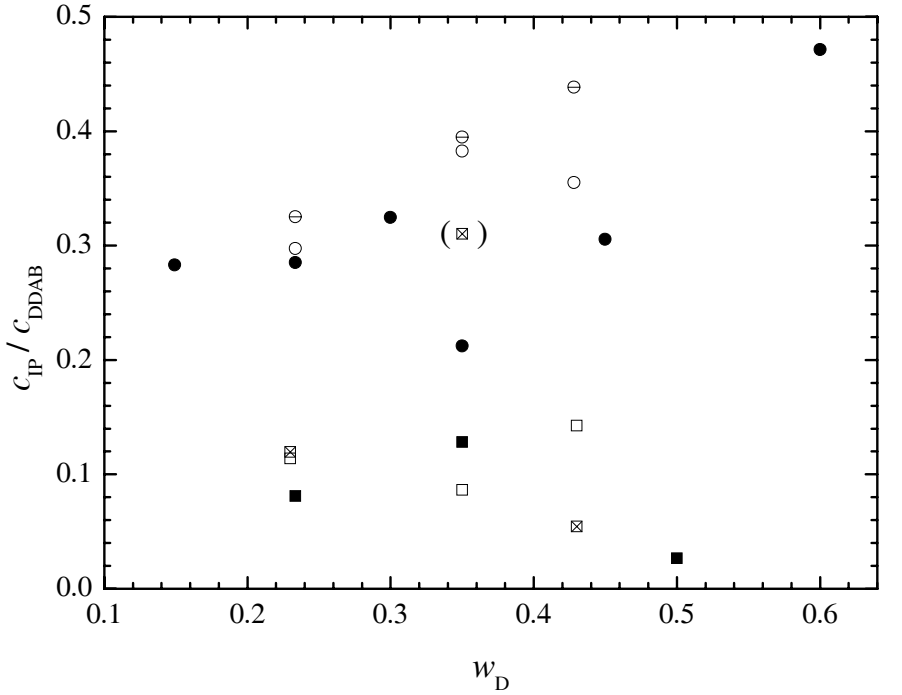

Figure 5.22: Relative ion-pair concentration, c_{IP}/c_{DDAB}, of DDAB/NaBr(aq)/D microemulsions as a function of the dodecane mass fraction, w_D, at co-electrolyte concentration, c, and 25 °C assuming the CIP model. Values given in brackets are the surfactant/water ratios, w_{DDAB}/w_W. ■: (0.358), $c = 0$; □: (0.358), $c = 1$ mM; ⊠: (0.358), $c = 7$ mM; •: (0.667), $c = 0$; ○: (0.667), $c = 1$ mM; ⊖: (0.667), $c = 10$ mM.

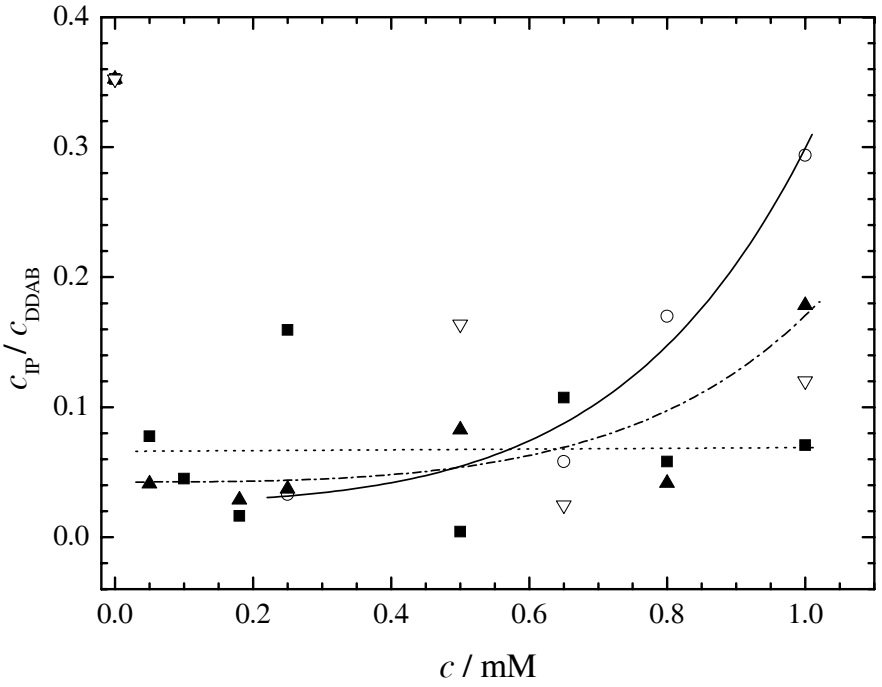

Figure 5.23: Relative ion-pair concentration, c_{IP}/c_{DDAB}, of DDAB/XBr(aq)/D microemulsions as a function of the co-electrolyte concentration, c, at $w_{DDAB}/w_W = 0.216$, $w_D = 0.35$ (point 21x) and 25 °C assuming the CIP model. ■: LiBr; ○: NaBr; ▲: CsBr; ▽: $(CH_3)_4NBr$; lines are given as a visual aid.

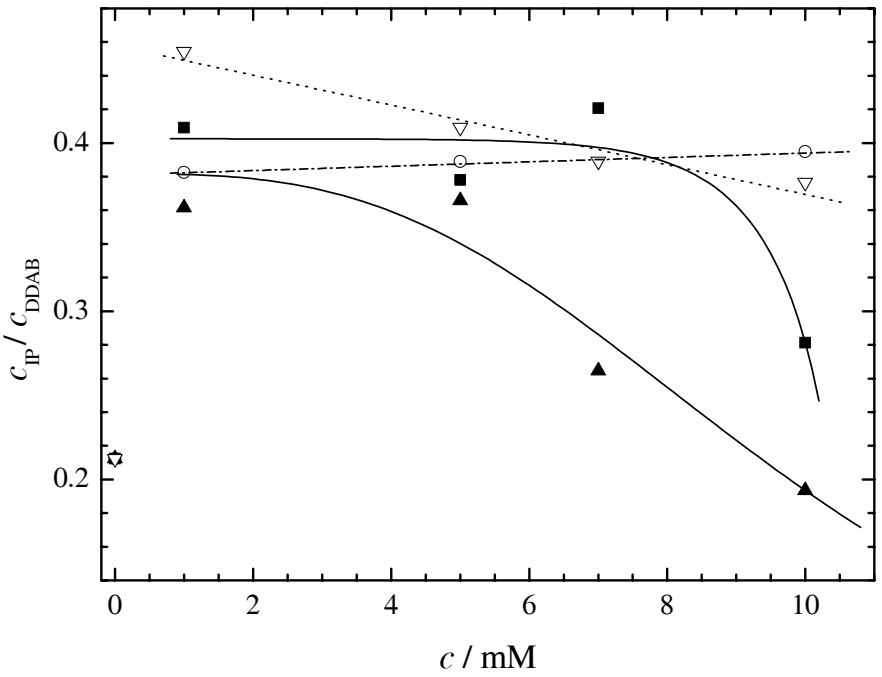

Figure 5.24: Relative ion-pair concentration, c_{IP}/c_{DDAB}, of DDAB/XBr(aq)/D microemulsions as a function of the co-electrolyte concentration, c, at $w_{DDAB}/w_W = 0.667$, $w_D = 0.35$ (point 23x) and 25 °C assuming the CIP model. ■: LiBr; ○: NaBr; ▲: CsBr; ▽: $(CH_3)_4NBr$; lines are given as a visual aid.

It is not obvious how to interpret these experimental findings. If it is assumed that process 4 can be ascribed to an ion-pair rotation, Figures 5.23 and 5.24 suggest that the DDAB ion-pair concentration varies as a function of co-ion addition. As the number of DDAB ion pairs that are able to rotate in a W/O droplet is limited by geometric constraints at the interface, this means that the co-ions are located in the interfacial area (where they also influence the interfacial-water dynamics, see above) and modify the geometry of the interface. This conclusion agrees well with the concept of Ninham *et al.* that '(1) adsorption of cations occurs, driven by dispersion forces; (2) once they are there they act as defects that induce a large change in a highly ordered cooperative interfacial water structure.'[134] Furthermore, despite the inaccuracy of the relaxation parameters of process 4, there is some evidence of an ion-specific effect, similar to the sequence $(CH_3)_4NBr > LiBr > NaBr \gg CsBr$ found by Murgia *et al.* for the stability of DDAB/W/decane microemulsions upon co-electrolyte addition.[144]

As already discussed in section 4.4, the rotational movement of ion pairs is not the only conceivable interpretation of process 4. As an alternative, this relaxation may be ascribed to small uncorrelated motions of single counterions within the aqueous subphase, giving rise to a small total dipole moment of the water droplet (see Figure 4.21). On the basis of the present data, it is not possible to decide which of these two models should be preferred. However, the conclusions drawn in this section on the basis of the ion-pairing model remain valid if we assume counterion rearrangements to account for process 4. In this case, the observed variations of the relaxation parameters upon co-ion addition also suggest that the latter modify the interfacial structure, given that the large majority of the counterions is located near the interface.[74]

5.2.4 Influence on Interfacial Polarisation

As discussed in section 4.5, relaxation processes 2 and 3 of the present spectra can be ascribed to surface counterion diffusion in the OHP and radial counterion diffusion in the diffuse double layer, respectively (see Figure 4.27). Since the high-frequency relaxation data strongly suggest that the co-ions (*i.e.* the cations of the co-electrolyte) are located near the interface and modify its geometrical structure, the parameters of these interfacial-polarisation processes would also be affected by co-ion addition.

Figures 5.28 and 5.32 show that the amplitude S_3 and the relaxation time τ_3 of process 3 decrease considerably upon addition of the co-electrolytes LiBr, NaBr, CsBr and $(CH_3)_4NBr$ without any ion-specific differences. Hence, we may conclude that in the water-rich region of the L_2 phase the radial diffusion of ions located in the diffuse double layer is hampered by the addition of co-ions, whereas the relaxation time of this process is shortened. Figures 5.25 to 5.27 and 5.29 to 5.31, comparing τ_3 and S_3 of the systems DDAB/W/D and DDAB/NaBr(aq)/D for various samples within L_2, show some deviations, but no perceptible trend upon co-ion addition.

In the case of process 2, reflecting the diffusion of counterions in the OHP along the surface, a pronounced decrease in both S_2 and τ_2 (Figures 5.36 and 5.41) can be observed for all investigated co-electrolytes in the water-rich part of L_2 ($W = 119$). As we have con-

cluded from the water-relaxation processes, the addition of co-ions evokes less connectivity between the water droplets, leading to more spherically-shaped particles than in a salt-free system; this trend is particularly pronounced at the water-rich edge of L_2. These structural changes apparently coincide with a reduced counterion diffusion along the surface of the W/O droplet. For systems at $W = 39$, exhibiting stronger percolation effects, the situation is somewhat different. Upon addition of NaBr, the relaxation time τ_2 increases, whereas it shows a strong decrease for CsBr, a slight decrease for $(CH_3)_4NBr$ and some scattering for LiBr (Figure 5.37); the amplitude S_2 shows roughly the same behaviour (Figure 5.42). This finding is difficult to explain, but as in the case of the water-rich sample, the dynamics of surface counterion diffusion are influenced by the added co-ions. In addition, this effect seems to be ion-specific. As for process 3, comparisons of S_2 and τ_2 of DDAB/W/D and DDAB/NaBr(aq)/D for various sample compositions throughout L_2 (Figures 5.33 to 5.35 and 5.38 to 5.40) do not reveal any identifiable trends.

In summary, the relaxation parameters of the interfacial-polarisation processes 2 and 3 are significantly influenced by the addition of co-ions, and even an ion-specific effect may be observable at $W = 39$. This result supports the view that co-ions are located near the interface and modify its structure.

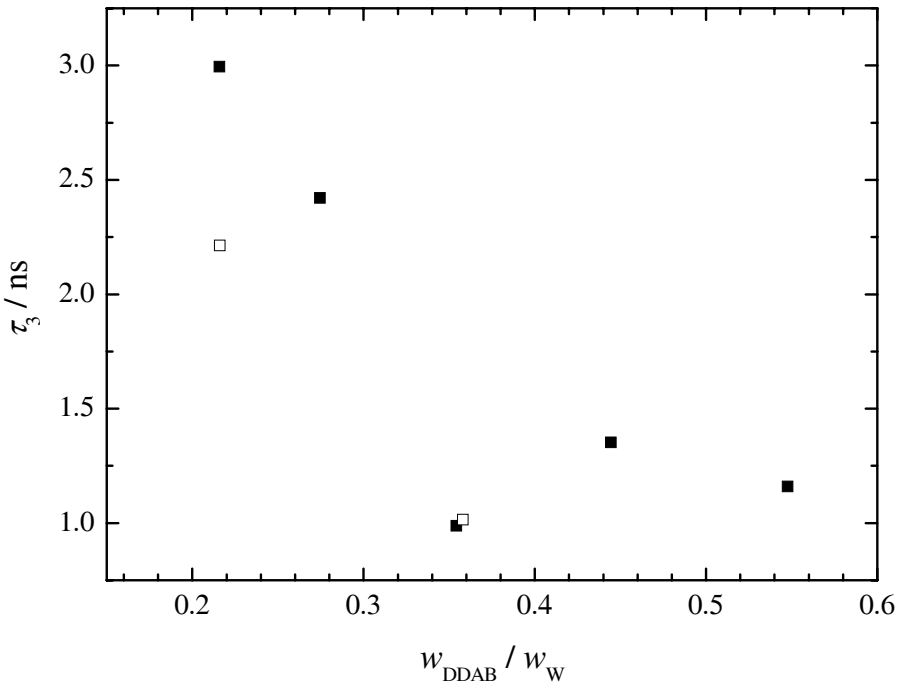

Figure 5.25: Relaxation times τ_3 of DDAB/NaBr(aq)/D microemulsions as a function of the surfactant/water ratio, w_{DDAB}/w_W, at $w_D = 0.35$, co-electrolyte concentration, c, and 25 °C. ■: $c = 0$; □: $c = 1$ mM.

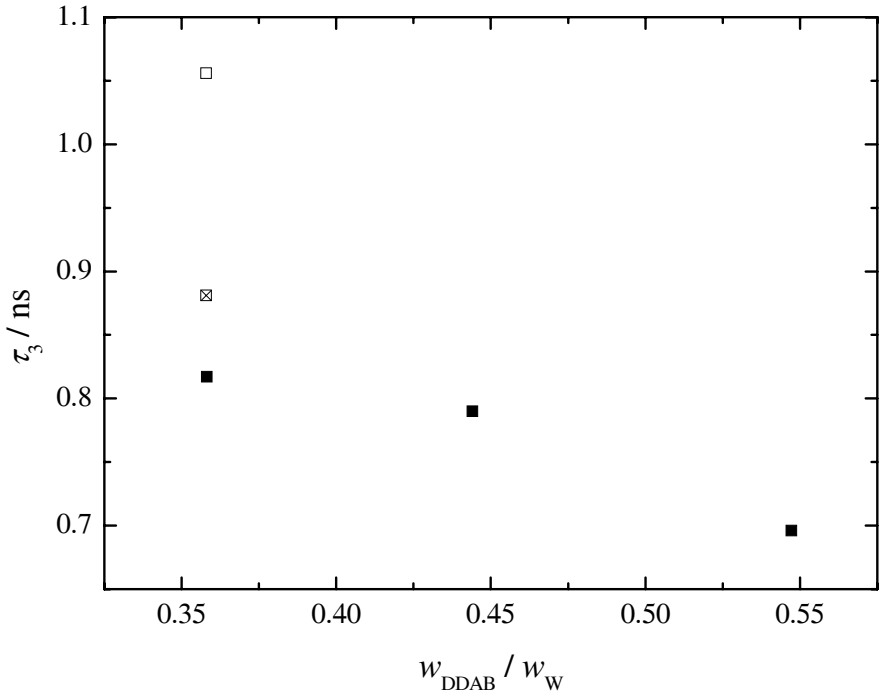

Figure 5.26: Relaxation times τ_3 of DDAB/NaBr(aq)/D microemulsions as a function of the surfactant/water ratio, $w_{\mathrm{DDAB}}/w_{\mathrm{W}}$, at $w_{\mathrm{D}} = 0.23$, co-electrolyte concentration, c, and 25 °C. ■: $c = 0$; □: $c = 1$ mM; ⊠: $c = 7$ mM.

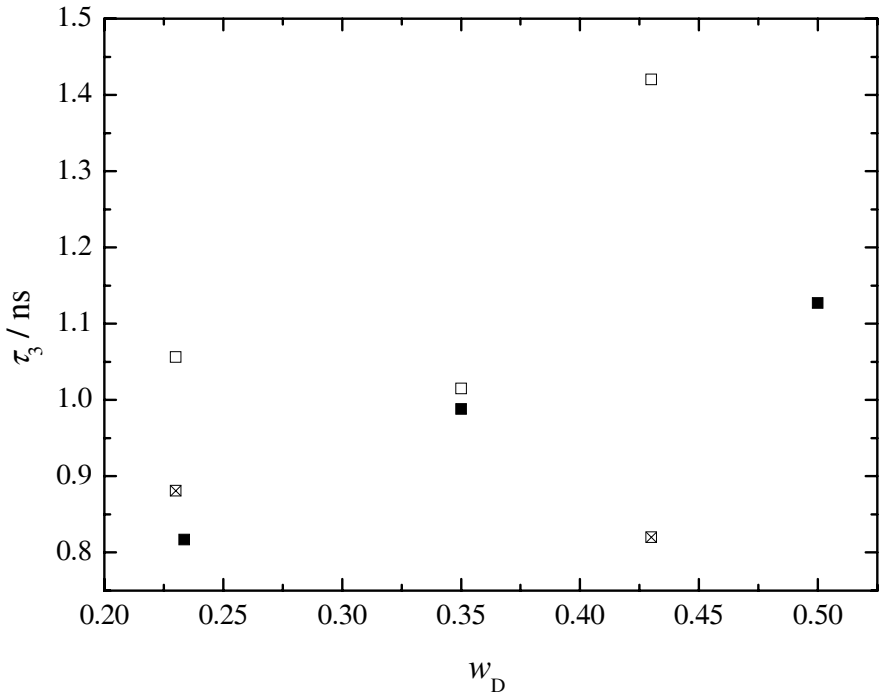

Figure 5.27: Relaxation times τ_3 of DDAB/NaBr(aq)/D microemulsions as a function of the dodecane mass fraction, w_{D}, at $w_{\mathrm{DDAB}}/w_{\mathrm{W}} = 0.358$, co-electrolyte concentration, c, and 25 °C. ■: $c = 0$; □: $c = 1$ mM; ⊠: $c = 7$ mM.

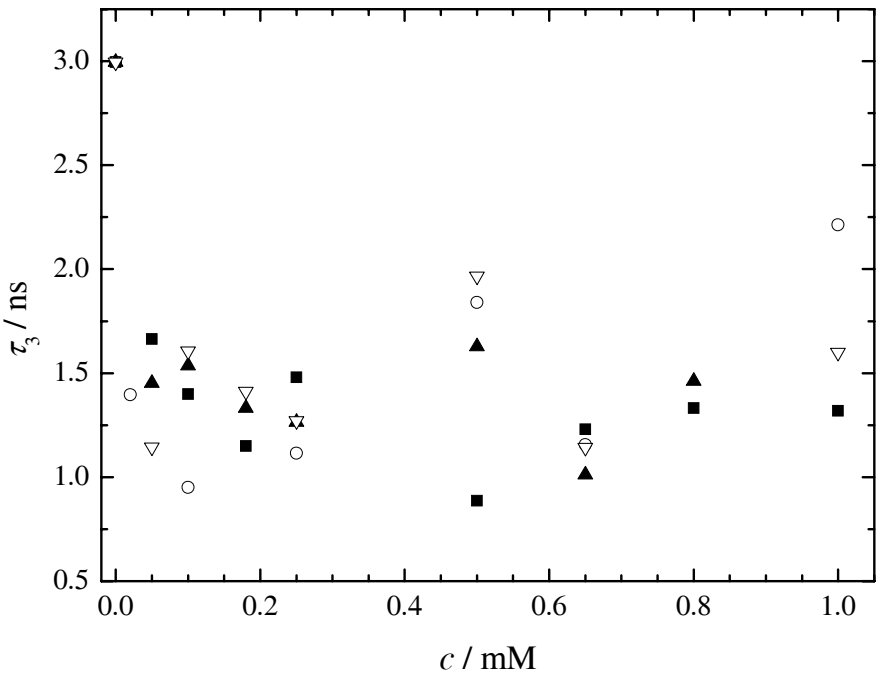

Figure 5.28: Relaxation times τ_3 of DDAB/XBr(aq)/D microemulsions as a function of the co-electrolyte concentration, c, at $w_{\mathrm{DDAB}}/w_{\mathrm{W}} = 0.216$, $w_{\mathrm{D}} = 0.35$ (point $21x$) and 25 ℃. ■: LiBr; ○: NaBr; ▲: CsBr; ▽: $(CH_3)_4NBr$.

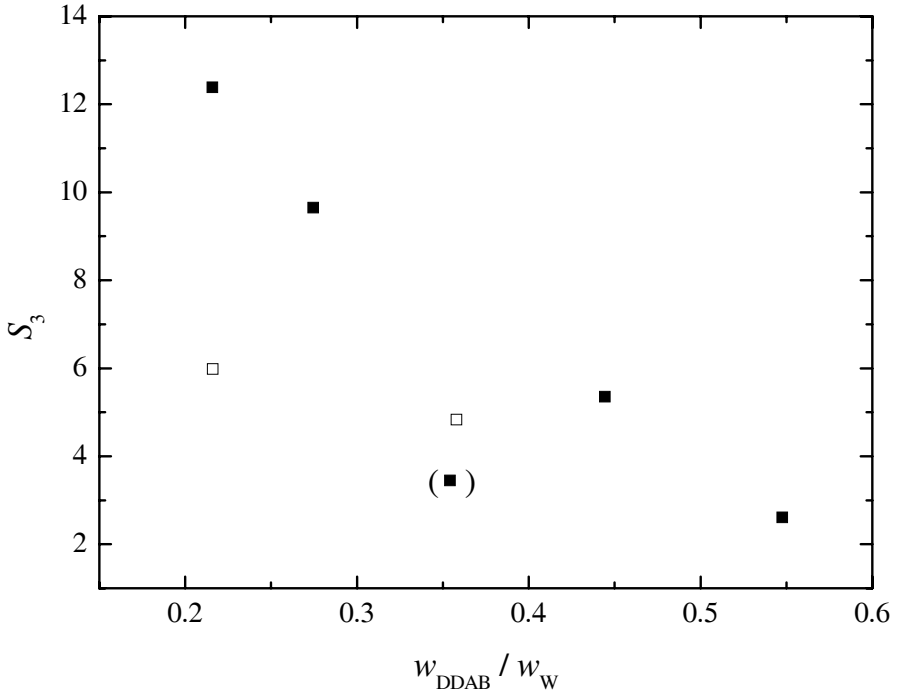

Figure 5.29: Relaxation amplitudes S_3 of DDAB/NaBr(aq)/D microemulsions as a function of the surfactant/water ratio, $w_{\mathrm{DDAB}}/w_{\mathrm{W}}$, at $w_{\mathrm{D}} = 0.35$, co-electrolyte concentration, c, and 25 ℃. ■: $c = 0$; □: $c = 1$ mM.

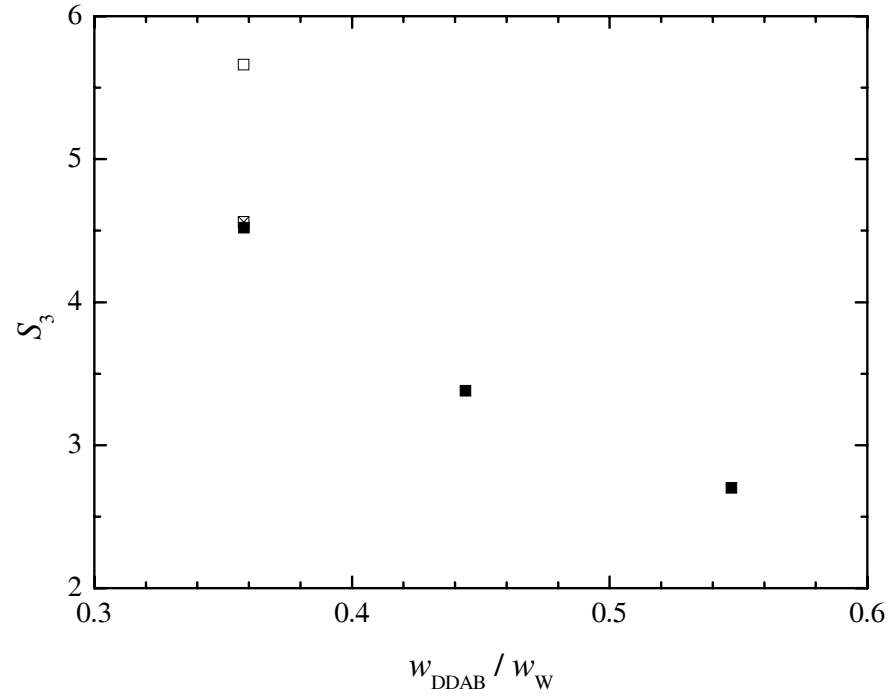

Figure 5.30: Relaxation amplitudes S_3 of DDAB/NaBr(aq)/D microemulsions as a function of the surfactant/water ratio, $w_{\mathrm{DDAB}}/w_{\mathrm{W}}$, at $w_{\mathrm{D}} = 0.23$, co-electrolyte concentration, c, and 25 °C. ■: $c = 0$; □: $c = 1$ mM; ⊠: $c = 7$ mM.

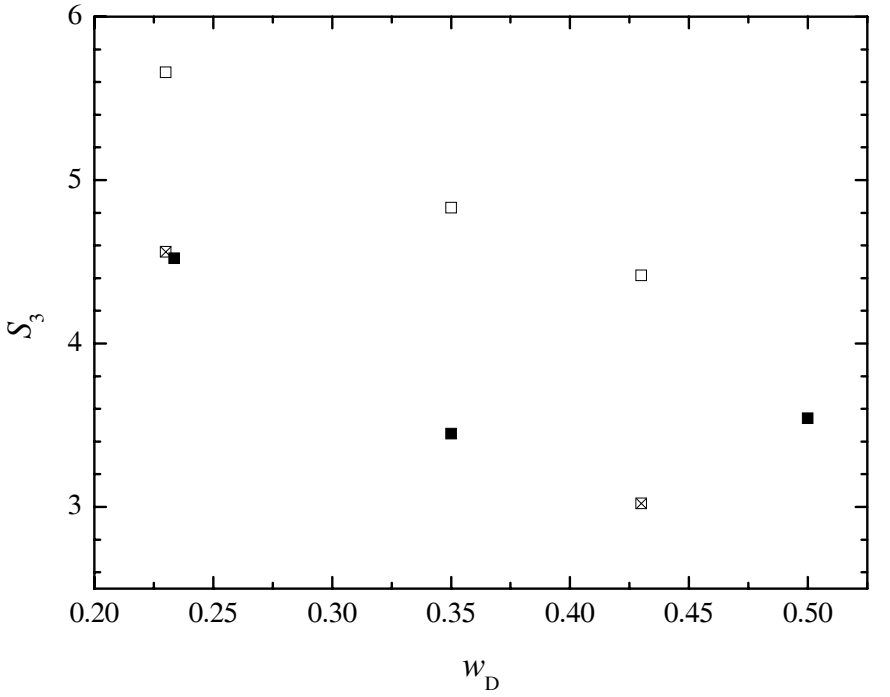

Figure 5.31: Relaxation amplitudes S_3 of DDAB/NaBr(aq)/D microemulsions as a function of the dodecane mass fraction, w_{D}, at $w_{\mathrm{DDAB}}/w_{\mathrm{W}} = 0.358$, co-electrolyte concentration, c, and 25 °C. ■: $c = 0$; □: $c = 1$ mM; ⊠: $c = 7$ mM.

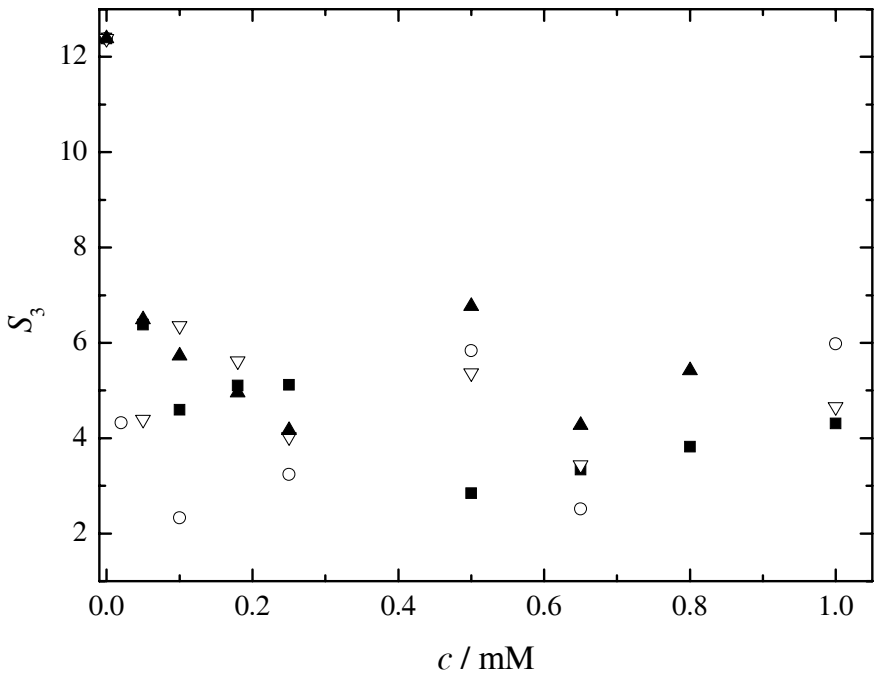

Figure 5.32: Relaxation amplitudes S_3 of DDAB/XBr(aq)/D microemulsions as a function of the co-electrolyte concentration, c, at $w_{\mathrm{DDAB}}/w_{\mathrm{W}} = 0.216$, $w_{\mathrm{D}} = 0.35$ (point $21x$) and 25 ℃. ■: LiBr; ○: NaBr; ▲: CsBr; ▽: $(CH_3)_4NBr$.

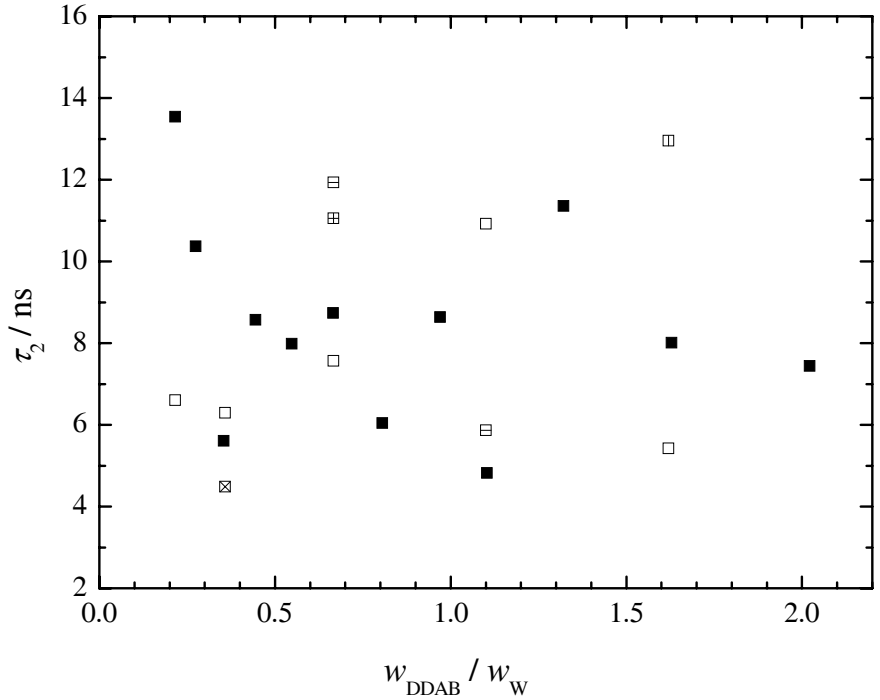

Figure 5.33: Relaxation times τ_2 of DDAB/NaBr(aq)/D microemulsions as a function of the surfactant/water ratio, $w_{\mathrm{DDAB}}/w_{\mathrm{W}}$, at $w_{\mathrm{D}} = 0.35$, co-electrolyte concentration, c, and 25 ℃. ■: $c = 0$; □: $c = 1$ mM; ⊞: $c = 5$ mM; ⊠: $c = 7$ mM; ⊟: $c = 10$ mM; ◫: $c = 25$ mM.

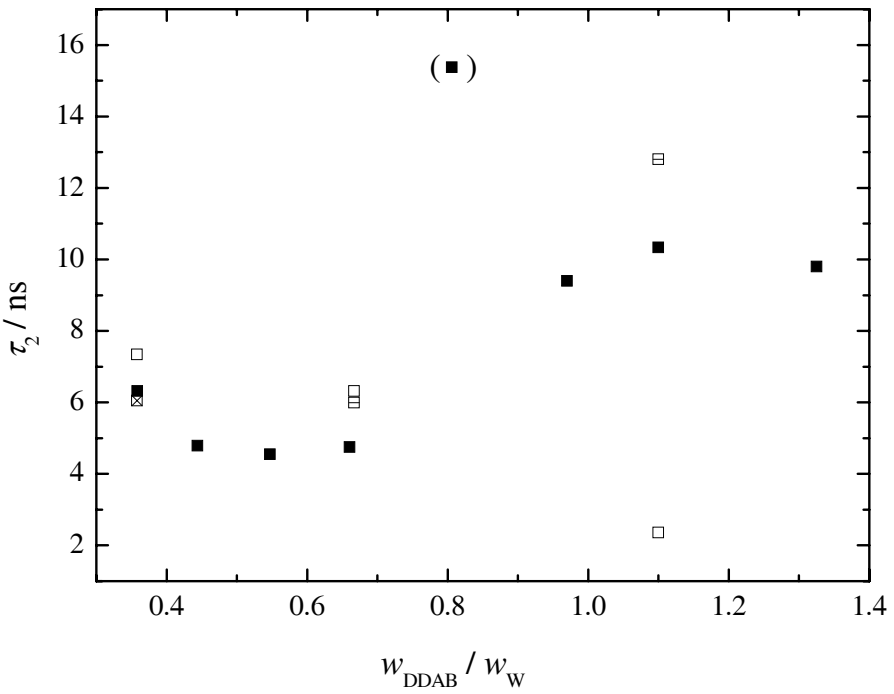

Figure 5.34: Relaxation times τ_2 of DDAB/NaBr(aq)/D microemulsions as a function of the surfactant/water ratio, w_{DDAB}/w_W, at $w_D = 0.23$, co-electrolyte concentration, c, and 25 °C. ■: $c = 0$; □: $c = 1$ mM; ⊠: $c = 7$ mM; ⊟: $c = 10$ mM.

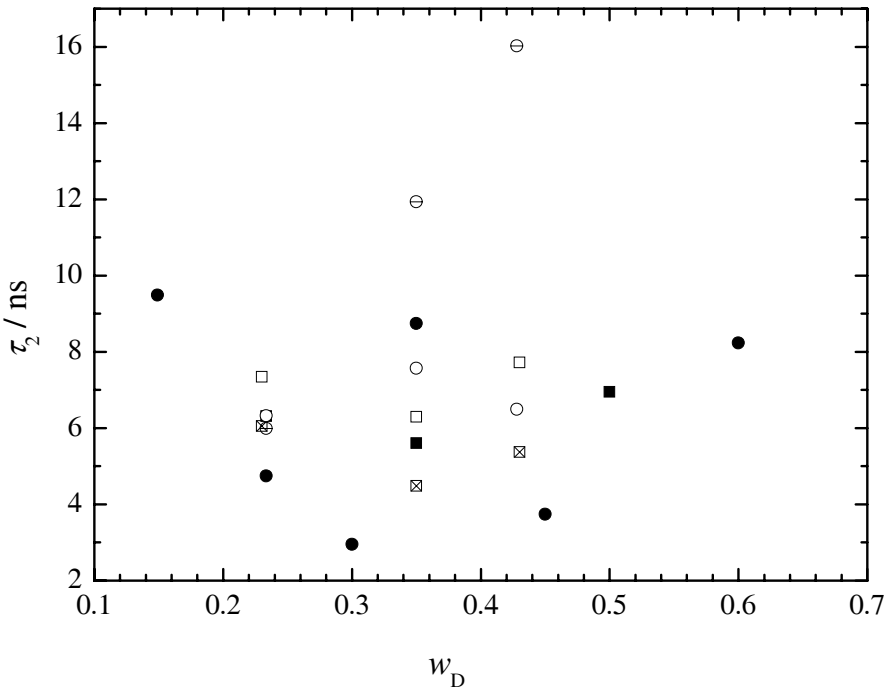

Figure 5.35: Relaxation times τ_2 of DDAB/NaBr(aq)/D microemulsions as a function of the dodecane mass fraction, w_D, at co-electrolyte concentration, c, and 25 °C. Values given in brackets are the surfactant/water ratios, w_{DDAB}/w_W. ■: (0.358), $c = 0$; □: (0.358), $c = 1$ mM; ⊠: (0.358), $c = 7$ mM; •: (0.667), $c = 0$; ○: (0.667), $c = 1$ mM; ⊖: (0.667), $c = 10$ mM.

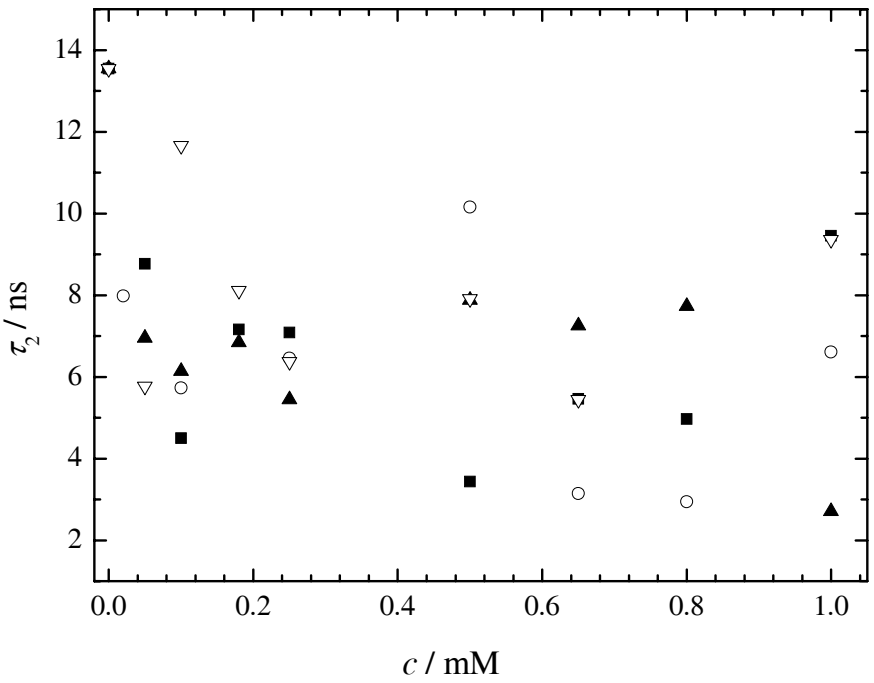

Figure 5.36: Relaxation times τ_2 of DDAB/XBr(aq)/D microemulsions as a function of the co-electrolyte concentration, c, at $w_{\mathrm{DDAB}}/w_{\mathrm{W}} = 0.216$, $w_{\mathrm{D}} = 0.35$ (point $21x$) and 25 ℃. ■: LiBr; ○: NaBr; ▲: CsBr; ▽: $(CH_3)_4NBr$.

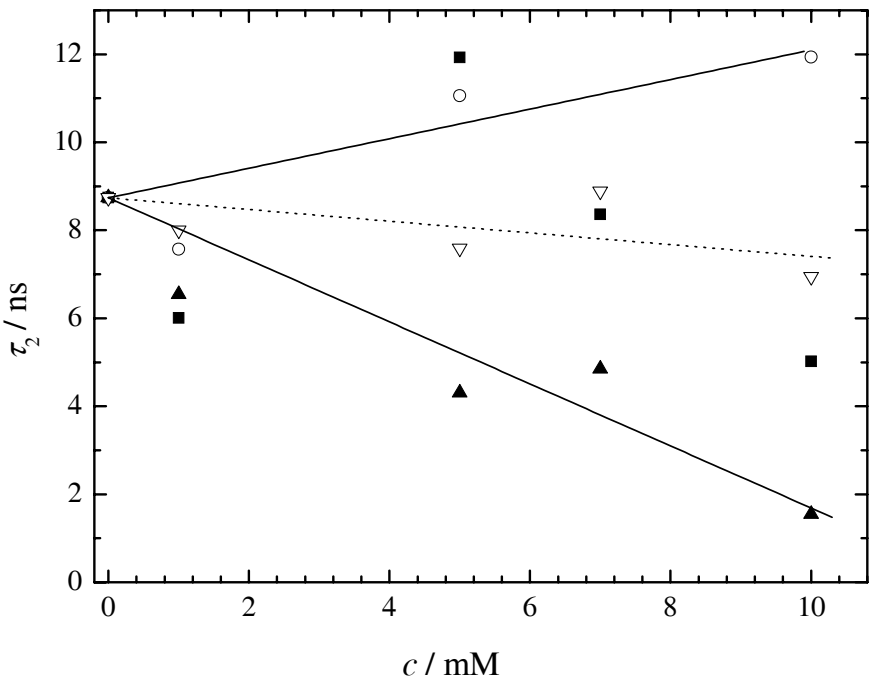

Figure 5.37: Relaxation times τ_2 of DDAB/XBr(aq)/D microemulsions as a function of the co-electrolyte concentration, c, at $w_{\mathrm{DDAB}}/w_{\mathrm{W}} = 0.667$, $w_{\mathrm{D}} = 0.35$ (point $23x$) and 25 ℃. ■: LiBr; ○: NaBr; ▲: CsBr; ▽: $(CH_3)_4NBr$; lines are given as a visual aid.

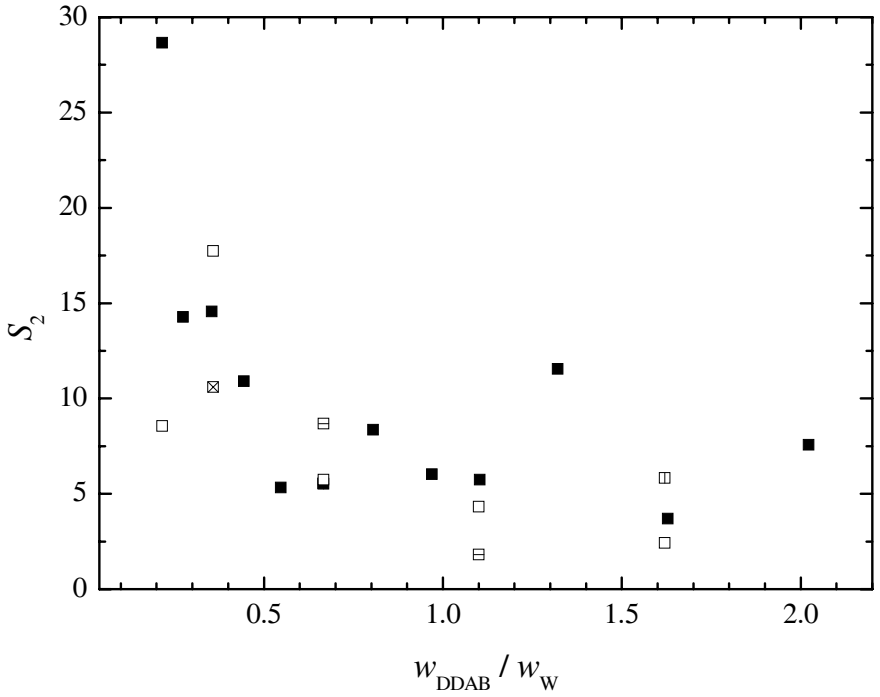

Figure 5.38: Relaxation amplitudes S_2 of DDAB/NaBr(aq)/D microemulsions as a function of the surfactant/water ratio, w_{DDAB}/w_W, at $w_D = 0.35$, co-electrolyte concentration, c, and 25 ℃. ■: $c = 0$; □: $c = 1$ mM; ⊞: $c = 5$ mM; ⊠: $c = 7$ mM; ⊟: $c = 10$ mM; ◫: $c = 25$ mM.

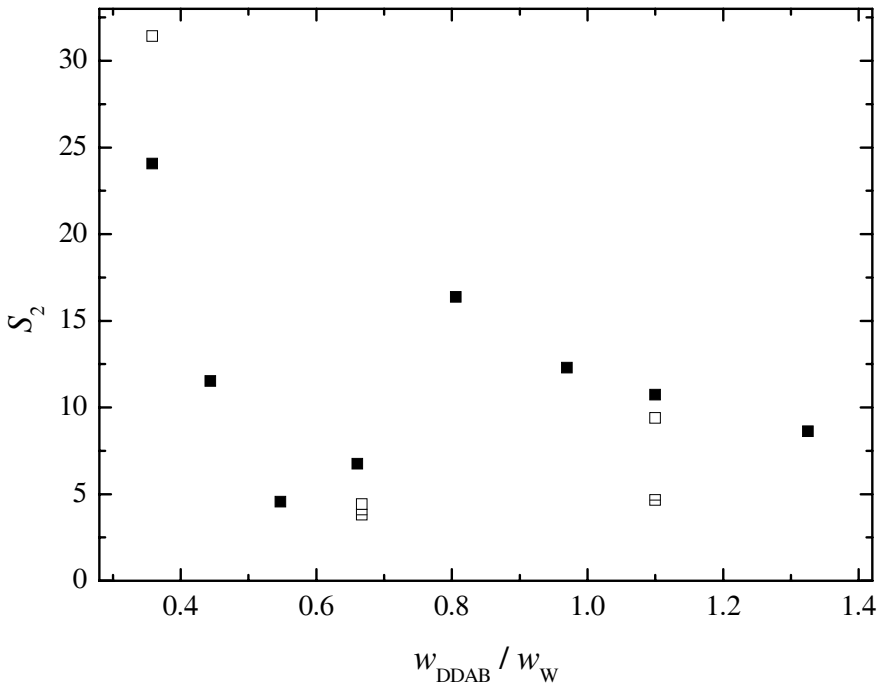

Figure 5.39: Relaxation amplitudes S_2 of DDAB/NaBr(aq)/D microemulsions as a function of the surfactant/water ratio, w_{DDAB}/w_W, at $w_D = 0.23$, co-electrolyte concentration, c, and 25 ℃. ■: $c = 0$; □: $c = 1$ mM; ⊠: $c = 7$ mM; ⊟: $c = 10$ mM.

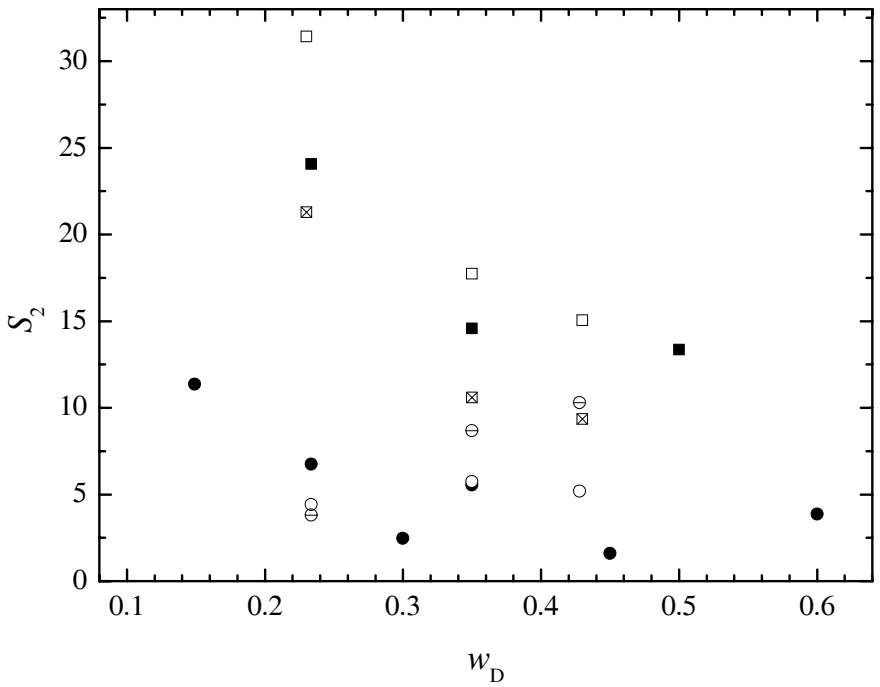

Figure 5.40: Relaxation amplitudes S_2 of DDAB/NaBr(aq)/D microemulsions as a function of the dodecane mass fraction, w_D, at co-electrolyte concentration, c, and 25 °C. Values given in brackets are the surfactant/water ratios, w_{DDAB}/w_W. ■: (0.358), $c = 0$; □: (0.358), $c = 1$ mM; ⊠: (0.358), $c = 7$ mM; •: (0.667), $c = 0$; ○: (0.667), $c = 1$ mM; ⊖: (0.667), $c = 10$ mM.

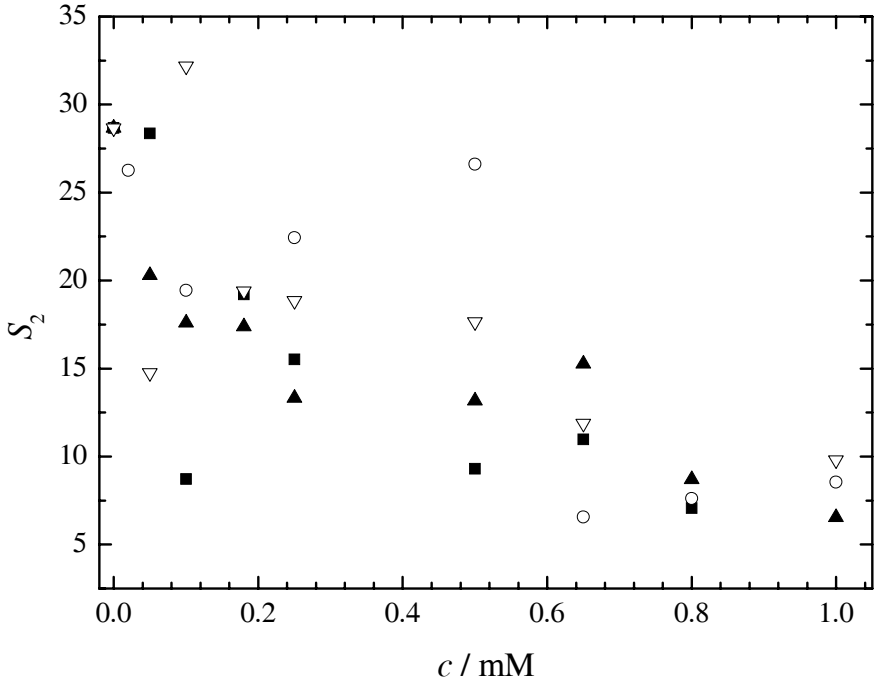

Figure 5.41: Relaxation amplitudes S_2 of DDAB/XBr(aq)/D microemulsions as a function of the co-electrolyte concentration, c, at $w_{DDAB}/w_W = 0.216$, $w_D = 0.35$ (point 21x) and 25 °C. ■: LiBr; ○: NaBr; ▲: CsBr; ▽: $(CH_3)_4NBr$.

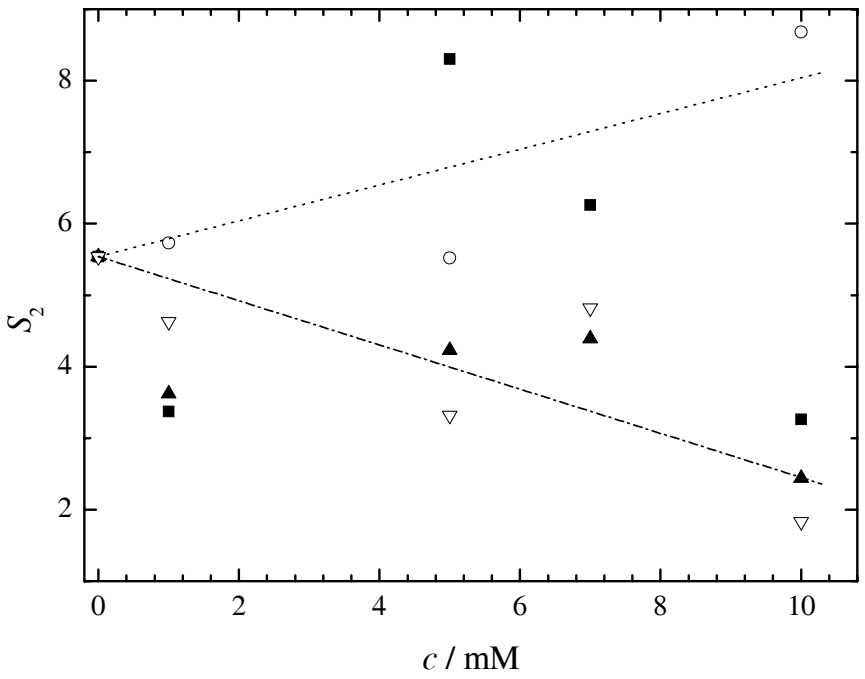

Figure 5.42: Relaxation amplitudes S_2 of DDAB/XBr(aq)/D microemulsions as a function of the co-electrolyte concentration, c, at $w_{\mathrm{DDAB}}/w_{\mathrm{W}} = 0.667$, $w_{\mathrm{D}} = 0.35$ (point $23x$) and 25 °C. ■: LiBr; ○: NaBr; ▲: CsBr; ▽: $(CH_3)_4NBr$; lines are given as a visual aid.

5.2.5 Influence on Transport of Charge Carriers

As outlined in section 4.5.2, process 1 reflects the transport of charge carriers between adjacent water droplets or along a percolation cluster. It has already been mentioned that the quality of the fitting parameters of this process is somewhat deficient, as only a minor part of process 1 is located within the frequency range experimentally accessible to our instruments (Figure 3.6). The S_1 and τ_1 data plotted in Figures 5.43 to 5.52 should therefore be regarded with caution.

However, the decrease in τ_1 and especially S_1 at point $21x$ ($W = 119$, Figures 5.46 and 5.51) is so distinctive that it is unlikely to arise solely from any inadequacies in the data. Figure 5.51 shows that S_1 almost vanishes for a co-electrolyte concentration of $c = 1$ mM. This dramatic decrease can be rationalised within the framework of our previous interpretation of the co-ion effect. On the basis of the high-frequency relaxation data, co-ion addition reduces the connectivity between the water droplets (see section 5.2.2), consistent with other findings.[149,176] Consequently, the distances between adjacent water droplets increase, particularly in the water-rich parts of L_2, thus complicating the transport of charge carriers, which is reflected in process 1.

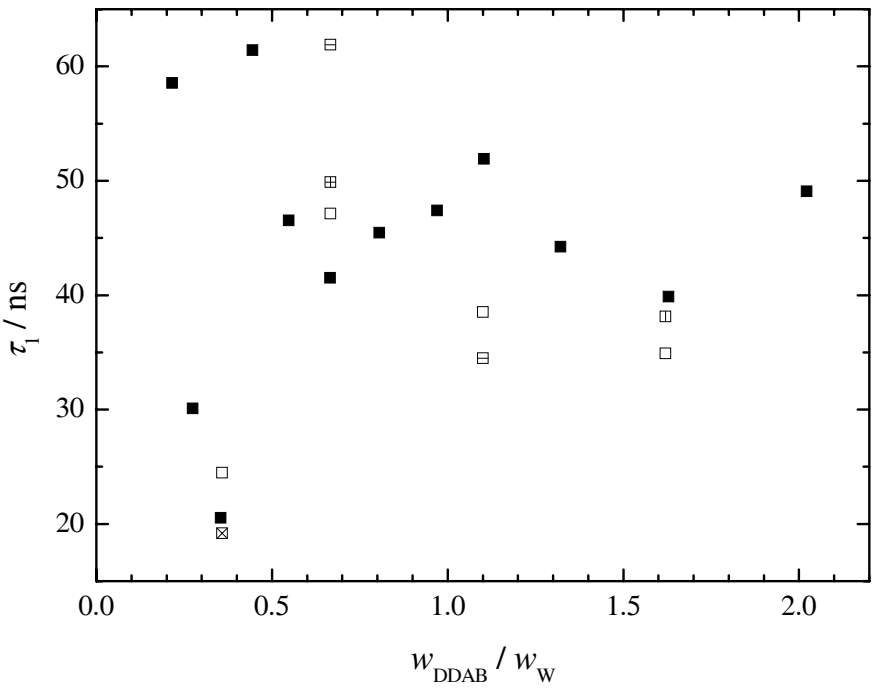

Figure 5.43: Relaxation times τ_1 of DDAB/NaBr(aq)/D microemulsions as a function of the surfactant/water ratio, w_{DDAB}/w_W, at $w_D = 0.35$, co-electrolyte concentration, c, and 25 °C. ■: $c = 0$; □: $c = 1$ mM; ⊞: $c = 5$ mM; ⊠: $c = 7$ mM; ⊟: $c = 10$ mM; ◫: $c = 25$ mM.

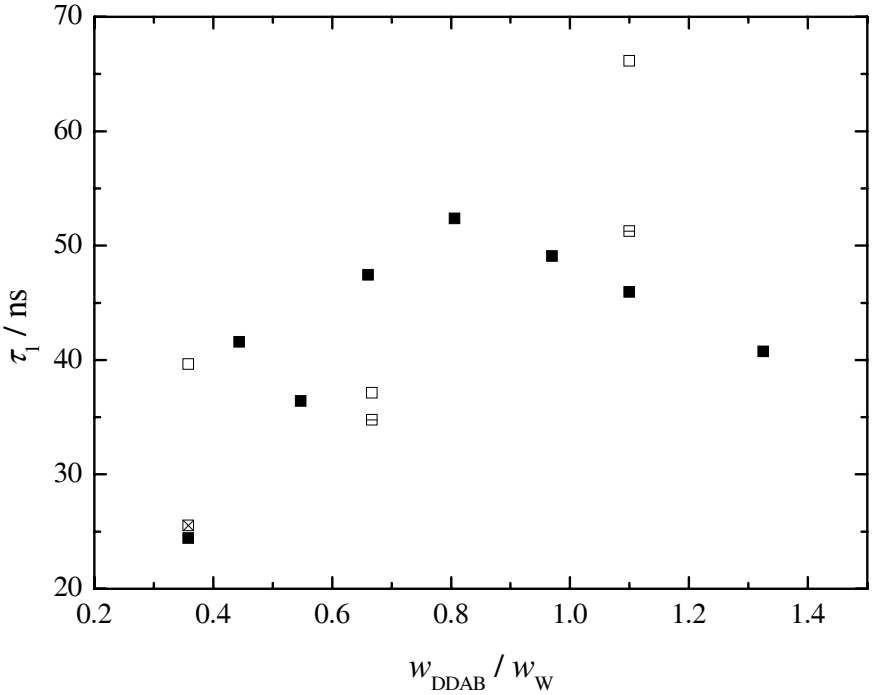

Figure 5.44: Relaxation times τ_1 of DDAB/NaBr(aq)/D microemulsions as a function of the surfactant/water ratio, w_{DDAB}/w_W, at $w_D = 0.23$, co-electrolyte concentration, c, and 25 °C. ■: $c = 0$; □: $c = 1$ mM; ⊠: $c = 7$ mM; ⊟: $c = 10$ mM.

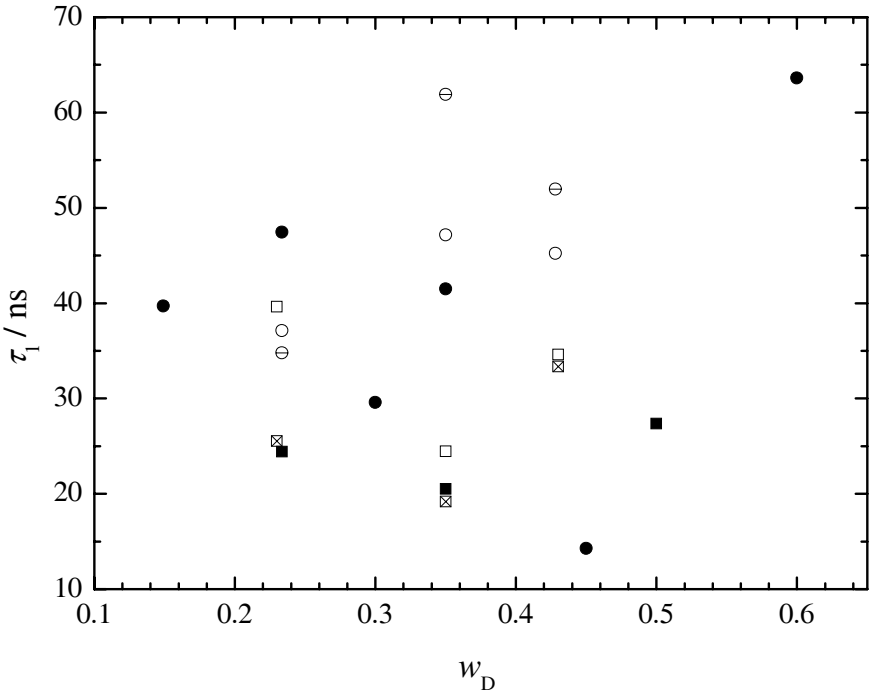

Figure 5.45: Relaxation times τ_1 of DDAB/NaBr(aq)/D microemulsions as a function of the dodecane mass fraction, w_D, at co-electrolyte concentration, c, and 25 °C. Values given in brackets are the surfactant/water ratios, w_{DDAB}/w_W. ■: (0.358), $c = 0$; □: (0.358), $c = 1$ mM; ⊠: (0.358), $c = 7$ mM; •: (0.667), $c = 0$; ○: (0.667), $c = 1$ mM; ⊖: (0.667), $c = 10$ mM.

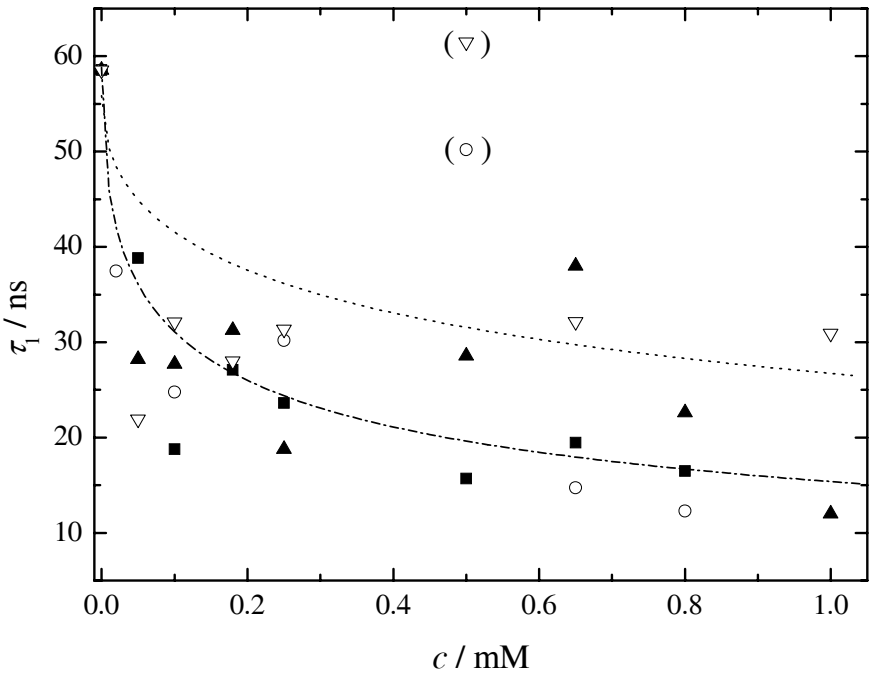

Figure 5.46: Relaxation times τ_1 of DDAB/XBr(aq)/D microemulsions as a function of the co-electrolyte concentration, c, at $w_{DDAB}/w_W = 0.216$, $w_D = 0.35$ (point 21x) and 25 °C. ■: LiBr; ○: NaBr; ▲: CsBr; ▽: $(CH_3)_4NBr$; lines are given as a visual aid.

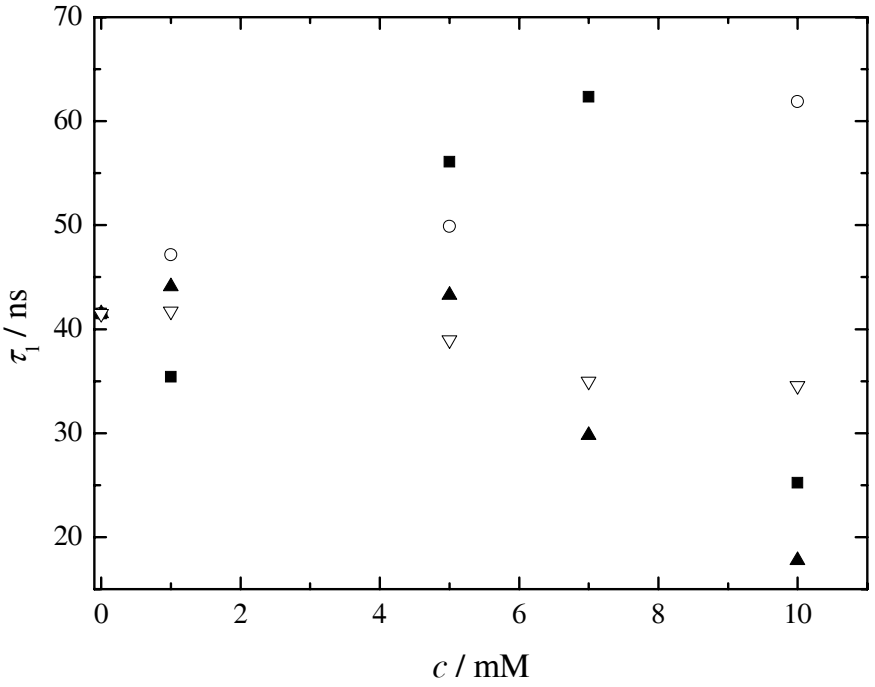

Figure 5.47: Relaxation times τ_1 of DDAB/XBr(aq)/D microemulsions as a function of the co-electrolyte concentration, c, at $w_{\mathrm{DDAB}}/w_{\mathrm{W}} = 0.667$, $w_{\mathrm{D}} = 0.35$ (point $23x$) and 25 ℃. ■: LiBr; ○: NaBr; ▲: CsBr; ▽: $(CH_3)_4NBr$.

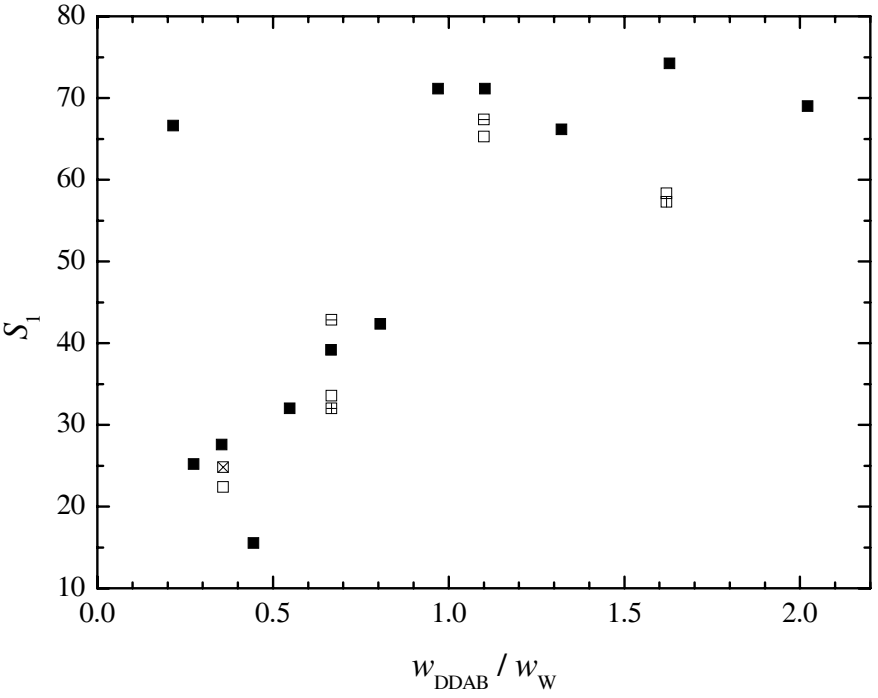

Figure 5.48: Relaxation amplitudes S_1 of DDAB/NaBr(aq)/D microemulsions as a function of the surfactant/water ratio, $w_{\mathrm{DDAB}}/w_{\mathrm{W}}$, at $w_{\mathrm{D}} = 0.35$, co-electrolyte concentration, c, and 25 ℃. ■: $c = 0$; □: $c = 1$ mM; ⊞: $c = 5$ mM; ⊠: $c = 7$ mM; ⊟: $c = 10$ mM; ◫: $c = 25$ mM.

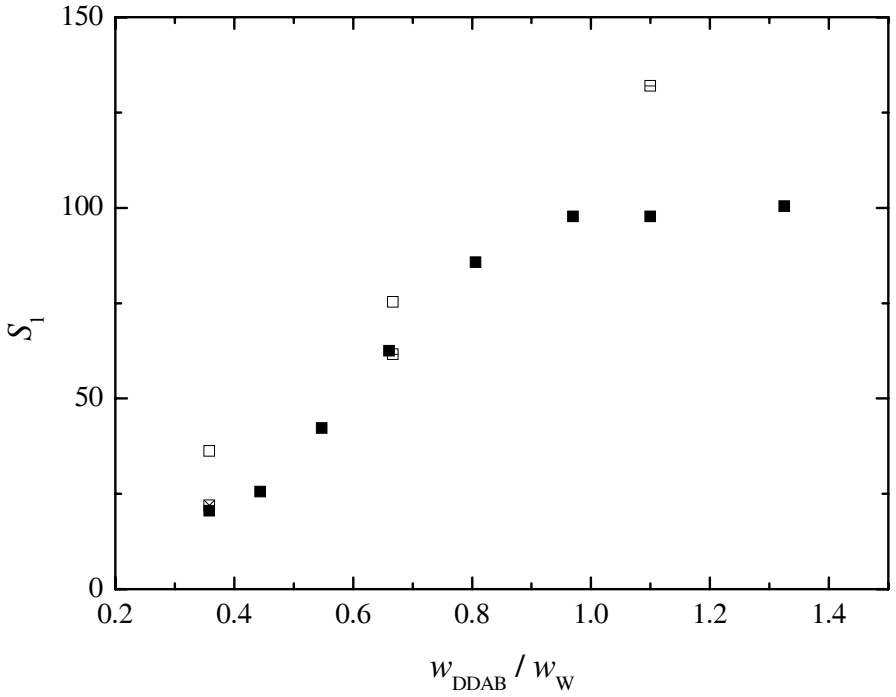

Figure 5.49: Relaxation amplitudes S_1 of DDAB/NaBr(aq)/D microemulsions as a function of the surfactant/water ratio, w_{DDAB}/w_W, at $w_D = 0.23$, co-electrolyte concentration, c, and 25 °C. ■: $c = 0$; □: $c = 1$ mM; ⊠: $c = 7$ mM; ⊟: $c = 10$ mM.

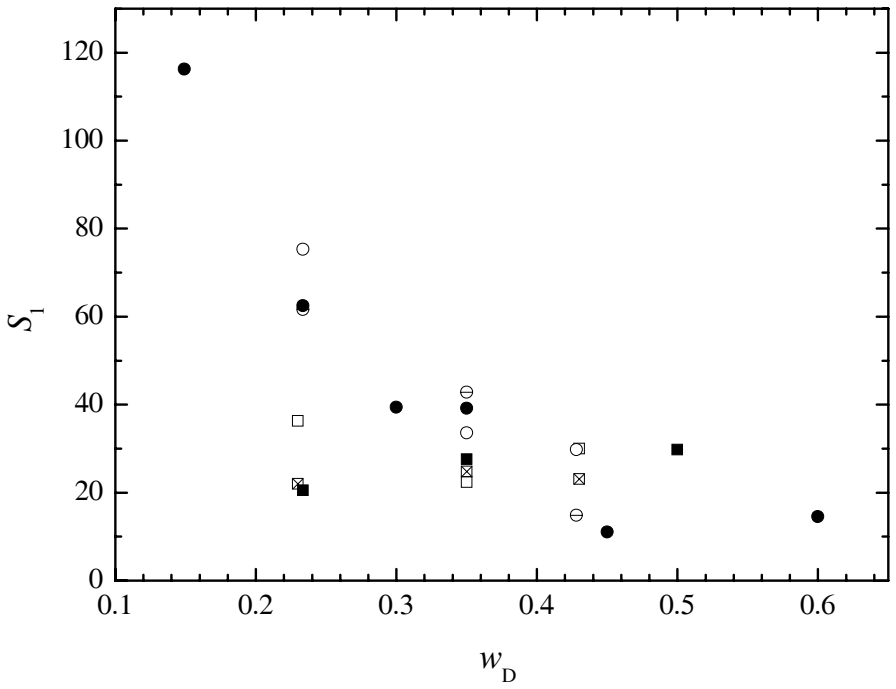

Figure 5.50: Relaxation amplitudes S_1 of DDAB/NaBr(aq)/D microemulsions as a function of the dodecane mass fraction, w_D, at co-electrolyte concentration, c, and 25 °C. Values given in brackets are the surfactant/water ratios, w_{DDAB}/w_W. ■: (0.358), $c = 0$; □: (0.358), $c = 1$ mM; ⊠: (0.358), $c = 7$ mM; •: (0.667), $c = 0$; ○: (0.667), $c = 1$ mM; ⊖: (0.667), $c = 10$ mM.

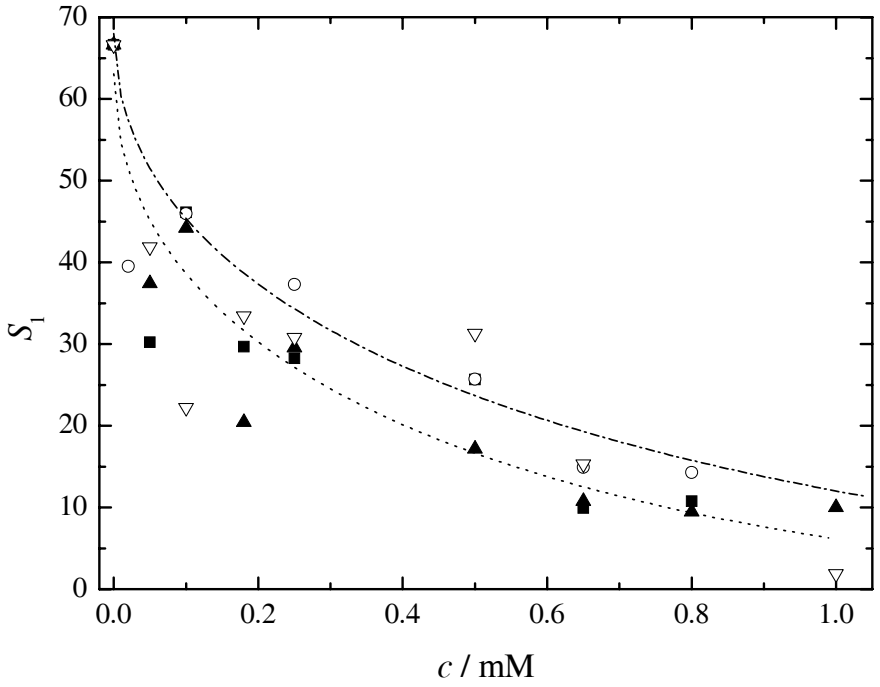

Figure 5.51: Relaxation amplitudes S_1 of DDAB/XBr(aq)/D microemulsions as a function of the co-electrolyte concentration, c, at $w_{\mathrm{DDAB}}/w_{\mathrm{W}} = 0.216$, $w_{\mathrm{D}} = 0.35$ (point 21x) and 25 ℃. ■: LiBr; ○: NaBr; ▲: CsBr; ▽: $(CH_3)_4NBr$; lines are given as a visual aid.

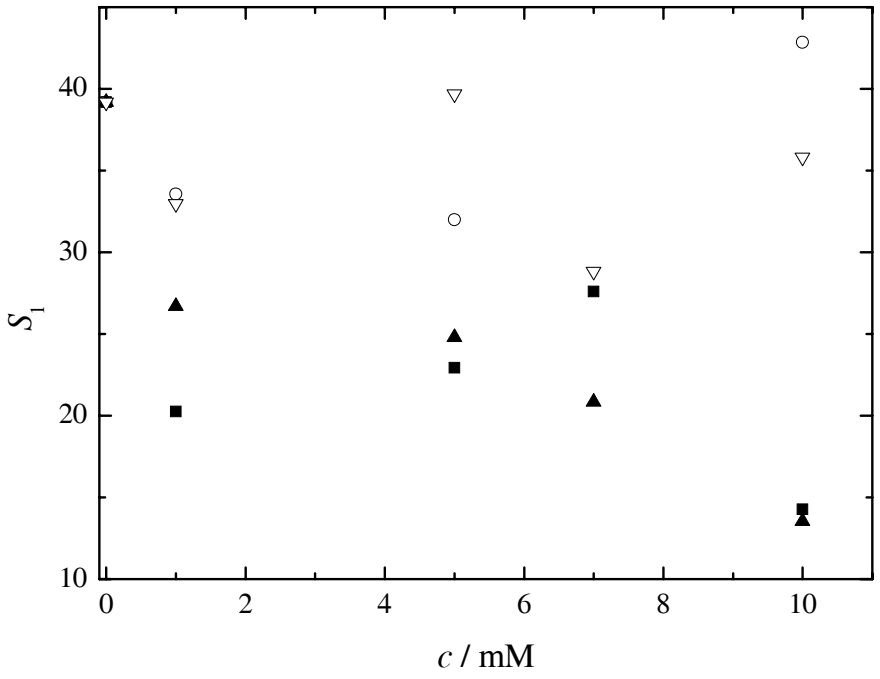

Figure 5.52: Relaxation amplitudes S_1 of DDAB/XBr(aq)/D microemulsions as a function of the co-electrolyte concentration, c, at $w_{\mathrm{DDAB}}/w_{\mathrm{W}} = 0.667$, $w_{\mathrm{D}} = 0.35$ (point 23x) and 25 ℃. ■: LiBr; ○: NaBr; ▲: CsBr; ▽: $(CH_3)_4NBr$.

5.2.6 Summary

Analysis of the present dielectric spectra of DDAB/XBr(aq)/D microemulsions leads to the following conclusions concerning co-ion effects.

- The co-ion effect is only important for the water-rich parts of the L_2 phase. For the largest water/surfactant ratio investigated in this work, $W = 119$, replacing water by aqueous solutions of LiBr, NaBr, CsBr or $(CH_3)_4NBr$ of $c \leq 1$ mM leads to a significant decrease in both ε' and ε''. This is an extraordinary result given that dielectric spectra of aqueous solutions at such concentrations are indistinguishable from that of pure water. In contrast, for the lowest water/surfactant ratios studied in this work ($W \lesssim 16$) a co-ion effect can hardly be detected.

- The co-ion effect is decreasing *gradually* with decreasing water/surfactant ratio. There are no indications of a 'threshold' exhibiting a strong variation in the co-ion sensitivity of the dielectric spectra. This behaviour appears to be analogous to the gradual increase in conductivity with decreasing water/surfactant ratio, which reflects the increasing percolation of the system DDAB/W/D. Hence, it may be concluded that a decrease of the co-ion effect is linked to an increase in percolation.

- Co-ions are located near the interface of the W/O droplets and modify the interfacial geometry. All interfacial relaxation processes, such as counterion diffusion or surfactant ion-pair rotations, are influenced by co-ion addition.

- Co-ion addition provokes a loss in connectivity between the W/O droplets and a transition from ellipsoidal to more spherical droplets.

- The variation of some (but not all) of the relaxation parameters with addition of different co-ions indicates that ion-specific effects may be observable.

Summary and Conclusions

Motivation

Microemulsions play a considerable role in current research activities – from technical applications to the elucidation of biological systems. In the past years numerous investigations led to a better understanding of this field; however, some essential aspects are still unexplained.

It is the aim of this work to apply dielectric relaxation spectroscopy (DRS) to ionic microemulsion systems. Unlike classical spectroscopic techniques (*e.g.* IR, Raman or NMR spectroscopy), which basically are only able to monitor molecular dynamics and short-range interactions, DRS is sensitive to collective modes of hydrogen bond systems and the reorientation of transient dipolar aggregates; thus, this method can provide valuable information about the dynamics of cooperative processes and about the structural consequences arising from that. DRS appears to be particularly suitable for the investigation of microemulsions, as it already revealed some characteristic relaxation processes caused by hydrate water molecules surrounding hydrophobic[43,190] and hydrophilic[185] ions and micelles of various surfactants.[7,8,88] However, only few DRS studies on ionic microemulsion systems have been performed and most of them have been conducted in the 1980s or early 1990s, in a time when this method had to struggle with considerable experimental inadequacies (see *e.g.* refs.[23,32,54,60,66,78,109,132,153,157,159,175,188]). Generally speaking, only a very limited number of data points could be recorded, which made it difficult to find a meaningful interpretation. In particular, those early studies were always limited to a frequency range of $\nu \lesssim 20$ GHz, which means that the water relaxation area could not be analyzed appropriately;[201] however, the behaviour of the water network confined in a microemulsion droplet is one of the most exciting features these systems exhibit.

Therefore, this work wants to harness the potentials state-of-the-art DRS instrumentation nowadays provides for a thorough investigation of ionic microemulsions over a wide range of frequencies ($0.005 \leq \nu/\mathrm{GHz} \leq 89$), putting a special emphasis on the water relaxation processes. Microemulsions consisting of didodecyldimethylammonium bromide (DDAB), water (W) and *n*-dodecane (D) were chosen for this study, as this system exhibits a very unusual effect: when pure water is replaced by extremely weakly concentrated aqueous solutions of sodium bromide or sodium sulfate ($1 \lesssim c/\mathrm{mM} \lesssim 27$ for NaBr) a dramatic shrinking of the DDAB/W/D microemulsion phase, L_2, takes place.[175] The reason for this *co-ion effect* is still obscure; as the bromide concentration in the solution remains virtually

constant at such a tiny electrolyte addition, it is obviously due to a cationic effect. Elucidating this phenomenon would certainly mean a major step towards an understanding of the co-ion influence on ionic microemulsions and of polyelectrolyte solutions in general.

Furthermore, DDAB/W/D appears to be particularly suitable for a detailed investigation, as is a relatively simply-structured microemulsion system. Since a co-surfactant is not required, it consists of only three components; additionally, the surfactant DDAB is known to be located at the water/oil interface, as it is very sparingly soluble in both water and dodecane. A water-in-oil (W/O) microemulsion is formed over wide areas of the DDAB/W/D phase diagram.

Data Acquisition

To study the co-ion effect on DDAB/W/D microemulsions, the following experimental strategy was pursued. First, the 'salt-free' system DDAB/W/D was thoroughly investigated over its entire microemulsion phase, L_2. As a next step, exploration measurements of DDAB/NaBr(aq)/D microemulsions were performed over large parts of L_2 to identify appropriate points for a detailed investigation of the co-ion effect. Finally, two of these points were selected, and extended concentration series of the systems DDAB/LiBr(aq)/D, DDAB/NaBr(aq)/D, DDAB/CsBr(aq)/D and DDAB/$(CH_3)_4$NBr(aq)/D were recorded.

All dielectric spectra were measured at standard temperature (T = 298.15 K) using different experimental techniques for different frequency ranges:

- a time-domain reflectometer (TDR, Regensburg University) for $0.005 \lesssim \nu/\mathrm{GHz} \lesssim 0.2$
- a vector network analyzer (VNA, Murdoch University, Perth, Australia) for $0.2 \lesssim \nu/\mathrm{GHz} \leq 20$
- two waveguide interferometers (IFM, Regensburg University) for $27 \leq \nu/\mathrm{GHz} \leq 89$

Additionally, FTIR spectra were recorded for a selection of DDAB/W/D and some of the DDAB/NaBr(aq)/D samples, density data were measured for most samples, and conductivity data could be obtained from the low-frequency TDR results.

Results

All dielectric spectra of the system DDAB/W/D could be described best using a superposition of six or five Debye equations (6D/5D model), depending on the W/DDAB ratio. The following process assignment could be established.

- The relaxation times of process 1 ($\tau_1 \approx 40$ ns) are in a range that is typical of the transport of charge carriers between adjacent water droplets or along a percolation cluster.[85,122,199] A similar relaxation has been observed by Schrödle *et al.* for non-ionic microemulsions.[169]

- Relaxation processes 2 and 3 ($\tau_2 \approx 8$ ns, $\tau_3 \approx 800$ ps) can be both ascribed to interfacial polarisation effects. According to a model proposed by Kozlovich *et al.* these processes reflect the surface counterion diffusion in the outer Helmholtz plane (OHP) and the radial counterion diffusion in the diffuse double layer, respectively.[132] Process 2 could be modelled on the basis of the Maxwell-Wagner approach assuming ellipsoidal water particles in oil. Process 3 is gradually decreasing with decreasing W/DDAB ratio until it becomes too small to be detected at $W \approx 40$, thus reducing the 6D model to a 5D model.

- Process 4 ($60 \lesssim \tau_4/\text{ps} \lesssim 280$) is a reflexion of uncorrelated movements of ionic species present in the microemulsion. This relaxation may possibly be ascribed to the rotation of DDAB contact ion pairs (CIPs), as the τ_4 values compare favourably with the relaxation times predicted by the Stokes-Debye-Einstein equation. In addition to this, Camardo *et al.* detected a similar process for AOT/H_2O/oil microemulsions, which they described as an ion-pairing process.[45] However, it remains unclear how surfactant ion pairs should be able to rotate within the geometrical confinement of the W/O interface. Alternatively, process 4 may be ascribed to uncorrelated counterion rearrangements within the aqueous subphase, thus giving rise to a small total dipole moment of the water droplet.

- Both processes 5 and 6 ($\tau_5 \approx 12$ ps, $\tau_6 \approx 3$ ps) are on a timescale which is typical of the cooperative relaxation of a water network. However, their relaxation times deviate considerably from each other and from the bulk-water value, 8.32 ps.[168] A comparison of the developing of the relaxation parameters as a function of the W/DDAB ratio with that of the infrared data leads to the conclusion that process 5 reflects the water network present in the core of the aqueous phase (*core water*), whereas process 6 can be ascribed to water near the interface (*interfacial water*). Because of the extremely high Br^- counterion concentration near the interface,[74] there is a scarcity of water in this area so that some H_2O-H_2O bonds must be substituted by the much weaker H_2O-Br^- bonds, which explains the short relaxation times τ_6 of this process. A similar phenomenon has been observed for the water network in H_2O/dioxane mixtures.[170,171]

It is important to note that all relaxation parameters, but also the density and the conductivity data, show smooth variations with varying W/DDAB ratio. No evidence could be found for a sudden percolation 'threshold', as proposed by Barnes *et al.*[11]

Exploration measurements of the system DDAB/NaBr(aq)/D revealed that the sensitivity of the dielectric data towards the addition of the co-ion Na^+ is gradually decreasing with decreasing W/DDAB ratio. As this developing was found to be analogous to that of the conductivity data, it was concluded that the co-ion effect is decreasing with increasing percolation. As for the 'salt-free' spectra, a 6D/5D model yields the best fitting results.

A detailed investigation of the effect exerted by the co-ions Li^+, Na^+, Cs^+ and $(CH_3)_4N^+$ on the dielectric relaxation processes led to the following results.

- At high W/DDAB ratios, both the amplitude S_1 and the relaxation time τ_1 decrease upon co-ion addition; this finding suggests that co-ions reduce the connectivity between the water droplets.

- The relaxation parameters of processes 2 and 3, which are both due to interfacial polarisation, are significantly influenced by the addition of co-ions. Hence, it appears plausible to conclude that co-ions are located near the interface and modify its geometrical structure, as proposed by Ninham *et al.*[134] For $W = 39$, an ion-specific effect may be observable.

- Also the relaxation parameters of process 4 are considerably influenced by co-ion addition. As both possible assignments, the rotation of DDAB ion pairs and an uncorrelated counterion movement, are processes happening near the interface, this finding confirms the conclusion drawn from processes 2 and 3.

- As the relaxation times τ_5 and τ_6 are hardly affected by the addition of co-ions, it becomes evident that the water network is not significantly influenced by the co-ion effect. The Kirkwood factor of the core water, g_5, is decreasing upon co-ion addition, which can be interpreted in terms of a transition from ellipsoidal to rather spherically-shaped water droplets, consistent with the loss of connectivity between the droplets outlined above. In contrast, the Kirkwood factor of the interfacial water, g_6, is scattering, which again indicates that the interface is modified by the addition of co-ions.

Conclusions

Putting all these pieces of information together, the following overall view of DDAB/W/D microemulsions arises.

- Except for very high D fractions, which have not been investigated in this study, DDAB/W/D microemulsion systems appear to be close to the percolation point over the entire L_2 phase. With decreasing W/DDAB ratio, a gradual increase in percolation can be observed; however, no sudden changes could be detected.

- The water droplets or their aggregates present in DDAB/W/D microemulsions are of spheroidal rather than of spherical shape.

- The large majority of the Br^- counterions is located near the interface, giving rise to extraordinarily high interfacial electrolyte concentrations. Two interfacial counterion polarisation processes could be detected.

- The dynamics of the water network confined in a microemulsion droplet differ significantly from those of bulk water. Core water exhibits a strengthened network, probably because of the unique geometrical environment. In contrast, the interfacial water network is considerably weakened, which is due to the extremely high Br^- concentrations near the interface.

- One relaxation process may be interpreted in terms of the rotational movement of surfactant ion pairs. This would imply that the interface is less rigid than previously assumed. However, the underlying relaxation may also be due to the uncorrelated movement of Br^- ions within the aqueous subphase.

- The co-ion effect previously observed for NaBr and Na_2SO_4 [175] is also present for LiBr, CsBr and $(CH_3)_4NBr$; this effect decreases gradually with increasing percolation.

- Co-ions are located near the interface and modify its geometrical structure. Furthermore, they evoke a loss in connectivity between the water droplets, giving rise to a transition from ellipsoidal to rather spherical particles.

- Some (but not all) of the relaxation parameters indicate that ion-specific effects may be observable.

Prospects for the Future

As has been highlighted in this work, dielectric relaxation spectroscopy is a very efficient experimental tool for the investigation of microemulsions, a veritable treasure trove of information. However, in order to benefit from all the merits this method can provide an extension of the frequency range currently accessible in our laboratories would be more than desirable. As can be seen from the present spectra, frequencies well below 5 MHz should be investigated so that process 1 can be resolved adequately. Also the high-frequency limit should be extended far beyond 89 GHz to allow a complete coverage of process 6.

Interpretation of the water relaxation processes has been complicated by the fact that the Kirkwood factors, g_5 and g_6, of the water network present in a W/O microemulsion droplet are unknown. A lot of additional information could be extracted from the dielectric spectra if these values could be determined, *i.e.* if a deeper insight could be gained into the relative alignment of water dipoles confined in a microemulsion droplet. Simulation studies certainly have the potential to make a decisive contribution to elucidate this question.

List of Figures

List of Tables

Bibliography

[1] M. Allen, D. F. Evans, D. J. Mitchell and B. W. Ninham
'Interfacial Tension of Ionic Microemulsions'
J. Phys. Chem. **91**, 2320-2324 (1987)

[2] A. P. Altshuller
'The Shapes of Particles from Dielectric Constant Studies of Suspensions'
J. Phys. Chem. **58**, 544-547 (1954)

[3] L. R. Angel, D. F. Evans and B. W. Ninham
'Three-Component Ionic Microemulsions'
J. Phys. Chem. **87**, 538-540 (1983)

[4] K. Asami
'Characterization of Heterogeneous Systems by Dielectric Spectroscopy'
Prog. Polym. Sci. **27**, 1617-1659 (2002)

[5] C. Baar
'Dielektrische Relaxation von Natriumchlorid-Lösungen in Formamid und N-Methylformamid'
Diploma Thesis, Regensburg University, Regensburg (1997)

[6] C. Baar
'Dielektrische Relaxation kationischer Tenside. Alkalitrimethylammoniumhalogenide in wässriger Lösung'
PhD Thesis, Regensburg University, Regensburg (2000)

[7] C. Baar, R. Buchner and W. Kunz
'Dielectric Relaxation of Cationic Surfactants in Aqueous Solution.
1. Solvent Relaxation'
J. Phys. Chem. B, **105**, 2906-2913 (2001)

[8] C. Baar, R. Buchner and W. Kunz
'Dielectric Relaxation of Cationic Surfactants in Aqueous Solution.
2. Solute Relaxation'
J. Phys. Chem. B, **105**, 2914-2922 (2001)

[9] A. J. Bard and L. R. Faulkner
'Electrochemical Methods'
Wiley, New York (1980)

[10] I. S. Barnes, S. T. Hyde, B. W. Ninham, P.-J. Derian, M. Drifford, G. G. Warr and T. N. Zemb
'The Disordered Open Connected Model of Microemulsions'
Progr. Colloid Polym. Sci. **76**, 90-95 (1988)

[11] I. S. Barnes, S. T. Hyde, B. W. Ninham, P.-J. Derian, M. Drifford and T. N. Zemb
'Small-Angle X-ray Scattering from Ternary Microemulsions Determines Microstructure'
J. Phys. Chem. **92**, 2286-2293 (1988)

[12] J. Barthel
'Abschlußbericht zum Forschungsvorhaben BA 223/20-1'
Regensburg University (1992)

[13] J. Barthel, K. Bachhuber, R. Buchner, H. Hetzenauer and M. Kleebauer
'A Computer-Controlled System of Transmission Lines for the Determination of the Complex Permittivity of Lossy Liquids between 8.5 and 90 GHz'
Ber. Bunsenges. Phys. Chem. **95**, 853-859 (1991)

[14] J. Barthel and R. Buchner, in: R. A. Meyers (ed.)
'Encyclopedia of Physical Science and Technology, 1990 Yearbook'
Academic Press, New York (1990)

[15] J. Barthel and R. Buchner
'Dielectric Permittivity and Relaxation of Electrolyte Solutions and Their Solvents'
Chem. Soc. Rev. **21**, 263-270 (1992)

[16] J. Barthel, R. Buchner, P.-N. Eberspächer, M. Münsterer, J. Stauber and B. Wurm
'Dielectric Relaxation Spectroscopy of Electrolyte Solutions. Recent Developments and Prospects'
J. Mol. Liq. **78**, 83-109 (1998)

[17] J. Barthel, R. Buchner and H. Steger
'Dielectric Properties of Liquid Mixtures'
Wiss. Zeitschr. THLM **31**, 409-423 (1989)

[18] J. Barthel, R. Buchner and E. Wismeth
'FTIR Spectroscopy of Ion Solvation of $LiClO_4$ and LiSCN in Acetonitrile, Benzonitrile, and Propylene Carbonate'
J. Solution Chem. **29**, 937-954 (2000)

[19] J. Barthel, H. Hetzenauer and R. Buchner
'Dielectric Relaxation of Aqueous Electrolyte Solutions. I. Solvent Relaxation of 1:2, 2:1, and 2:2 Electrolyte Solutions'
Ber. Bunsenges. Phys. Chem. **96**, 988-997 (1992)

[20] J. Barthel, H. Hetzenauer and R. Buchner
'Dielectric Relaxation of Aqueous Electrolyte Solutions. II. Ion-Pair Relaxation of 1:2, 2:1, and 2:2 Electrolytes'
Ber. Bunsenges. Phys. Chem. **96**, 1424-1432 (1992)

[21] D. Bertolini, M. Cassettari, G. Salvetti, E. Tombari and S. Veronesi
'Time Domain Reflectometry to Study the Dielectric Properties of Liquids: Some Problems and Solutions'
Rev. Sci. Instrum. **62**, 450-456 (1991)

[22] P. R. Bevington
'Data Reduction and Error Analysis for the Physical Sciences'
McGraw-Hill, New York (1969)

[23] S. Bhattacharya, J. P. Stokes, M. W. Kim and J. S. Huang
'Percolation in an Oil-Continuous Microemulsion'
Phys. Rev. Lett. **55**, 1884-1887 (1985)

[24] J. R. Birch and T. J. Parker
'Dispersive Fourier Transform Spectrometry'
in: K. J. Button (ed.)
'Infrared and Millimeter Waves. Vol. 2. Instrumentation.'
Academic Press, New York (1979)

[25] D. V. Blackham and R. D. Pollard
'An Improved Technique for Permittivity Measurements Using a Coaxial Probe'
IEEE Trans. Instr. Meas. **46**, 1093-1099 (1997)

[26] F. D. Blum, S. Pickup, B. Ninham, S. J. Chen and D. F. Evans
'Structure and Dynamics in Three-Component Microemulsions'
J. Phys. Chem. **89**, 711-713 (1985)

[27] C. J. F. Böttcher and P. Bordewijk
'Theory of Electric Polarisation', Vols. 1 and 2
Elsevier, Amsterdam (1978)

[28] C. Boned and J. Peyrelasse
'Etude de la permittivité complexe d'ellipsoides disperses dans un milieu continu. Analyses théorique et numérique'
Colloid Polymer Sci. **261**, 600-612 (1983)

[29] C. Boned and J. Peyrelasse
'Percolation in Microemulsions'
J. Surface Sci. Technol. **7**, 1-31 (1991)

[30] C. Boned, J. Peyrelasse and Z. Saidi
'Dynamic Percolation of Spheres in a Continuum: The Case of Microemulsions'
Phys. Rev. E **47**, 468-478 (1993)

[31] F. Bordi, C. Cametti, P. Codastefano, F. Sciortino, P. Tartaglia and J. Rouch
'Dielectric Properties of Highly Concentrated Water-in-Oil Microemulsions'
Progr. Colloid Polym. Sci. **105**, 298-301 (1997)

[32] F. Bordi, C. Cametti and A. Di Biasio
'High-Frequency Dielectric Polarization Mechanism in Water-in-Oil Microemulsions Below Percolation'
Progr. Colloid Polym. Sci. **115**, 44-49 (2000)

[33] M. Born
'Optik: ein Lehrbuch der elektromagnetischen Lichttheorie'
Springer, Berlin (1972)

[34] J. E. Boyd, A. Briskman, C. M. Sayes, D. Mittleman and V. Colvin
'Terahertz Vibrational Modes of Inverse Micelles'
J. Phys. Chem. B **106**, 6346-6353 (2002)

[35] M. H. Boyle
'The Electrical Properties of Heterogeneous Mixtures Containing an Oriented Spheroidal Dispersed Phase'
Colloid Polym. Sci. **263**, 51-57 (1985)

[36] J.-B. Brubach, A. Mermet, A. Filabozzi, A. Gerschel, D. Lairez, M. P. Krafft and P. Roy
'Dependence of Water Dynamics upon Confinement Size'
J. Phys. Chem. B **105**, 430-435 (2001)

[37] R. Buchner
'Dielectric Sepctroscopy of Solutions'
in: J. Samios and V. A. Durov (eds.)
'Novel Approaches to the Structure and Dynamics of Liquids: Experiments, Theories and Simulations'
NATO Science Ser. II, Vol. 133, *Kluwer*, Dordrecht (2004)

[38] R. Buchner and J. Barthel
'Dielectric Relaxation in Solutions'
Annu. Rep. Prog. Chem. Sect. C **91**, 71-105 (1994)

[39] R. Buchner and J. Barthel
'Kinetic Processes in the Liquid Phase Studied by High Frequency Permittivity Measurements'
J. Mol. Liq. **63**, 55-75 (1995)

[40] R. Buchner and J. Barthel
'A Time Domain Reflectometer for Dielectric Relaxation Spectroscopy of Electrolyte Solutions'
Ber. Bunsenges. Phys. Chem. **101**, 1509-1516 (1997)

[41] R. Buchner, J. Barthel and J. Stauber
'The Dielectric Relaxation of Water between 0 °C and 35 °C'
Chem. Phys. Lett. **306**, 57-63 (1999)

[42] R. Buchner, G. T. Hefter and P. M. May
'Dielectric Relaxation of Aqueous NaCl Solutions'
J. Phys. Chem. A **103**, 1-9 (1999)

[43] R. Buchner, C. Hölzl, J. Stauber and J. Barthel
'Dielectric Spectroscopy of Ion-Pairing and Hydration in Aqueous Tetra-*n*-alkylammonium Halide Solutions'
Phys. Chem. Chem. Phys. **4**, 2169-2179 (2002)

[44] A. L. R. Bug, S. A. Safran, G. S. Grest and I. Webman
'Do Interactions Raise or Lower a Percolation Threshold?'
Phys. Rev. Lett. **55**, 1896-1899 (1985)

[45] M. Camardo, M. D'Angelo, D. Fioretto, G. Onori, L. Palmieri and A. Santucci
'Dielectric Relaxation of Microemulsions'
Progr. Colloid Polym. Sci. **100**, 177-181 (1996)

[46] C. Cametti, P. Codastefano, A. Di Biasio, P. Tartaglia and S. H. Chen
'Dynamic Scaling of Dielectric Relaxation in Sodium Di(2-ethylhexyl)sulfosuccinate-Water-Decane Microemulsions near the Percolation Threshold'
Phys. Rev. A **40**, 1962-1966 (1989)

[47] C. Cametti, P. Codastefano, P. Tartaglia, S.-H. Chen and J. Rouch
'Electrical Conductivity and Percolation Phenomena in Water-in-Oil Microemulsions'
Phys. Rev. A **45**, R5358-R5361 (1992)

[48] E. A. S. Cavell, P. C. Knight and M. A. Sheikh
'Dielectric Relaxation in Nonaqueous Solutions. 2. Solutions of Tri(n-butyl)ammonium Picrate and Iodide in Polar Solvents'
J. Chem. Soc. Faraday Trans. **67**, 2225-2233 (1971)

[49] A. Chandra, D. Wei and G. N. Patey
'Dielectric Relaxation of Electrolyte Solutions: Is There Really a Kinetic Dielectric Decrement?'
J. Chem. Phys. **98**, 4959-4966 (1993)

[50] S. H. Chen, T. L. Lin and J. S. Huang
'Structure and Phase Transitions of a Three-Component Microemulsion System: AOT / Water / Alkane'
in: S. A. Safran and N. A. Clark (eds.)
'Physics of Complex and Supermolecular Fluids'
Wiley, New York (1987)

[51] S. J. Chen, D. F. Evans and B. W. Ninham
'Properties and Structure of Three-Component Ionic Microemulsions'
J. Phys. Chem. **88**, 1631-1634 (1984)

[52] V. Chen, D. F. Evans and B. W. Ninham
'Counterion and Co-Ion Specificity in Ionic Microemulsions'
J. Phys. Chem. **91**, 1823-1826 (1987)

[53] V. Chen, G. G. Warr, D. F. Evans and F. G. Prendergast
'Curvature and Geometric Constraints as Determinants of Microemulsion Structure: Evidence from Fluorescence Anisotropy Measurements'
J. Phys. Chem. **92**, 768-773 (1988)

[54] S. I. Chou and D. O. Shah
'Dielectric Relaxation of Oil-External Microemulsions'
J. Phys. Chem. **85**, 1480-1485 (1981)

[55] M. Clausse
'Dielectric Properties of Emulsions and Related Systems'
in: P. Becher (ed.)
'Encyclopedia of Emulsion Technology', Vol. 1
Marcel Dekker, New York (1983)

[56] K. S. Cole and R. H. Cole
'Dispersion and Absorption in Dielectrics. I. Alternating-Current Characteristics'
J. Chem. Phys. **9**, 341-351 (1941)

[57] K. S. Cole and R. H. Cole
'Dispersion and Absorption in Dielectrics. II. Direct-Current Characteristics'
J. Chem. Phys. **10**, 98-105 (1942)

[58] R. H. Cole
'Evaluation of Dielectric Behavior by Time Domain Spectroscopy.
II. Complex Permittivity'
J. Phys. Chem. **79**, 1469-1474 (1975)

[59] R. H. Cole, J. G. Berberian, S. Mashimo, G. Chryssikos, A. Burns and E. Tombari
'Time Domain Reflection Methods for Dielectric Measurements to 10 GHz'
J. Appl. Phys. **66**, 793-802 (1989)

[60] R. H. Cole, G. Delbos, P. Winsor IV, T. K. Bose and J. M. Moreau
'Study of Dielectric Properties of Water/Oil and Oil/Water Microemulsions by Time Domain and Resonance Cavity Methods'
J. Phys. Chem. **89**, 3338-3343 (1985)

[61] R. H. Cole, S. Mashimo and P. Winsor, IV
'Evaluation of Dielectric Behavior by Time Domain Spectroscopy.
3. Precision Difference Methods'
J. Phys. Chem. **84**, 786-793 (1980)

[62] CRC-Handbook of Chemistry and Physics. 1995-1996, 75^{th} edition
CRC Press, Boca Raton (1995)

[63] D. Cringus, J. Lindner, M. T. W. Milder, M. S. Pshenichnikov, P. Vöhringer and D. A. Wiersma
'Femtosecond Water Dynamics in Reverse-Micellar Nanodroplets'
Chem. Phys. Lett. **408**, 162-168 (2005)

[64] I. M. Cuccovia, L. G. Dias, F. A. Maximiano and H. Chaimovich
'Analysis of the Bromide Ion Distribution in the Water Pool of Reverse Micelles of Hexadecyltrimethylammonium Bromide in Chloroform/*n*-Dodecane and Isooctane/*n*-Hexanol by Chemical Trapping'
Langmuir **17**, 1060-1068 (2001)

[65] I. R. Dagg and G. E. Reesor
'Dielectric Loss Measurements on Nonpolar Liquids in the Microwave Region 8 to 12 GHz'
Can. J. Phys. **52**, 29-32 (1974)

[66] M. D'Angelo, D. Fioretto, G. Onori, L. Palmieri and A. Santucci
'Study of the Dynamics of Water / Aerosol OT / *n*-Heptane System by Dielectric Relaxation Measurements'
Colloid Polym. Sci. **273**, 899-905 (1995)

[67] I. Danielsson and B. Lindman
'The Definition of Microemulsion'
Colloids Surf. **3**, 391-392 (1981)

[68] D. W. Davidson and R. H. Cole
'Dielectric Relaxation in Glycerol'
J. Chem. Phys. **18**, 1417 (1950)

[69] D. W. Davidson and R. H. Cole
'Dielectric Relaxation in Glycerol, Propylene Glycol, and n-Propanol'
J. Chem. Phys. **19**, 1484-1490 (1951)

[70] P. Debye
'Polar Molecules'
Dover Publications, New York, reprint of 1st edition (1929)

[71] P. G. de Gennes
'Percolation: quelques systèmes nouveaux'
J. Phys. (Paris) **41**, C3-17 (1980)

[72] B. Derrida, D. Stauffer, H. J. Herrmann and J. Vannimenus
'Transfer Matrix Calculation of Conductivity in Three-Dimensional Random Resistor Networks at Percolation Threshold'
J. Phys. (Paris) Lett. **44**, L701-L706 (1983)

[73] H.-D. Dörfler
'Grenzflächen und kolloid-disperse Systeme: Physik und Chemie'
Springer, Berlin & Heidelberg (2002)

[74] A. M. Dokter, S. Woutersen and H. J. Bakker
'Ultrafast Dynamics of Water in Cationic Micelles'
J. Chem. Phys. **126**, 124507 (2007)

[75] J. L. Dote and D. Kivelson
'Hydrodynamic Rotational Friction Coefficients for Nonspheroidal Particles'
J. Phys. Chem. **87**, 3889-3893 (1983)

[76] J. L. Dote, D. Kivelson and R. N. Schwartz
'A Molecular Quasi-Hydrodynamic Free-Space Model for Molecular Rotational Relaxation in Liquids'
J. Phys. Chem. **85**, 2169-2180 (1981)

[77] K. Dransfeld and P. Kienle
'Physik II. Elektrodynamik'
Oldenbourg, Munich (1986)

[78] B. R. Epstein, K. R. Foster and R. A. Mackay
'Microwave Dielectric Properties of Ionic and Nonionic Microemulsions'
J. Colloid Interface Sci. **95**, 218-227 (1983)

[79] D. F. Evans, D. J. Mitchell and B. W. Ninham
'Oil, Water, and Surfactant: Properties and Conjectured Structure of Simple Microemulsions'
J. Phys. Chem. **90**, 2817-2825 (1986)

[80] J. Fahrenfort
'Attenuated Total Reflection. A New Principle for the Production of Useful Infra-Red Reflection Spectra of Organic Compounds'
Spectrochim. Acta **17**, 698-709 (1961)

[81] J. Fahrenfort
'The Methods and Results of Dispersion Studies'
in: M. Davies (ed.)
'Infra-Red Spectroscopy and Molecular Structure. An Outline of the Principles'
Elsevier, London (1963)

[82] H. Falkenhagen
'Theorie der Elektrolyte'
Hirzel, Leipzig (1971)

[83] Y. Feldman, N. Kozlovich, Y. Alexandrov, R. Nigmatullin and Y. Ryabov
'Mechanism of the Cooperative Relaxation in Microemulsions near the Percolation Threshold'
Phys. Rev. E **54**, 5420-5427 (1996)

[84] Y. Feldman, N. Kozlovich, I. Nir and N. Garti
'Dielectric Relaxation in Sodium Bis(2-ethylhexyl)sulfosuccinate-Water-Decane Microemulsions near the Percolation Temperature Threshold'
Phys. Rev. E **51**, 478-491 (1995)

[85] Y. Feldman, N. Kozlovich, I. Nir, N. Garti, V. Archipov, Z. Idiyatullin, Y. Zuev and V. Fedotov
'Mechanism of Transport of Charge Carriers in the Sodium Bis(2-ethylhexyl) Sulfosuccinate - Water - Decane Microemulsion near the Percolation Temperature Threshold'
J. Phys. Chem. **100**, 3745-3748 (1996)

[86] H. Fellner-Feldegg
'The Measurement of Dielectrics in the Time Domain'
J. Phys. Chem. **73**, 616-623 (1969)

[87] H. Fellner-Feldegg
'A Thin-Sample Method for the Measurement of Permeability, Permittivity, and Conductivity in the Frequency and Time Domain'
J. Phys. Chem. **76**, 2116-2122 (1972)

[88] P. Fernandez, S. Schrödle, R. Buchner and W. Kunz
'Micelle and Solvent Relaxation in Aqueous Sodium Dodecylsulfate Solutions'
ChemPhysChem **4**, 1065-1072 (2003)

[89] K. Fontell, A. Ceglie, B. Lindman and B. Ninham
'Some Observations on Phase Diagrams and Structure in Binary and Ternary Systems of Didodecyldimethylammonium Bromide'
Acta Chem. Scand. A **40**, 247-256 (1986)

[90] H. Fricke
'The Maxwell-Wagner Dispersion in a Suspension of Ellipsoids'
J. Phys. Chem. **57**, 934-937 (1953)

[91] H. Fröhlich
'Theory of Dielectrics: Dielectric Constant and Dielectric Loss'
2nd ed., *Clarendon Press*, Oxford (1968)

[92] B. Gestblom and J. Sjöblom
'Dielectric Properties of Some Microemulsion Systems Containing Electrolytes'
Langmuir **4**, 360-364 (1988)

[93] K. Ghowsi and R. J. Gale
'Some Aspects of the High Frequency Conductance of Electrolytes'
J. Electrochem. Soc. **136**, 2806-2811 (1989)

[94] G. Giammona, F. Goffredi, V. Turco Liveri and G. Vassallo
'Water Structure in Water/AOT/n-Heptane Microemulsions by FT-IR Spectroscopy'
J. Colloid Interface Sci. **154**, 411-415 (1992)

[95] J. H. Gibbs, C. Cohen, P. D. Fleming III and H. Porosoff
'Toward a Model for Liquid Water'
in: R. L. Kay (ed.)
'The Physical Chemistry of Aqueous Systems'
Plenum, New York (1973)

[96] S. H. Glarum
'Dielectric Relaxation of Isoamyl Bromide'
J. Chem. Phys. **33**, 639-643 (1960)

[97] D. N. Glew and N. S. Rath
'H_2O, HDO, and CH_3OH Infrared Spectra and Correlation with Solvent Basicity and Hydrogen Bonding'
Can. J. Chem. **49**, 837-856 (1971)

[98] G. S. Greschner
'Maxwellgleichungen'
Hüthig & Wepf, Basel (1981)

[99] G. S. Grest, I. Webman, S. A. Safran and A. L. R. Bug
'Dynamic Percolation in Microemulsions'
Phys. Rev. A **33**, 2842-2845 (1986)

[100] K. Günther and D. Heinrich
'Dielektrizitätskonstante, Permeabilität, elektrische Leitfähigkeit, Wärmeleitfähigkeit und Diffusionskonstante von Gemisehen mit kugelförmigen Teilchen (gitterförmige und statistische Anordnung)'
Z. Physik **185**, 345-374 (1965)

[101] T. Hanai
'Electrical Properties of Emulsions'
in: P. Sherman (ed.)
'Emulsion Science'
Academic Press, London (1968)

[102] T. Hanai, K. Asami and N. Koizumi
'Dielectric Theory of Concentrated Suspensions of Shell-Spheres in Particular Reference to the Analysis of Biological Cell Suspensions'
Bull. Inst. Chem. Res. **57**, 297-305 (1979)

[103] M. R. Harpham, B. M. Ladanyi, N. E. Levinger and K. W. Herwig
'Water Motion in Reverse Micelles Studied by Quasielastic Neutron Scattering and Molecular Dynamics Simulation'
J. Chem. Phys. **121**, 7855-7868 (2004)

[104] N. J. Harrick
'Surface Chemistry from Spectral Analysis of Totally Internally Reflected Radiation'
J. Phys. Chem. **64**, 1110-1114 (1960)

[105] N. J. Harrick
'Internal Reflection Spectroscopy'
Wiley, New York (1967)

[106] J. B. Hasted
'Liquid Water: Dielectric Properties'
in: F. Franks (ed.)
'Water: A Comprehensive Treatise'
Vol. 1, *Plenum*, New York (1972)

[107] H. Hauser, G. Haering, A. Pande and P. L. Luisi
'Interaction of Water with Sodium Bis(2-ethyl-1-hexyl) Sulfosuccinate in Reversed Micelles'
J. Phys. Chem. **93**, 7869-7876 (1989)

[108] S. Havriliak and S. Negami
'A Complex Plane Analysis of α-Dispersions in Some Polymer Systems'
J. Polym. Sci., Part C **14**, 99-103 (1966)

[109] R. Henze and U. Schreiber
'Dielectric Relaxation Measurements on Aerosol-OT/Water/Cyclohexane - Solutions at Low Water Content'
Colloid Polym. Sci. **263**, 164-172 (1985)

[110] N. E. Hill
'Theoretical Treatment of Permittivity and Loss'
in: N. E. Hill, W. E. Vaughan, A. H. Price and M. Davies
'Dielectric Properties and Molecular Behaviour'
Van Nostrand, London (1969)

[111] T. P. Hoar and J. H. Schulman
'Transparent Water-in-Oil Dispersions: The Oleopathic Hydro-Micelle'
Nature **152**, 102-103 (1943)

[112] C. Hölzl
'Dielektrische Relaxation von Benzonitril und Butylencarbonat sowie verbesserte Auswertemethoden von TDR-Messungen'
Diploma Thesis, Regensburg University, Regensburg (1995)

[113] C. Hölzl
'Optimierung einer TDR-Apparatur zur Untersuchung der dielektrischen Relaxation von H_2O, D_2O und wäßrigen Tetraalkylammoniumbromidlösungen'
PhD Thesis, Regensburg University, Regensburg (1998)

[114] P. Huang Kenéz, G. Carlström, I. Furó and B. Halle
'Counterion Spin Relaxation in Microemulsion Droplets'
J. Phys. Chem. **96**, 9524-9531 (1992)

[115] J. B. Hubbard
'Dielectric Dispersion and Dielectric Friction in Electrolyte Solutions. II.'
J. Chem. Phys. **68**, 1649-1664 (1978)

[116] J. B. Hubbard, P. Colonomos and P. G. Wolynes
'Molecular Theory of Solvated Ion Dynamics. III. The Kinetic Dielectric Decrement'
J. Chem. Phys. **71**, 2652-2661 (1979)

[117] J. B. Hubbard and L. Onsager
'Dielectric Dispersion and Dielectric Friction in Electrolyte Solutions. I.'
J. Chem. Phys. **67**, 4850-4857 (1977)

[118] J. Hunger
'Einfluss des Hydrotrops 1-Pentanol auf die dielektrische Relaxation von Natriumdodecylsulfat Mizellen
Diploma Thesis, Regensburg University, Regensburg (2006)

[119] T. Isono
'Density, Viscosity, and Electrolytic Conductivity of Concentrated Aqueous Electrolyte Solutions at Several Temperatures. Alkaline-Earth Chlorides, $LaCl_3$, Na_2SO_4, $NaNO_3$, NaBr, KNO_3, KBr, and $Cd(NO_3)_2$'
J. Chem. Eng. Data **29**, 45-52 (1984)

[120] J. Israelachvili
'Intermolecular and Surface Forces'
2nd ed., *Academic Press*, London (1991)

[121] M. O. Iwunze
'Reductive Voltammetry of Berberine Hydrochloride in Bicontinuous Microemulsion'
Bulletin of Electrochemistry **18**, 81-86 (2002)

[122] A. Jada, J. Lang and R. Zana
'Relation between Electrical Percolation and Rate Constant for Exchange of Material between Droplets in Water in Oil Microemulsions'
J. Phys. Chem. **93**, 10-12 (1989)

[123] W. Jahn and R. Strey
'Microstructure of Microemulsions by Freeze Fracture Electron Microscopy'
J. Phys. Chem. **92**, 2294-2301 (1988)

[124] T. K. Jain, M. Varshney and A. Maitra
'Structural Studies of Aerosol OT Reverse Micellar Aggregates by FT-IR Spectroscopy'
J. Phys. Chem. **93**, 7409-7416 (1989)

[125] U. Kaatze
'The Dielectric Properties of Water in its Different States of Interaction'
J. Solution Chem. **26**, 1049-1112 (1997)

[126] G. N. Kamau and J. F. Rusling
'Enhanced Rates of Organic Dehalogenations in a Microemulsion Using Adsorbed Metal Phthalocyanines on Electrodes'
Langmuir **12**, 2645-2649 (1996)

[127] P. Karpe and E. Ruckenstein
'Effect of Hydration Ratio on the Degree of Counterion Binding and pH Distribution in Reverse Micelles with Aqueous Core'
J. Colloid Interf. Sci. **137**, 408-424 (1990)

[128] T. Keyes and D. Kivelson
'Depolarized Light Scattering: Theory of the Sharp and Broad Rayleigh Lines'
J. Chem. Phys. **56**, 1057-1065 (1972)

[129] J. G. Kirkwood
'The Dielectric Polarization of Polar Liquids'
J. Chem. Phys. **7**, 911-919 (1939)

[130] D. Kivelson and P. Madden
'Theory of Dielectric Relaxation'
Mol. Phys. **30**, 1749-1780 (1975)

[131] D. Kivelson and P. Madden
'Comments on the Dielectric Relaxation of Small Parts of a Large System'
J. Phys. Chem. **88**, 6557-6559 (1984)

[132] N. Kozlovich, A. Puzenko, Y. Alexandrov and Y. Feldman
'Effect of Charge Density Fluctuations Within a Droplet on Dielectric Polarization of Ionic Microemulsions'
Colloids Surf. A **140**, 299-312 (1998)

[133] O. Kratky, H. Leopold and H. Stabinger
'Dichtemessung an Flüssigkeiten und Gasen auf 10^{-6} g/cm^3 bei 0.6 cm^3 Präparatvolumen'
Z. Angew. Phys. **27**, 273-277 (1969)

[134] W. Kunz, P. Lo Nostro and B. W. Ninham
'The Present State of Affairs with Hofmeister Effects'
Curr. Opin. Colloid Interface Sci. **9**, 1-18 (2004)

[135] M. Laguës
'Electrical Conductivity of Microemulsions: a Case of Stirred Percolation'
J. Phys. (Paris) Lett. **40**, L331-L333 (1979)

[136] M. J. Lawrence and G. D. Rees
'Microemulsion-Based Media as Novel Drug Delivery Systems'
Adv. Drug Delivery Rev. **45**, 89-121 (2000)

[137] U. Lenz and H. Hoffmann
'Dynamic Behaviour of Ternary Microemulsions Consisting of Didodecyldimethylammoniumbromide, Water and Hydrocarbon'
Ber. Bunsenges. Phys. Chem. **96**, 809-815 (1992)

[138] H. Levine and C. H. Papas
'Theory of the Circular Diffraction Antenna'
J. Appl. Phys. **22**, 29-43 (1951)

[139] N. E. Levinger
'Water in Confinement'
Science **298**, 1722-1723 (2002)

[140] H. MacDonald, B. Bedwell and E. Gulari
'FTIR Spectroscopy of Microemulsion Structure'
Langmuir **2**, 704-708 (1986)

[141] Y. Marcus
'Ion Properties'
Marcel Dekker, New York (1997)

[142] D. W. Marquardt
'An Algorithm for Least-Squares Estimation of Nonlinear Parameters'
J. Soc. Indust. Appl. Math. **11**, 431-441 (1963)

[143] F. M. Menger, J. A. Donohue and R. F. Williams
'Catalysis in Water Pools'
J. Am. Chem. Soc. **95**, 286-288 (1973)

[144] S. Murgia, M. Monduzzi and B. W. Ninham
'Hofmeister Effects in Cationic Microemulsions'
Curr. Opin. Colloid Interface Sci. **9**, 102-106 (2004)

[145] S. Murgia, F. Portesani, B. W. Ninham and M. Monduzzi
'Interaction of Sodium Ions with Cationic Surfactant Interfaces'
Chem. Eur. J. **12**, 7889-7898 (2006)

[146] W. Niesel
'Die Dielektrizitätskonstanten heterogener Mischkörper aus isotropen und anisotropen Substanzen'
Ann. Physik **445**, 336-348 (1952)

[147] R. Nozaki and T. K. Bose
'Broadband Complex Permittivity Measurements by Time-Domain Spectroscopy'
IEEE Trans. Instrum. Meas. **39**, 945-951 (1990)

[148] G. Onori and A. Santucci
'IR Investigations of Water Structure in Aerosol OT Reverse Micellar Aggregates'
J. Phys. Chem. **97**, 5430-5434 (1993)

[149] G. Onori and A. Santucci
'Hydration and Dynamics of Aerosol OT Microemulsions: Infrared and Microwave Dielectric Spectroscopy'
Trends in Chemical Physics **4**, 215-225 (1996)

[150] L. Onsager
'Electric Moments of Molecules in Liquids'
J. Am. Chem. Soc. **58**, 1486-1493 (1936)

[151] A. L. Oppenheim
'Ancient Mesopotamia – Portrait of a Dead Civilization'
University of Chicago Press, Chicago (1964)

[152] J. T. G. Overbeek
'The First Rideal Lecture. Microemulsions, a Field at the Border Between Lyophobic and Lyophilic Colloids'
Faraday Discuss. Chem. Soc. **65**, 7-19 (1978)

[153] M. Paillette
'Interfacial Charges Manifestations: Kerr and Dielectric Constants Relaxations Studies in a Microemulsion System'
Physica A **157**, 548-554 (1989)

[154] H. Pauly and H. P. Schwan
'Über die Impedanz einer Suspension von kugelförmigen Teilchen mit einer Schale'
Z. Naturforsch. **14b**, 125-131 (1959)

[155] E. Pehl
'Mikrowellentechnik'
Vol. 2, *Hüthig*, Heidelberg (1984)

[156] M. H. Pellat
'Polarisation réelle des diélectriques. Conséquences de cette polarisation'
Ann. Chim. Phys. **18**, 150-181 (1899)

[157] J. Peyrelasse and C. Boned
'Conductivity, Dielectric Relaxation, and Viscosity of Ternary Microemulsions: The Role of the Experimental Path and the Point of View of Percolation Theory'
Phys. Rev. A **41**, 938-954 (1990)

[158] D. Polder and J. H. van Santen
'The Effective Permeability of Mixtures of Solids'
Physica **12**, 257-271 (1946)

[159] A. Ponton, T. K. Bose and G. Delbos
'Dielectric Study of Percolation in an Oil-Continuous Microemulsion'
J. Chem. Phys. **94**, 6879-6886 (1991)

[160] A. Ponton, R. Nozaki and T. K. Bose
'Dielectric Relaxation Study of Oil-Continuous Microemulsion Systems'
J. Chem. Phys. **97**, 8515-8521 (1992)

[161] J. G. Powles
'Dielectric Relaxation and the Internal Field'
J. Chem. Phys. **21**, 633-637 (1953)

[162] E. S. Rittner
'Binding Energy and Dipole Moment of Alkali Halide Molecules'
J. Chem. Phys. **19**, 1030-1035 (1951)

[163] D. E. Rosenfeld and C. A. Schmuttenmaer
'Dynamics of Water Confined Within Reverse Micelles'
J. Phys. Chem. B **110**, 14304-14312 (2006)

[164] T. Sato and R. Buchner
'The Cooperative Dynamics of the H-bond System in 2-Propanol/Water Mixtures: Steric Hindrance Effects of Nonpolar Head Group'
J. Chem. Phys. **119**, 10789-10800 (2003)

[165] T. G. Scholte
'Theory of the Dielectric Constant of Polar Liquids'
Physica **15**, 437-449 (1949)

[166] B. Schrader
'Infrared and Raman Spectroscopy. Methods and Applications'
VCH, Weinheim (1995)

[167] S. Schrödle
'Struktur und Dynamik von Oligoethylenglykolen und verwandten Systemen'
Diploma Thesis, Regensburg University, Regensburg (2002)

[168] S. Schrödle
'Effects of Non-Ionic Surfactants and Related Compounds on the Cooperative and Molecular Dynamics of their Aqueous Solutions'
PhD Thesis, Regensburg University, Regensburg (2005)

[169] S. Schrödle, R. Buchner and W. Kunz
'Percolating Microemulsions of Nonionic Surfactants Probed by Dielectric Spectroscopy'
ChemPhysChem **6**, 1051-1055 (2005)

[170] S. Schrödle, B. Fischer, H. Helm and R. Buchner
'Picosecond Dynamics and Microheterogenity of Water + Dioxane Mixtures'
J. Phys. Chem. A **111**, 2043-2046 (2007)

[171] S. Schrödle, G. Hefter and R. Buchner
'Dielectric Spectroscopy of Hydrogen Bond Dynamics and Microheterogenity of Water + Dioxane Mixtures'
J. Phys. Chem. B **111**, 5946-5955 (2007)

[172] J. H. Schulman, W. Stoeckenius and L. M. Prince
'Mechanism of Formation and Structure of Micro Emulsions by Electron Microscopy'
J. Phys. Chem. **63**, 1677-1680 (1959)

[173] J. W. Shield, H. D. Ferguson, A. S. Bommarius and T. A. Hatton
'Enzymes in Reversed Micelles as Catalysts for Organic-Phase Synthesis Reactions'
Ind. Eng. Chem. Fundam. **25**, 603-612 (1986)

[174] T. Shikata and S. Imai
'Dielectric Relaxation of Surfactant Micellar Solutions'
Langmuir **14**, 6804-6810 (1998)

[175] J. Sjöblom, R. Skurtveit, J. O. Saeten and B. Gestblom
'Structural Changes in the Microemulsion System Didodecyldimethylammonium Bromide / Water / Dodecane as Investigated by Means of Dielectric Spectroscopy'
J. Colloid Interface Sci. **141**, 329-337 (1991)

[176] R. Skurtveit and U. Olsson
'A Self-Diffusion Study of the Microstructure in Didodecyldimethylammonium Bromide-Dodecane-Brine Microemulsions'
J. Phys. Chem. **95**, 5353-5358 (1991)

[177] R. Skurtveit and U. Olsson
'Microstructure near the Oil Corner of a Ternary Microemulsion'
J. Phys. Chem. **96**, 8640-8646 (1992)

[178] M. Śmiechowski and J. Stangret
'Molecular Picture of Hydroxide Anion Hydration in Aqueous Solutions Studied by FT-IR ATR Spectroscopy'
J. Mol. Struct. **834-836**, 239-248 (2007)

[179] A. Sommerfeld
'Vorlesungen über Theoretische Physik, Band III, Elektrodynamik'
4$^{\text{th}}$ edition, *Akademische Verlagsgesellschaft*, Leipzig (1964)

[180] H. Steger
'Dielektrische Eigenschaften wasserreicher Ethanol-Wasser-Mischungen im Frequenzbereich 0.95 bis 39.0 GHz und ihre Beeinflussung durch Elektrolytzusatz'
PhD Thesis, Regensburg University, Regensburg (1985)

[181] A. Stoppa
'Kooperative Dynamik von Acetonitril und dessen wässrigen Mischungen'
Diploma Thesis, Regensburg University, Regensburg (2006)

[182] D. Tabor
'Babylonian Lecanomancy: An Ancient Text on the Spreading of Oil on Water'
J. Colloid Interf. Sci. **75**, 240-245 (1980)

[183] The International Association for the Properties of Water and Steam
Release on the IAPWS Industrial Formulation 1997 for the Thermodynamic Properties of Water and Steam
IAPWS Meeting, Erlangen, September 1997

[184] D. J. Tobias and M. L. Klein
'Molecular Dynamics Simulations of a Calcium Carbonate / Calcium Sulfonate Reverse Micelle'
J. Phys. Chem. **100**, 6637-6648 (1996)

[185] A. Tromans, P. M. May, G. Hefter, T. Sato and R. Buchner
'Ion Pairing and Solvent Relaxation Processes in Aqueous Solutions of Sodium Malonate and Sodium Succinate'
J. Phys. Chem. B **108**, 13789-13795 (2004)

[186] M. A. van Dijk
'Dielectric Study of Percolation Phenomena in a Microemulsion'
Phys. Rev. Lett. **55**, 1003-1005 (1985)

[187] M. A. van Dijk, G. Casteleijn, J. G. H. Joosten and Y. K. Levine
'Percolation in Oil-Continuous Microemulsions. A Dielectric Study of Aerosol OT / Water / Isooctane'
J. Chem. Phys. **85**, 626-631 (1986)

[188] M. A. van Dijk, J. G. H. Joosten, Y. K. Levine and D. Bedeaux
'Dielectric Study of Temperature-Dependent Aerosol OT / Water / Isooctane Microemulsion Structure'
J. Phys. Chem. **93**, 2506-2512 (1989)

[189] W. Wachter
'Dielektrische Relaxation wässriger 1:1-Elektrolytlösungen. Die Hydratation von Anionen und ihr Einfluss auf die Hofmeister-Serie'
Diploma Thesis, Regensburg University, Regensburg (2004)

[190] W. Wachter, R. Buchner and G. Hefter
'Hydration of Tetraphenylphosphonium and Tetraphenylborate Ions by Dielectric Relaxation Spectroscopy'
J. Phys. Chem. B **110**, 5147-5154 (2006)

[191] W. Wachter, Š. Fernandez, R. Buchner and G. Hefter
'Ion Association and Hydration in Aqueous Solutions of LiCl and Li_2SO_4 by Dielectric Spectroscopy'
J. Phys. Chem. B **111**, 9010-9017 (2007)

[192] W. Wachter, W. Kunz, R. Buchner and G. Hefter
'Is There an Anionic Hofmeister Effect on Water Dynamics? Dielectric Spectroscopy of Aqueous Solutions of NaBr, NaI, $NaNO_3$, $NaClO_4$, and NaSCN'
J. Phys. Chem. A **109**, 8675-8683 (2005)

[193] G. E. Walrafen
'Raman Spectral Studies of the Effects of Electrolytes on Water'
J. Chem. Phys. **36**, 1035-1042 (1962)

[194] G. G. Warr
'Shear and Elongational Rheology of Ternary Microemulsions'
Colloids Surf. A **103**, 273-279 (1995)

[195] G. G. Warr, R. Sen, D. F. Evans and J. E. Trend
'Microemulsion Formation and Phase Behavior of Dialkyldimethylammonium Bromide Surfactants'
J. Phys. Chem. **92**, 774-783 (1988)

[196] E. Wismeth
'FTIR-Spektroskopische Untersuchungen zur Solvatation und Assoziation von Lithiumsalzen in dipolar aprotischen Lösungsmitteln'
PhD Thesis, Regensburg University, Regensburg (1996)

[197] M. Wong, J. K. Thomas and T. Nowak
'Structure and State of H_2O in Reversed Micelles. 3.'
J. Am. Chem. Soc. **99**, 4730-4736 (1977)

[198] L. Yang and K. Zhao
'Dielectric Model and Theoretical Analysis of Cationic Reverse Micellar Solutions in CTAB/Isooctane/*n*-Hexanol/Water Systems'
Langmuir **23**, 8732-8739 (2007)

[199] R. Zana, J. Lang and D. Canet
'Ternary Water-in-Oil Microemulsions Made of Cationic Surfactants, Water, and Aromatic Solvents. 3. Self-Diffusion Studies in Relation to Exchange of Material between Droplets and Percolation'
J. Phys. Chem. **95**, 3364-3367 (1991)

[200] S. Zhang and J. F. Rusling
'Dechlorination of Polychlorinated Biphenyls on Soils and Clay by Electrolysis in a Bicontinuous Microemulsion'
Environ. Sci. Technol. **29**, 1195-1199 (1995)

[201] K. Zhao, K. He and S. Wei
'Progress in the Study of Molecular Organized Assemblies by Dielectric Relaxation Spectroscopy'
Progress in Natural Science **16**, 221-230 (2006)

[202] D.-L. Zhou, H. Carrero and J. F. Rusling
'Radical vs Anionic Pathway in Mediated Electrochemical Reduction of Benzyl Bromide in a Bicontinuous Microemulsion'
Langmuir **12**, 3067-3074 (1996)

[203] D.-L. Zhou, J. Gao and J. F. Rusling
'Kinetic Control of Reactions of Electrogenerated Co(I)Macrocycles with Alkyl Bromides in a Bicontinuous Microemulsion'
J. Am. Chem. Soc. **117**, 1127-1134 (1995)

Regensburg, den 14. November 2007

Wolfgang Wachter